Politecnico di Milano
Dipartimento di Elettronica, Informatica e Bioingegneria
Doctoral Programme In Systems and Control

A Newton-Euler approach to modelling and control of flexible manipulators

Doctoral Dissertation of:
Bruno Scaglioni

Supervisor:
Prof. Gianni Ferretti

Tutor:
Prof. Luca Bascetta

The Chair of the Doctoral Program:
Prof. Andrea Bonarini

2016 – XXIX Cycle

Contents

Abstract

Modelling and control of flexible lightweight manipulators has been matter of research since the late 80s. Nevertheless, the interest on this topic is still intense. Manipulators where structural flexibility deserve to be considered in the design stage can be found in a range of applications including traditional industrial robots, nuclear materials manipulation, agricultural and space robotics as well as in autonomous vehicle applications. The introduction of lightweight robots is a driver of innovation when trending technologies require decreasing power consumption and low manipulator masses in view of increasing performances requirements. The aforementioned trends encourage the use of lightweight manipulators and the development of related technologies, but whenever high performances are required, a severe issue arises: vibrations. The main subject of this thesis is the development of a closed-form model of three-dimensional flexible manipulator with links of general shape and the synthesis of a two-timescale control system able to improve the performances of the manipulator and substantially increase damping with respect to the classical P/PI control structure. The resulting performance are achieved by means of a controller acting on the robot joints in a "fast" timescale, coupled with a traditional system acting on the "slow" timescale. A compact model of a generic three-dimensional flexible body was initially developed in an object-oriented modelling framework, namely Modelica, and based on the floating frame of reference (FFR) formulation. The equations of motion have been formulated in the Newton-Euler form, allowing a complete calculation of the Coriolis and gyroscopic terms of the inertial forces for the elastic degrees of freedom. The model allows considering bodies of general shape through the calculation of shape functions, which describe the geometry, as the result of the modal analysis performed by finite elements packages. The results achieved in the development of the generic body model have then been exploited in the development of a closed-form model of flexible manipulator. The proposed model is based on the adoption of the spatial vector notation, which allows to combine the equations of motion of the links calculated in the previous step, leading to a multilink three-dimensional model in closed form with respect to the joint angles and the modal coordinates. The motion equations can be computed for links with arbitrary shape and cardinality; hence, the model results to be highly adaptable and computationally efficient. The model has been validated by

means of comparison with literature benchmarks obtained with the classical multibody approach and with experiments collected on a real manipulator. Despite its efficiency and accuracy, the closed form model is not suitable for real-time control and active vibration damping due to its inherent complexity, hence an approximated model based on the integral manifold approach has been developed starting from the complete model previously described. The approximated model has therefore been compared with the original closed-form model and with experimental data retrieved from the MERIt dataset. The subsystems resulting from the adoption of the integral manifold approximation are in fact two: a "slow" nonlinear subsystem, which can be controlled by means of classical techniques, and a "fast" linear subsystem, whose dynamic matrices exhibit a dependency on the state of the "slow" subsystem, namely the spatial configuration of the robot. A control technique is finally presented for the family of the "fast" subsystems, which is based on advanced nonconvex H-infinity control. The overall control system provides better performances with respect of the classical techniques, allowing a consistent vibration damping and a substantial increase in the control bandwidth. Future developments will concern controllability and observability analysis on the vibration system and a state estimator for the "fast" subsystem, based on considerations related to the use of sensors, such as the strain gauges position, in conjunction with the analysis of the shape functions relating the strain to the modal variables.

Sommario

La modellazione ed il controllo di manipolatori flessibili lightweight è oggetto di ricerca sin dalla fine degli anni 80, ciononostante, questo tema è ancora di grande interesse sia industriale che scientifico. Esistono numerosi campi applicativi dove la flessibilità strutturale dei manipolatori non può essere trascurata, si pensi ad esempio alla manipolazione di scorie nucleari, la robotica agricola e spaziale cosi come le applicazioni di manipolazione su veicoli. L'introduzione di robots leggeri è inoltre un importante driver tecnologico nelle applicazioni che richiedono basso cosumo energetico ed alte prestazioni dinaniche, pertanto l'uso di manipolatori leggeri e lo sviluppo delle relative tecnologie di modellazione e controllo è fortemente incoraggiato dalle richieste del mercato. Sfortunatamente l'uso di strutture leggere abbinate ad alte prestazioni conduce inevitabilmente al problema delle vibrazioni. L'argomento principale di questa tesi è lo sviluppo di un modello tridimensionale in forma chiusa di manipolatore flessible e la sintesi di un sistema di controllo a due scale di tempo in grado di migliorare le performances del manipolatore attraverso lo smorzamento attivo delle vibrazioni. Le suddette prestazioni vengono raggiunte attraverso un controllore agente sui giunti del manipolatore in una scala di tempo veloce, accoppiato con un classico schema di controllo del moto, agente sulla scala di tempo lenta. Inizialmente, è stato sviluppato un modello di corpo flessibile generico e object-oriented, basato sulla formulazione floating frame of reference. Le equazioni di moto sono state formulate secondo l'approccio di Newton-Eulero, permettendo il calcolo completo dei termini giroscopici e di Coriolos per le forze d'inerzia agenti sui gradi di libertà elastici. La generalità del modello è stata ottenuta attraverso il calcolo di funzioni di forma che descrivono la geometria, come risultato di una fase di pre-processing portata a termine da solutori ad elementi finiti. I risultati ottenuti nello sviluppo del modello di corpo generico sono stati sfruttati per mettere a punto un modello in forma chiusa di manipolatore flessibile. Il suddetto modello è basato sull'adozione della spatial vector notation, che permette di combinare le equazioni di moto dei links, creando un modello di manipolatore flessibile multilink in forma chiusa rispetto alle variabili di giunto ed alle coordinate modali. Le equazioni di moto possono essere risolte per links di qualsiasi forma e cardinalità, di conseguenza il modello è particolarmente versatile e computazionalmente efficiente. Il modello è stato validato attraverso il confronto con esperimenti effettuati su

un manipolatore reale. Nonostante l'efficienza e l'accuratezza che caratterizzano il modello in forma chiusa, quest'ultimo risulta poco adatto alla sintesi di sistemi di controllo attivo di vibrazioni, a causa della complessità intrinseca che lo caratterizza. Conseguentemente, è stato sviluppato un modello approssimato, basato sull'approccio integral manifold. Il suddetto modello è stato poi confrontato con il modello originale e con i dati sperimentali ottenuti dal dataset MERIt. L'adozione dell'approccio integral manifold ha permesso di dividere il modello originale in due sottosistemi: un sistema "lento" non lineare, controllato con tecniche classiche, ed un sistema "veloce" lineare tempo variante, le cui matrici presentano una dipendenza dallo state del sistema lento. Infine, è stata presentata una tecnica di controllo per la famiglia dei sistemi "veloci" basata sul controllo H-infinito non convesso e nonsmooth. Il sistema di controllo complessivo permette di incrementare sensibilmente le performances rispetto alle tecniche classiche.

Chapter 1

Introduction

Lightweight manipulators are used nowadays in a wide variety of applications ranging from the replacement of human action in hazardous environment to agricultural robotics, mobile robotics, robotic surgery and the well known field of space robotics. Although the adoption of robotic manipulators is widely spread in every industrial field, most of the existing industrial manipulators are designed with the aim of maximizing the structural stiffness in order to reduce the vibrations of the end-effector and achieve a good position accuracy. This high stiffness is often achieved by using heavy materials and bulky design which necessarily yield inefficiency in terms of performances, dexterity and power consumption, the last of which is gaining great attention in the recent trends of industrial innovation, as shown by the presence of several European and National projects on the topic of energy efficiency in industrial environments.

The use of lightweight structures in industrial scenarios is an interesting alternative to the classic approach, and several advances are expected. Compared to the conventional heavy robots, manipulators with flexible structures have the potential advantage of lower costs, higher operational speed, greater payload-to-manipulator weight ratio, lower energy consumption and safer operation due to low inertia. This approach presents however a drawback: reduced masses and extended workspaces enhance the effects of structural flexibility, yielding to vibrations as a consequence of low stiffness. The structural vibrations appear to be one of the main obstacles tht prevent the design of control loops with high bandwidth and accurate positioning capability. It has been estimated that many cumulative hours have been spent in order to damp down the vibration in the remote manipulator system in a Space Station-assembly Shuttle mission [40].

In this scenario, an accurate modelling of the system and an efficient control technique acquire crucial importance, however, a robotic system with flexible links is governed by a system of nonlinear partial differential equations aimed to describe the distributed flexibility. The exact solution of such system is not practically feasible and the infinite dimensional model imposes several constraints on the design of the controller as well. In the 90's and

00's decades, such a challenging problem has attracted several researchers leading to brilliant results: an exaustive review on modelling can be found in [123] while good a survey on control approaches is in [14]. The interest in the topic seems to have somehow decreased since the mid 00's due to the great amount of literature developed so far and to the complexity and peculiarity of the problem at hand. Although, some relevant scientific work has been recently carried out [68, 82, 115, 119, 137, 158] and, as shown by a recent review [117], some open problems can still be tackled in this area and further advances can be made.

To the author's knowledge, the majority of the research has been carried out on single-link or planar two-links manipulators where links with uniform shape are considered [14, 123], while a general approach for modelling three-dimensional manipulators with links of general shape is still missing. Moreover, linearised approaches to the links' flexibility are considered, hence there is the need of incorporating large deformations, geometrical stiffening and composite materials. This thesis aims to give a substantial contribution in this field by developing a complete, closed-form model for three-dimensional flexible manipulators with links of general shape based on the Newton-Euler formulation of the motion equations. Subsequently, a control-oriented, approximated model, based on the integral manifold approach [135] is sinthesized, and finally, a control strategy based on a non smooth and non convex optimization, originally described in [7] is proposed. Another substantial contribution of this thesis is the development of an object-oriented model of flexible body for multibody simulation purposes, based on the same Newton-Euler formulation, which has been carried out as a first step towards the synthesis of the closed-form model. However, this object-oriented model represents an ancillary result as it contains a complete description of the calculation of the quadratic and Coriolis terms of the inertial forces acting on the elastic degrees of freedom. To the author's knowledge this is a brand new result with respect to literature.

1.1 Approaches to distributed flexibility

Flexible manipulators are described by continuous non linear dynamical systems characterized by an infinite number of degrees of freedom, hence a complete mathematical description should be based upon nonlinear partial differential equations, which can hardly be tackled for simulation and control design purposes. As a consequence, it is necessary to introduce methods to describe the distributed flexibility with a finite number of parameters. Three approaches are generally used in order to derive approximated models: lumped parameters, assumed modes method (AMM) and finite elements method (FEM).

Historically, the first and simplest adopted approach consists in developing a lumped parameters method [62, 89, 154, 160]. In this method each

flexible link is divided into a finite number of rigid links connected by joints, and flexibility is represented by springs that restrict the joints' motion. Actually, this method has been rarely used since the 90' because of the roughness of the approximation and the difficulty in determining a physical meaning for the springs' stiffness. Moreover, the addition of a further degree of freedom to an existing model causes a variation of all the frequencies, yielding a model difficult to refine and maintain.

The Assumed modes method is widely used in literature [17, 19, 22, 35, 78, 111, 157]. In this approach, links' flexibility is described through the use of shape functions defined over the entire extension of the link. These functions are based on spatial mode eigenfunctions and usually are represented by truncated modal series. Although this method is conceptually simple, the best selection of modal shapes and boundary conditions is not trivial, an example of clamped boundary conditions can be found in [17], while in [8] pinned-pinned boundary conditions, and in [11] free-free conditions are used. On the other hand, in the Finite Element formulation [114, 116, 149], shape functions are defined over small subdomains of the link as polynomial functions and the choice of boundary conditions can be treated in a straightforward manner. This approach is usually considered a suitable method in the context of design of robotic systems [66, 138] but lacks of performances and tractability when coming to simulation and control. A thorough comparison of the two approaches has been reported by Theodore and Ghosal in [140]. In particular, they recommend the assumed modes model formulation for discretization of manipulator links with uniform cross-sectional geometries and single-link manipulators, whereas the finite elements formulation is recommended for complex cross-sectional geometries and for multilink manipulators. It must be pointed out that AMM is usually adopted in the case of simple geometries where global shape functions can be analytically computed, while FEM formulation is usually not feasible for any real time or control application, as the cardinality of the state variables dramatically increases in the case of complex geometries.

Assuming that the modes shapes are time-invariant, formulation of the shape functions does not necessarily enter in the motion equations of the manipulator. In fact, once suitable boundary conditions have been imposed (see in particular [35,140] for the AMM and [58] for the FEM), and the shape functions have been completely defined, they need to be evaluated at the tip of the links only, while the spatial dependence is resolved by integration over the spatial domain of the links, introducing a number of constant parameters characterizing the mechanical properties. In turn, solid modelling packages for finite element analisys (FEA) can be conveniently used for the off-line computation of the above-mentioned parameters, particularly in the case of complex geometries, performing also an orthonormalization of mode shapes [96], which is of great importance for model simplification. Without using such tools, the analysis is almost always limited to the adoption of the Euler-

Bernoulli or Timoshenko beam model for the flexible links [17, 78, 114, 116, 140, 157].

In this thesis, the latter approach has been followed, thus the model reduction feature provided by several FE commercial codes has been exploited. In fact, most commercial FEA packages [2, 30, 95] can reduce the huge number of nodal coordinates to a much smaller number of modal coordinates (two or three in the case of robotic manipulators, according to [140]). This task is usually carried out by means of the classical Craig-Bampton method [28] or other recently proposed methods [73, 77, 100], and the flexible body parameters are stored either in ASCII or binary files after the analysis. Subsequently, the data describing the flexible link can be used to build the dynamic model of the manipulator.

1.2 Approaches to dynamic modelling

Different schemes for modelling of the flexible manipulators' dynamics have been proposed in literature, the equations of motion of the manipulator can be obtained by means of the Euler-Lagrange or the Newton-Euler approach. In the first case the mathematical model is derived from energy principles following the same conceptual scheme adopted for rigid manipulators, but differently from the simple rigid systems, a potential energy is stored by virtue of the deflections of the links, as well as kinetic energy is expressed by means of links' deflection rate. The Lagrange-Euler formulation results in a symbolic, closed form, dynamic model of the manipulator, and it is best suited for study of dynamic properties and analysis of control schemes. Several examples of dynamic models of manipulators that use a Lagrangian approach can be found in literature[1] for single link [21, 56, 57, 98], two-links [105, 143] and multilink [34, 35, 128]. However, in the Euler-Lagrange approach the model of the manipulator is obtained as a whole, in closed form, by means of the symbolic computation of the derivatives of potential and kinetic energies. This can be considered as an obstacle for the development of a modular model with respect to the number of links. Moreover, to the knowledge of the author, there is no result in literature which describes a complete computation of the Coriolis and centripetal terms of the inertia forces for the elastic degrees of freedom of a three dimensional body in the Lagrangian approach.

On the contrary of the Lagrange-Euler formulation, in the Newton-Euler formulation the motion equations are outlined separately for each (floating) link and formalized on the D'Alambert's principle. The forward propagation of the kinematic quantities, common to the Lagrange-Euler approach, is followed by a backward propagation of forces/torques from the tip to the base, and by a projection of the joint constraint forces on the axes of motion. Several examples of single link [112], two-links [53, 103] and multilink [18, 70]

[1] The list of examples cited here is not exaustive, see [123] for a complete rieview

manipulators' models can be found in literature, however, the Newton-Euler formulation is usually adopted in multibody system dynamic analysis, where components representing the objects are connected in order to form complex mechanisms. In this context the Newton-Euler formulation is more suitable to a modular approach with respect to the Lagrangian formulation. The Newton-Euler approach is also generally preferred [71] for implementation of real-time, model-based control schemes, because of its computational efficiency. The computational procedure described above is generally computed with a recursive approach [63,69,156].

In this thesis, the dynamic model of the manipulator is obtained by means of the Newton-Euler approach and the adoption of the spatial vector notation [43, 44, 50]. Differently from all the other formulations based on the Newton-Euler equations, the model is here obtained in closed form with respect to the joint angles and the global vector of elastic coordinates, furthermore the inertia matrix and the nonlinear quadratic velocity terms are explicitly computed in the same context. The model input data are given by the number of links' modal coordinates, the inertia invariants, the structural stiffness matrices, the shape function matrices relevant to the links' connectors, and the undeformed relative positions between connectors. It must be pointed out that the computation of a closed form model for three-dimensional manipulators with multiple links of general shape is a totally new result in the field of flexible manipulators' modelling.

1.3 Choice of the coordinates system

The choice of the coordinates system for the description of the flexible manipulators' links configurations represents a more difficult problem with respect to the rigid robots, in the latter case, given the vector of joint state angles and derivatives, the kinematic configuration of the manipulator is known. Conversely, in the first case the finite set of state variables describing the deformation can be expressed in terms of relative nodal displacements and infinitesimal rotations with respect to the undeformed configuration or in terms of absolute coordinates. The first approach is the most widely adopted in the field of flexible manipulators and multibody dynamics [60, 108, 109, 113, 150] and it known as Floating Frame of Reference formulation (FFR), thoroughly described in [124]. In the FFR formulation, each body is attached to a moving frame of reference undergoing large (rigid) motion, while the (small) elastic displacements are obtained in local coordinates with respect to the reference frame. It must be pointed out that the inertia terms of the equations of motion are highly nonlinear in the FFR formulation. Conversely, in the case of large deformation problems, an approach based on the adoption of absolute coordinates for the flexible state variables can be effective. This formulation is known as Absolute Nodal Coordinate Formulation (ANCF) [124,124,125]. The ANCF, adopting absolute

displacements and global slopes as nodal coordinates, results in a constant mass matrix, zero centripetal ad Coriolis inertia forces, and highly nonlinear elastic terms, even in the case of linear elastic behaviour. An interesting comparison between the two approaches can be found in [97].

On the other hand, in order to model large deformations within the FFR formulation, it is possible to subdivide a body into several flexible components or *substructures*, adopting for each substructure a FFR formulation [151]. Using this approach (or *substructuring* method), it is usually necessary to formulate the substructure compatibility constraints, to be imposed at the substructures interfaces, explicitly. For the sake of completeness it must be mentioned that, as recently pointed out by Heckmann [58], the substructuring method is a technique to find a specific solution for a specific problem but it is not systemically supported as the ANCF formulation, and requires skilled modelers (in particular, using more substructures does not necessarily improve the accuracy of the solution).

In this thesis, an approach based on the FFR formulation has been adopted, as the flexible dynamical behaviour of the manipulators considered in this context can be confined to the case of small deflections. Anyway it will be shown how to adopt substructuring in order to cope with the issues related to high flexibility.

1.4 Control design

Plentiful work has been carried out in the literature investigating the control of flexible manipulators [14,117], particularly on the single-link robots, where the dynamics is not geometry-dependent and hence linear. Furthermore, the task of controlling a flexible robot turns out to be tough when coming to multi-link manipulator, because of the spatial configuration dependency of the dynamics. The control problems of a flexible robotic arm can be classified in four main objectives, listed here in increasing order of difficulty [14]:

- End effector positioning problems
- Rest to rest end effector motion in fixed time
- Trajectory tracking in the joint space
- Trajectory tracking in the operational space (end-effector trajectory tracking)

The classical positioning problem, which can be recap in the first and second objectives described above, is the easiest and the first developed approach [80, 101, 120]. A linear feedback together with a constant feedforward action has been shown to asymptotically stabilize the system [36] when some structural damping is present. Conversely, if the passive damping is not present, a classical linear control based on the linearisation of the manipulator's dynamics around the desired final position can be designed [133, 134].

As far as rest to rest motion is concerned, the problem has been investigated by several researchers [15,20,93,152]. A remarkable result consists in a feed-forward approach for both single link and multilink manipulators, developed in [31].

When coming to tracking problems, which concern the third and fourth task listed above, a nonlinear control strategy that takes into account the complex coupling between the flexible dynamics of the links and the motion of the manipulator is required. On the other hand, the tip trajectory tracking is considered the toughest control problem for flexible manipulators as the non-colocated relation between the torque input and the tip position give rise to unstable zero dynamic, thus a direct inversion of the dynamics would lead to closed loop internal instability. Due to the great interest on this topic, a great amount of approaches can be found in literature ranging from the applications of colocated and non colocated PD regulators [36, 74, 75, 120, 148], computed torque methods [24, 32, 33] based on the input/output linearization, adaptive control [9, 153] based on lagrangian dynamics, sliding mode control [23], or even neural network based algorithms [64, 84]. Moreover, several results have been obtained in the field of robust and optimal control [3, 10, 67, 91, 132, 144] which has been widely used in literature due to the guaranteed robustness and stability properties of the system with respect to unmodeled dynamics. Nevertheless, the problem of synthesizing a robust controller for such a complex family of systems is not trivial, on top of that, the results found in literature are highly tailored on the specific problem at hand, usually represented by a single link or two links manipulators. An additional approach that deserves to be mentioned, exploits the natural two-time scale nature of the dynamics of flexible manipulators. This mathod has been initially developed by means of the singular perturbation approach [128] and further developed in the context of the integral manifold approach [92, 129, 136, 155]. In this cases, two different controllers are used, a "*slow*" controller tracks the desired trajectory while a "*fast*" controller stabilizes the flexible dynamics. This approach yields a substantial reduction of the design complexity at the expense of an approximate tracking. In this work the integral manifold approach has been followed together with an innovative approach based on constrained robust control. The closed-form model has been adapted in the context of the integral manifold, leading to a control-oriented model of the flexible manipulator. This model is constituted by two interacting subsystems loperating in two different time scales. Finally, two independent controllers have been computed, the synthesis of the "*slow*" controller follows an approach based on the method described in [128], while the "*fast*" controller exploits a new result in the field of robust control based on a non smooth and non convex optimization of the controller with respect to a mixed H_2/H_∞ cost function and subject to structural contraints, thoroughly described in [6, 7].

1.5 Chapters summary

Chapter 2 describes the development of the equations of motion for the generic flexible body model, the formulation is based on the Newton-Euler equations and relies on the calculation of nine *inertia invariants* which can be computed by means of a FE preprocessing stage. The described formulation is based on the FFR approach and includes the full computation of the Coriolis and centripetal terms of the inertial forces which constitutes a fresh result with respect to literature. The model is then implemented in an object-oriented framework and validated with respect to literature benchmarks.
Chapter 3 introduces the three dimensional model of flexible manipulator. The model is obtained in closed form with respect to the joint angles and the modal elastic variables and is based on the aggregation of the models of the single links by means of the spatial vector notation. Further extensions of the model are presented which account for links with high flexibility and for the presence of payloads. In order to validate the model, some simulations are shown where the manipulator's model is compared against benchmarks from literature and against a dataset obtained by means of an experimental platform.
Chapter 4 describes the derivation of a control-oriented, approximated model, based on the previously developed closed-form. A brief description of the adopted integral manifold approach is initially performed, then, the formal derivation of the approximated model is carried out and the computational procedure, which yields the derivation of two approximated subsystems is shown. Finally, the approximation is validated with respect to literature benchmarks and the aforementioned experimental platform, and the differences with the complete closed-form model are discueesd.
Chapter 5 finally discusses an approach to the control of flexible manipulators based on the approximated model developed in Chapter 4. An approach based on the classical robust control is initially described and applied. Subsequently, due to poor performances in the controller performances, a novel approach based on the optimization of the robust controller, subject to additional structural and performances constraints is applied. The obtained results demonstrate the effectiveness of the proposed approach.

Chapter 2

Object oriented model of general flexible body

The first step related to the development of a flexible manipulator model is constituted by the realization of a reliable model for the generic flexible body. In this chapter the construction and testing of the aforementioned model will be described. The model is based on the FFR approach introduced in Chapter 1 and on the Newton-Euler formulation of the motion equations, extensively described in [124]. The model has been developed in the context of an and object-oriented framework. The motivation of this choice follows the last trends in the modeling of manipulators and, more generally, of mechatronic systems. In these contexts the *modular* and *acausal* approach are gaining relevance both in academic and industrial environments [47] as they provide effective tools in order to master the complexity of large cyber-physical models by means of the component modelling paradigm. Whenever a modular approach is adopted, the modelling effort is focused on the development of the equations of the single component, and system-level model organization is managed by means of the definition of standard component interfaces. The object-oriented framework is the natural choice in order to tackle this complexity.

It must be pointed out that the work illustrated in this chapter constitutes the base for the results described in the following chapters on one hand, but on the other hand it can be considered as an independent research result, being the first example of generic object-oriented body model fully described in terms of its equations and code. The developed model constitutes a step forward in terms of generality with respect to the state of the art due to the capability of representing bodies of general shape. The data describing the body are retrieved from a finite element preprocessing stage, allowing the shape and material of the body to be arbitrary. The FE preprocessing stage is extensively described in Appendix [48].

2.1 Object oriented flexible multibody - State of the art

Object-oriented modelling techniques and tools have started emerging at the end of the 70's (e.g., ASCEND [110], OMOLA [86], gPROMS [102], MOSES [81]). As a main result of this research, some specific paradigms have been stated [118] and implemented in the Modelica language [139], and some modelling and simulation environments have been designed, both commercial (Dymola [29], MathModelica [85], SimulationX [42]) and open-source (OpenModelica [51]). Coming to the specific case of multibody systems, and sticking to the Modelica language, although the presented ideas are more general, the adoption of a fully modular approach requires the description of the dynamics of every single body in terms of *local* variables, while the interaction between different bodies has to be described using the *connectors* of the standard Modelica multibody library [104]. A connector is associated with a reference frame, so that a connection is equivalent to a rigid junction of the two connector frames. The connector assumes the cut force and torque as *flow* variables [118], while the *effort* variables are given by the position of the origin of the connector frame with respect to the world frame and by an *orientation object*[1], describing the relative orientation between the world frame and the connector frame. The local description of the body's dynamics which is a peculiar characteristic of the Modelica paradigm naturally calls for the FFR approach, previously described. There exist two Modelica libraries able to process the output of FE codes and produce a flexible body model compatible with the Modelica Multibody Standard Library. The first has been developed by the German Aerospace Center (DLR) [59] and distributed by Modelon AB., the other is distributed by Claytex Services Ltd. The DLR FlexibleBodies library simply provides two Modelica classes (models): one for the beam model (`Beam`) and one for general flexible bodies exported from FE codes (`ModalBody`). The results of the FE analysis performed by several general purpose codes (Abaqus [30], Ansys [2], MSC.Nastran [95]) are first processed by another commercial code: FEMBS, distributed by SIMPACK AG [131], performing modal reduction in a two-step process. Guyan or Craig-Bampton reduction methods are applied in the first step to keep the flexible body input file to FEMBS small, while in the second reduction step the modes of interest (i.e. in the frequency range of interest) for multi-body simulation are selected. The reduced modal representation is then stored in a Standard Input Data (SID) file [122, 147], an object-oriented data structure developed to define a standard format to exchange data between FE and MBS codes. When a `ModalBody` class is instantiated the user has just to specify the name of the

[1] The internal representation of the orientation (i.e., the parametrization of the relative rotation matrix) in the Modelica multibody library is completely masked to the user. In addition to that, the orientation object is endowed with methods to compute rotation matrices and angular velocities, to rotate vectors, etc., so that knowledge about the actual description form of orientation is not necessary.

SID file containing the modal description of the body.

The Claytex library directly generates the Modelica model of a flexible body from the output of the model reduction process performed by three FE codes: namely Nastran, Genesis and Abaqus. It must be pointed out that none of the aforementioned libraries is open-source, hence there is no way to inspect the code and understand which dynamic terms are considered, particularly no description of the Coriolis and gyroscopic terms of the inertial forces are provided.However, the correct description of these terms (provided here) can be crucial in applications where high angular speeds are considered. Moreover, the DLR FlexibleBodies library requires the use of an external commercial code, namely FEMBS, in order to produce the Modelica model while the model described here is completely open-source and freely available.

With reference to the fundamental step of FE model reduction, in addition to classical techniques, such as the modal truncation [27] or the component mode synthesis [28], several other techniques have been recently investigated [45, 46], taking into account specific criteria, such as computability for large scale systems, stability preservation, quality of the reduced order model, model error evaluation, model tuning in a given frequency range, and more. For example, reduction methods based on Krylov subspaces, singular value decomposition (SVD), Gramian matrices, proper orthogonal decomposition (POD) have been considered and implemented in the software package Morembs [100], which gives the user a tool for selecting several model order reduction techniques.

2.2 Motion equations of the flexible body

2.2.1 Kinematics

To start the treatise, it is convenient to recall the generalized Newton-Euler equations for a generic unconstrained flexible body, formulated with respect to a local reference frame rigidly attached to the body itself [121, 124] and, based on that, to introduce the inertia invariants, assuming a continuous mass distribution.

The position (in local coordinates) of a point on a flexible body, see Fig. 2.1, is given by:

$$\bar{\mathbf{u}} = \bar{\mathbf{u}}_0 + \bar{\mathbf{u}}_f \ ,$$

where $\bar{\mathbf{u}}_0$ is the "undeformed" (i.e., rigid) position vector and $\bar{\mathbf{u}}_f$ is the deformation contribution to position (i.e., the deformation field).

If small elastic deflections are considered, the infinite dimensional deformation field on the body can be approximated by a functional basis space with finite dimension, say M, so that the vector $\bar{\mathbf{u}}_f$ can be expressed by the finite dimensional product

$$\bar{\mathbf{u}}_f = \mathbf{S}\mathbf{q} \tag{2.1}$$

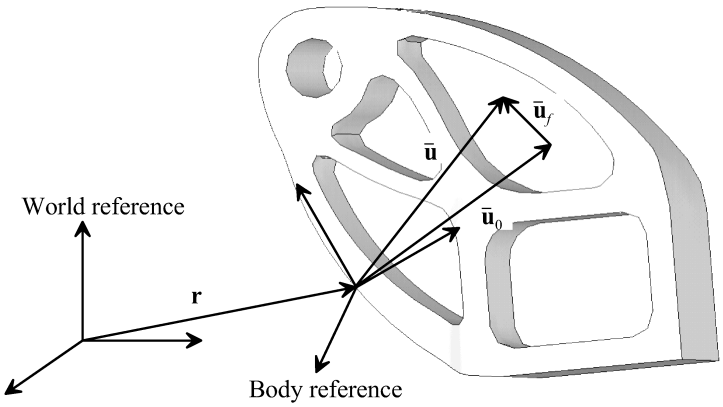

Figure 2.1: Floating reference system

where $\mathbf{S}$ is the $[3 \times M]$ shape functions matrix (i.e., a matrix of functions defined over the body domain and used as a basis to describe the deformation field of the body itself) and $\mathbf{q}$ is the M-dimensional vector of deformation degrees of freedom.

The position of a point on a deformable body can then be expressed in world reference as

$$\mathbf{p} = \mathbf{r} + \mathbf{A}\bar{\mathbf{u}} = \mathbf{r} + \mathbf{A}\bar{\mathbf{u}}_0 + \mathbf{A}\mathbf{S}\mathbf{q} \ ,$$

where $\mathbf{r}$ is the vector identifying the origin of the body local reference system and $\mathbf{A}$ is the rotation matrix for the body reference system.

The representation of a generic flexible body in world reference requires then $6+M$ d.o.f. (6 corresponding to rigid displacements and rotations and M to the deformation field), i.e.,

$$\mathbf{q} = \left[\begin{array}{ccc} \mathbf{r}^T & \theta^T & \mathbf{q}^T \end{array} \right]^T \ ,$$

where θ represents the undeformed body orientation angles.

2.2.2 Dynamics

The motion equations for a generic flexible body, expressed in the local reference frame, can be developed applying the principle of virtual work [90, 118], yielding

$$\left[\begin{array}{ccc} m\mathbf{I}_3 & m\tilde{\bar{\mathbf{d}}}_C^T & \bar{\mathbf{C}}_t^T \\ m\tilde{\bar{\mathbf{d}}}_C & \bar{\mathbf{J}} & \bar{\mathbf{C}}_r^T \\ \bar{\mathbf{C}}_t & \bar{\mathbf{C}}_r & \mathbf{M}_e \end{array} \right] \left[\begin{array}{c} \ddot{\mathbf{r}} - \bar{\mathbf{g}} \\ \dot{\bar{\omega}} \\ \ddot{\mathbf{q}} \end{array} \right] = \left[\begin{array}{c} \mathbf{0}_3 \\ \mathbf{0}_3 \\ -\mathbf{K}_e\mathbf{q} - \mathbf{D}_e\dot{\mathbf{q}} \end{array} \right] + \left[\begin{array}{c} \mathbf{h}_\omega^r \\ \mathbf{h}_\omega^\theta \\ \mathbf{h}_\omega^f \end{array} \right] + \left[\begin{array}{c} \mathbf{h}_e^r \\ \mathbf{h}_e^\theta \\ \mathbf{h}_e^f \end{array} \right] \ , \tag{2.2}$$

where $\ddot{\mathbf{r}}$, $\dot{\bar{\omega}}$, $\ddot{\mathbf{q}}$ are the linear, angular and deformation accelerations respectively expressed in the local reference frame, $\bar{\mathbf{g}}$ is the gravity acceleration, $\mathbf{I}_3$ is the 3×3 identity matrix, $\mathbf{M}_e$, $\mathbf{D}_e$, $\mathbf{K}_e$ are the structural mass, damping

and stiffness matrix respectively, $\mathbf{h}^r_\omega$, $\mathbf{h}^\theta_\omega$, $\mathbf{h}^f_\omega$ are the vectors of gyroscopic and centripetal terms and $\mathbf{h}^r_e$, $\mathbf{h}^\theta_e$, $\mathbf{h}^f_e$ are the vectors of external forces, applied at the body connectors (recall the discussion in Section 1).

The terms in the generalized mass matrix depend on some inertia invariants, which in turn depend on the shape functions and on the body mass distribution[2] The dependency of the terms of the mass matrix with respect of the invariants is the following, recalling that $\mathbf{S} = \left[\begin{array}{cccc} \mathbf{s}_1 & \mathbf{s}_2 & \dots & \mathbf{s}_M \end{array}\right]$:

$$
\begin{aligned}
m &= \int_V \rho \, \mathrm{d}V = I^1 \ , && (2.3)\\
m\tilde{\bar{\mathbf{d}}}_C &= \int_V \rho\tilde{\bar{\mathbf{u}}} \, \mathrm{d}V = \int_V \rho\tilde{\bar{\mathbf{u}}}_0 \, \mathrm{d}V + \int_V \rho\widetilde{(\mathbf{Sq})} \, \mathrm{d}V \\
&= \int_V \rho\tilde{\bar{\mathbf{u}}}_0 \, \mathrm{d}V + \sum_{i=1}^{M} \left(\int_V \rho\tilde{\mathbf{s}}_i \, \mathrm{d}V \right) q_i = \tilde{\mathbf{I}}^2 + \sum_{i=1}^{M} \tilde{\mathbf{I}}^3_i q_i \ , && (2.4)\\
\bar{\mathbf{C}}^T_t &= \int_V \rho\mathbf{S} \, \mathrm{d}V = \int_V \rho \left[\begin{array}{cccc} \mathbf{s}_1 & \mathbf{s}_2 & \dots & \mathbf{s}_M \end{array}\right] \mathrm{d}V \\
&= \left[\begin{array}{cccc} \mathbf{I}^3_1 & \mathbf{I}^3_2 & \dots & \mathbf{I}^3_M \end{array}\right], && (2.5)\\
\bar{\mathbf{C}}^T_r &= \int_V \rho\tilde{\bar{\mathbf{u}}}\mathbf{S} \, \mathrm{d}V = \int_V \rho\tilde{\bar{\mathbf{u}}}_0\mathbf{S} \, \mathrm{d}V + \int_V \rho\widetilde{(\mathbf{Sq})}\mathbf{S} \, \mathrm{d}V \\
&= \int_V \rho\tilde{\bar{\mathbf{u}}}_0\mathbf{S} \, \mathrm{d}V + \sum_{i=1}^{M} \left(\int_V \rho\tilde{\mathbf{s}}_i\mathbf{S} \, \mathrm{d}V \right) q_i = \mathbf{I}^4 + \sum_{i=1}^{M} \mathbf{I}^5_i q_i, && (2.6)\\
\mathbf{M}_e &= \int_V \rho\mathbf{S}^T\mathbf{S} \, \mathrm{d}V = \mathbf{I}^6, && (2.7)\\
\bar{\mathbf{J}} &= \int_V \rho\tilde{\bar{\mathbf{u}}}^T\tilde{\bar{\mathbf{u}}} \, \mathrm{d}V = \int_V \rho\tilde{\bar{\mathbf{u}}}^T_0\tilde{\bar{\mathbf{u}}}_0 \, \mathrm{d}V + \int_V \rho\tilde{\bar{\mathbf{u}}}^T_0\widetilde{(\mathbf{Sq})} \, \mathrm{d}V \\
&\quad + \int_V \rho\widetilde{(\mathbf{Sq})}^T\tilde{\bar{\mathbf{u}}}_0 \, \mathrm{d}V + \int_V \rho\widetilde{(\mathbf{Sq})}^T\widetilde{(\mathbf{Sq})} \, \mathrm{d}V \\
&= \int_V \rho\tilde{\bar{\mathbf{u}}}^T_0\tilde{\bar{\mathbf{u}}}_0 \, \mathrm{d}V - \sum_{i=1}^{M} \left(\int_V \rho\tilde{\mathbf{s}}_i\tilde{\bar{\mathbf{u}}}_0 \, \mathrm{d}V \right) q_i \\
&\quad - \sum_{i=1}^{M} \left(\int_V \rho\tilde{\bar{\mathbf{u}}}_0\tilde{\mathbf{s}}_i \, \mathrm{d}V \right) q_i - \sum_{i=1}^{M}\sum_{j=1}^{M} \left(\int_V \rho\tilde{\mathbf{s}}_i\tilde{\mathbf{s}}_j \, \mathrm{d}V \right) q_i q_j \\
&= \mathbf{I}^7 - \sum_{i=1}^{M} \left(\mathbf{I}^{8T}_i + \mathbf{I}^8_i \right) q_i - \sum_{i=1}^{M}\sum_{j=1}^{M} \mathbf{I}^9_{ij} q_i q_j && (2.8)
\end{aligned}
$$

Where $\tilde{\mathbf{v}}$ is the skew-symmetric matrix associated to vector $\mathbf{v}$.

[2] The kinematic quantities carrying a *bar* like "$\bar{\mathbf{r}}ar$" are referred to the FFR, while the same quantities without the *bar* are referred to the world reference frame

2.2.3 The gyroscopic and centripetal terms

The vectors of gyroscopic and centripetal terms relevant to the rigid degrees of freedom are given by

$$\mathbf{h}_\omega^r = -\bar{\boldsymbol{\omega}} \times \bar{\boldsymbol{\omega}} \times m\bar{\mathbf{d}}_C - 2\bar{\boldsymbol{\omega}} \times \bar{\mathbf{C}}_t^T \dot{\mathbf{q}} \ , \tag{2.9}$$

$$\mathbf{h}_\omega^\theta = -\bar{\boldsymbol{\omega}} \times \bar{\mathbf{J}}\bar{\boldsymbol{\omega}} - \dot{\bar{\mathbf{J}}}\bar{\boldsymbol{\omega}} - \bar{\boldsymbol{\omega}} \times \bar{\mathbf{C}}_r^T \dot{\mathbf{q}} \ , \tag{2.10}$$

where

$$\dot{\bar{\mathbf{J}}} = -\sum_{i=1}^{M} \left(\mathbf{I}_i^{8T} + \mathbf{I}_i^8 \right) \dot{q}_i - \sum_{i=1}^{M} \sum_{j=1}^{M} \mathbf{I}_{ij}^9 (\dot{q}_i q_j + q_i \dot{q}_j), \tag{2.11}$$

The computation of the vector relevant to the elastic degrees of freedom is much more involved and requires the definition of two more inertia invariants. The equations required to calculate the aforementioned terms are reported here, while the full computation and proof are reported in Appendix A

The final formula of the vector is:

$$\begin{aligned} \mathbf{h}_\omega^f = & \begin{bmatrix} \bar{\omega}_1 \left(\sum_{i=1}^3 \mathbf{d}_{ii} \right) - \bar{\boldsymbol{\omega}}^T \mathbf{D}_1 \\ \bar{\omega}_2 \left(\sum_{i=1}^3 \mathbf{d}_{ii} \right) - \bar{\boldsymbol{\omega}}^T \mathbf{D}_2 \\ \bar{\omega}_3 \left(\sum_{i=1}^3 \mathbf{d}_{ii} \right) - \bar{\boldsymbol{\omega}}^T \mathbf{D}_3 \end{bmatrix}^T \bar{\boldsymbol{\omega}} \\ & -2 \left[\bar{\omega}_1 \left(\mathbf{I}_{32}^{11} - \mathbf{I}_{23}^{11} \right) + \bar{\omega}_2 \left(\mathbf{I}_{13}^{11} - \mathbf{I}_{31}^{11} \right) + \bar{\omega}_3 \left(\mathbf{I}_{21}^{11} - \mathbf{I}_{12}^{11} \right) \right] \dot{\mathbf{q}} \ , \end{aligned} \tag{2.12}$$

Starting from the definition:

$$\begin{aligned} \mathbf{h}_\omega^f &= -\int_V \rho \mathbf{S}^T \tilde{\bar{\boldsymbol{\omega}}}^2 \bar{\mathbf{u}} \ \mathrm{d}V - 2 \int_V \rho \mathbf{S}^T \ \tilde{\bar{\boldsymbol{\omega}}} \mathbf{S} \dot{\mathbf{q}} \ \mathrm{d}V \\ &= \left(\int_V \rho \left[-\widetilde{(\bar{\boldsymbol{\omega}} \times \bar{\mathbf{u}})} \mathbf{S} \right]^T \ \mathrm{d}V \right) \bar{\boldsymbol{\omega}} - 2 \left(\int_V \rho \mathbf{S}^T \tilde{\bar{\boldsymbol{\omega}}} \mathbf{S} \mathrm{d}V \right) \dot{\mathbf{q}}, \end{aligned} \tag{2.13}$$

and defining $\mathbf{S}^T = \begin{bmatrix} \hat{\mathbf{s}}_1^T & \hat{\mathbf{s}}_2^T & \hat{\mathbf{s}}_3^T \end{bmatrix}$ one obtains

$$\begin{aligned} \mathbf{h}_\omega^f = & \left(\int_V \rho \begin{bmatrix} \bar{\omega}_1 \bar{\mathbf{u}}^T \mathbf{S} - \bar{\boldsymbol{\omega}}^T \bar{u}_1 \mathbf{S} \\ \bar{\omega}_2 \bar{\mathbf{u}}^T \mathbf{S} - \bar{\boldsymbol{\omega}}^T \bar{u}_2 \mathbf{S} \\ \bar{\omega}_3 \bar{\mathbf{u}}^T \mathbf{S} - \bar{\boldsymbol{\omega}}^T \bar{u}_3 \mathbf{S} \end{bmatrix}^T \ \mathrm{d}V \right) \bar{\boldsymbol{\omega}} \\ & -2 \left(\bar{\omega}_1 \int_V \rho \left(\hat{\mathbf{s}}_3^T \hat{\mathbf{s}}_2 - \hat{\mathbf{s}}_2^T \hat{\mathbf{s}}_3 \right) \ \mathrm{d}V \right) \dot{\mathbf{q}} \\ & -2 \left(\bar{\omega}_2 \int_V \rho \left(\hat{\mathbf{s}}_1^T \hat{\mathbf{s}}_3 - \hat{\mathbf{s}}_3^T \hat{\mathbf{s}}_1 \right) \ \mathrm{d}V \right) \dot{\mathbf{q}} \\ & -2 \left(\bar{\omega}_3 \int_V \rho \left(\hat{\mathbf{s}}_2^T \hat{\mathbf{s}}_1 - \hat{\mathbf{s}}_1^T \hat{\mathbf{s}}_2 \right) \ \mathrm{d}V \right) \dot{\mathbf{q}}, \end{aligned} \tag{2.14}$$

which yields (2.12), by defining

$$\mathbf{D}_i = \begin{bmatrix} \mathbf{d}_{i1} \\ \mathbf{d}_{i2} \\ \mathbf{d}_{i3} \end{bmatrix} = \int_V \rho \bar{\mathbf{u}}_i \mathbf{S} \ \mathrm{d}V \ , \quad \mathbf{I}_{ij}^{11} = \int_V \rho \hat{\mathbf{s}}_i^T \hat{\mathbf{s}}_j \ \mathrm{d}V \quad i,j = 1,2,3 \tag{2.15}$$

In turn, matrix $\mathbf{D}_i$ is given by:

$$\begin{aligned}
\mathbf{D}_i &= \int_V \rho \bar{\mathbf{u}}_i \mathbf{S}\, \mathrm{d}V = \int_V \rho \left(\bar{\mathbf{u}}_0 + \mathbf{S}\mathbf{q}\right)_i \mathbf{S}\, \mathrm{d}V \\
&= \int_V \rho \bar{\mathbf{u}}_{0i} \mathbf{S}\, \mathrm{d}V + \int_V \rho \left(\mathbf{S}\mathbf{q}\right)_i \mathbf{S}\, \mathrm{d}V = \begin{bmatrix} \mathbf{I}_{i1}^{10} \\ \mathbf{I}_{i2}^{10} \\ \mathbf{I}_{i3}^{10} \end{bmatrix} + \int_V \rho \hat{\mathbf{s}}_i \mathbf{q} \mathbf{S}\, \mathrm{d}V \\
&= \begin{bmatrix} \mathbf{I}_{i1}^{10} \\ \mathbf{I}_{i2}^{10} \\ \mathbf{I}_{i3}^{10} \end{bmatrix} + \int_V \rho \mathbf{q}^T \hat{\mathbf{s}}_i^T \mathbf{S}\, \mathrm{d}V \\
&= \begin{bmatrix} \mathbf{I}_{i1}^{10} \\ \mathbf{I}_{i2}^{10} \\ \mathbf{I}_{i3}^{10} \end{bmatrix} + \begin{bmatrix} \mathbf{q}^T \mathbf{I}_{i1}^{11} \\ \mathbf{q}^T \mathbf{I}_{i2}^{11} \\ \mathbf{q}^T \mathbf{I}_{i3}^{11} \end{bmatrix} \quad i = 1, 2, 3,
\end{aligned} \tag{2.16}$$

where $(\mathbf{v})_i$ is the i-th element of vector $\mathbf{v}$ and

$$\begin{bmatrix} \mathbf{I}_{i1}^{10} \\ \mathbf{I}_{i2}^{10} \\ \mathbf{I}_{i3}^{10} \end{bmatrix} = \int_V \rho \bar{\mathbf{u}}_{0i} \mathbf{S}\, \mathrm{d}V \quad i = 1, 2, 3, \tag{2.17}$$

Invariants $\mathbf{I}_{ij}^{10}$ and $\mathbf{I}_{ij}^{11}$ may be however computed from invariants $\mathbf{I}_i^8$ and $\mathbf{I}_{ij}^9$ in fact, recalling that

$$\begin{aligned}
\mathbf{I}_i^8 &= \int_V \rho \begin{bmatrix} -\bar{u}_{03} s_{3i} - \bar{u}_{02} s_{2i} & \bar{u}_{02} s_{1i} & \bar{u}_{03} s_{1i} \\ \bar{u}_{01} s_{2i} & -\bar{u}_{03} s_{3i} - \bar{u}_{01} s_{1i} & \bar{u}_{03} s_{2i} \\ \bar{u}_{01} s_{3i} & \bar{u}_{02} s_{3i} & -\bar{u}_{02} s_{2i} - \bar{u}_{01} s_{1i} \end{bmatrix} \mathrm{d}V, \\
\mathbf{I}_{ij}^9 &= \int_V \rho \begin{bmatrix} -s_{3i} s_{3j} - s_{2i} s_{2j} & s_{2i} s_{1j} & s_{3i} s_{1j} \\ s_{1i} s_{2j} & -s_{3i} s_{3j} - s_{1i} s_{1j} & s_{3i} s_{2j} \\ s_{1i} s_{3j} & s_{2i} s_{3j} & -s_{2i} s_{2j} - s_{1i} s_{1j} \end{bmatrix} \mathrm{d}V,
\end{aligned}$$

one obtains

$$\left(\mathbf{I}_{ij}^{10}\right)_k = \begin{cases} \left(\mathbf{I}_k^8\right)_{ji} & i \neq j = 1, 2, 3 \quad k = 1, \ldots, M \\ \frac{1}{2}\left[\left(\mathbf{I}_k^8\right)_{ii} - \left(\mathbf{I}_k^8\right)_{ll} - \left(\mathbf{I}_k^8\right)_{mm}\right] & \begin{matrix} i = j = 1, 2, 3 \\ l, m = 1, 2, 3 \end{matrix} \quad k = 1, \ldots, M \end{cases}$$

$$\left(\mathbf{I}_{ij}^{11}\right)_{kl} = \begin{cases} \left(\mathbf{I}_{kl}^9\right)_{ji} & i \neq j = 1, 2, 3 \quad k, l = 1, \ldots, M \\ \frac{1}{2}\left[\left(\mathbf{I}_{kl}^9\right)_{ii} - \left(\mathbf{I}_{kl}^9\right)_{mm} - \left(\mathbf{I}_{kl}^9\right)_{nn}\right] & \begin{matrix} i = j = 1, 2, 3 \\ m, n = 1, 2, 3 \end{matrix} \quad k, l = 1, \ldots, M \end{cases}$$

Matrix $\mathbf{D}_e$, modeling the dissipative properties of the material, is defined as $\mathbf{D}_e = \alpha \mathbf{M}_e + \beta \mathbf{K}_e$, where α and β are the so-called Rayleigh damping coefficients.

2.2.4 External forces

Assuming N_c connectors attached to a flexible body the vectors of external forces are given by

$$\mathbf{h}_e^r = \sum_{i=1}^{N_c} \bar{\mathbf{f}}_i, \tag{2.18}$$

$$\mathbf{h}_e^\theta = \sum_{i=1}^{N_c} \left(\bar{\tau}_i + \tilde{\bar{\mathbf{l}}}_i \bar{\mathbf{f}}_i \right) , \tag{2.19}$$

$$\mathbf{h}_e^f = \sum_{i=1}^{N_c} \left(\mathbf{S}_i^T \bar{\mathbf{f}}_i + \hat{\mathbf{S}}_i^T \bar{\tau}_i \right) , \tag{2.20}$$

where $\bar{\mathbf{f}}_i$ and $\bar{\tau}_i$ are the forces and torques acting at the connector frames projected on the local reference frame, $\bar{\mathbf{l}}_i$ is the position vector from the origin of the local body reference frame to the origin of the connector frame, $\mathbf{S}_i$ and $\hat{\mathbf{S}}_i$ are the slices of the modal matrix corresponding to the translational and rotational d.o.f. of connectors. Note that

$$\bar{\mathbf{l}}_i = \bar{\mathbf{u}}_{0i} + \mathbf{S}_i \mathbf{q}, \tag{2.21}$$

with $\bar{\mathbf{u}}_{0i}$ being the undeformed position of the i-th connector.

In order to project the forces and torques acting at the connector frames on the local reference frame, *small* rotations of the connectors due to body deformation must be taken into account. These small rotations can be still obtained by a modal superposition as

$$\theta_i = \begin{bmatrix} \theta_{i1} \\ \theta_{i2} \\ \theta_{i3} \end{bmatrix} = \hat{\mathbf{S}}_i \mathbf{q} , \tag{2.22}$$

so that the rotation matrix between the deformed and the undeformed connector orientation can be defined as

$$\hat{\mathbf{A}}_i = \mathbf{I}_3 + \tilde{\theta}_i = \begin{bmatrix} 1 & -\theta_{i3} & \theta_{i2} \\ \theta_{i3} & 1 & -\theta_{i1} \\ -\theta_{i2} & \theta_{i1} & 1 \end{bmatrix} , \tag{2.23}$$

Therefore, if $\bar{\mathbf{A}}_i$ is the (constant) rotation matrix between the connector frame and the local frame in the undeformed configuration, the projection of the force $\mathbf{f}_i$ and the torque τ_i acting at the connector frame i is given by:

$$\bar{\mathbf{f}}_i = \hat{\mathbf{A}}_i \bar{\mathbf{A}}_i \mathbf{f}_i, \tag{2.24}$$

$$\bar{\tau}_i = \hat{\mathbf{A}}_i \bar{\mathbf{A}}_i \tau_i, \tag{2.25}$$

To cope with the connector structure it is also necessary to compute the kinematic quantities $\mathbf{A}_i$ and $\mathbf{p}_i$ relevant to each connector, thus the rotation

Table 2.1: Flexible body data

M	Number of deformation d.o.f.
$I^1, \mathbf{I}^2, \mathbf{I}^3_i, \mathbf{I}^4, \mathbf{I}^5_i, \mathbf{I}^6, \mathbf{I}^7, \mathbf{I}^8_i, \mathbf{I}^9_{ij}, \mathbf{I}^{10}_{ij}, \mathbf{I}^{11}_{ij}$	Inertia invariants
$\mathbf{D}_e, \mathbf{K}_e$	Structural damping and stiffness matrix
N_c	Number of connectors
$\mathbf{S}_i, \hat{\mathbf{S}}_i$	Slices of the modal matrix of connectors d.o.f.
$\bar{\mathbf{u}}_{0i}, \bar{\mathbf{A}}_i$	Undeformed position and orientation of connectors

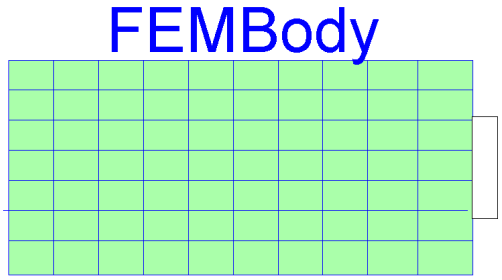

Figure 2.2: Modelica model of a general flexible body

matrix between the frame connector and the world reference frame and the position of the origin of the connector frame with respect to the world frame. This leads to

$$\mathbf{A}_i = \mathbf{A}\hat{\mathbf{A}}_i\bar{\mathbf{A}}_i, \tag{2.26}$$

$$\mathbf{p}_i = \mathbf{r} + \mathbf{A}\bar{\mathbf{l}}_i, \tag{2.27}$$

As a result, the set of data describing a flexible body can be summarized as in Table 2.1.

2.3 Structure of the Modelica model

The Modelica model of a general flexible body (Fig. 2.2) is characterized by an array of N_c multibody connectors, while the data in Table 2.1 have been suitably collected in the Modelica record `BodyData`. The record is defined as `replaceable`:

```
replaceable parameter FEMData.BodyData data;
```

so that it is possible, by exploiting the features of the Modelica language, to assign a different data record to each FEMBody instance, by simply replacing the record in the model declaration, as in

```
FEMBody FlexPendulum(redeclare FEMData.PendulumData data,
        alpha=1,
        beta=0.5,
        d=1);
```

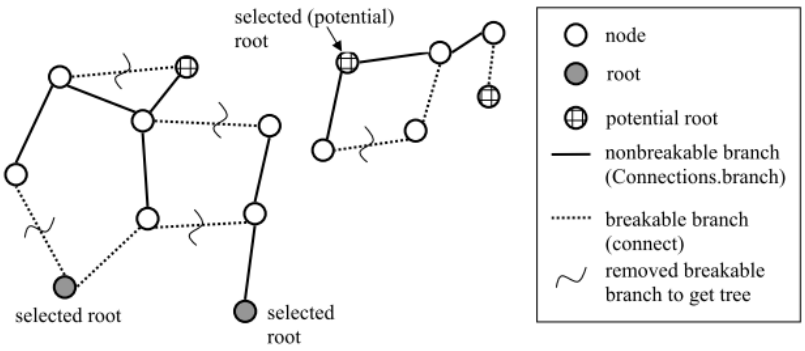

Figure 2.3: Example of virtual connection graph

where `alpha`, `beta`, `d` are the parameters defining the damping matrix $\mathbf{D}_e$.

An important question arises when considering the state variables introduced by the model. The standard Modelica multibody library [104] defines a *virtual connection graph* (2.3) in order to handle overdetermined differential-algebraic equations (DAE) systems, generated by connections among models. When a model is a component of a tree structure, thus directly or indirectly connected to a *root*, its kinematic variables are calculated as algebraic functions of some state variables, corresponding to another node of the tree. In the opposite case, 12 state variables and a root node, attached to a connector, must be introduced in order to describe the body orientation and position.

It must be pointed out that, when dealing with rigid bodies, the spatial relation between connectors is purely algebraic, thus any connector can become a root, since said algebraic relations can be inverted by the symbolic manipulator. On the other hand, in the FFR approach, every quantity of the flexible body is referred to the body reference frame, say `FFR`, without necessarily having a connector attached; it is then natural to define the frame `FFR` as a root. Otherwise, the quantities $\bar{\mathbf{r}}$, $\dot{\bar{\mathbf{r}}}$, $\ddot{\bar{\mathbf{r}}}$, $\mathbf{A}$, $\bar{\omega}$, $\dot{\bar{\omega}}$ are obtained from one of the body connectors, according to eqs. (2.26,2.27).

The spatial relationships among frame `FFR` and connector frames are however more involved with respect to the rigid body case, due to the presence of elastic d.o.f., hence, for the sake of efficiency it is necessary to find out which connector belongs to the tree path, say connector `A` (`rooted(A.R)=true`), and to explicitly reverse the equations relevant to that connector. Thus, the kinematic quantities of the frame `FFR` are explicitly defined from the kinematic quantities of frame `A` and, in turn, the kinematic quantities of all other connectors are defined from the kinematic quantities of frame `FFR`.

2.4 Validation of the model

Being focused on a general object-oriented formulation of flexible multibody systems, this paper adopts the classical modal approach, based on the model reduction performed by several packages in order to interface the results of the FEM modelling with ADAMS [96]. As a result of the model reduction step, most of the data reported in Table 2.1 are stored in a binary Modal Neutral File (`.mnf`), in turn converted into an ASCII file (`.mtx`). The inertia invariants $\mathbf{I}_{ij}^{10}$ and $\mathbf{I}_{ij}^{11}$ however, are not stored in the `.mnf` and `.mtx` files, so they are computed by two Modelica functions according to eqs. (2.18) and (2.18), when the `BodyData` record is instantiated, i.e.,

```
parameter Real inv10[3,3,M] = FEMPackage.calcInv10(M,inv8);
parameter Real inv11[3,3,M,M] = FEMPackage.calcInv11(M,inv9);
```

In this work, the FEM models have been created with Abaqus [30], which is endowed with a specific tool for the generation of the `.mnf` file. The procedure [99] consists of two steps, in the first a modal eigenvalues analysis must be performed, in the second the modal reduction process is carried out, inertia invariants are calculated and the `.mnf` file containing the relevant data is created.

As far as the choice of the boundary conditions is concerned, it must be pointed out that it largely depends on the problem at hand. In this respect, a comprehensive survey is reported in [58] where, in the case of chain and tree-structured multibody systems, it is suggested to align the boundary conditions with the local d.o.f. of the connecting joints.

To generate the ASCII file containing the Modelica `BodyData` record, a parsing software tool has been built. The only data required to define the Modelica model, and not stored in the `.mtx` file, are the number and the spatial layout of the connector frames on the body. Accordingly, the parsing tool ask the user to specify an input list representing the FEM nodes in which Modelica connectors must be placed.

Several different numerical examples have been considered, so as to thoroughly test and validate the body model. Particular care has been taken in the choice of the aforementioned examples as all of them has been found in literature. In the opinion of the author the comparison with experiments and simulation carried out by other researchers is a fundamental step of validation. In the following subsections the most significant test cases are briefly reported, comparing the results obtained with an analytical flexible beam model previously developed in Modelica, whose description can be found in [118]. It must be pointed out that both the analytical model and the literature benchmarks are limited to a planar deformation field while the model here presented is characterized by a three-dimensional field, hence the examples here presented must be considered for validation purposes but the model has been used in further simulations where 3D flexibility is crucial [48]

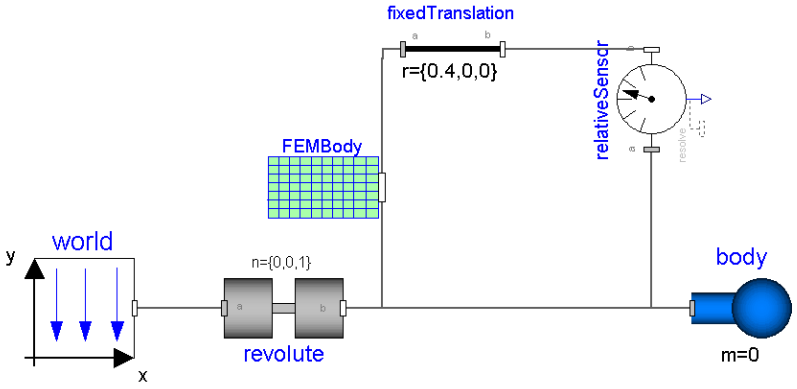

Figure 2.4: Modelica model of the flexible pendulum.

All simulations have been performed on a workstation equipped with an Intel Xeon 4Ghz and 2Gb RAM processor, and the CPU simulation times have been reported. However, it must be pointed out that the CPU time varies largely, depending on the damping ratio, the numerical solver and the numerical tolerance.

2.4.1 Flexible pendulum

The first benchmark example is taken from [41], where a flexible rod swings under the action of gravity.

The Modelica model of the system is sketched in Fig. 2.4: the flexible body is connected to the world reference frame through a revolute joint and to a massless body on the opposite tip. In order to observe the tip deflection a `RelativeSensor` component has been used.

While in the case of the analytical beam model the FFR is always placed in one of the beam ends (referring to Fig. 2.4 it is attached to the joint connector), in the case of a model derived by numerical modal reduction the FFR corresponds to the global coordinate system adopted in the FE solid modelling step.

The rod has a length $L = 0.4$ m, a cross sectional area $A = 0.0018$ m^2 and a density $\rho = 5540$ kg/m^3. Differently from [41], in FEM-based models it is not possible to assign the second moment of area arbitrarily, as it is indirectly calculated in the FEM preprocessing stage. In order to mantain the same body data used in [41] the quantity $E \times J$ (second moment of area $\times$ Young's modulus) was kept coherent with [41], assuming a round section for the rod ($J = \pi r^4/4$ m^4). The FEM beam model has been therefore created with Abaqus, characterized by 20 nodes and 20 `B31` one-dimensional elements. Then, after the frequency and substructuring analysis steps, a number of 15 eigenmodes was retained.

The DASSL integration algorithm was adopted, with a tolerance of $1 \times$

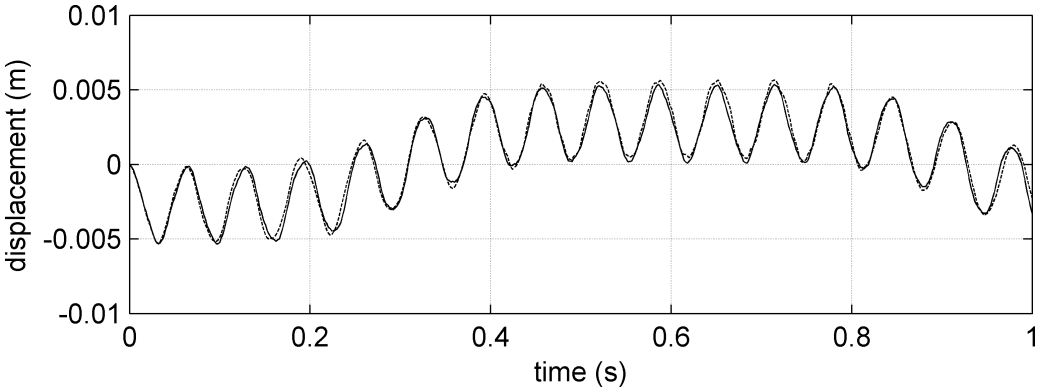

Figure 2.5: Flexible pendulum tip displacement. Solid line: FEM model, dashed line: analytical model.

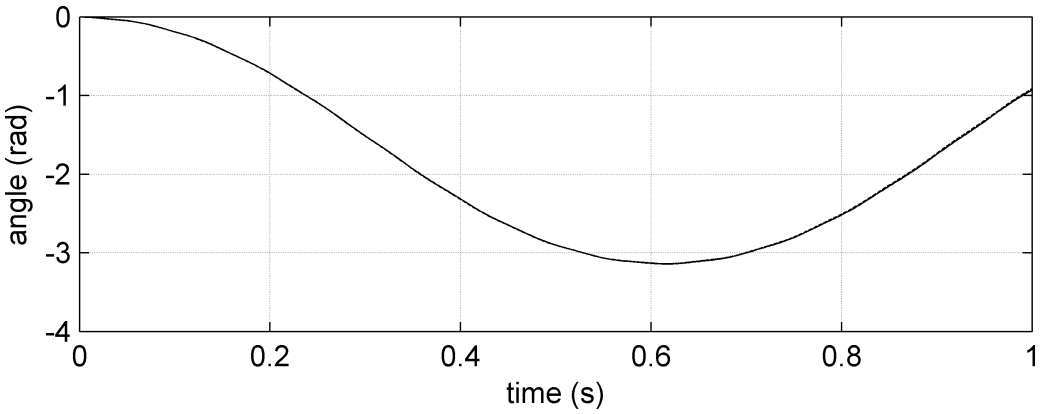

Figure 2.6: Flexible pendulum swing angle. Solid line: FEM model, dashed line: analytical model.

10^{-6}, and the simulation required 0.062 s of CPU time. The results were compared with those obtained in [49], where the same beam was modeled analytically, in this case the simulation required 0.032 s of CPU time. Figure 2.5 shows the translational displacement of the pendulum tip in the motion direction, namely the distance between the tip of the flexible beam and the tip of a rigid beam, while Fig. 2.6 shows the swing angle, namely the relative orientation between the connector frames at both ends of the flexible beam in the plane of motion. As it is apparent, the results obtained with the FEM model (solid line) are in good accordance with the analytic one (dashed line) and with the experiment reported in [41].

2.4.2 Elastic slider crank mechanism

The elastic slider-crank mechanism is one of the most widely used benchmark for flexible multibody systems simulation, and involves a closed chain [22,54, 87]. In this respect, here the same simulation experiment considered in [41]

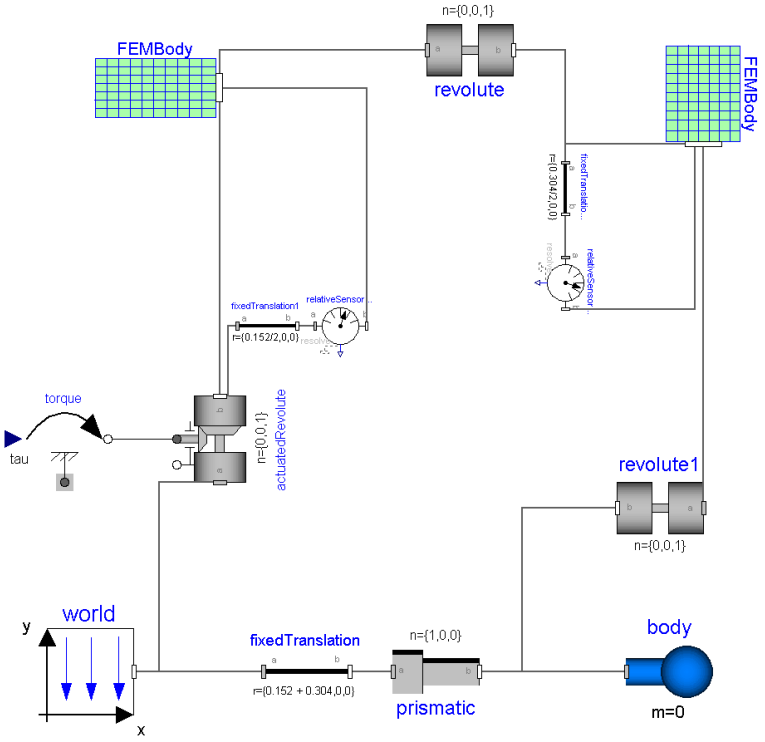

Figure 2.7: The slider-crank simulation scheme.

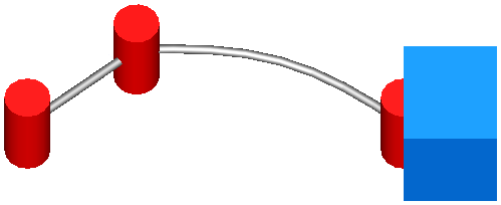

Figure 2.8: The elastic slider-crank model.

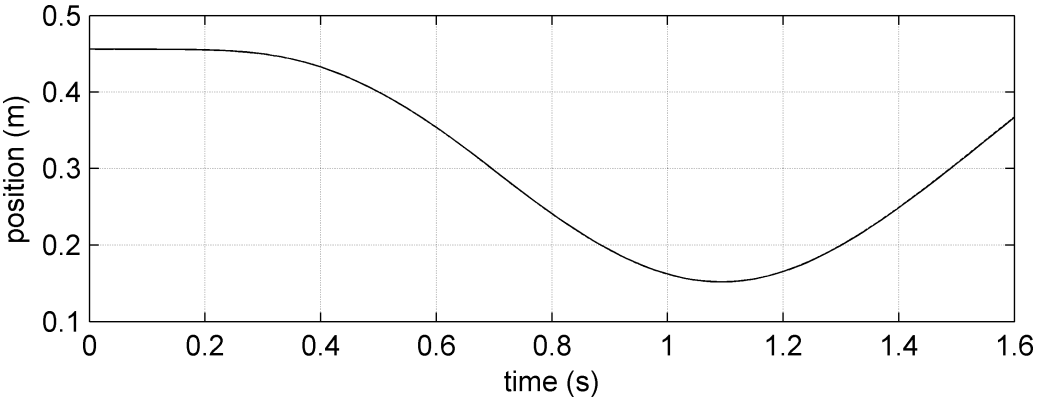

Figure 2.9: Position of the slider block. Solid line: FEM model, dashed line: analytical model.

and [49] has been performed. The Modelica model, composed by a flexible crankshaft, a flexible rod and a rigid massless slider block, connected with frictionless revolute and prismatic joints, is shown in Figs. 2.7 and 2.8.

A round section beam was considered for the rod, with a length $L = 0.304$ m, a cross sectional radius $r = 0.005$ m, and a density $\rho = 2767$ kg/m^3. The second moment of area was $J = 4.909 \times 10^{-10}$ m^4, calculated as in Section 2.4.1, with the aim of keeping the quantity $E \times J$ consistent with [41] and [49]; the elasticity modulus E was set to 1×10^9 N/m^2. The FEM rod model was computed as a beam containing 30 `B31` nodes, and 15 eigenmodes were retained.

The crankshaft was characterized by the same physical parameters of the rod but the length, which was $L = 0.152$ m, and the elasticity modulus: $E = 5 \times 10^7$ N/m^2; the FEM model was made by 15 `B31` elements, and 10 eigenmodes were retained.

In accordance with [41] and [49], a simulation time of 1.6 seconds was assumed, while driving the crankshaft with the following torque:

$$\tau = \begin{cases} M(t) = 0.01(1 - e^{-t/0.167}), & t \leq 0.7 \text{ s} \\ 0, & t > 0.7 \text{ s} \end{cases} \tag{2.28}$$

The simulation was performed with a RADAU algorithm and a tolerance of 10^{-6} and the simulation CPU time was 28.42 s, while the simulation of the analytic beam model required a CPU time of 21.14 s. Figures 2.9 and 2.10 compare again the results obtained with both analytical (dashed line) and FEM (solid line) beam model, which are also in good accordance with [41].

2.4.3 The spin-up manouver

The classical FFR formulation adopted here is based on a linear strain-displacement relationship in the definition of the elastic potential energy. This approach leads to efficient simulations and small number of elastic

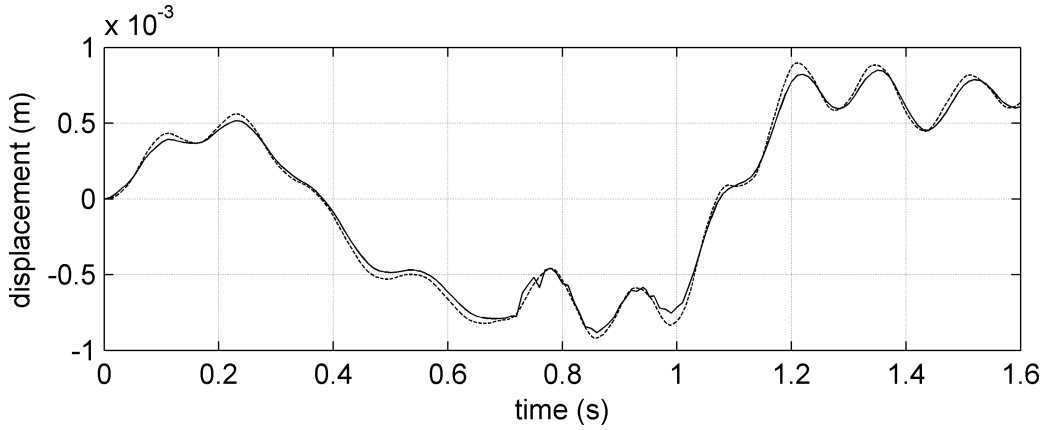

Figure 2.10: Displacement of the rod's middle point. Solid line: FEM model, dashed line: analytical model.

coordinates but lacks of accuracy when the deformation field is inherently nonlinear (large deformations) and higher order terms in the strain energy must be taken into account. Typical examples of this phenomenon are the elicopter and wind turbine blades where the bodies are subject to great deformations due to loads, but also the cases of beams subject to axial loads is of interest. This effect is referred to in literature as *geometrical stiffening*. Thorough treatise can be found in [16, 88, 107, 126]

Among the various methods proposed in the literature to account for the geometrical stiffening [16, 88, 151] the easiest one is the application of the *substructuring* technique [151], dividing a flexible body into smaller rigidly connected substructures, each one described by a local FFR. In this way, although each substructure is characterized by small deformations, the whole assembled structure can represent very large deformations. One of the main advantages of this approch is that the models based on the FFR formulation can be used by rigidly connecting them, on the other hand the number of state variables grealty increases with the number of substructures and some effects like axial deformation due to bending are still not reproduced. Several methods other then substructuring have been proposed in literature, based on the inertial coordinates representation, but this family of methods produce models that are heavily dependent on the geometry and whose description is not possible in terms of the local coordinates. The classical spin-up manoeuver problem, another frequently used benchmark in flexible multibody simulation in order to point out geometrical stiffening [126, 127, 145], is here considered. A flexible beam rotates about an axis passing through one of its ends, according to the following law [126]:

$$\theta(t) = \begin{cases} \frac{\Omega}{T}\left[\frac{t^2}{2} + (\frac{T}{2\pi})^2(\cos(\frac{2\pi t}{T}) - 1)\right], & t < T \\ \Omega(t - T/2), & t \geq T \end{cases} \tag{2.29}$$

thus, the spin-up manoeuver starts at $t = 0$ and ends at $t = T$, reaching a

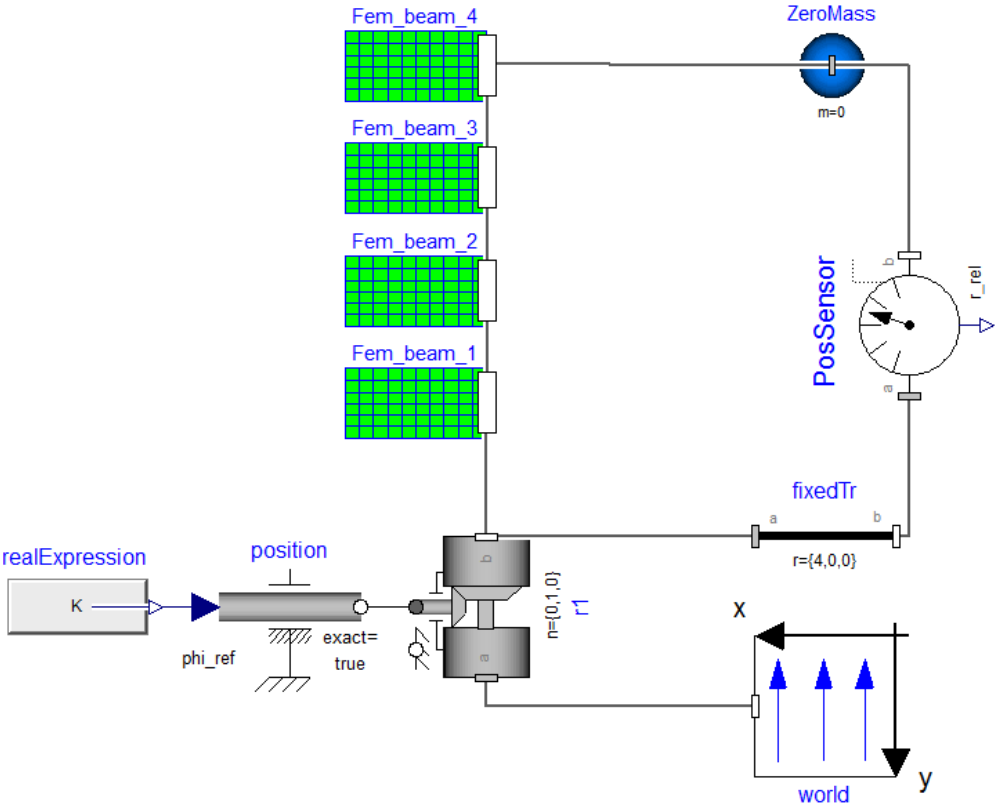

Figure 2.11: Beam substructuring.

constant angular velocity Ω.

It is worth noticing that the analytical model considers a planar deformation field, while the FEM model considers a 3D deformation field. As such, in order to compare the results obtained with both models, in a first simulation experiment gravity was not considered. The following data were assumed for the beam: length $L = 8$ m, cross sectional area $A = 7.299 \times 10^{-5}$ m^2 and density $\rho = 2767$ kg/m^3. As in the other experiments the product $E \times J$ was kept coherent, so the following value was assumed for modulus of elasticity $E = 1.3359 \times 10^{12}$ N/m^2.

Three different simulation experiments were performed, corresponding to the target angular velocities of $\Omega = 2$ rad/s, $\Omega = 4$ rad/s and $\Omega = 10$ rad/s and the deflection of the tip, namely the difference between the tips of a rigid and a flexible beam in the plane of motion, was recorded [126]. In the case of $\Omega = 2$ rad/s and $\Omega = 4$ rad/s the FEM beam model was substructured in 4 elements (Fig. 2.11), each one with a length $L = 2$ m and consisting of 20 `B31` nodes, 15 eigenmodes were retained, while in the case of $\Omega = 10$ the beam was substructured in 8 elements, each one with a length $L = 1$ m.

Figure 2.12 shows a comparison between the results obtained with the analytic beam model (dashed line) and the FEM model (solid line), as it

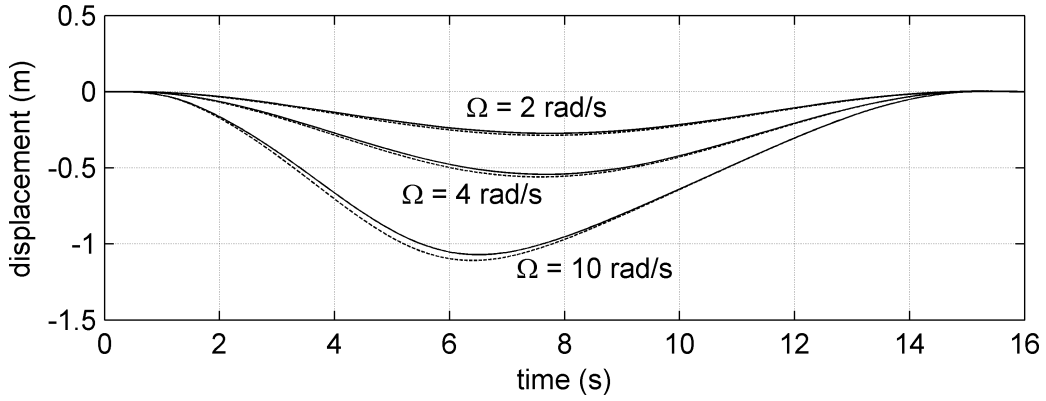

Figure 2.12: Tip deflection in spin up manouver at different angular velocities. Solid line: FEM model, dashed line: analytical model.

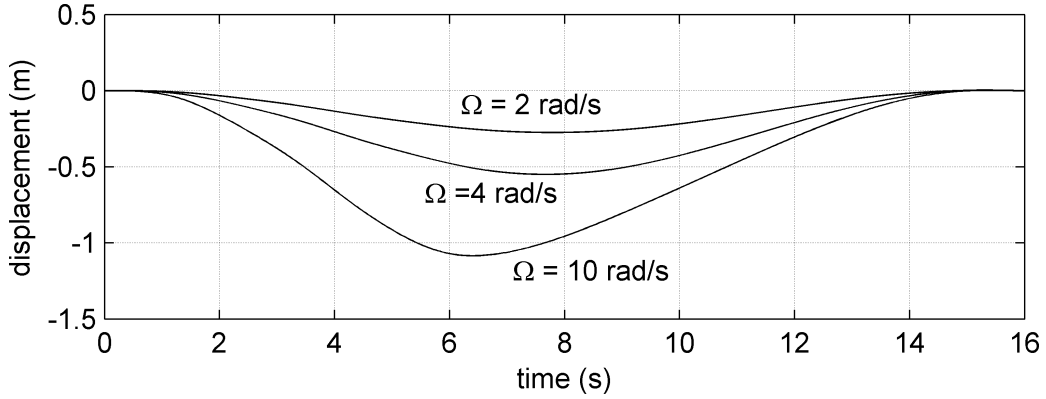

Figure 2.13: Tip deflection in the plane of motion with gravity at different angular velocities.

is apparent, a good agreement was obtained. The simulations based on the analytic beam model took 0.22 s of CPU time for $\Omega = 2$ rad/s and $\Omega = 4$ rad/s, 0.40 s for $\Omega = 10$ rad/s, while the simulations based on the FEM model took 2.06, s 2.65 s, and 3.71 s respectively.

In a second set of simulation experiments, gravity was added along the negative y-axis, retaining the model data of the previous simulations. As shown in Fig. 2.13, the deflection of the beam tip in the plane of motion is de facto unchanged. On the other hand, the displacement along the y-axis (Fig. 2.14) showed the 3D effects of centripetal terms, raising up the tip of the beam. The CPU time requested in these simulation experiments resulted longer, namely 6.59 s, 7.64 s and 10.03 s for $\Omega = 2$ rad/s, $\Omega = 4$ rad/s and $\Omega = 10$ rad/s respectively.

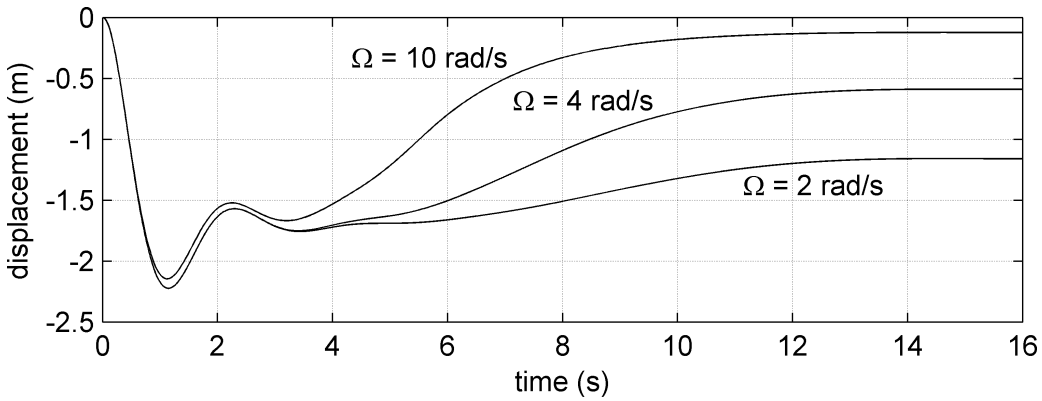

Figure 2.14: Tip deflection along y axis with gravity at different angular velocities.

Chapter 3

Closed form Newton-Euler of flexible manipulators

In this chapter one of the main results of the thesis is described. A dynamic model of flexible manipulators, based on the Newton-Euler approach and on the adoption of the spatial vector notation [43,44,50], is developed. A similar approach has been also adopted in [18], while in [1] a recursive formulation is obtained, in which the Newton-Euler motion equations are derived for links and joints in terms of position and orientation of the FFR. In [76] a $O(n)$ mass matrix inversion method using Lie derivatives has been also proposed. The model is obtained in closed form with respect to the joint angles and the global vector of elastic coordinates, furthermore the inertia matrix and the nonlinear quadratic velocity terms are explicitly computed in the same context.

The model is based on the generic body model described in Chapter 2, hence the input data (namely the inertia invariants) can be analytically computed according to either AMM or FEM formulation or, in case of complex geometries, can be extracted as the output of a finite element preprocessing stage. The ability to extract the data from FE models leads to a greatly pliable models, in fact it is possible to account for links of general shape and material.

The closed form Newton-Euler dynamic model of flexible manipulators is then validated by comparing a simulation obtained with a Matlab implementation against the multibody approach in a classical example often proposed in literature. A further simulation is carried out in order to compare the model against experimental results provided by the MERIt dataset. The MERIt project [83], developed by the Technische Universität Dortmund, which the author would primarily like to thank, makes freely available a set of measurement data carried out by the TUDOR experimental flexible robot.

Notwithstanding the original aim of MERIt is the identification of manipulator's dynamics, in the context of this work a subset of the experi-

Table 3.1: Link data

M_i	Number of modal coordinates
$I_i^1, \boldsymbol{I}_i^2, \boldsymbol{I}_{j,i}^3, \boldsymbol{I}_i^4, \boldsymbol{I}_{j,i}^5, \boldsymbol{I}_i^6, \boldsymbol{I}_i^7, \boldsymbol{I}_{j,i}^8, \boldsymbol{I}_{jk,i}^9$	Inertia invariants
$\boldsymbol{K}_{e,i}$	Structural stiffness matrix
$\boldsymbol{S}_i, \hat{\boldsymbol{S}}_i$	Shape functions matrices
$\bar{\boldsymbol{u}}_{0i}$	Undeformed relative position between FFRs
$\hat{\boldsymbol{z}}'_{i-1}$	Joint rotation axis

ments provided by the dataset has been reproduced by means of the Matlab/Simulink simulation environment, and results have been compared with the measurements, with the aim of validating the closed form model.

3.1 Equations of motion of the flexible manipulator

The dynamic model of the flexible manipulator will be derived in the following closed form:

$$\boldsymbol{\mathcal{M}}_{\theta\theta}(\boldsymbol{\theta},\boldsymbol{q})\ddot{\boldsymbol{\theta}} + \boldsymbol{\mathcal{M}}_{\theta q}(\boldsymbol{\theta},\boldsymbol{q})\ddot{\boldsymbol{q}} + \boldsymbol{\mathcal{C}}_{\theta}(\boldsymbol{\theta},\boldsymbol{q},\dot{\boldsymbol{\theta}},\dot{\boldsymbol{q}}) = \boldsymbol{\tau}, \tag{3.1}$$

$$\boldsymbol{\mathcal{M}}_{\theta q}^T(\boldsymbol{\theta},\boldsymbol{q})\ddot{\boldsymbol{\theta}} + \boldsymbol{\mathcal{M}}_{qq}(\boldsymbol{\theta},\boldsymbol{q})\ddot{\boldsymbol{q}} + \boldsymbol{\mathcal{D}}_e\dot{\boldsymbol{q}} + \boldsymbol{\mathcal{K}}_e\boldsymbol{q} + \boldsymbol{\mathcal{C}}_{\boldsymbol{q}}(\boldsymbol{\theta},\boldsymbol{q},\dot{\boldsymbol{\theta}},\dot{\boldsymbol{q}}) = \boldsymbol{0}, \tag{3.2}$$

where $\boldsymbol{\theta} = \text{col}\{\theta_i\} \in \mathbb{R}^N$, $\boldsymbol{q} = \text{col}\{\boldsymbol{q}_i\} \in \mathbb{R}^M$, $\boldsymbol{\tau} = \text{col}\{\tau_i\} \in \mathbb{R}^N$, and θ_i, $\boldsymbol{q}_i$, τ_i, are the joint angles, the M_i-dimensional vector of modal coordinates of link i and the joint torques respectively. Furthermore $M = \sum_{i=1}^N M_i$. Thus, all matrices and vectors in eqs. (3.1,3.2) will be directly computed starting from link data, summarized in Table 3.1.

3.1.1 Kinematics

Let the local FFR attached to link i be $\{O_i, \boldsymbol{x}_i, \boldsymbol{y}_i, \boldsymbol{z}_i\}$, as shown by Fig. 3.1), and let $\{O'_i, \boldsymbol{x}'_i, \boldsymbol{y}'_i, \boldsymbol{z}'_i\}$ be another local reference frame, having the same orientation of the FFR frame in the undeformed configuration and with the origin O'_i coinciding with the origin O_{i+1} of the FFR of the next link in the chain. The angle θ_i is the coordinate of the joint connecting link i to link $i-1$, while $\hat{\boldsymbol{z}}'_{i-1}$ is the axis of rotation in the frame $\{O'_{i-1}, \boldsymbol{x}'_{i-1}, \boldsymbol{y}'_{i-1}, \boldsymbol{z}'_{i-1}\}$.

Remark 1. Some of the definitions given in this Chapter have alredy been given in Chapter 2, the author believes that for the sake of clarity and cleraness of the tractation some redundancy can be suitable.

Remark 2. The notation adopted to describe the undeformed configuration is redundant with respect to the notations usually adopted in robotics, i.e., the Denavit-Hartenberg notation [37]. However, it is compliant with the description of bodies in FEM packages and with the notation adopted in Chapter 2, which is necessary to describe distributed flexibility in case of complex geometries of links.

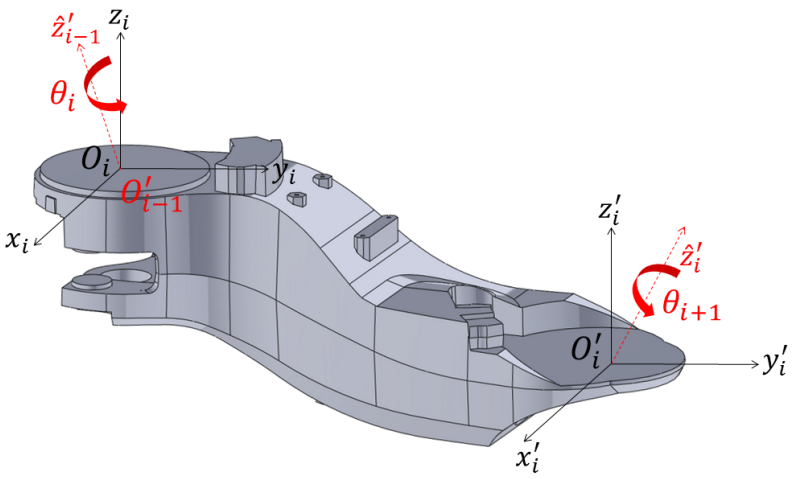

Figure 3.1: Reference frames.

If small elastic deflections are considered, the infinite dimensional deformation field on the body can be approximated by a functional basis space with finite dimension, say M_i, so that the position $\boldsymbol{p}_{i+1}$ of the origin O_{i+1} of the $(i+1)$-th frame with respect to the world reference frame is given by:

$$\boldsymbol{p}_{i+1} = \boldsymbol{p}_i + \boldsymbol{p}_{i+1,i} \ , \tag{3.3}$$

$$\boldsymbol{p}_{i+1,i} = \boldsymbol{A}_i \bar{\boldsymbol{u}}_i = \boldsymbol{A}_i \bar{\boldsymbol{u}}_{0,i} + \boldsymbol{A}_i \boldsymbol{S}_i \boldsymbol{q}_i \ , \tag{3.4}$$

where $\boldsymbol{A}_i$ is the (3×3) rotation matrix relating the FFR and the world reference frame, $\bar{\boldsymbol{u}}_{0,i}$ is the position vector relating the two frames in the undeformed configuration[1], $\boldsymbol{S}_i$ is the $[3 \times M_i]$ shape function matrix (i.e., a matrix of functions defined over the body domain and used as a basis to describe the deformation field of the body itself) and $\boldsymbol{q}_i$ is the M_i-dimensional vector of modal coordinates. Accordingly, the relation between the linear accelerations of the two frames, for $i = 1, \ldots, (N-1)$, is given by:

$$\dot{\boldsymbol{v}}_{i+1} = \dot{\boldsymbol{v}}_i - \tilde{\boldsymbol{p}}_{i+1,i} \dot{\boldsymbol{\omega}}_i + \boldsymbol{A}_i \boldsymbol{S}_i \ddot{\boldsymbol{q}}_i + \dot{\boldsymbol{v}}'_{i+1} \ , \tag{3.5}$$

$$\dot{\boldsymbol{v}}'_{i+1} = \boldsymbol{\omega}_i \times (\boldsymbol{\omega}_i \times \boldsymbol{p}_{i+1,i} + \boldsymbol{A}_i \boldsymbol{S}_i \dot{\boldsymbol{q}}_i) \ , \tag{3.6}$$

where $\tilde{\boldsymbol{p}}$ is the skew-symmetric matrix associated to vector $\boldsymbol{p}$. For $i = 0$, instead, it is:

$$\dot{\boldsymbol{v}}_1 = \dot{\boldsymbol{v}}'_1 \ , \tag{3.7}$$

$$\dot{\boldsymbol{v}}'_1 = -\boldsymbol{g} \ , \tag{3.8}$$

where $\boldsymbol{g}$ is the gravity acceleration in the world frame. In this way it is possible to easily account for gravitational terms in the motion equations.

[1] The bar above a vector indicates that the vector is expressed with reference to the local FFR.

The rotation matrix $\boldsymbol{A}_{i+1}$ of the $(i+1)$-th frame with respect to the world frame is in turn related to the rotation matrix $\boldsymbol{A}_i$ as follows:

$$\boldsymbol{A}_{i+1} = \boldsymbol{A}_i \hat{\boldsymbol{A}}_i \bar{\boldsymbol{A}}_i \ , \tag{3.9}$$

$$\hat{\boldsymbol{A}}_i = \boldsymbol{U} + \widetilde{\left(\hat{\boldsymbol{S}}_i \boldsymbol{q}_i\right)} \ , \tag{3.10}$$

$$\bar{\boldsymbol{A}}_i = \bar{\boldsymbol{A}}_i(\hat{\boldsymbol{z}}'_i, \theta_{i+1}) \ , \tag{3.11}$$

where $\boldsymbol{U}$ is the 3×3 identity matrix, and matrix $\hat{\boldsymbol{A}}_i$ defines *small* rotations of the frame $\{O'_i, \boldsymbol{x}'_i, \boldsymbol{y}'_i, \boldsymbol{z}'_i\}$ with respect to the FFR due to body deformation, obtained by a modal superposition through the $[3 \times M_i]$ shape function matrix $\hat{\boldsymbol{S}}_i$, while matrix $\bar{\boldsymbol{A}}_i$ defines a rotation of the frame $\{O_i, \boldsymbol{x}_{i+1}, \boldsymbol{y}_{i+1}, \boldsymbol{z}_{i+1}\}$ of an angle θ_{i+1} about an axis defined in the frame $\{O'_i, \boldsymbol{x}'_i, \boldsymbol{y}'_i, \boldsymbol{z}'_i\}$ by the constant unit vector $\hat{\boldsymbol{z}}'_i$.

The angular velocity and acceleration of the $(i+1)$-th frame, for $i = 1, \ldots, (N-1)$, are therefore given by:

$$\boldsymbol{\omega}_{i+1} = \boldsymbol{\omega}_i + \boldsymbol{A}_i \hat{\boldsymbol{S}}_i \dot{\boldsymbol{q}}_i + \boldsymbol{A}_i \hat{\boldsymbol{A}}_i \hat{\boldsymbol{z}}'_i \dot{\theta}_{i+1} \ , \tag{3.12}$$

$$\dot{\boldsymbol{\omega}}_{i+1} = \dot{\boldsymbol{\omega}}_i + \boldsymbol{A}_i \hat{\boldsymbol{A}}_i \hat{\boldsymbol{z}}'_i \ddot{\theta}_{i+1} + \boldsymbol{A}_i \hat{\boldsymbol{S}}_i \ddot{\boldsymbol{q}}_i + \dot{\boldsymbol{\omega}}'_{i+1} \ , \tag{3.13}$$

$$\dot{\boldsymbol{\omega}}'_{i+1} = \boldsymbol{\omega}_i \times \left(\boldsymbol{A}_i \hat{\boldsymbol{S}}_i \dot{\boldsymbol{q}}_i + \boldsymbol{A}_i \hat{\boldsymbol{A}}_i \hat{\boldsymbol{z}}'_i \dot{\theta}_{i+1}\right) + \boldsymbol{A}_i \widetilde{\left(\hat{\boldsymbol{S}}_i \dot{\boldsymbol{q}}_i\right)} \hat{\boldsymbol{z}}'_i \dot{\theta}_{i+1} \ , \tag{3.14}$$

while for $i = 0$,

$$\boldsymbol{\omega}_1 = \boldsymbol{A}_0 \hat{\boldsymbol{A}}_0 \hat{\boldsymbol{z}}'_0 \dot{\theta}_1 \quad (\boldsymbol{A}_0 = \hat{\boldsymbol{A}}_0 = \boldsymbol{U}), \tag{3.15}$$

$$\dot{\boldsymbol{\omega}}_1 = \boldsymbol{A}_0 \hat{\boldsymbol{A}}_0 \hat{\boldsymbol{z}}'_0 \ddot{\theta}_1 + \dot{\boldsymbol{\omega}}'_1 \ , \tag{3.16}$$

$$\dot{\boldsymbol{\omega}}'_1 = \boldsymbol{0} \tag{3.17}$$

Adopting the spatial vector notation [43, 44, 50], thus defining

$$\dot{\boldsymbol{V}}_i = \begin{bmatrix} \dot{\boldsymbol{\omega}}_i, \\ \dot{\boldsymbol{v}}_i \end{bmatrix} \in \mathbb{R}^6, \quad \dot{\boldsymbol{V}}'_i = \begin{bmatrix} \dot{\boldsymbol{\omega}}'_i \\ \dot{\boldsymbol{v}}'_i \end{bmatrix} \in \mathbb{R}^6, \quad \boldsymbol{P}_i = \begin{bmatrix} \boldsymbol{U} & \boldsymbol{0} \\ -\tilde{\boldsymbol{p}}_{i+1,i} & \boldsymbol{U} \end{bmatrix} \in \mathbb{R}^{6\times6}, \tag{3.18}$$

$$\boldsymbol{B}_{\theta,i} = \begin{bmatrix} \boldsymbol{A}_i \hat{\boldsymbol{A}}_i \hat{\boldsymbol{z}}_i \\ \boldsymbol{0} \end{bmatrix} \in \mathbb{R}^6, \quad \boldsymbol{B}_{q,i} = \begin{bmatrix} \boldsymbol{A}_i \hat{\boldsymbol{S}}_i \\ \boldsymbol{A}_i \boldsymbol{S}_i \end{bmatrix} \in \mathbb{R}^{6\times M_i}, \tag{3.19}$$

eqs. (3.5) and (3.13) can be collected into:

$$\dot{\boldsymbol{V}}_i - \boldsymbol{P}_{i-1} \dot{\boldsymbol{V}}_{i-1} = \boldsymbol{B}_{\theta,i-1} \ddot{\theta}_i + \boldsymbol{B}_{q,i-1} \ddot{\boldsymbol{q}}_{i-1} + \dot{\boldsymbol{V}}'_i. \tag{3.20}$$

In turn, defining with N the number of the links, and with $M = \sum_{i=1}^{N} M_i$ the number of elastic variables, it is possible to collect all the equations (3.20) into a single global equation of the form

$$\boldsymbol{\mathcal{P}}^T \dot{\boldsymbol{\mathcal{V}}} = \boldsymbol{\mathcal{B}}_\theta \ddot{\boldsymbol{\theta}} + \boldsymbol{\mathcal{B}}_q \ddot{\boldsymbol{q}} + \dot{\boldsymbol{\mathcal{V}}}', \tag{3.21}$$

with $\dot{\boldsymbol{\mathcal{V}}} = \text{col}\{\dot{\boldsymbol{V}}_i\} \in \mathbb{R}^{6N}$, $\dot{\boldsymbol{\mathcal{V}}}' = \text{col}\{\dot{\boldsymbol{V}}_i'\} \in \mathbb{R}^{6N}$

$$\boldsymbol{\mathcal{P}} = \begin{bmatrix} \boldsymbol{U} & -\boldsymbol{P}_1^T & \boldsymbol{0} & \dots & \boldsymbol{0} & \boldsymbol{0} \\ \boldsymbol{0} & \boldsymbol{U} & -\boldsymbol{P}_2^T & \dots & \boldsymbol{0} & \boldsymbol{0} \\ \boldsymbol{0} & \boldsymbol{0} & \boldsymbol{U} & \dots & \boldsymbol{0} & \boldsymbol{0} \\ \vdots & \vdots & \vdots & \ddots & \vdots & \vdots \\ \boldsymbol{0} & \boldsymbol{0} & \boldsymbol{0} & \dots & \boldsymbol{U} & -\boldsymbol{P}_{N-1}^T \\ \boldsymbol{0} & \boldsymbol{0} & \boldsymbol{0} & \dots & \boldsymbol{0} & \boldsymbol{U} \end{bmatrix} \in \mathbb{R}^{6N \times 6N}, \tag{3.22}$$

$$\boldsymbol{\mathcal{B}}_\theta = \begin{bmatrix} \boldsymbol{B}_{\theta,0} & \boldsymbol{0} & \boldsymbol{0} & \dots & \boldsymbol{0} & \boldsymbol{0} \\ \boldsymbol{0} & \boldsymbol{B}_{\theta,1} & \boldsymbol{0} & \dots & \boldsymbol{0} & \boldsymbol{0} \\ \boldsymbol{0} & \boldsymbol{0} & \boldsymbol{B}_{\theta,2} & \dots & \boldsymbol{0} & \boldsymbol{0} \\ \vdots & \vdots & \vdots & \ddots & \vdots & \vdots \\ \boldsymbol{0} & \boldsymbol{0} & \boldsymbol{0} & \dots & \boldsymbol{B}_{\theta,N-2} & \boldsymbol{0} \\ \boldsymbol{0} & \boldsymbol{0} & \boldsymbol{0} & \dots & \boldsymbol{0} & \boldsymbol{B}_{\theta,N-1} \end{bmatrix} \in \mathbb{R}^{6N \times N}, \tag{3.23}$$

$$\boldsymbol{\mathcal{B}}_q = \begin{bmatrix} \boldsymbol{0} & \boldsymbol{0} & \boldsymbol{0} & \dots & \boldsymbol{0} & \boldsymbol{0} \\ \boldsymbol{B}_{q,1} & \boldsymbol{0} & \boldsymbol{0} & \dots & \boldsymbol{0} & \boldsymbol{0} \\ \boldsymbol{0} & \boldsymbol{B}_{q,2} & \boldsymbol{0} & \dots & \boldsymbol{0} & \boldsymbol{0} \\ \vdots & \vdots & \vdots & \ddots & \vdots & \vdots \\ \boldsymbol{0} & \boldsymbol{0} & \boldsymbol{0} & \dots & \boldsymbol{0} & \boldsymbol{0} \\ \boldsymbol{0} & \boldsymbol{0} & \boldsymbol{0} & \dots & \boldsymbol{B}_{q,N-1} & \boldsymbol{0} \end{bmatrix} \in \mathbb{R}^{6N \times M}. \tag{3.24}$$

3.1.2 Dynamics

The motion equations for the flexible links are the same equations described in Chapter 2 where an additional index i is added to the terms in order to identify the *i-th* link. Equation 2.2 is revised as:

$$\begin{bmatrix} m_i\boldsymbol{U} & m_i\tilde{\bar{\boldsymbol{d}}}_{C,i}^T & \bar{\boldsymbol{C}}_{t,i}^T \\ m_i\tilde{\bar{\boldsymbol{d}}}_{C,i} & \bar{\boldsymbol{J}}_i & \bar{\boldsymbol{C}}_{r,i}^T \\ \bar{\boldsymbol{C}}_{t,i} & \bar{\boldsymbol{C}}_{r,i} & \boldsymbol{M}_{e,i} \end{bmatrix} \begin{bmatrix} \dot{\bar{\boldsymbol{v}}}_i \\ \dot{\bar{\boldsymbol{\omega}}}_i \\ \ddot{\boldsymbol{q}}_i \end{bmatrix} = \begin{bmatrix} \boldsymbol{0}_3 \\ \boldsymbol{0}_3 \\ -\boldsymbol{K}_{e,i}\boldsymbol{q}_i - \boldsymbol{D}_{e,i}\dot{\boldsymbol{q}}_i \end{bmatrix} + \begin{bmatrix} \boldsymbol{h}_{\omega,i}^r \\ \boldsymbol{h}_{\omega,i}^\theta \\ \boldsymbol{h}_{\omega,i}^f \end{bmatrix} + \begin{bmatrix} \boldsymbol{h}_{e,i}^r \\ \boldsymbol{h}_{e,i}^\theta \\ \boldsymbol{h}_{e,i}^f \end{bmatrix} \tag{3.25}$$

As a consequence, all equations from 2.3 to 2.20 must be revised accordingly. A complete description cam be found in [13]

Collecting the torque and force in a spatial vector $\boldsymbol{F}_i = \begin{bmatrix} \boldsymbol{n}_i^T & \boldsymbol{f}_i^T \end{bmatrix}^T \in \mathbb{R}^6$, and projecting the motion equations relevant to the angular and linear accelerations on the world frame one obtains

$$\boldsymbol{I}_{vv,i}\dot{\boldsymbol{V}}_i + \boldsymbol{I}_{vq,i}\ddot{\boldsymbol{q}}_i - \boldsymbol{C}_{v,i} = \boldsymbol{F}_i - \boldsymbol{P}_i^T\boldsymbol{F}_{i+1}, \tag{3.26}$$

where

$$\boldsymbol{I}_{vv,i} = \begin{bmatrix} \boldsymbol{A}_i \bar{\boldsymbol{J}}_i \boldsymbol{A}_i^T & m_i \boldsymbol{A}_i \tilde{\bar{\boldsymbol{d}}}_{C,i} \boldsymbol{A}_i^T \\ m_i \boldsymbol{A}_i \tilde{\bar{\boldsymbol{d}}}_{C,i}^T \boldsymbol{A}_i^T & m_i \boldsymbol{U} \end{bmatrix} \in \mathbb{R}^{6\times 6}, \tag{3.27}$$

$$\boldsymbol{I}_{vq,i} = \begin{bmatrix} \boldsymbol{A}_i \bar{\boldsymbol{C}}_{r,i}^T \\ \boldsymbol{A}_i \bar{\boldsymbol{C}}_{t,i}^T \end{bmatrix} \in \mathbb{R}^{6\times M_i}, \quad \boldsymbol{C}_{v,i} = \begin{bmatrix} \boldsymbol{A}_i \boldsymbol{h}_{\omega,i}^{\theta} \\ \boldsymbol{A}_i \boldsymbol{h}_{\omega,i}^{r} \end{bmatrix} \in \mathbb{R}^{6}, \tag{3.28}$$

A single global equation can be again obtained by defining $\boldsymbol{\mathcal{I}}_{vv} = \text{diag}\{\boldsymbol{I}_{vv,i}\} \in \mathbb{R}^{6N\times 6N}$, $\boldsymbol{\mathcal{F}} = \text{col}\{\boldsymbol{F}_i\} \in \mathbb{R}^{6N}$, $\boldsymbol{\mathcal{C}}_v = \text{col}\{\boldsymbol{C}_{v,i}\} \in \mathbb{R}^{6N}$ and

$$\boldsymbol{\mathcal{I}}_{vq} = \begin{bmatrix} \boldsymbol{I}_{vq,1} & \boldsymbol{0} & \boldsymbol{0} & \dots & \boldsymbol{0} & \boldsymbol{0} \\ \boldsymbol{0} & \boldsymbol{I}_{vq,2} & \boldsymbol{0} & \dots & \boldsymbol{0} & \boldsymbol{0} \\ \boldsymbol{0} & \boldsymbol{0} & \boldsymbol{I}_{vq,3} & \dots & \boldsymbol{0} & \boldsymbol{0} \\ \vdots & \vdots & \vdots & \ddots & \vdots & \vdots \\ \boldsymbol{0} & \boldsymbol{0} & \boldsymbol{0} & \dots & \boldsymbol{I}_{vq,N-1} & \boldsymbol{0} \\ \boldsymbol{0} & \boldsymbol{0} & \boldsymbol{0} & \dots & \boldsymbol{0} & \boldsymbol{I}_{vq,N} \end{bmatrix} \in \mathbb{R}^{6N\times M} \tag{3.29}$$

as follows

$$\boldsymbol{\mathcal{I}}_{vv}\dot{\boldsymbol{\mathcal{V}}} + \boldsymbol{\mathcal{I}}_{vq}\ddot{\boldsymbol{q}} - \boldsymbol{\mathcal{C}}_v = \boldsymbol{\mathcal{P}}\boldsymbol{\mathcal{F}}. \tag{3.30}$$

A global equation can be also obtained for the dynamics of the elastic coordinates which, according to (2.2), are defined by:

$$\boldsymbol{I}_{vq,i}^T \dot{\boldsymbol{V}}_i + \boldsymbol{M}_{e,i}\ddot{\boldsymbol{q}}_i = -\boldsymbol{K}_{e,i}\boldsymbol{q}_i - \boldsymbol{D}_{e,i}\dot{\boldsymbol{q}}_i + \boldsymbol{h}_{\omega,i}^f - \boldsymbol{B}_{q,i}^T \boldsymbol{F}_{i+1}. \tag{3.31}$$

Defining $\boldsymbol{\mathcal{M}}_e = \text{diag}\{\boldsymbol{M}_{e,i}\} \in \mathbb{R}^{M\times M}$, $\boldsymbol{\mathcal{K}}_e = \text{diag}\{\boldsymbol{K}_{e,i}\} \in \mathbb{R}^{M\times M}$, $\boldsymbol{\mathcal{D}}_e = \text{diag}\{\boldsymbol{D}_{e,i}\} \in \mathbb{R}^{M\times M}$, $\boldsymbol{\mathcal{C}}_f = \text{col}\{\boldsymbol{h}_{\omega,i}^f\} \in \mathbb{R}^{M}$ one obtains

$$\boldsymbol{\mathcal{I}}_{vq}^T \dot{\boldsymbol{\mathcal{V}}} + \boldsymbol{\mathcal{M}}_e\ddot{\boldsymbol{q}} + \boldsymbol{\mathcal{D}}_e\dot{\boldsymbol{q}} + \boldsymbol{\mathcal{K}}_e\boldsymbol{q} - \boldsymbol{\mathcal{C}}_f = -\boldsymbol{\mathcal{B}}_q^T \boldsymbol{\mathcal{F}} \tag{3.32}$$

3.1.3 Closed form model

By solving eq. (3.21) with respect to $\dot{\boldsymbol{\mathcal{V}}}$, and eq. (3.30) with respect to $\boldsymbol{\mathcal{F}}$, and substituting in eq. (3.32) one obtains eq. (3.2):

$$\boldsymbol{\mathcal{M}}_{\theta q}^T \ddot{\boldsymbol{\theta}} + \boldsymbol{\mathcal{M}}_{qq}\ddot{\boldsymbol{q}} + \boldsymbol{\mathcal{D}}_e\dot{\boldsymbol{q}} + \boldsymbol{\mathcal{K}}_e\boldsymbol{q} + \boldsymbol{\mathcal{C}}_{\boldsymbol{q}} = \boldsymbol{0} \tag{3.33}$$

where

$$\begin{aligned} \boldsymbol{\mathcal{M}}_{\theta q}^T &= \left\{ \left(\boldsymbol{\mathcal{I}}_{vq}^T \boldsymbol{\mathcal{P}}^{-T}\right) + \left[\boldsymbol{\mathcal{B}}_q^T \left(\boldsymbol{\mathcal{P}}^{-1}\boldsymbol{\mathcal{I}}_{vv}\boldsymbol{\mathcal{P}}^{-T}\right)\right] \right\} \boldsymbol{\mathcal{B}}_\theta, & (3.34) \\ \boldsymbol{\mathcal{M}}_{qq} &= \boldsymbol{\mathcal{M}}_e + \boldsymbol{\mathcal{B}}_q^T \left(\boldsymbol{\mathcal{P}}^{-1}\boldsymbol{\mathcal{I}}_{vv}\boldsymbol{\mathcal{P}}^{-T}\right) \boldsymbol{\mathcal{B}}_q \\ &\quad + \left[\left(\boldsymbol{\mathcal{I}}_{vq}^T \boldsymbol{\mathcal{P}}^{-T}\right) \boldsymbol{\mathcal{B}}_q\right] + \left[\left(\boldsymbol{\mathcal{I}}_{vq}^T \boldsymbol{\mathcal{P}}^{-T}\right) \boldsymbol{\mathcal{B}}_q\right]^T, & (3.35) \\ \boldsymbol{\mathcal{C}}_q &= \left\{ \left(\boldsymbol{\mathcal{I}}_{vq}^T \boldsymbol{\mathcal{P}}^{-T}\right) + \left[\boldsymbol{\mathcal{B}}_q^T \left(\boldsymbol{\mathcal{P}}^{-1}\boldsymbol{\mathcal{I}}_{vv}\boldsymbol{\mathcal{P}}^{-T}\right)\right] \right\} \dot{\boldsymbol{\mathcal{V}}}' \\ &\quad - \boldsymbol{\mathcal{B}}_q^T \left(\boldsymbol{\mathcal{P}}^{-1}\boldsymbol{\mathcal{C}}_v\right) - \boldsymbol{\mathcal{C}}_f. & (3.36) \end{aligned}$$

It must be recalled that matrix $\boldsymbol{\mathcal{P}}$ is invertible, and that its inverse is the upper-triangular matrix

$$\boldsymbol{\mathcal{P}}^{-1} = \begin{bmatrix} \boldsymbol{U} & \boldsymbol{P}_{2,1}^T & \boldsymbol{P}_{3,1}^T & \dots & \boldsymbol{P}_{N-1,1}^T & \boldsymbol{P}_{N,1}^T \\ \boldsymbol{0} & \boldsymbol{U} & \boldsymbol{P}_{3,2}^T & \dots & \boldsymbol{P}_{N-1,2}^T & \boldsymbol{P}_{N,2}^T \\ \boldsymbol{0} & \boldsymbol{0} & \boldsymbol{U} & \dots & \boldsymbol{P}_{N-1,3}^T & \boldsymbol{P}_{N,3}^T \\ \vdots & \vdots & \vdots & \ddots & \vdots & \vdots \\ \boldsymbol{0} & \boldsymbol{0} & \boldsymbol{0} & \dots & \boldsymbol{U} & \boldsymbol{P}_{N,N-1}^T \\ \boldsymbol{0} & \boldsymbol{0} & \boldsymbol{0} & \dots & \boldsymbol{0} & \boldsymbol{U} \end{bmatrix} \in \mathbb{R}^{6N \times 6N} \tag{3.37}$$

being

$$\boldsymbol{P}_i = \boldsymbol{P}_{i+1,i}, \quad \boldsymbol{P}_{i,k} = \boldsymbol{P}_{i,j}\boldsymbol{P}_{j,k}, \quad \boldsymbol{P}_{i,j}^{-1} = \boldsymbol{P}_{j,i}. \tag{3.38}$$

The efficient computation of the inverse of the $\boldsymbol{\mathcal{P}}$ matrix is particularly relevant as it appears in many terms of the mass matrix.

The joint input torque τ_i is equal to the scalar product between the i-th joint rotation axis and the torque $\boldsymbol{n}_i$

$$\tau_i = \left(\boldsymbol{A}_{i-1}\hat{\boldsymbol{A}}_{i-1}\hat{\boldsymbol{z}}'_{i-1}\right)^T \boldsymbol{n}_i = \begin{bmatrix} \left(\boldsymbol{A}_{i-1}\hat{\boldsymbol{A}}_{i-1}\hat{\boldsymbol{z}}'_{i-1}\right)^T & \boldsymbol{0} \end{bmatrix} \boldsymbol{F}_i = \boldsymbol{B}_{\theta,i-1}^T \boldsymbol{F}_i, \tag{3.39}$$

so that

$$\boldsymbol{\tau} = \boldsymbol{\mathcal{B}}_\theta^T \boldsymbol{\mathcal{F}} \tag{3.40}$$

from which eq. (3.1) follows

$$\boldsymbol{\mathcal{M}}_{\theta\theta}\ddot{\boldsymbol{\theta}} + \boldsymbol{\mathcal{M}}_{\theta q}\ddot{\boldsymbol{q}} + \boldsymbol{\mathcal{C}}_\theta = \boldsymbol{\tau} \tag{3.41}$$

where

$$\boldsymbol{\mathcal{M}}_{\theta\theta} = \left[\boldsymbol{\mathcal{B}}_\theta^T \left(\boldsymbol{\mathcal{P}}^{-1}\boldsymbol{\mathcal{I}}_{vv}\boldsymbol{\mathcal{P}}^{-T}\right)\right]\boldsymbol{\mathcal{B}}_\theta, \tag{3.42}$$

$$\boldsymbol{\mathcal{C}}_\theta = \left[\boldsymbol{\mathcal{B}}_\theta^T \left(\boldsymbol{\mathcal{P}}^{-1}\boldsymbol{\mathcal{I}}_{vv}\boldsymbol{\mathcal{P}}^{-T}\right)\right]\dot{\boldsymbol{\mathcal{V}}}' - \boldsymbol{\mathcal{B}}_\theta^T \left(\boldsymbol{\mathcal{P}}^{-1}\boldsymbol{\mathcal{C}}_v\right). \tag{3.43}$$

The described procedure contains the complete calculation for all the terms of eqns. 3.1 and 3.2 which describe a closed form model of manipulator in terms of the joint angles and elastic variables, leading to one of the main results of this work.

Remark 3. Starting from matrices $\boldsymbol{\mathcal{I}}_{vv}$ and $\boldsymbol{\mathcal{I}}_{vq}$ the computation of the manipulator inertia matrix requires the computation of eight matrix products,

namely:

$$\begin{aligned}
\boldsymbol{\mathcal{M}}_1 &= \boldsymbol{\mathcal{P}}^{-1}\boldsymbol{\mathcal{I}}_{vv}\boldsymbol{\mathcal{P}}^{-T}, && (3.44)\\
\boldsymbol{\mathcal{M}}_2 &= \boldsymbol{\mathcal{M}}_1\boldsymbol{\mathcal{B}}_\theta, && (3.45)\\
\boldsymbol{\mathcal{M}}_3 &= \boldsymbol{\mathcal{B}}_\theta^T\boldsymbol{\mathcal{M}}_2, && (3.46)\\
\boldsymbol{\mathcal{M}}_4 &= \boldsymbol{\mathcal{B}}_q^T\boldsymbol{\mathcal{M}}_2, && (3.47)\\
\boldsymbol{\mathcal{M}}_5 &= \boldsymbol{\mathcal{B}}_q^T\boldsymbol{\mathcal{M}}_1\boldsymbol{\mathcal{B}}_q, && (3.48)\\
\boldsymbol{\mathcal{M}}_6 &= \boldsymbol{\mathcal{I}}_{vq}^T\boldsymbol{\mathcal{P}}^{-T}, && (3.49)\\
\boldsymbol{\mathcal{M}}_7 &= \boldsymbol{\mathcal{M}}_6\boldsymbol{\mathcal{B}}_q, && (3.50)\\
\boldsymbol{\mathcal{M}}_8 &= \boldsymbol{\mathcal{M}}_6\boldsymbol{\mathcal{B}}_\theta, && (3.51)
\end{aligned}$$

To this aim, suitable algorithms and data structures can be used, taking advantage of the sparse structure of the matrices.

Remark 4. When mode shapes are ortonormalized, as usually done by FEM packages [96], an identity matrix is obtained for $\boldsymbol{M}_{e,i} = \boldsymbol{I}_i^6$, while the stiffness matrix $\boldsymbol{K}_{e,i}$ is a diagonal matrix, whose elements are the squares of mode frequencies.

3.1.4 Adding an external force at the tip

In order to model interactions of the end effector with external objects, the model can be extended to account for an external wrench acting at the tip of the manipulator.

If $\boldsymbol{F}_e = \begin{bmatrix} \boldsymbol{n}_e^T & \boldsymbol{f}_e^T \end{bmatrix}^T \in \mathbb{R}^6$ is the wrench exerted on link N at the origin of the frame $\{O'_N, \boldsymbol{x}'_N, \boldsymbol{y}'_N, \boldsymbol{z}'_N\}$, eqs. (3.30) and (3.32) modify as it follows:

$$\begin{aligned}
\boldsymbol{\mathcal{I}}_{vv}\dot{\boldsymbol{\mathcal{V}}} + \boldsymbol{\mathcal{I}}_{vq}\ddot{\boldsymbol{q}} - \boldsymbol{\mathcal{C}}_v &= \boldsymbol{\mathcal{P}}\boldsymbol{\mathcal{F}} + \tilde{\boldsymbol{\mathcal{P}}}\boldsymbol{F}_e, && (3.52)\\
\boldsymbol{\mathcal{I}}_{vq}^T\dot{\boldsymbol{\mathcal{V}}} + \boldsymbol{\mathcal{M}}_e\ddot{\boldsymbol{q}} + \boldsymbol{\mathcal{D}}_e\dot{\boldsymbol{q}} + \boldsymbol{\mathcal{K}}_e\boldsymbol{q} - \boldsymbol{\mathcal{C}}_f &= -\boldsymbol{\mathcal{B}}_q^T\boldsymbol{\mathcal{F}} + \tilde{\boldsymbol{\mathcal{B}}}_q^T\boldsymbol{F}_e, && (3.53)
\end{aligned}$$

where

$$\tilde{\boldsymbol{\mathcal{P}}} = \begin{bmatrix} \boldsymbol{0} \\ \boldsymbol{0} \\ \boldsymbol{0} \\ \vdots \\ \boldsymbol{0} \\ \boldsymbol{P}_N^T \end{bmatrix} \in \mathbb{R}^{6N\times 6}, \quad \tilde{\boldsymbol{\mathcal{B}}}_q^T = \begin{bmatrix} \boldsymbol{0} \\ \boldsymbol{0} \\ \boldsymbol{0} \\ \vdots \\ \boldsymbol{0} \\ \boldsymbol{B}_{q,N}^T \end{bmatrix} \in \mathbb{R}^{M\times 6} \qquad (3.54)$$

so that the following holds

$$\begin{aligned}
\boldsymbol{\mathcal{M}}_{\theta\theta}\ddot{\boldsymbol{\theta}} + \boldsymbol{\mathcal{M}}_{\theta q}\ddot{\boldsymbol{q}} + \boldsymbol{\mathcal{C}}_\theta &= \boldsymbol{\tau} + \boldsymbol{\mathcal{B}}_\theta^T\boldsymbol{\mathcal{P}}^{-1}\tilde{\boldsymbol{\mathcal{P}}}\boldsymbol{F}_e, && (3.55)\\
\boldsymbol{\mathcal{M}}_{\theta q}^T\ddot{\boldsymbol{\theta}} + \boldsymbol{\mathcal{M}}_{qq}\ddot{\boldsymbol{q}} + \boldsymbol{\mathcal{D}}_e\dot{\boldsymbol{q}} + \boldsymbol{\mathcal{K}}_e\boldsymbol{q} + \boldsymbol{\mathcal{C}}_{\boldsymbol{q}} &= \left(\tilde{\boldsymbol{\mathcal{B}}}_q^T + \boldsymbol{\mathcal{B}}_q^T\boldsymbol{\mathcal{P}}^{-1}\tilde{\boldsymbol{\mathcal{P}}}\right)\boldsymbol{F}_e, && (3.56)
\end{aligned}$$

3.1.5 Adding a payload at the tip

Assume $\{O'_N, \boldsymbol{x}'_N, \boldsymbol{y}'_N, \boldsymbol{z}'_N\}$ as the end-effector frame and model the payload as a rigid body with m_p, $\boldsymbol{I}_p$ and $\bar{\boldsymbol{r}}_p$ defining its mass, inertia tensor and vector locating its center of mass with respect to the end-effector frame respectively.

Applying the Newton-Euler equations to the payload, considered as a floating body and subject to the wrench $-\boldsymbol{F}_e$, gives

$$\begin{aligned} \tilde{\bar{\boldsymbol{r}}}_p\dot{\bar{\boldsymbol{v}}}_p + \boldsymbol{I}_p\dot{\bar{\boldsymbol{\omega}}}_p &= -\bar{\boldsymbol{\omega}}_p \times \boldsymbol{I}_p\bar{\boldsymbol{\omega}}_p - \bar{\boldsymbol{n}}_e, & (3.57)\\ m_p\dot{\bar{\boldsymbol{v}}}_p + \tilde{\bar{\boldsymbol{r}}}_p^T\dot{\bar{\boldsymbol{\omega}}}_p &= -\bar{\boldsymbol{\omega}}_p \times (\bar{\boldsymbol{\omega}}_p \times \bar{\boldsymbol{r}}_p) - \bar{\boldsymbol{f}}_e, & (3.58) \end{aligned}$$

and projecting the said equations on the absolute frame through the matrix $\boldsymbol{A}_p = \boldsymbol{A}_N\hat{\boldsymbol{A}}_N$, while defining $\dot{\boldsymbol{V}}_p = \begin{bmatrix} \dot{\bar{\boldsymbol{\omega}}}_p^T & \dot{\bar{\boldsymbol{v}}}_p^T \end{bmatrix}^T \in \mathbb{R}^6$ yields

$$\boldsymbol{F}_e = -\boldsymbol{\mathcal{I}}_{vv,p}\dot{\boldsymbol{V}}_p - \boldsymbol{\mathcal{C}}_{v,p}, \tag{3.59}$$

where

$$\begin{aligned} \boldsymbol{\mathcal{I}}_{vv,p} &= \begin{bmatrix} \boldsymbol{A}_p\boldsymbol{I}_p\boldsymbol{A}_p^T & \boldsymbol{A}_p\tilde{\bar{\boldsymbol{r}}}_p \\ \boldsymbol{A}_p\tilde{\bar{\boldsymbol{r}}}_p^T & m_p\boldsymbol{U} \end{bmatrix}, & (3.60)\\ \boldsymbol{\mathcal{C}}_{v,p} &= \begin{bmatrix} \boldsymbol{\omega}_p \times \boldsymbol{A}_p\boldsymbol{I}_p\boldsymbol{A}_p^T\boldsymbol{\omega}_p \\ \boldsymbol{\omega}_p \times (\boldsymbol{\omega}_p \times \boldsymbol{A}_p\bar{\boldsymbol{r}}_p) \end{bmatrix}, & (3.61) \end{aligned}$$

Recalling that $\dot{\boldsymbol{V}}_p$ can be obtained as:

$$\begin{aligned} \dot{\boldsymbol{V}}_p &= \tilde{\boldsymbol{\mathcal{P}}}^T\dot{\boldsymbol{\mathcal{V}}} + \tilde{\boldsymbol{\mathcal{B}}}_q\ddot{\boldsymbol{q}} + \dot{\boldsymbol{V}}'_{N+1} & (3.62)\\ \dot{\boldsymbol{V}}'_{N+1} &= \begin{bmatrix} \boldsymbol{\omega}_N \times \left(\boldsymbol{A}_N\hat{\boldsymbol{S}}_N\dot{\boldsymbol{q}}_N\right), \\ \boldsymbol{\omega}_N \times (\boldsymbol{\omega}_N \times \boldsymbol{p}_{N+1,N} + \boldsymbol{A}_N\boldsymbol{S}_N\dot{\boldsymbol{q}}_N) \end{bmatrix}, & (3.63) \end{aligned}$$

substituting (3.63) in (3.59) and (3.59) in (3.52), (3.53) one obtains:

$$\begin{aligned} \hat{\boldsymbol{\mathcal{I}}}_{vv}\dot{\boldsymbol{\mathcal{V}}} + \hat{\boldsymbol{\mathcal{I}}}_{vq}\ddot{\boldsymbol{q}} - \hat{\boldsymbol{\mathcal{C}}}_v &= \boldsymbol{\mathcal{P}}\boldsymbol{\mathcal{F}}, & (3.64)\\ \hat{\boldsymbol{\mathcal{I}}}_{vq}^T\dot{\boldsymbol{\mathcal{V}}} + \hat{\boldsymbol{\mathcal{M}}}_e\ddot{\boldsymbol{q}} + \boldsymbol{\mathcal{D}}_e\dot{\boldsymbol{q}} + \boldsymbol{\mathcal{K}}_e\boldsymbol{q} - \hat{\boldsymbol{\mathcal{C}}}_f &= -\boldsymbol{\mathcal{B}}_q^T\boldsymbol{\mathcal{F}}, & (3.65) \end{aligned}$$

where

$$\begin{aligned} \hat{\boldsymbol{\mathcal{I}}}_{vv} &= \boldsymbol{\mathcal{I}}_{vv} + \tilde{\boldsymbol{\mathcal{P}}}\boldsymbol{\mathcal{I}}_{vv,p}\tilde{\boldsymbol{\mathcal{P}}}^T, & (3.66)\\ \hat{\boldsymbol{\mathcal{I}}}_{vq} &= \boldsymbol{\mathcal{I}}_{vq} + \tilde{\boldsymbol{\mathcal{P}}}\boldsymbol{\mathcal{I}}_{vv,p}\tilde{\boldsymbol{\mathcal{B}}}_q, & (3.67)\\ \hat{\boldsymbol{\mathcal{C}}}_v &= \boldsymbol{\mathcal{C}}_v - \tilde{\boldsymbol{\mathcal{P}}}\left(\boldsymbol{\mathcal{I}}_{vv,p}\dot{\boldsymbol{V}}'_N + \boldsymbol{\mathcal{C}}_{v,p}\right), & (3.68)\\ \hat{\boldsymbol{\mathcal{M}}}_e &= \boldsymbol{\mathcal{M}}_e + \tilde{\boldsymbol{\mathcal{B}}}_q^T\boldsymbol{\mathcal{I}}_{vv,p}\tilde{\boldsymbol{\mathcal{B}}}_q, & (3.69)\\ \hat{\boldsymbol{\mathcal{C}}}_f &= \boldsymbol{\mathcal{C}}_f - \tilde{\boldsymbol{\mathcal{B}}}_q^T\left(\boldsymbol{\mathcal{I}}_{vv,p}\dot{\boldsymbol{V}}'_N + \boldsymbol{\mathcal{C}}_{v,p}\right), & (3.70) \end{aligned}$$

Therefore, equations (3.1) and (3.2) still follow by simply replacing $\boldsymbol{\mathcal{I}}_{vv}$, $\boldsymbol{\mathcal{I}}_{vq}$, $\boldsymbol{\mathcal{C}}_v$, $\boldsymbol{\mathcal{M}}_e$, $\boldsymbol{\mathcal{C}}_f$ in (3.34) and (3.36), while (3.42) and (3.43) are replaced with $\hat{\boldsymbol{\mathcal{I}}}_{vv}$, $\hat{\boldsymbol{\mathcal{I}}}_{vq}$, $\hat{\boldsymbol{\mathcal{C}}}_v$, $\hat{\boldsymbol{\mathcal{M}}}_e$, $\hat{\boldsymbol{\mathcal{C}}}_f$.

3.1.6 Modeling highly flexible manipulators

In order to cope with a high flexibility, link i can be subdivided into more rigidly connected flexible elements or substructures, as shown in Fig. 3.2, each one described through a FFR approach introducing M_k modal coordinates. Define with N_e the total number of elements of the whole manipulator and with $M = \sum_{k=1}^{N_e} M_k$ the total number of modal coordinates.

Let $\theta_i = \theta^e_{\bar{k}}, i = 1, \ldots, N$ denote the "real" joint angle between element $\bar{k}-1$ and $\bar{k}$ and consider a "dummy" joint angle θ^e_k if a rigid connection exists between element $k-1$ and k, thus $\theta^e_k = 0$, $\dot{\theta}^e_k = 0$, $\ddot{\theta}^e_k = 0$. In the latter case it is also:

$$\boldsymbol{A}_{k+1} = \boldsymbol{A}_k \hat{\boldsymbol{A}}_k = \boldsymbol{A}_k \left[\boldsymbol{I} + \widetilde{\left(\hat{\boldsymbol{S}}_k \boldsymbol{q}_k \right)} \right], \tag{3.71}$$

$$\dot{\boldsymbol{\omega}}_{k+1} = \dot{\boldsymbol{\omega}}_k + \boldsymbol{A}_k \hat{\boldsymbol{S}}_k \ddot{\boldsymbol{q}}_k + \dot{\boldsymbol{\omega}}'_{k+1}, \tag{3.72}$$

$$\dot{\boldsymbol{\omega}}'_{k+1} = \boldsymbol{\omega}_k \times \boldsymbol{A}_k \hat{\boldsymbol{S}}_k \dot{\boldsymbol{q}}_k \tag{3.73}$$

$$\dot{\boldsymbol{V}}_k - \boldsymbol{P}_{k-1} \dot{\boldsymbol{V}}_{k-1} = \boldsymbol{B}_{q,k-1} \ddot{\boldsymbol{q}}_{k-1} + \dot{\boldsymbol{V}}'_k \tag{3.74}$$

By comparing eq. (3.20) with eq. (3.74) it is immediately apparent that the model remains formally identical by removing the columns of matrix $\boldsymbol{\mathcal{B}}_\theta$ corresponding to the "dummy" joint angles and with matrices $\boldsymbol{\mathcal{B}}_q$ and $\boldsymbol{\mathcal{B}}_\theta$ having dimensions $6N_e \times M$ and $6N_e \times N$ respectively.

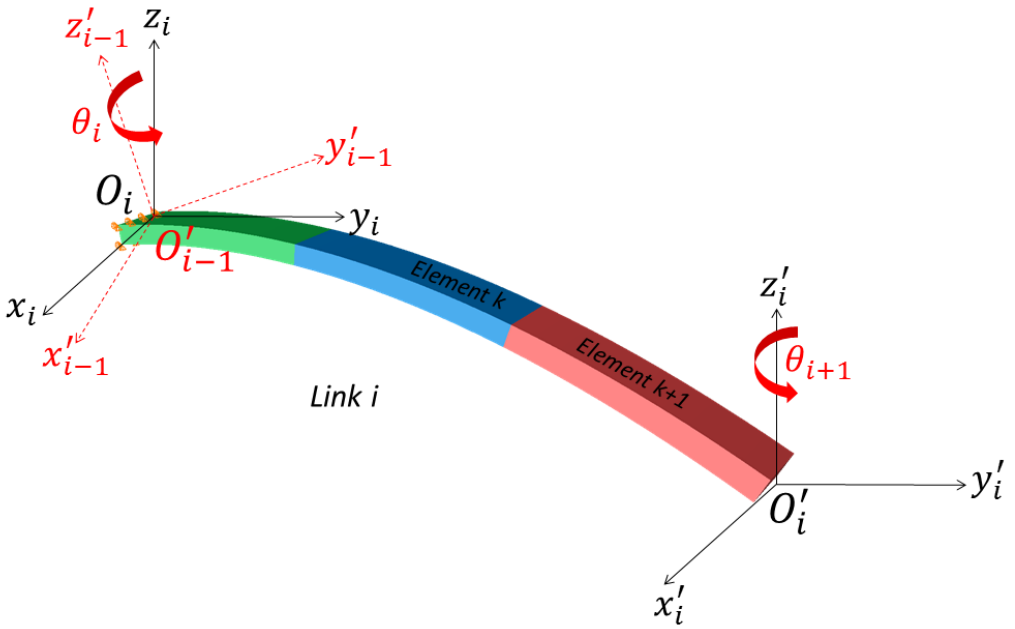

Figure 3.2: Substructuring a highly flexible bar into $k+1$ segments

3.2 Validation of the model

The validation of the model has been carried out in two steps, the results obtained by implementing and simulating model (3.1,3.2) in MATLAB have been first compared with the results obtained by simulating the same system in other multibody environments. Two simulation scenarios have been chosen, the model has been initially compared with a literature benchmark used also in Chapter 2; then a different simulation scenario has been considered, where a planar robot with two links is subject to low-speed and high-speed movements, in this case the results are compared with a different sotware, namely MSC/Adams [94] which relies on a Lagrangian formulation for the flexible degrees of freedom. As a second step, the model of an experimental manipulator has been implemented and the simulation has been compared with experimental results provided by the MERIt dataset ([83]), which contains several measurements carried out on the TUDOR experimental platform, a three DOFs elastic manipulator designed by the Technische Universität Dortmund.

3.2.1 Simulations - Slider crank

The first considered scenario is the same described in Section 2.4.2 which has been selected for several reasons:

- This experiment on the slider-crank mechanism is a widely known benchmark used in literature.
- The mechanism is in fact a closed kinematic chain which requires a feedback force on the tip in order to be simulated within this framework. An efficient way to cope with this problem is described below.
- The same benchmark has been used in Chapter 2 in order to validate the object-oriented body model, in this context the model has been used in a slightly different way, in order to maximise the similarity between the two. This is supposed to further validate and demonstrate the pliability of the general approach.

The links' data (Tab. 3.1) have been obtained as the result of a FE preprocessing followed by a modal reduction step [28], the procedure adopted in order to obtain the data is basically the same described in Section 2.4.2. It must be however pointed out that the prismatic joint previously adopted in order to constrain the tip of the slider to move along the $\boldsymbol{x}$ axis closes a kinematic chain, and actually defines an overall differential-algebraic equation (DAE) system. Since the simulation of this DAE system resulted very difficult to be tackled by MATLAB solvers from a numerical point of view, the kinematic constraint has been replaced by a very stiff spring-damper system, acting on the tip of the slider along the $\boldsymbol{y}$ axis, with a stiffness constant $K = 1 \times 10^5$ N/m and a damping $D = 100$ Ns/m. For the sake

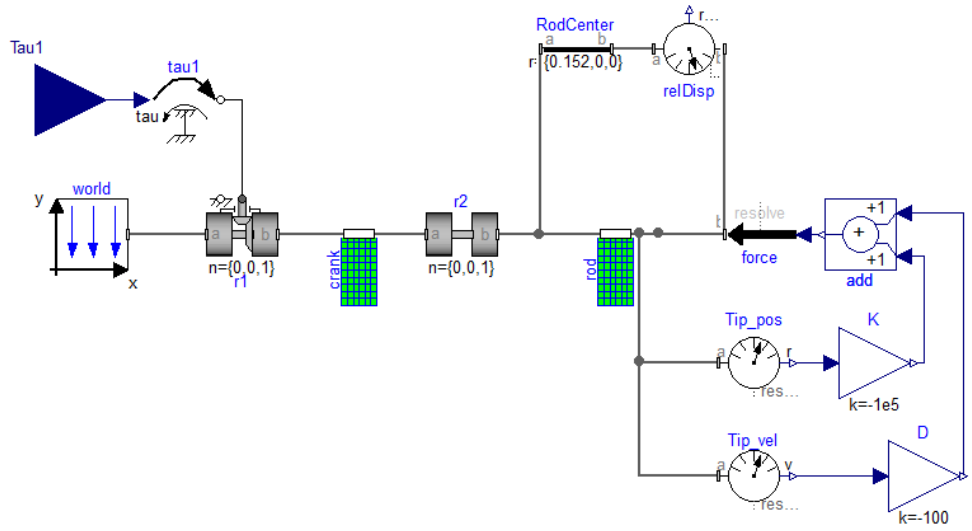

Figure 3.3: Dymola model scheme of the slider crank.

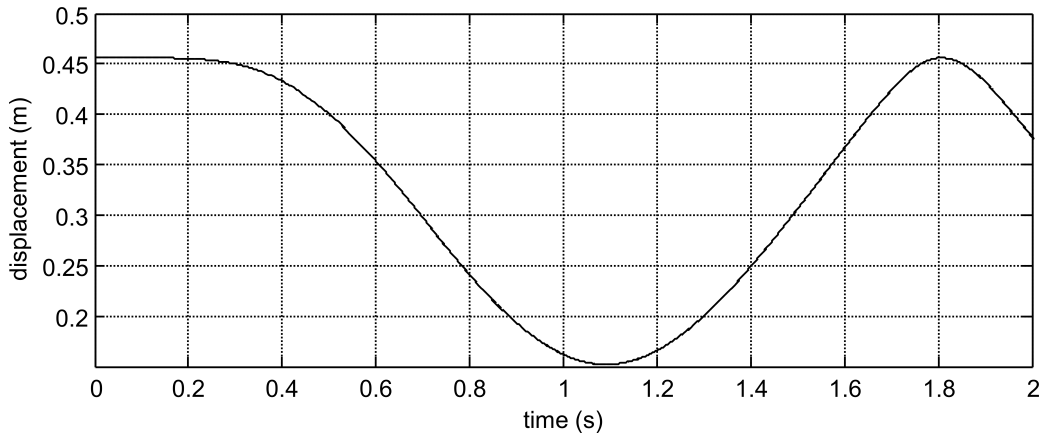

Figure 3.4: Displacement of the slider along the x axis obtained with the Dymola simulation (dashed line), and with the MATLAB simulation (solid line).

of comparison, the Modelica model previously described has been modified in order to be as much similar as possible with the MATLAB simulation model, Fig. 3.3 shows the relevant Dymola model scheme.

The DASSL solver has been used in Dymola, while the `ode15s` solver has been used in MATLAB.

Figure 3.4 shows the displacement of the slider along the $\boldsymbol{x}$ axis, obtained with the MATLAB (solid line) and Dymola (dashed line) simulation; as it is apparent, the two plots are indistinguishable. Some difference between the two simulations is appreciable in Fig. 3.5, where the transverse displacements of the rod center with respect to a rigid motion are shown. The results are in agreement with the benchmark reported in [41] and with the

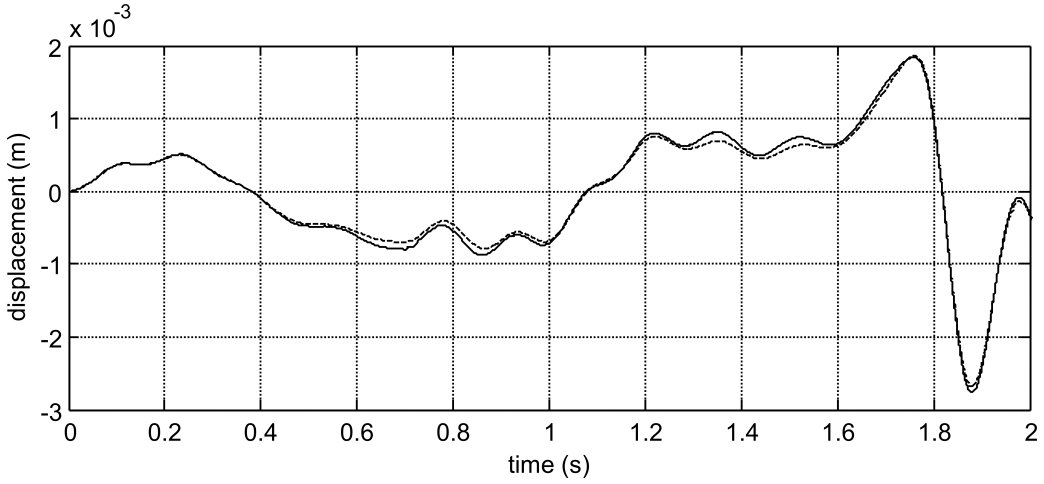

Figure 3.5: Transverse displacements of the rod center with respect to a rigid motion obtained with the Dymola simulation (dashed line), and with the MATLAB simulation (solid line).

results reported in Chapter 2. It must be pointed out that the provided example represents a planar mechanism while the model is suited for three dimensional dynamics, but literature lacks of 3D widely used benchmarks.

3.2.2 Experimental validation

In order to show the effectiveness of the modelling technique here proposed, we will now develop the model of the TUDOR experimental platform, a three DOFs elastic manipulator designed by the Technische Universität Dortmund.

Notwithstanding the original aim of MERIt is the identification of manipulator's dynamics, in the context of this work a subset of the experiments provided by the dataset has been reproduced by means of the Matlab/Simulink simulation environment, and results have been compared with the measurements, with the aim of validating the closed form model.

The equivalent kinematics of the manipulator, whose complete description can be found in [84], is depicted in Fig. 3.6. The first link is rigid, and the first actuated joint moves the robot in the X-Z horizontal plane. Hence, in the context of this work, only the second and third links are considered, making the remaining system equivalent to a planar flexible robot. The second and third joints operate on the X-Y vertical plane, acting on joint angles θ_1 and θ_2. The manipulator kinematics is structured in order to have gravity acting on the negative Y direction. The elastic links, labelled l_1 and l_2, are constituted by spring steel rods with rectangular cross section. The rods are oriented in order to have the great flexibility in the motion plane. Links, joints and motors data are summarized in Tabs. 3.2 and 3.3.

As for the measurement system, strain gauges are placed on each elastic rod, strains are measured at 46 mm and 260 mm from the root of the first

Table 3.2: Tudor Link data

	Link 1	Link 2
Length	440 mm	410 mm
Width	15 mm	15 mm
Height	4 mm	4 mm
Density	7800 Kg/m^3	7800 Kg/m^3
Young Modulus	200 GPa	200 GPa

Table 3.3: Tudor Joint data

	Joint 1	Joint 2
Motor model	EC-max40	EC-max30
Rotor and gear Inertia	9.41×10^{-6} Kgm^2	0.82×10^{-6} Kgm^2
Torque constant	44.8 mNm/A	12.9 mNm/A
Gear Ratio	320 : 1	246 : 1
Mass	1.6680 Kg	0.5885 Kg

rod, and 45 mm and 235 mm from the root of the second rod. It must be considered however, that the initial part of each link is clamped due to mechanical connection to the joint. The length of the clamp along the X direction is 31 mm for the first link, and 28 mm for the second one. In Fig. 3.7, strain gauge positions and clamped parts are shown.

The manipulator can be equipped with a variable payload on the tip, the dataset includes experiments with different payloads, namely 0, 100, 200, 300 and 400 g. Nine tests are provided for every payload condition, and in every test a different pseudo-random set point is generated for the joint angles θ_1 and θ_2.

Summarizing, the experimental measurements provided by the MERIt dataset are: joint angles and velocities, motor currents and the strain measured by the sensors.

The link data, summarized in Table 3.1, have been obtained by means of a FE modal reduction stage, similarly to the data of the slider-crank mechanism outspread in the previous section.

Both links have been modelled with beam elements, as shown in Fig. 3.8, adopting an automatic procedure for node placement, except for the nodes corresponding to the strain sensor positions. Three nodes have been placed at a distance of 1.5 mm each, in the position corresponding to each strain gauge, in order to obtain the strain value from the nodal displacements.

For each flexible link, only 3 eigenmodes have been considered (see Table 3.4), the 2$^{\text{nd}}$ eigenmode has been discarded, because it is a bending mode in the out-of-plane direction, where no strain gauge are present in the experimental setup. Though the number of eigenmodes is low, it has revealed adequate to correctly represent the flexible dynamics of TUDOR. An higher

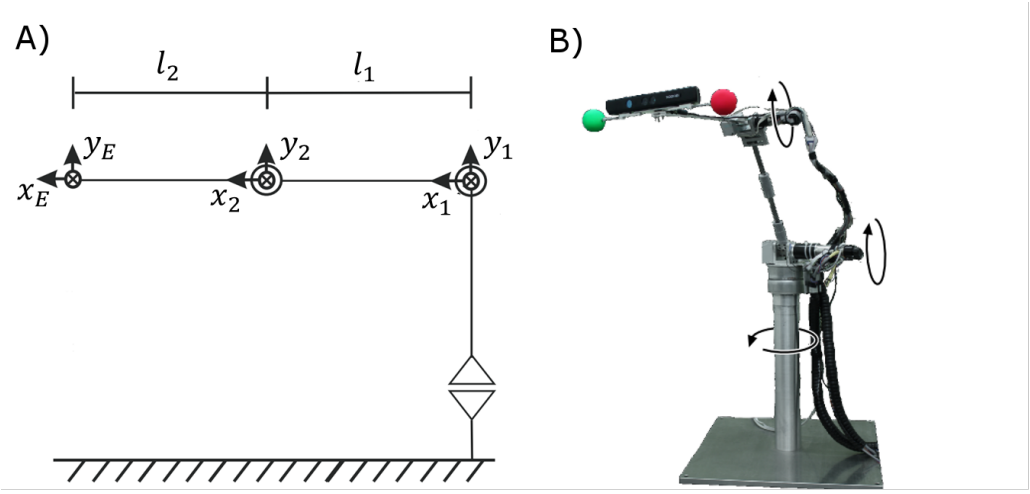

Figure 3.6: Equivalent kinematic (A) and picture (B) of the robot of the TUDOR experimental platform.

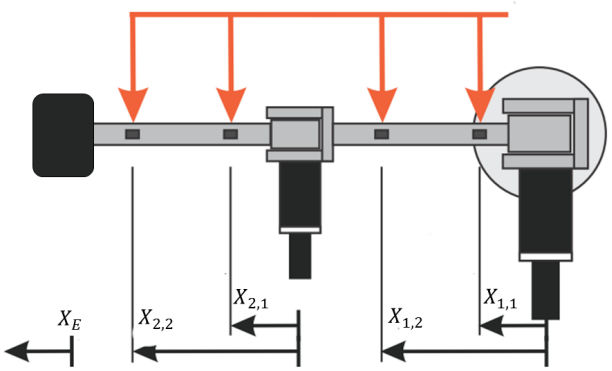

Figure 3.7: Locations of the strain gauges along the robot.

Table 3.4: Considered eigenfrequencies

Link 1		Link 2	
Mode number	Frequency (Hz)	Mode number	Frequency (Hz)
1	4.7	1	22.9
3	75.6	3	143.44
4	241.3	4	401.33

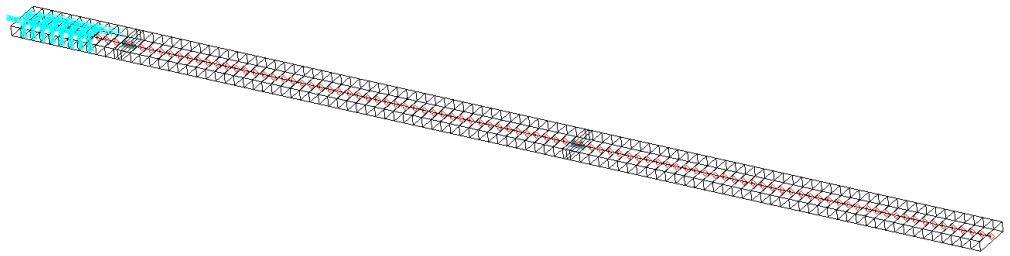

Figure 3.8: Mesh of the FEM model of a link.

precision could be achieved with more eigenmodes causing, however, an increased computational burden.

The boundary conditions adopted in the FE analysis have great influence on the mode shapes of the flexible links, manipulator's links are clamped at one end, hence the nodes corresponding to the clamped part have been constrained in the FE model. Furthermore, clamping the first node of the link intrinsically guarantees that the FFR is placed in the above mentioned node, hence the hypotesis of placing the FFR in the base flexible links is satisfied.

The motor and gear inertia related to the actuator on θ_2 are considered in the FE modelling stage by applying a concentrated mass fixed on the first link's tip, while the payload on the manipulator's tip is considered in the closed form model.

In order to correctly simulate the motion of the manipulator, a closed-loop approach has been adopted. The commanded joint angles have been used as set points for two PID controllers that have been manually tuned with the aim of correctly reproduce the behaviour of the TUDOR manipulator in terms of joint positions. The closed loop approach has been chosen in order to compensate the effects of friction and rotary inertia, while focusing the attention on the flexible dynamics.

MERIt, includes only joint, current and link strain, no absolute or relative displacement of the links is provided. On the contrary, the model described in sec. 3.1 determines only displacements and orientation of the nodes with respect to the FFR. Absolute nodal positions can then be computed. In order to compare experimental results with simulations, link strains at the stain

gauge positions have been derived from the nodal displacements. The beam elements are 1D from the FE perspective, hence, the strain on the surface of the beam must be computed starting from the transversal deflection. The deflection of three consecutive nodes, placed at a relative distance of 1.5 mm have been calculated by means of the $\boldsymbol{S}_i$ shape matrices. Then, recalling that the FFR presents no deflection, a cubic function $\Omega(x) = Ax^3 + Bx^2 + Cx$, describing deflection along the beam length, has been interpolated in the four nodes (FFR and three nodes around the gauge position). Finally, considering that strain is proportional to the second derivative of the deflection with respect to the beam length coordinate x, we can compute the strain $\epsilon(i)$ at point x_i along the beam as follows: $\epsilon(i) = (6Ax_i + 2B)(h_{section}/2)$.

Remark 5. The approach adopted here in order to derive the strain is feasible for beam-like structures. In the case of more complex FE models it is possible to obtain some *strain matrices*, namely $\mathbf{S_i^{st}}$ which directly relate the strain of a FE node i to the modal coordinates through a linear relationship of the kind:

$$\epsilon(i) = \mathbf{S_i^{st}}\mathbf{q} \tag{3.75}$$

For the sake of space limitation, only results related to experiments with a payload of 400 gr. are reported here. All the figures shown in this Section present a comparison between MERIt experimental data, represented by a black solid line, and simulation results, represented by a dashed grey line. First of all, Figs. 3.9 and 3.10 report the joint angles. Though, PID position regulators have been manually tuned, the response generated by the model is so closed to the experimental one that the two curves overlap. On the other hand, concerning the validation of the flexible dynamics, it can be noticed that there is again a good accordance between the simulated model and experimental data. In particular, Figs. 3.11-3.14 show a comparison between the strain gauge measurements and the strain computed by the model, at the same positions, while Fig.3.15 shows a zoom of the strain at $X_{1,1}$ in a small time window. These figures reveal that small differences between simulated and experimental data are due to the effect of material damping, which is a parameter difficult to identify without specific experiments, and static measurement offsets, as it can be seen when the manipulator is stationary (see, e.g., the first 10 seconds of Fig.3.11).

In order to confirm the results of the time domain analysis, a frequency analysis of the strains has been performed as well. Figs. 3.16-3.19 show a comparison between the frequency response of the strain gauge measurements and the strains computed using the model. These figures reveal, again, a good accordance between model and experimental data. In particular, a resonance around 2 Hz is shown by the simulation and experimental data as well. Strains on $X_{1,2}$ and $X_{2,2}$ for an experiment with a 200 g. payload are briefly reported in Figs. 3.20 and 3.21.

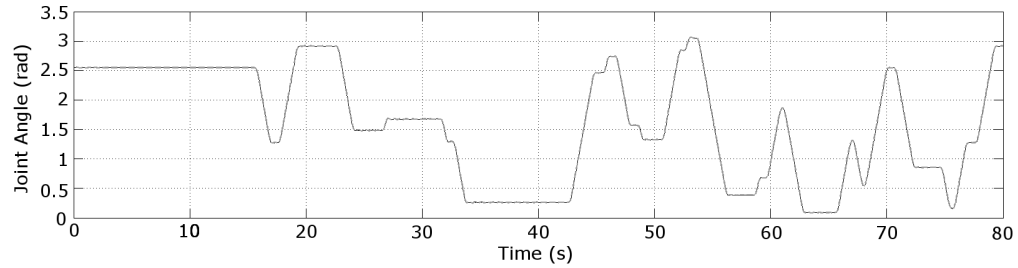

Figure 3.9: First joint angle θ_1, Experimental results (dashed line), and MATLAB simulation (solid line).

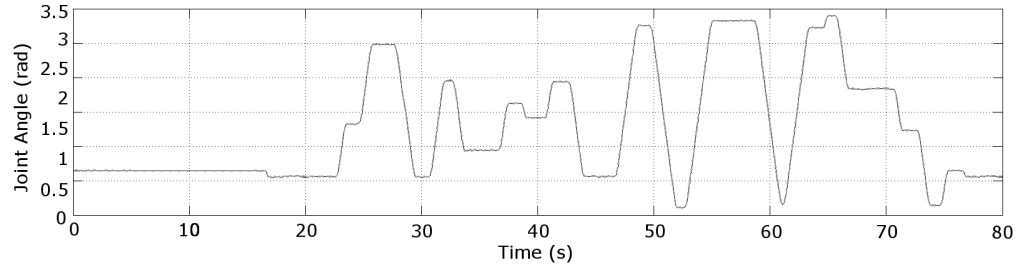

Figure 3.10: Second joint angle θ_2, Experimental results (dashed line), and MATLAB simulation (solid line).

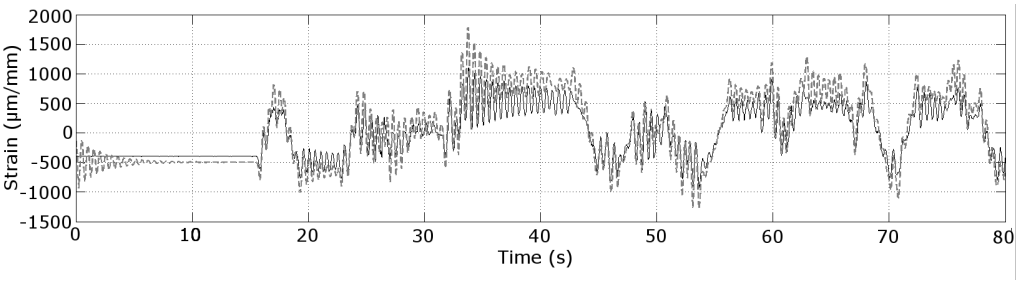

Figure 3.11: Comparison between the strain gauge measurements and the strain computed by the model at the position $X_{1,1}$, Experimental results (dashed line), and MATLAB simulation (solid line).

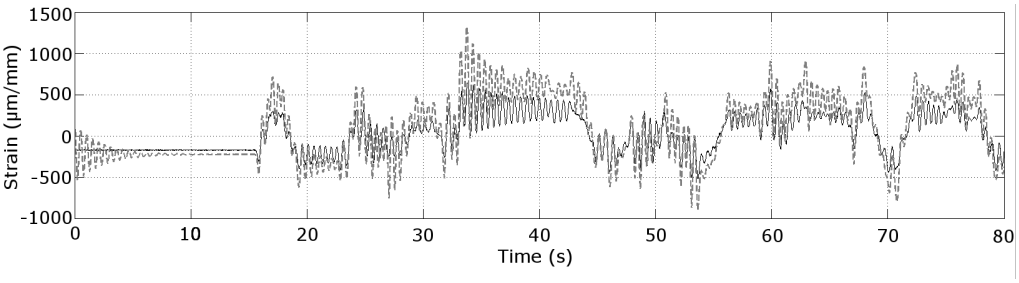

Figure 3.12: Comparison between the strain gauge measurements and the strain computed by the model at the position $X_{1,2}$, Experimental results (dashed line), and MATLAB simulation (solid line).

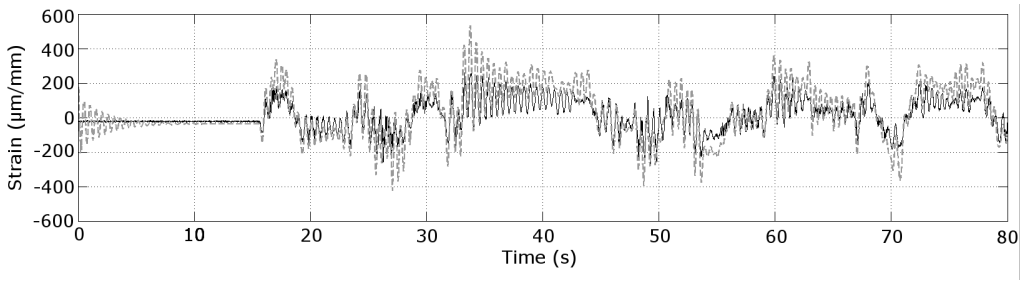

Figure 3.13: Comparison between the strain gauge measurements and the strain computed by the model at the position $X_{2,1}$, Experimental results (dashed line), and MATLAB simulation (solid line).

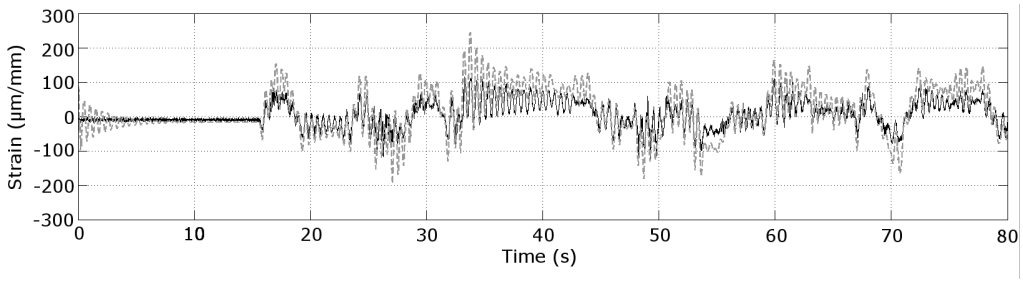

Figure 3.14: Comparison between the strain gauge measurements and the strain computed by the model at the position $X_{2,2}$, Experimental results (dashed line), and MATLAB simulation (solid line).

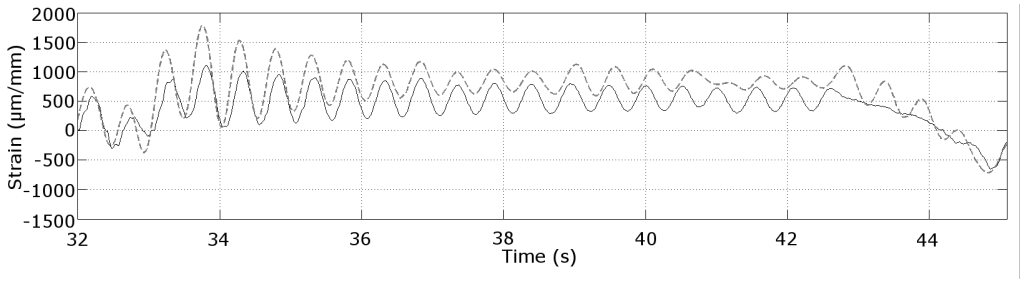

Figure 3.15: Comparison between the strain gauge measurements and the strain computed by the model at the position $X_{1,1}$, Experimental results (dashed line), and MATLAB simulation (solid line).

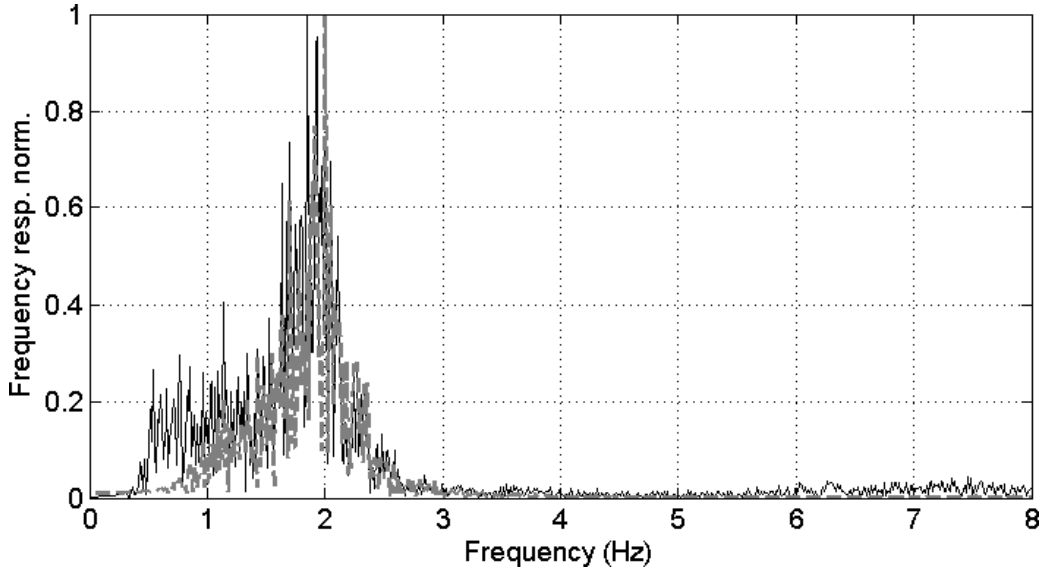

Figure 3.16: Comparison between the FFT of the strain computed by the model and Dymola simulations at the position $X_{1,1}$, Experimental results (dashed line), and MATLAB simulation (solid line).

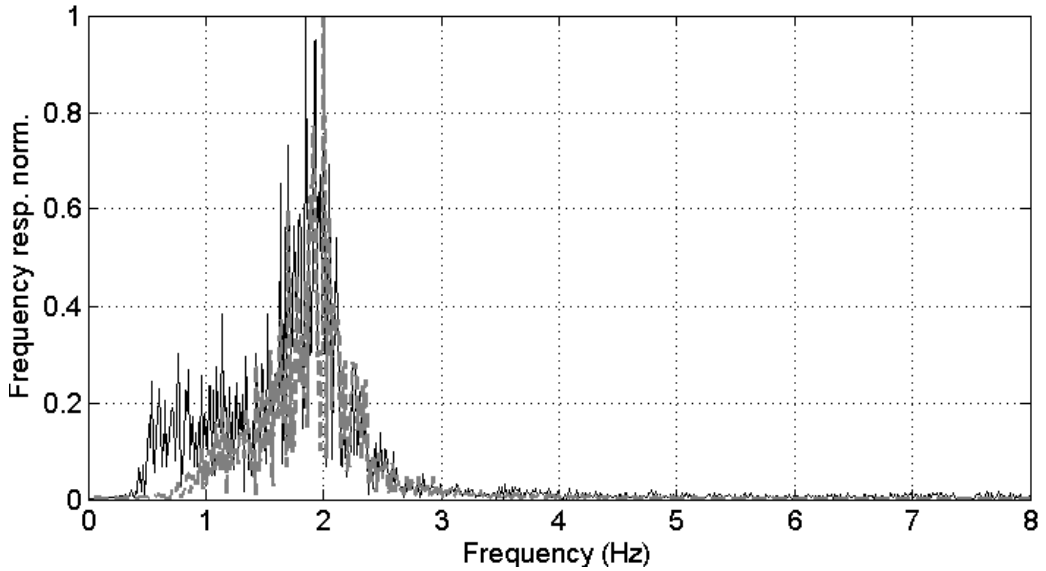

Figure 3.17: Comparison between the FFT of the strain computed by the model and Dymola simulations at the position $X_{1,2}$, Experimental results (dashed line), and MATLAB simulation (solid line).

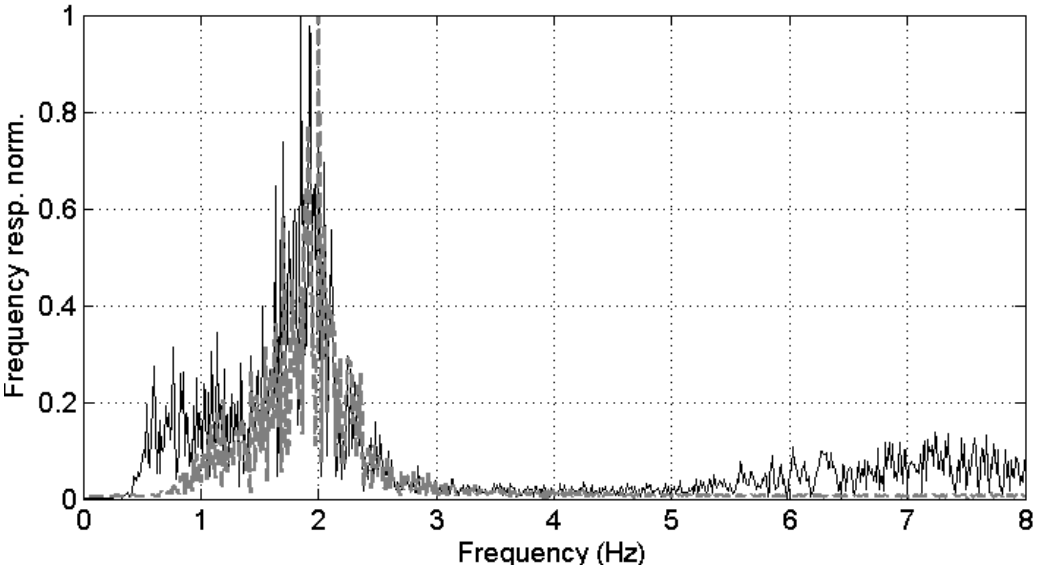

Figure 3.18: Comparison between the FFT of the strain computed by the model and Dymola simulations at the position $X_{2,1}$, Experimental results (dashed line), and MATLAB simulation (solid line).

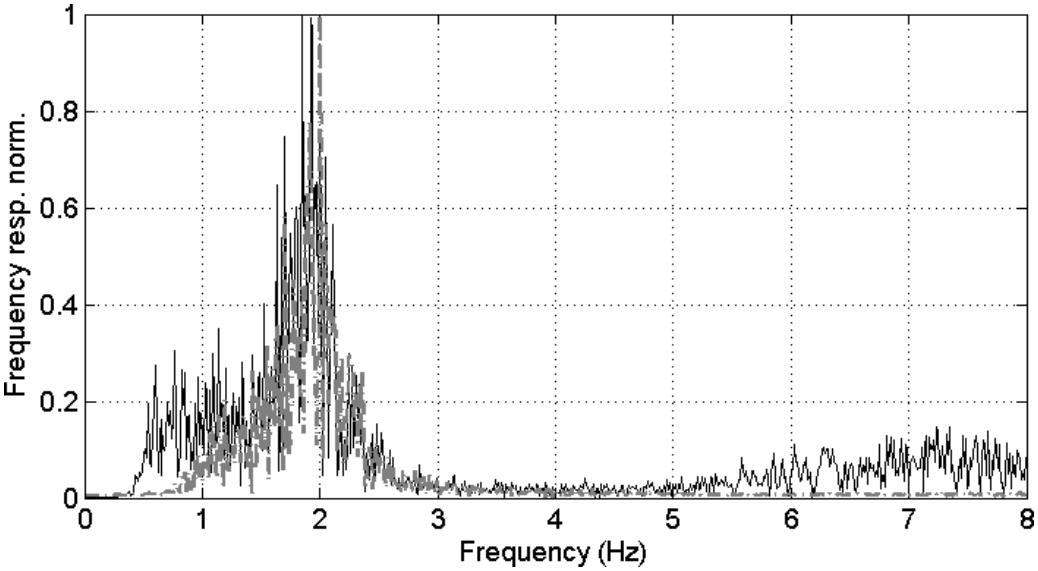

Figure 3.19: Comparison between the FFT of the strain computed by the model and Dymola simulations at the position $X_{2,2}$, Experimental results (dashed line), and MATLAB simulation (solid line).

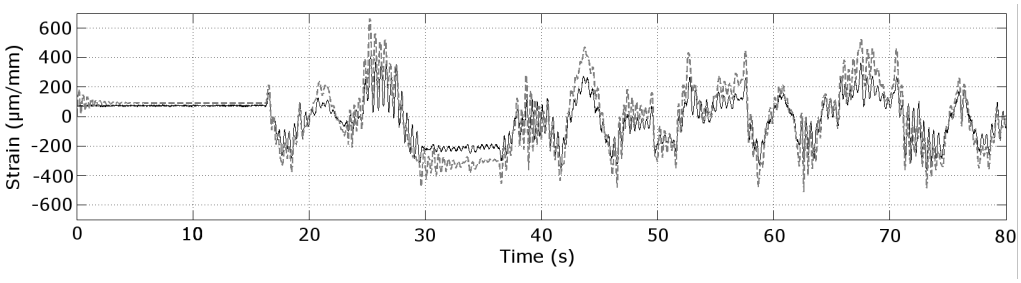

Figure 3.20: Comparison between the strain gauge measurements and the strain computed by the model at the position $X_{2,1}$, Experimental results (dashed line), and MATLAB simulation (solid line) - payload 200 gr.

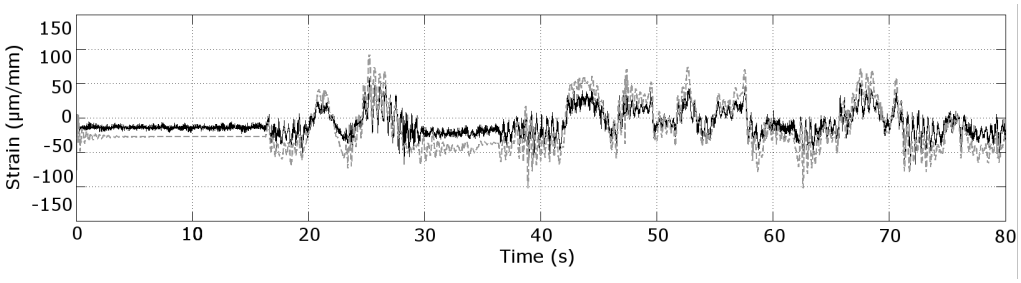

Figure 3.21: Comparison between the strain gauge measurements and the strain computed by the model at the position $X_{2,2}$, Experimental results (dashed line), and MATLAB simulation (solid line) - payload 200 gr.

Chapter 4

Development of a control oriented model

The closed form model described in Chapter 3 is suited for dynamic analysis and simulation but it is affected by several issues when coming to model based control. The model is inherently nonlinear, hence many control synthesis techniques related to model based optimization appear unfeasible or cannot guarantee stability properties, moreover the computational burden required to implement control schemes which rely upon real-time simulation can negatively affect the performances of the control systems. A common approach for the synthesis of control for such complex systems is to derive a simplified model for example by linearizing or by neglecting "fast" dynamics. Unfortunately, when coping with the control of flexible manipulators, the fast dynamics are represented by vibrations and therefore a model based control should rely upon a model where these dynamics are correctly represented.

The techniques based upon the singular perturbation (SP) approach [128], along with the composite control theory [26, 79], allow to overcome this issue by means of a model separation based on time scaling. The aforementioned SP methodologies consider a reduced simplified model in first instance, which is meant to capture the dominant phenomenon characterized by slow dynamics. In second instance the neglected phenomena are carried out by defining a second reduced model as a correction of the simplified one. Furthermore, exploiting the theoretical framework provided by the composite control theory, a separate control law for each subsystem can be synthesized.

A flexible manipulator naturally exhibits a two-time scale behaviour where the rigid overall motion represent the slowest phenomenon, while the parasitic phenomenon can be associated to the vibrations induced by disturbances or by the motion control. As a consequence, a control problem related to vibration damping in flexible manipulators naturally recalls a modeling approach based on the SP.

In this chapter a model based on the SP method is presented. In fact,

an additional step with respect to the classical SP is here disclosed; the model is developed by means of the integral manifold (IM) approach [72,129], which can be considered as an extension of SP. The IM technique is aimed to overcome the limits of the classical SP by obtaining the reduced order models with an $O(\varepsilon^p)$ approximation, conversely to the $O(\varepsilon)$ approximation adopted in the SP.

4.1 Introduction to the singular perturbation theory

Consider the following singular perturbation model of generic ODE:

$$\dot{x} = f(x, z, u, \varepsilon, t) \tag{4.1}$$
$$\varepsilon \dot{z} = g(x, z, u, \varepsilon, t) \tag{4.2}$$

With the following conditions:

$$x(t_0) = x_0 \tag{4.3}$$
$$z(t_0) = z_0 \tag{4.4}$$

where and $x \in \mathbb{R}^{\mathbb{N}}, z \in \mathbb{R}^{\mathbb{M}}$ are the state variables, u is the vector of control inputs and , ε is a small positive scalar called perturbation parameter. Assume also that f and g are continuously differentiable with respect to all their arguments. Since the perturbation parameter ε is supposed to be small, the velocity $\dot{z} = g/\varepsilon$ can be large with respect to the velocity of the state variables x and therefore the state variables z are supposed to quickly approach a quasi-steady state trajectory. Conversely,the x state variables are are subject to slower transients. Therefore,the singularly perturbed dynamic system exhibits a two time scale behaviour, provided that the perturbation parameter is properly choosen. Loosely speaking, the z substate represents the "parasitic" phenomena which are responsible for the presence of higher order terms in the dynamic model. Supposing $\varepsilon = 0$ one finds an approximate solution of the initial problem which takes into account only the dominant phenomena. In this case, the dimension of the state space shrinks from $N + M$ to M, and the state equation (4.2) degenerates into the algebraic equation

$$0 = g(\bar{x}, \bar{z}, \bar{u}, 0, t) \tag{4.5}$$

where the bar here denotes that the variables belong to the system with $\varepsilon = 0$.

The model 4.1,4.2 is said to be in *standard form* if and only if equation 4.5 has $k \geq 0$ distinct real roots.

$$\bar{z} = \phi_i(\bar{x}, \bar{u}, t), \quad i = 1, 2, ...k \tag{4.6}$$

Assuming that the model (4.1,4.2) is in standard form, for every $i = 1, 2, ...k$ there exist a reduced order model obtained by substituting $\phi_i(\bar{x}, \bar{u}, t)$ into

equation 4.1 as follows:

$$\dot{\bar{x}} = f(\bar{x}, \phi_i(\bar{x}, \bar{u}, t), \bar{u}, 0, t) \tag{4.7}$$

Equation (4.7) represents the *quasi steady state* model where the state is supposed to converge when the z variables have rapidly converged to a root of (4.6), hence the model represents the slow part of (4.1,4.2). As a consequence $\bar{x}$ is an $O(\varepsilon)$ approximation of x uniformely in the interval $[t_0, T]$.

$$x = \bar{x}(t) + O(\varepsilon) \tag{4.8}$$

The z state variables do not undergo the the same approximation in the whole interval $[t_0, T]$. Consider a *quasi steady state* $\bar{z}$. The initial value at time t_0 is:

$$\bar{z}(t_0) = \bar{\phi}_i(\bar{x}(t_0), t_0) \tag{4.9}$$

which can significantly differ from the initial condition z_0. As a consequence, the approximation:

$$z = \bar{z}(t) + O(\varepsilon) \tag{4.10}$$

is conversely valid only after the original variable z converges to its *quasi steady state* $\bar{z}$ that is for $t \in [t_1, T]$, being $t_1 > t_0$. In the interval $[t_0, t_1]$ the system is subject to a transient, which deserves to be analyzed.

Consider the time variable τ defined as follows:

$$\tau = \frac{t - t_0}{\varepsilon} \tag{4.11}$$

The τ time is 0 at initial time and rapidly grows for $t > t_0$. The rate of growth depends on the ε parameter. The following differential relation holds:

$$\frac{d\tau}{dt} = \frac{1}{\varepsilon} \tag{4.12}$$

Then, consider a variable $\hat{z}(\tau)$ which represents the discrepancy between the original z and the approximation $\bar{z}$ in such way:

$$z = \bar{z}(t) + \hat{z}(\tau) \tag{4.13}$$

$\hat{z}$ is called *boundary layer correction* and is function of τ, because it vanishes as z tends to $\bar{z}$ after a fast transient.

In order to describe the transient it is possible to define a *boundary layer system*

$$\frac{d\hat{z}}{d\tau} = g(x_0, \hat{z}(\tau) + \bar{z}(t_0), 0, t_0), \quad \hat{z}(0) = z_0 - \bar{z}(t_0) \tag{4.14}$$

where x_0, t_0 and $\bar{z}$ can be considered as fixed in the τ-time scale.

It must be pointed out that the correctness of the approximation stated in eq (4.13) is related to the stability of the system (4.14). The proof (Tikhonov's theorem) can be found in [141], [61]. In order to formally derive

the approximations (4.8) and (4.13) consider the derivatives of x and z with respect to t and τ.

$$\dot{\bar{x}}(t) + \frac{d\hat{x}}{d\tau}\frac{d\tau}{dt} = f(\bar{x}+\hat{x}, \bar{z}+\hat{z}, \varepsilon, t) \tag{4.15}$$

$$\varepsilon\dot{\bar{z}}(t) + \varepsilon\frac{d\hat{z}}{d\tau}\frac{d\tau}{dt} = g(\bar{x}+\hat{x}, \bar{z}+\hat{z}, \varepsilon, t) \tag{4.16}$$

Substituting the quasi-steady-state reduced model (4.7) into (4.15) yelds

$$\frac{d\hat{x}}{d\tau} = \varepsilon[f(\bar{x}+\hat{x}, \bar{z}+\hat{z}, \varepsilon, t) - f(\bar{x}, \bar{z}, 0, t)] \tag{4.17}$$

As a consequence, when ε tends to 0, also $d\hat{x}/d\tau$ does, hence if $\varepsilon = 0$ and $\bar{x}(t_0) = x_0$, then $\hat{x}(\tau)$ is equal to 0. Moreover, given that the right hand side of 4.17 is bounded, then $x(t,\varepsilon) \to \bar{x}(t)$ and approximation 4.8 is valid. On the other hand equation 4.16 yelds

$$\frac{d\bar{z}(\tau)}{t\tau} = g(\bar{x}(t), \bar{z}(t)+\hat{z}(\tau), \varepsilon, t) - \varepsilon\dot{\bar{z}}, \quad \hat{z}(0) = z_0 - \bar{z}(t_0) \tag{4.18}$$

4.2 The singularly perturbed model of flexible manipulator

In this section, the singularly perturbed model of manipulator will be derived. Consider the closed-form model described in Chapter 3 where the damping is neglected[1]:

$$\begin{bmatrix} \boldsymbol{\mathcal{M}}_{\theta\theta} & \boldsymbol{\mathcal{M}}_{\theta q} \\ \boldsymbol{\mathcal{M}}_{\theta q}^T & \boldsymbol{\mathcal{M}}_{qq} \end{bmatrix} \begin{bmatrix} \ddot{\boldsymbol{\theta}} \\ \ddot{\boldsymbol{q}} \end{bmatrix} + \begin{bmatrix} \boldsymbol{\mathcal{C}}_\theta \\ \boldsymbol{\mathcal{C}}_{\boldsymbol{q}} \end{bmatrix} + \begin{bmatrix} \mathbf{0} \\ \boldsymbol{\mathcal{K}}_e \boldsymbol{q} \end{bmatrix} = \begin{bmatrix} \boldsymbol{\tau} \\ \mathbf{0} \end{bmatrix} \tag{4.19}$$

and consider the inverse of the inertia matrix as follows:

$$\begin{bmatrix} \boldsymbol{\mathcal{M}}_{\theta\theta} & \boldsymbol{\mathcal{M}}_{\theta q} \\ \boldsymbol{\mathcal{M}}_{\theta q}^T & \boldsymbol{\mathcal{M}}_{qq} \end{bmatrix}^{-1} = \begin{bmatrix} \boldsymbol{\mathcal{H}}_{\theta\theta} & \boldsymbol{\mathcal{H}}_{\theta q} \\ \boldsymbol{\mathcal{H}}_{q\theta} & \boldsymbol{\mathcal{H}}_{qq} \end{bmatrix} \tag{4.20}$$

The original model can be explicitly written as:

$$\ddot{\boldsymbol{\theta}} = -\boldsymbol{\mathcal{H}}_{\theta\theta}\boldsymbol{\mathcal{C}}_\theta - \boldsymbol{\mathcal{H}}_{\theta q}\boldsymbol{\mathcal{C}}_{\boldsymbol{q}} + \boldsymbol{\mathcal{H}}_{\theta\theta}\boldsymbol{u} - \boldsymbol{\mathcal{H}}_{\theta q}\boldsymbol{\mathcal{K}}_e\boldsymbol{q} \tag{4.21}$$

$$\ddot{\boldsymbol{q}} = -\boldsymbol{\mathcal{H}}_{q\theta}\boldsymbol{\mathcal{C}}_\theta - \boldsymbol{\mathcal{H}}_{qq}\boldsymbol{\mathcal{C}}_{\boldsymbol{q}} + \boldsymbol{\mathcal{H}}_{q\theta}\boldsymbol{u} - \boldsymbol{\mathcal{H}}_{qq}\boldsymbol{\mathcal{K}}_e\boldsymbol{q} \tag{4.22}$$

where $u = \tau$

Since the parasitic phenomenon which we want to confine in the boundary layer correction are the manipulator vibrations, it is convenient to relate the perturbation parameter to the system stiffness. Recalling that the stiffness matrix $\boldsymbol{\mathcal{K}}_e$ is supposed to be a diagonal one can define:

[1] The sngularly perturbed model described here and the Integral manifold model described in the following section are intended for control purposes, hence structural damping can be neglected as it positively contributes in vibration control.

$$k_e = \min\{k_{e,j,i}\} \ , \ \varepsilon = \frac{1}{\sqrt{k_e}} \tag{4.23}$$

A scaled stiffness matrix $\bar{\boldsymbol{\mathcal{K}}}_e$ is conveniently defined as follows:

$$\bar{\boldsymbol{\mathcal{K}}}_e = \varepsilon^2 \boldsymbol{\mathcal{K}}_e \tag{4.24}$$

It must be pointed out that, due to the characteristics of the model reduction exerted by the FE packages which orthogonalize the vibration modes, the stiffness matrix contains the squares of the links' natural frequencies. The perturbation parameter is consequently equal to the inverse of the links' lowest natural frequency.

Two subsets of the state variables can be defined:

$$\boldsymbol{x} = \begin{bmatrix} \boldsymbol{x}_1 \\ \boldsymbol{x}_2 \end{bmatrix} = \begin{bmatrix} \boldsymbol{\theta} \\ \dot{\boldsymbol{\theta}} \end{bmatrix} \ , \ \boldsymbol{z} = \begin{bmatrix} \boldsymbol{z}_1 \\ \boldsymbol{z}_2 \end{bmatrix} = \begin{bmatrix} \boldsymbol{\mathcal{K}}_e \boldsymbol{q} \\ \varepsilon \boldsymbol{\mathcal{K}}_e \dot{\boldsymbol{q}} \end{bmatrix} \tag{4.25}$$

and the equations (4.21,4.22) can be written as follows:

$$\begin{aligned} \dot{\boldsymbol{x}}_1 &= \boldsymbol{x}_2 \\ \dot{\boldsymbol{x}}_2 &= -\boldsymbol{\mathcal{H}}_{\theta\theta}(\boldsymbol{x}_1, \varepsilon^2 \bar{\boldsymbol{\mathcal{K}}}_e^{-1} \boldsymbol{z}_1) \boldsymbol{\mathcal{C}}_\theta(\boldsymbol{x}_1, \varepsilon^2 \bar{\boldsymbol{\mathcal{K}}}_e^{-1} \boldsymbol{z}_1, \boldsymbol{x}_2, \varepsilon \bar{\boldsymbol{\mathcal{K}}}_e^{-1} \boldsymbol{z}_2) \\ &\quad -\boldsymbol{\mathcal{H}}_{\theta q}(\boldsymbol{x}_1, \varepsilon^2 \bar{\boldsymbol{\mathcal{K}}}_e^{-1} \boldsymbol{z}_1) \boldsymbol{\mathcal{C}}_{\boldsymbol{q}}(\boldsymbol{x}_1, \varepsilon^2 \bar{\boldsymbol{\mathcal{K}}}_e^{-1} \boldsymbol{z}_1, \boldsymbol{x}_2, \varepsilon \bar{\boldsymbol{\mathcal{K}}}_e^{-1} \boldsymbol{z}_2) \\ &\quad +\boldsymbol{\mathcal{H}}_{\theta\theta}(\boldsymbol{x}_1, \varepsilon^2 \bar{\boldsymbol{\mathcal{K}}}_e^{-1} \boldsymbol{z}_1) \boldsymbol{u} - \boldsymbol{\mathcal{H}}_{\theta q}(\boldsymbol{x}_1, \varepsilon^2 \bar{\boldsymbol{\mathcal{K}}}_e^{-1} \boldsymbol{z}_1) \boldsymbol{z}_1 \end{aligned} \tag{4.26}$$

$$\begin{aligned} \varepsilon \dot{\boldsymbol{z}}_1 &= \boldsymbol{z}_2 \\ \varepsilon \bar{\boldsymbol{\mathcal{K}}}_e^{-1} \dot{\boldsymbol{z}}_2 &= -\boldsymbol{\mathcal{H}}_{q\theta}(\boldsymbol{x}_1, \varepsilon^2 \bar{\boldsymbol{\mathcal{K}}}_e^{-1} \boldsymbol{z}_1) \boldsymbol{\mathcal{C}}_\theta(\boldsymbol{x}_1, \varepsilon^2 \bar{\boldsymbol{\mathcal{K}}}_e^{-1} \boldsymbol{z}_1, \boldsymbol{x}_2, \varepsilon \bar{\boldsymbol{\mathcal{K}}}_e^{-1} \boldsymbol{z}_2) \\ &\quad -\boldsymbol{\mathcal{H}}_{qq}(\boldsymbol{x}_1, \varepsilon^2 \bar{\boldsymbol{\mathcal{K}}}_e^{-1} \boldsymbol{z}_1) \boldsymbol{\mathcal{C}}_{\boldsymbol{q}}(\boldsymbol{x}_1, \varepsilon^2 \bar{\boldsymbol{\mathcal{K}}}_e^{-1} \boldsymbol{z}_1, \boldsymbol{x}_2, \varepsilon \bar{\boldsymbol{\mathcal{K}}}_e^{-1} \boldsymbol{z}_2) \\ &\quad +\boldsymbol{\mathcal{H}}_{q\theta}(\boldsymbol{x}_1, \varepsilon^2 \bar{\boldsymbol{\mathcal{K}}}_e^{-1} \boldsymbol{z}_1) \boldsymbol{u} - \boldsymbol{\mathcal{H}}_{qq}(\boldsymbol{x}_1, \varepsilon^2 \bar{\boldsymbol{\mathcal{K}}}_e^{-1} \boldsymbol{z}_1) \boldsymbol{z}_1 \end{aligned} \tag{4.27}$$

Finally, following the singular perturbation theory, two subsystems can be derived from equations (4.26, 4.27). Considering (4.27) where $\varepsilon = 0$ and solving one obtains:

$$\begin{aligned} \bar{\boldsymbol{z}}_2 &= 0 \\ \bar{\boldsymbol{z}}_1 &= -\boldsymbol{\mathcal{H}}_{qq}^{-1}(\bar{\boldsymbol{x}}_1, 0) \boldsymbol{\mathcal{H}}_{q\theta}(\bar{\boldsymbol{x}}_1, 0) [\bar{\boldsymbol{u}} \boldsymbol{\mathcal{C}}_\theta(\bar{\boldsymbol{x}}_1, 0, \bar{\boldsymbol{x}}_2, 0)] \\ &\quad +\boldsymbol{\mathcal{C}}_{\boldsymbol{q}}(\bar{\boldsymbol{x}}_1, 0, \bar{\boldsymbol{x}}_2, 0) \end{aligned} \tag{4.28}$$

It must be recalled that $\boldsymbol{\mathcal{C}}_{\boldsymbol{q}}$ is inherently equal to zero if the elastic variables and their derivatives are zero.

The slow subsystem is derived from (4.26) considering $\varepsilon = 0$ and (4.28):

$$\begin{aligned} \dot{\bar{\boldsymbol{x}}}_1 &= \bar{\boldsymbol{x}}_2 \\ \dot{\bar{\boldsymbol{x}}}_2 &= \boldsymbol{\mathcal{H}}_{\theta\theta}(\bar{\boldsymbol{x}}_1, 0) + \boldsymbol{\mathcal{H}}_{\theta q}(\bar{\boldsymbol{x}}_1, 0) \boldsymbol{\mathcal{H}}_{qq}^{-1}(\bar{\boldsymbol{x}}_1, 0) \boldsymbol{\mathcal{H}}_{q\theta}(\bar{\boldsymbol{x}}_1, 0) [\bar{\boldsymbol{u}} \\ &\quad -\boldsymbol{\mathcal{C}}_\theta(\bar{\boldsymbol{x}}_1, 0, \bar{\boldsymbol{x}}_2, 0)] \end{aligned} \tag{4.29}$$

Applying the Shur complement[2] the slow subsystem can be rewritten as:

$$\begin{aligned} \dot{\bar{\boldsymbol{x}}}_1 &= \bar{\boldsymbol{x}}_2 \\ \dot{\bar{\boldsymbol{x}}}_2 &= \boldsymbol{\mathcal{M}}_{\theta\theta}^{-1}(\bar{\boldsymbol{x}}_1, 0)[\bar{\boldsymbol{u}} - \boldsymbol{\mathcal{C}}_\theta(\bar{\boldsymbol{x}}_1, 0, \bar{\boldsymbol{x}}_2, 0)] \end{aligned} \tag{4.30}$$

Which coincides with the rigid manipulator model.

Considering $\tau = t/\varepsilon$ as the fast timescale and $\boldsymbol{\eta}_1 = \boldsymbol{z}_1 - \bar{\boldsymbol{z}}_1$, $\boldsymbol{\eta}_2 = \boldsymbol{z}_2 - \bar{\boldsymbol{z}}_2$, the boundary layer system is:

$$\begin{aligned} \frac{d\boldsymbol{\eta}_1}{d\tau} &= \boldsymbol{\eta}_2 \\ \frac{d\boldsymbol{\eta}_2}{d\tau} &= -\boldsymbol{\mathcal{H}}_{qq}(\bar{\boldsymbol{x}}_1, 0)\boldsymbol{\eta}_1 + \boldsymbol{\mathcal{H}}_{q\theta}(\bar{\boldsymbol{x}}_1, 0)(\boldsymbol{u} - \bar{\boldsymbol{u}}) \end{aligned} \tag{4.31}$$

which is linear but parametric in the state of the slow subsystem.

4.3 The integral manifold approach

The singular perturbation approach is a powerful tool to decompose the complex model of manipulator described in Chapter 3, but it is based on the assumption that ε is sufficiently small to preserve the time-scale separation. This assumption can be critical as the manipulator stiffness decreases; the perturbation parameter consequently increases and the nominal bandwidth achieved by the slow controller must be consequently reduced. The integral manifold approach aims to overcome the $O(\varepsilon)$ approximation, in this theory, the reduced order subsystems are obtained by means of a $O(\varepsilon)^p$ approximation, allowing to cope with two timescale modelling of soft manipulators.

Definition 6. (Integral manifold definition)

Consider a n-dimensional surface Σ_t in the s-dimensional space R^s. The surface is defined by m equations, where $m = s - n$. These equations express m state variables as functions of the remaining n. If one considers surfaces that vary with time, explicit functions can be written as follows:

$$\Sigma_t : z = h(x, t) \qquad z \in R^m,\ x \in R^n \tag{4.32}$$

assuming that:

- $\partial h/\partial x$ exist, are continuous and have full rank
- $\partial h/\partial t$ exist, are continuous over the interval of interest, which should preferably be infinite.

[2] $\boldsymbol{\mathcal{M}}_{\theta\theta}^{-1}(\bar{\boldsymbol{x}}_1, 0) = \boldsymbol{\mathcal{H}}_{\theta\theta}(\bar{\boldsymbol{x}}_1, 0) + \boldsymbol{\mathcal{H}}_{\theta q}(\bar{\boldsymbol{x}}_1, 0)\boldsymbol{\mathcal{H}}_{qq}^{-1}(\bar{\boldsymbol{x}}_1, 0)\boldsymbol{\mathcal{H}}_{q\theta}(\bar{\boldsymbol{x}}_1, 0)$

Then, consider the dynamic system Δ_t:

$$\begin{aligned} \dot{x} &= f(x, z, t) \\ \dot{z} &= g(x, z, t), \end{aligned} \tag{4.33}$$

A surface Σ_t is an *integral manifold* for the system Δ_t if every solution $z(t), x(t)$ of Δ_t which is in the surface Σ_t at $t = t_0$ remains in Σ_t for all $t \in (t_0, t_1)$, that is

$$z(t) = h(x(t), t) \qquad t \in (t_0, t_1) \tag{4.34}$$

In practice, an *integral manifold* is a surface on which the system remains for all $t > t_0$ given that it is on the surface at $t = t_0$.

Definition 7. (Manifold condition)
If $\Sigma : z = h(x, t)$ satisfies the partial differential equation:

$$\frac{\partial h}{\partial t} + \frac{\partial h}{\partial x} f(x, h(x, t), t) = g(x, h(x, t), t) \tag{4.35}$$

the surface Σ is an integral manifold for the system (4.33)

If one can find the manifold equation $h(x, t)$, the system's dynamics is restricted to the manifold, so it can be described by the following n-th order system:

$$\dot{x} = f(x, h(x, t), t) \qquad x \in R^n \tag{4.36}$$

However, it must be recalled that the reduced-order system is an correct reduction only if the system's state belongs to the manifold at $t = t_0$, i.e. $z(t_0) = h(x(t_0), t_0)$. Whenever the system is not on the manifold at the initial state, the distance between the system's state $z(t)$ and the manifold can be described by a new set of coordinates, in turn:

$$\eta = z - h(x, t) \qquad \eta \in R^m \tag{4.37}$$

In order to obtain a description of the *off*-manifold one can differentiate η with respect to time, as follows:

$$\dot{\eta} = g(x, \eta + h(x, t), t) - \frac{\partial h}{\partial x} f(x, \eta + h(x, t), t) - \frac{\partial h}{\partial t} \tag{4.38}$$

Conversely, when the initial *off*-manifold transient ends, the system reaches an equilibrium with $\eta = 0$. During this phase the *on*-manifold system is described by equation 4.36. In the following section it will be shown how the integral manifold approach can be exploited in order to tackle with the flexible manipulators modelling, where the *on*-manifold subsystem represents the dominant phenomena and the *off*-manifold takes into account the fast dynamics.

4.4 An integral manifold model of flexible manipulators

Consider the flexible manipulator model described in the previous section; if the flexibility is described by $\boldsymbol{q} \in R^{n_c}$ modal state variables, an integral manifold Σ_e with dimension $2n_c$ can be introduced as follows:

$$\begin{aligned} \bar{\boldsymbol{z}}_1 &= \boldsymbol{h}_1(\boldsymbol{x}_1, \boldsymbol{x}_2, \boldsymbol{u}, \varepsilon) \\ \bar{\boldsymbol{z}}_2 &= \boldsymbol{h}_2(\boldsymbol{x}_1, \boldsymbol{x}_2, \boldsymbol{u}, \varepsilon) \end{aligned} \tag{4.39}$$

The application of the aforementioned manifold condition (4.35) to the system expressed in (4.26, 4.27) yelds to the following constraint:

$$\begin{aligned} \varepsilon \dot{\boldsymbol{h}}_1 &= \boldsymbol{h}_2 \\ \varepsilon \bar{\boldsymbol{\mathcal{K}}}_e^{-1} \dot{\boldsymbol{h}}_2 &= -\boldsymbol{\mathcal{H}}_{q\theta}(\boldsymbol{x}_1, \varepsilon^2 \bar{\boldsymbol{\mathcal{K}}}_e^{-1} \boldsymbol{h}_1) \boldsymbol{\mathcal{C}}_\theta(\boldsymbol{x}_1, \varepsilon^2 \bar{\boldsymbol{\mathcal{K}}}_e^{-1} \boldsymbol{h}_1, \boldsymbol{x}_2, \varepsilon \bar{\boldsymbol{\mathcal{K}}}_e^{-1} \boldsymbol{h}_2) \\ &\quad -\boldsymbol{\mathcal{H}}_{qq}(\boldsymbol{x}_1, \varepsilon^2 \bar{\boldsymbol{\mathcal{K}}}_e^{-1} \boldsymbol{h}_1) \boldsymbol{\mathcal{C}}_{\boldsymbol{q}}(\boldsymbol{x}_1, \varepsilon^2 \bar{\boldsymbol{\mathcal{K}}}_e^{-1} \boldsymbol{z}_1, \boldsymbol{x}_2, \varepsilon \bar{\boldsymbol{\mathcal{K}}}_e^{-1} \boldsymbol{z}_2) \\ &\quad +\boldsymbol{\mathcal{H}}_{q\theta}(\boldsymbol{x}_1, \varepsilon^2 \bar{\boldsymbol{\mathcal{K}}}_e^{-1} \boldsymbol{h}_1) \boldsymbol{u} - \boldsymbol{\mathcal{H}}_{qq}(\boldsymbol{x}_1, \varepsilon^2 \bar{\boldsymbol{\mathcal{K}}}_e^{-1} \boldsymbol{h}_1) \boldsymbol{h}_1 \end{aligned} \tag{4.40}$$

In order to determine an analytical expression of the manifold, the manifold condition (4.35) should be solved, however this requires the solution of partial differential equations which turns out to be a very tough task. In the following, an approximation of Σ_e based on a series expansion at the $O(\varepsilon^3)$ will be considered. Assume the series expansion relative to the manifold condition for $\boldsymbol{z}_1$ and $\boldsymbol{z}_2$ as follows:

$$\begin{aligned} \bar{\boldsymbol{z}}_1 &= \boldsymbol{h}_1(\boldsymbol{x}_1, \boldsymbol{x}_2, \bar{\boldsymbol{u}}, \boldsymbol{0}) + \frac{\partial \boldsymbol{h}_1(\boldsymbol{x}_1, \boldsymbol{x}_2, \bar{\boldsymbol{u}}, \varepsilon)}{\partial \varepsilon} \varepsilon + \frac{\partial^2 \boldsymbol{h}_1(\boldsymbol{x}_1, \boldsymbol{x}_2, \bar{\boldsymbol{u}}, \varepsilon)}{\partial \varepsilon^2} \varepsilon^2 + O(\varepsilon^3) \\ &= \boldsymbol{h}_1^0 + \boldsymbol{h}_1^1 \varepsilon + \boldsymbol{h}_1^2 \varepsilon^2 + O(\varepsilon^3) \qquad (4.41) \\ \bar{\boldsymbol{z}}_2 &= \boldsymbol{h}_2(\boldsymbol{x}_1, \boldsymbol{x}_2, \bar{\boldsymbol{u}}, \boldsymbol{0}) + \frac{\partial \boldsymbol{h}_2(\boldsymbol{x}_1, \boldsymbol{x}_2, \bar{\boldsymbol{u}}, \varepsilon)}{\partial \varepsilon} \varepsilon + \frac{\partial^2 \boldsymbol{h}_2(\boldsymbol{x}_1, \boldsymbol{x}_2, \bar{\boldsymbol{u}}, \varepsilon)}{\partial \varepsilon^2} \varepsilon^2 + O(\varepsilon^3) \\ &= \boldsymbol{h}_2^0 + \boldsymbol{h}_2^1 \varepsilon + \boldsymbol{h}_2^2 \varepsilon^2 + O(\varepsilon^3) \qquad (4.42) \\ \bar{\boldsymbol{u}} &= \bar{\boldsymbol{u}}^0 + \bar{\boldsymbol{u}}^1 \varepsilon + \bar{\boldsymbol{u}}^2 \varepsilon^2 + O(\varepsilon^3) \qquad (4.43) \end{aligned}$$

The approximated formulation of the manifold will be substitued in equation (4.40) in order to calculate the terms of the expansion explicitely. To this purpose, all the terms of eqns. (4.21,4.22) must be expanded consistently.

$$\begin{aligned}
\boldsymbol{\mathcal{H}}_{q\theta}(\boldsymbol{x}_1, \varepsilon^2\bar{\boldsymbol{\mathcal{K}}}_e^{-1}\boldsymbol{z}_1) &= \boldsymbol{\mathcal{H}}_{q\theta}(\boldsymbol{x}_1, \boldsymbol{0}) \\
&\quad +\varepsilon^2 \sum_{i=1}^{N}\sum_{j=1}^{M_i} \frac{1}{\bar{k}_{e,j,i}} \frac{\partial \boldsymbol{\mathcal{H}}_{q\theta}(\boldsymbol{\theta}, \boldsymbol{q})}{\partial q_{j,i}}\bigg|_{\boldsymbol{q}=\boldsymbol{0}} h^0_{1,j,i} + O(\varepsilon^3) \\
&= \boldsymbol{\mathcal{H}}_{q\theta}(\boldsymbol{x}_1, \boldsymbol{0}) + \varepsilon^2 \hat{\boldsymbol{\mathcal{H}}}_{q\theta}(\boldsymbol{x}_1, \boldsymbol{0}) + O(\varepsilon^3) \qquad (4.44) \\
\boldsymbol{\mathcal{H}}_{qq}(\boldsymbol{x}_1, \varepsilon^2\bar{\boldsymbol{\mathcal{K}}}_e^{-1}\boldsymbol{z}_1) &= \boldsymbol{\mathcal{H}}_{qq}(\boldsymbol{x}_1, \boldsymbol{0}) \\
&\quad +\varepsilon^2 \sum_{i=1}^{N}\sum_{j=1}^{M_i} \frac{1}{\bar{k}_{e,j,i}} \frac{\partial \boldsymbol{\mathcal{H}}_{qq}(\boldsymbol{\theta}, \boldsymbol{q})}{\partial q_{j,i}}\bigg|_{\boldsymbol{q}=\boldsymbol{0}} h^0_{1,j,i} + O(\varepsilon^3) \\
&= \boldsymbol{\mathcal{H}}_{qq}(\boldsymbol{x}_1, \boldsymbol{0}) + \varepsilon^2 \hat{\boldsymbol{\mathcal{H}}}_{qq}(\boldsymbol{x}_1, \boldsymbol{0}) + O(\varepsilon^3) \qquad (4.45)
\end{aligned}$$

$$\begin{aligned}
&\boldsymbol{\mathcal{C}}_\theta(\boldsymbol{x}_1, \varepsilon^2\bar{\boldsymbol{\mathcal{K}}}_e^{-1}\boldsymbol{z}_1, \boldsymbol{x}_2, \varepsilon\bar{\boldsymbol{\mathcal{K}}}_e^{-1}\boldsymbol{z}_2) = \boldsymbol{\mathcal{C}}_\theta(\boldsymbol{x}_1, \boldsymbol{0}, \boldsymbol{x}_2, \boldsymbol{0}) \\
&+\varepsilon^2 \sum_{i=1}^{N}\sum_{j=1}^{M_i} \frac{1}{\bar{k}_{e,j,i}} \frac{\partial \boldsymbol{\mathcal{C}}_\theta(\boldsymbol{\theta}, \boldsymbol{q}, \dot{\boldsymbol{\theta}}, \dot{\boldsymbol{q}})}{\partial q_{j,i}}\bigg|_{\boldsymbol{q}=\boldsymbol{0}} h^0_{1,j,i} \\
&+\varepsilon \sum_{i=1}^{N}\sum_{j=1}^{M_i} \frac{1}{\bar{k}_{e,j,i}} \frac{\partial \boldsymbol{\mathcal{C}}_\theta(\boldsymbol{\theta}, \boldsymbol{q}, \dot{\boldsymbol{\theta}}, \dot{\boldsymbol{q}})}{\partial \dot{q}_{j,i}}\bigg|_{\substack{\boldsymbol{q}=\boldsymbol{0} \\ \dot{\boldsymbol{q}}=\boldsymbol{0}}} \left(h^0_{2,j,i} + \varepsilon h^1_{2,j,i}\right) + O(\varepsilon^3) \qquad (4.46) \\
&= \boldsymbol{\mathcal{C}}_\theta(\boldsymbol{x}_1, \boldsymbol{0}, \boldsymbol{x}_2, \boldsymbol{0}) + \varepsilon\tilde{\boldsymbol{\mathcal{C}}}^0_\theta(\boldsymbol{x}_1, \boldsymbol{0}, \boldsymbol{x}_2, \boldsymbol{0}) \\
&+\varepsilon^2 \left(\hat{\boldsymbol{\mathcal{C}}}_\theta(\boldsymbol{x}_1, \boldsymbol{0}, \boldsymbol{x}_2, \boldsymbol{0}) + \tilde{\boldsymbol{\mathcal{C}}}^1_\theta(\boldsymbol{x}_1, \boldsymbol{0}, \boldsymbol{x}_2, \boldsymbol{0})\right)
\end{aligned}$$

$$\begin{aligned}
&\boldsymbol{\mathcal{C}}_{\boldsymbol{q}}(\boldsymbol{x}_1, \varepsilon^2\bar{\boldsymbol{\mathcal{K}}}_e^{-1}\boldsymbol{z}_1, \boldsymbol{x}_2, \varepsilon\bar{\boldsymbol{\mathcal{K}}}_e^{-1}\boldsymbol{z}_2) = \boldsymbol{\mathcal{C}}_{\boldsymbol{q}}(\boldsymbol{x}_1, \boldsymbol{0}, \boldsymbol{x}_2, \boldsymbol{0}) \\
&+\varepsilon^2 \sum_{i=1}^{N}\sum_{j=1}^{M_i} \frac{1}{\bar{k}_{e,j,i}} \frac{\partial \boldsymbol{\mathcal{C}}_{\boldsymbol{q}}(\boldsymbol{\theta}, \boldsymbol{q}, \dot{\boldsymbol{\theta}}, \dot{\boldsymbol{q}})}{\partial q_{j,i}}\bigg|_{\boldsymbol{q}=\boldsymbol{0}} h^0_{1,j,i} \\
&+\varepsilon \sum_{i=1}^{N}\sum_{j=1}^{M_i} \frac{1}{\bar{k}_{e,j,i}} \frac{\partial \boldsymbol{\mathcal{C}}_{\boldsymbol{q}}(\boldsymbol{\theta}, \boldsymbol{q}, \dot{\boldsymbol{\theta}}, \dot{\boldsymbol{q}})}{\partial \dot{q}_{j,i}}\bigg|_{\substack{\boldsymbol{q}=\boldsymbol{0} \\ \dot{\boldsymbol{q}}=\boldsymbol{0}}} \left(h^0_{2,j,i} + \varepsilon h^1_{2,j,i}\right) + O(\varepsilon^3) \qquad (4.47) \\
&= \boldsymbol{\mathcal{C}}_{\boldsymbol{q}}(\boldsymbol{x}_1, \boldsymbol{0}, \boldsymbol{x}_2, \boldsymbol{0}) + \varepsilon\tilde{\boldsymbol{\mathcal{C}}}^0_q(\boldsymbol{x}_1, \boldsymbol{0}, \boldsymbol{x}_2, \boldsymbol{0}) \\
&+\varepsilon^2 \left(\hat{\boldsymbol{\mathcal{C}}}_{\boldsymbol{q}}(\boldsymbol{x}_1, \boldsymbol{0}, \boldsymbol{x}_2, \boldsymbol{0}) + \tilde{\boldsymbol{\mathcal{C}}}^1_q(\boldsymbol{x}_1, \boldsymbol{0}, \boldsymbol{x}_2, \boldsymbol{0})\right)
\end{aligned}$$

where:

$$\begin{aligned}
&\bar{\boldsymbol{\mathcal{H}}}_{q\theta}(\boldsymbol{x}_1, \boldsymbol{0}) = \bar{\boldsymbol{\mathcal{K}}}_e \boldsymbol{\mathcal{H}}_{q\theta}(\boldsymbol{x}_1, \boldsymbol{0}) \ , \ \bar{\hat{\boldsymbol{\mathcal{H}}}}_{q\theta}(\boldsymbol{x}_1, \boldsymbol{0}) = \bar{\boldsymbol{\mathcal{K}}}_e \hat{\boldsymbol{\mathcal{H}}}_{q\theta}(\boldsymbol{x}_1, \boldsymbol{0}) \\
&\bar{\boldsymbol{\mathcal{H}}}_{qq}(\boldsymbol{x}_1, \boldsymbol{0}) = \bar{\boldsymbol{\mathcal{K}}}_e \boldsymbol{\mathcal{H}}_{qq}(\boldsymbol{x}_1, \boldsymbol{0}) \ , \ \bar{\hat{\boldsymbol{\mathcal{H}}}}_{qq}(\boldsymbol{x}_1, \boldsymbol{0}) = \bar{\boldsymbol{\mathcal{K}}}_e \hat{\boldsymbol{\mathcal{H}}}_{qq}(\boldsymbol{x}_1, \boldsymbol{0})
\end{aligned} \qquad (4.48)$$

The partial derivatives of $\boldsymbol{\mathcal{H}}_{\theta\theta}, \boldsymbol{\mathcal{H}}_{\theta q}, \boldsymbol{\mathcal{H}}_{q\theta}$ and $\boldsymbol{\mathcal{H}}_{qq}$[3] with respect to the modal coordinates can be calculated recalling that [4]:

[3] In the following, the arguments of $\boldsymbol{\mathcal{H}}_{\theta\theta}, \boldsymbol{\mathcal{H}}_{\theta q}, \boldsymbol{\mathcal{H}}_{q\theta}, \boldsymbol{\mathcal{H}}_{qq}, \boldsymbol{\mathcal{C}}_\theta, \boldsymbol{\mathcal{C}}_{\boldsymbol{q}}$, their derivatives and their expansions will be omitted for the sake of brevity. The aforementioned quantities are always evaluated in $\boldsymbol{z}_1 = \boldsymbol{z}_2 = 0$

[4] $M^{-1}M = I$,
$M^{-1'}M + M^{-1}M' = 0$,
$M^{-1'} = M^{-1}M'M^{-1}$

$$\begin{bmatrix} \frac{\partial \boldsymbol{\mathcal{H}}_{\theta\theta}}{\partial q_{j,i}} & \frac{\partial \boldsymbol{\mathcal{H}}_{\theta q}}{\partial q_{j,i}} \\ \frac{\partial \boldsymbol{\mathcal{H}}_{q\theta}}{\partial q_{j,i}} & \frac{\partial \boldsymbol{\mathcal{H}}_{qq}}{\partial q_{j,i}} \end{bmatrix} = - \begin{bmatrix} \boldsymbol{\mathcal{H}}_{\theta\theta} & \boldsymbol{\mathcal{H}}_{\theta q} \\ \boldsymbol{\mathcal{H}}_{q\theta} & \boldsymbol{\mathcal{H}}_{qq} \end{bmatrix} \begin{bmatrix} \frac{\partial \boldsymbol{\mathcal{M}}_{\theta\theta}}{\partial q_{j,i}} & \frac{\partial \boldsymbol{\mathcal{M}}_{\theta q}}{\partial q_{j,i}} \\ \frac{\partial \boldsymbol{\mathcal{M}}_{\theta q}^{T}}{\partial q_{j,i}} & \frac{\partial \boldsymbol{\mathcal{M}}_{qq}}{\partial q_{j,i}} \end{bmatrix} \begin{bmatrix} \boldsymbol{\mathcal{H}}_{\theta\theta} & \boldsymbol{\mathcal{H}}_{\theta q} \\ \boldsymbol{\mathcal{H}}_{q\theta} & \boldsymbol{\mathcal{H}}_{qq} \end{bmatrix} \tag{4.49}$$

While the partial derivatives of the components of the mass matrix can be calculated starting from the terms of equations (3.5-3.32) as described in Appendix B.

As mentioned before, the approximated formulation of the manifold is substituted in equation (4.40), yelding the reduced order on-manifold system:

$$\varepsilon \dot{\boldsymbol{h}}_1^0 + \varepsilon^2 \dot{\boldsymbol{h}}_1^1 = \boldsymbol{h}_2^0 + \boldsymbol{h}_2^1 \varepsilon + \boldsymbol{h}_2^2 \varepsilon^2 \tag{4.50}$$

$$\begin{aligned} \varepsilon \dot{\boldsymbol{h}}_2^0 + \varepsilon^2 \dot{\boldsymbol{h}}_2^1 = & - \left(\bar{\boldsymbol{\mathcal{H}}}_{q\theta} + \varepsilon^2 \bar{\hat{\boldsymbol{\mathcal{H}}}}_{q\theta} \right) \left[\boldsymbol{\mathcal{C}}_\theta + \varepsilon \tilde{\boldsymbol{\mathcal{C}}}_\theta^0 + \varepsilon^2 \left(\hat{\boldsymbol{\mathcal{C}}}_\theta + \tilde{\boldsymbol{\mathcal{C}}}_\theta^1 \right) \right] \\ & - \left(\bar{\boldsymbol{\mathcal{H}}}_{qq} + \varepsilon^2 \bar{\hat{\boldsymbol{\mathcal{H}}}}_{qq} \right) \left[\boldsymbol{\mathcal{C}}_{\boldsymbol{q}} + \varepsilon \tilde{\boldsymbol{\mathcal{C}}}_q^0 + \varepsilon^2 \left(\hat{\boldsymbol{\mathcal{C}}}_{\boldsymbol{q}} + \tilde{\boldsymbol{\mathcal{C}}}_q^1 \right) \right] \\ & + \left(\bar{\boldsymbol{\mathcal{H}}}_{q\theta} + \varepsilon^2 \bar{\hat{\boldsymbol{\mathcal{H}}}}_{q\theta} \right) \left(\bar{\boldsymbol{u}}^0 + \bar{\boldsymbol{u}}^1 \varepsilon + \bar{\boldsymbol{u}}^2 \varepsilon^2 \right) \\ & - \left(\bar{\boldsymbol{\mathcal{H}}}_{qq} + \varepsilon^2 \bar{\hat{\boldsymbol{\mathcal{H}}}}_{qq} \right) \left(\boldsymbol{h}_1^0 + \boldsymbol{h}_1^1 \varepsilon + \boldsymbol{h}_1^2 \varepsilon^2 \right) \end{aligned} \tag{4.51}$$

The equivalent powers of ε are equated, obtaining:

$$\boldsymbol{h}_1^0 = -\bar{\boldsymbol{\mathcal{H}}}_{qq}^{-1} \bar{\boldsymbol{\mathcal{H}}}_{q\theta} \left(\boldsymbol{\mathcal{C}}_\theta - \bar{\boldsymbol{u}}^0 \right) - \boldsymbol{\mathcal{C}}_{\boldsymbol{q}} \tag{4.52}$$

$$\boldsymbol{h}_1^1 = -\bar{\boldsymbol{\mathcal{H}}}_{qq}^{-1} \bar{\boldsymbol{\mathcal{H}}}_{q\theta} \bar{\boldsymbol{u}}^1 \tag{4.53}$$

$$\begin{aligned} \boldsymbol{h}_1^2 = & \bar{\boldsymbol{\mathcal{H}}}_{qq}^{-1} \left[-\bar{\boldsymbol{\mathcal{H}}}_{q\theta} \left(\hat{\boldsymbol{\mathcal{C}}}_\theta + \tilde{\boldsymbol{\mathcal{C}}}_\theta^1 - \bar{\boldsymbol{u}}^2 \right) - \bar{\hat{\boldsymbol{\mathcal{H}}}}_{q\theta} \left(\boldsymbol{\mathcal{C}}_\theta - \bar{\boldsymbol{u}}^0 \right) - \bar{\hat{\boldsymbol{\mathcal{H}}}}_{qq} \left(\boldsymbol{\mathcal{C}}_{\boldsymbol{q}} + \boldsymbol{h}_1^0 \right) - \dot{\boldsymbol{h}}_2^1 \right] \\ & - \hat{\boldsymbol{\mathcal{C}}}_q - \tilde{\boldsymbol{\mathcal{C}}}_q^1 \end{aligned} \tag{4.54}$$

$$\boldsymbol{h}_2^0 = \boldsymbol{0} \;\Rightarrow\; \dot{\boldsymbol{h}}_2^0 = \boldsymbol{0} \;,\; \tilde{\boldsymbol{\mathcal{C}}}_\theta^0 = \boldsymbol{0} \;,\; \tilde{\boldsymbol{\mathcal{C}}}_q^0 = \boldsymbol{0} \tag{4.55}$$

$$\boldsymbol{h}_2^1 = \dot{\boldsymbol{h}}_1^0 \tag{4.56}$$

$$\boldsymbol{h}_2^2 = \dot{\boldsymbol{h}}_1^1 \tag{4.57}$$

In order to obtain the equations of the on-manifold subsystem it is possible to substitute the expansions of the matrices into equation (4.26), obtaining:

$$\dot{\boldsymbol{x}}_1 = \boldsymbol{x}_2 \tag{4.58}$$

$$\begin{aligned} \dot{\boldsymbol{x}}_2 = & -(\boldsymbol{\mathcal{H}}_{\theta\theta} + \varepsilon^2 \hat{\boldsymbol{\mathcal{H}}}_{qq})(\boldsymbol{\mathcal{C}}_\theta + \varepsilon^2 [\hat{\boldsymbol{\mathcal{C}}}_\theta + \tilde{\boldsymbol{\mathcal{C}}}_\theta^1]) \\ & -(\boldsymbol{\mathcal{H}}_{\theta q} + \varepsilon^2 \hat{\boldsymbol{\mathcal{H}}}_{\theta q})(\boldsymbol{\mathcal{C}}_{\boldsymbol{q}} + \varepsilon^2 [\hat{\boldsymbol{\mathcal{C}}}_q + \tilde{\boldsymbol{\mathcal{C}}}_q^1]) \\ & -(\boldsymbol{\mathcal{H}}_{\theta\theta} + \varepsilon^2 \hat{\boldsymbol{\mathcal{H}}}_{\theta\theta})(\bar{\boldsymbol{u}}^0 + \varepsilon \bar{\boldsymbol{u}}^1 + \varepsilon^2 \bar{\boldsymbol{u}}^2) \\ & -(\boldsymbol{\mathcal{H}}_{\theta q} + \varepsilon^2 \hat{\boldsymbol{\mathcal{H}}}_{\theta q})(\bar{\boldsymbol{h}}^0 + \varepsilon \bar{\boldsymbol{h}}^1 + \varepsilon^2 \bar{\boldsymbol{h}}^2) \end{aligned} \tag{4.59}$$

which, considering only the terms up to ε^2 and grouping the equal powers of ε yelds:

$$\begin{aligned}
\dot{\boldsymbol{x}}_1 &= \boldsymbol{x}_2 && (4.60)\\
\dot{\boldsymbol{x}}_2 &= -\boldsymbol{\mathcal{H}}_{\theta\theta}\left[\boldsymbol{\mathcal{C}}_\theta - \left(\bar{\boldsymbol{u}}^0 + \bar{\boldsymbol{u}}^1\varepsilon + \bar{\boldsymbol{u}}^2\varepsilon^2\right)\right] - \boldsymbol{\mathcal{H}}_{\theta q}\left(\boldsymbol{\mathcal{C}}_{\boldsymbol{q}} + \bar{\boldsymbol{z}}_1\right)\\
&\quad -\varepsilon^2\left[\boldsymbol{\mathcal{H}}_{\theta\theta}\left(\hat{\boldsymbol{\mathcal{C}}}_\theta + \tilde{\boldsymbol{\mathcal{C}}}^1_\theta\right) + \hat{\boldsymbol{\mathcal{H}}}_{\theta\theta}\left(\boldsymbol{\mathcal{C}}_\theta - \bar{\boldsymbol{u}}^0\right)\right]\\
&\quad -\varepsilon^2\left[\boldsymbol{\mathcal{H}}_{\theta q}\left(\hat{\boldsymbol{\mathcal{C}}}_q + \tilde{\boldsymbol{\mathcal{C}}}^1_q\right) + \hat{\boldsymbol{\mathcal{H}}}_{\theta q}\left(\boldsymbol{\mathcal{C}}_{\boldsymbol{q}} + \boldsymbol{h}^0_1\right)\right] && (4.61)
\end{aligned}$$

The initial discrepancy describing the distance of the $\boldsymbol{z}$ from the manifold can be described by a new set of coordinates, defined as follows:

$$\begin{aligned}
\boldsymbol{\eta}_1 &= \boldsymbol{z}_1 - \boldsymbol{h}_1(\boldsymbol{x}_1, \boldsymbol{x}_2, \boldsymbol{u}, \varepsilon)\\
\boldsymbol{\eta}_2 &= \boldsymbol{z}_2 - \boldsymbol{h}_2(\boldsymbol{x}_1, \boldsymbol{x}_2, \boldsymbol{u}, \varepsilon)
\end{aligned} \qquad (4.62)$$

Introducing a fast time scale $\tau = t/\varepsilon$ and differentiating with respect to τ the $\boldsymbol{\eta}$ coordinates one obtains:

$$\begin{aligned}
\frac{\mathrm{d}\boldsymbol{\eta}_1}{\mathrm{d}\tau} &= \varepsilon\frac{\mathrm{d}\boldsymbol{\eta}_1}{\mathrm{d}t}\\
&= \varepsilon\dot{\boldsymbol{z}}_1 - \varepsilon\dot{\boldsymbol{h}}_1\\
&= \varepsilon\frac{1}{\varepsilon}\boldsymbol{z}_2 - \varepsilon\frac{1}{\varepsilon}\boldsymbol{h}_2\\
&= \boldsymbol{\eta}_2 && (4.63)\\
\frac{\mathrm{d}\boldsymbol{\eta}_2}{\mathrm{d}\tau} &= \varepsilon\dot{\boldsymbol{z}}_2 - \varepsilon\dot{\boldsymbol{h}}_2\\
&= -(\boldsymbol{\mathcal{H}}_{q\theta} + \varepsilon^2\hat{\boldsymbol{\mathcal{H}}}_{q\theta})(\boldsymbol{\mathcal{C}}_\theta + \varepsilon\tilde{\boldsymbol{\mathcal{C}}}^0_\theta + \varepsilon^2[\boldsymbol{\mathcal{C}}_\theta + \tilde{\boldsymbol{\mathcal{C}}}^1_\theta])\\
&\quad -(\boldsymbol{\mathcal{H}}_{qq} + \varepsilon^2\hat{\boldsymbol{\mathcal{H}}}_{qq})(\boldsymbol{\mathcal{C}}_{\boldsymbol{q}} + \varepsilon\tilde{\boldsymbol{\mathcal{C}}}^0_q + \varepsilon^2[\boldsymbol{\mathcal{C}}_{\boldsymbol{q}} + \tilde{\boldsymbol{\mathcal{C}}}^1_q])\\
&\quad +(\boldsymbol{\mathcal{H}}_{q\theta} + \varepsilon^2\hat{\boldsymbol{\mathcal{H}}}_{q\theta})(\bar{\boldsymbol{u}} + \boldsymbol{u}_f) - (\boldsymbol{\mathcal{H}}_{qq} + \varepsilon^2\hat{\boldsymbol{\mathcal{H}}}_{qq})\boldsymbol{z}_1\\
&\quad +(\boldsymbol{\mathcal{H}}_{q\theta} + \varepsilon^2\hat{\boldsymbol{\mathcal{H}}}_{q\theta})(\boldsymbol{\mathcal{C}}_\theta + \varepsilon\tilde{\boldsymbol{\mathcal{C}}}^0_\theta + \varepsilon^2[\boldsymbol{\mathcal{C}}_\theta + \tilde{\boldsymbol{\mathcal{C}}}^1_\theta])\\
&\quad +(\boldsymbol{\mathcal{H}}_{qq} + \varepsilon^2\hat{\boldsymbol{\mathcal{H}}}_{qq})(\boldsymbol{\mathcal{C}}_{\boldsymbol{q}} + \varepsilon\tilde{\boldsymbol{\mathcal{C}}}^0_q + \varepsilon^2[\boldsymbol{\mathcal{C}}_{\boldsymbol{q}} + \tilde{\boldsymbol{\mathcal{C}}}^1_q])\\
&\quad -(\boldsymbol{\mathcal{H}}_{q\theta} + \varepsilon^2\hat{\boldsymbol{\mathcal{H}}}_{q\theta})\bar{\boldsymbol{u}} - (\boldsymbol{\mathcal{H}}_{qq} + \varepsilon^2\hat{\boldsymbol{\mathcal{H}}}_{qq})\boldsymbol{h}_1 && (4.64)
\end{aligned}$$

Which can be simplified, yelding the final equations for the off-manifold subsystem:

$$\begin{aligned}
\frac{\mathrm{d}\boldsymbol{\eta}_1}{\mathrm{d}\tau} &= \boldsymbol{\eta}_2\\
\frac{\mathrm{d}\boldsymbol{\eta}_2}{\mathrm{d}\tau} &= -\left(\bar{\boldsymbol{\mathcal{H}}}_{qq} + \varepsilon^2\bar{\hat{\boldsymbol{\mathcal{H}}}}_{qq}\right)\boldsymbol{\eta}_1 + \left(\bar{\boldsymbol{\mathcal{H}}}_{q\theta} + \varepsilon^2\bar{\hat{\boldsymbol{\mathcal{H}}}}_{q\theta}\right)\boldsymbol{u}_f
\end{aligned} \qquad (4.65)$$

where $\boldsymbol{u}_f = \boldsymbol{u} - \bar{\boldsymbol{u}}$ is the fast control input, and

$$\boldsymbol{\eta}(0) = \boldsymbol{z}_0(t_0) - \bar{\boldsymbol{z}}(t_0) \tag{4.66}$$

are the initial conditions of the fast variables.

It can be easily observed that the system (4.65) is the $O(\varepsilon^3)$ refinement of the singular perturbation system described in Section 4.2. The system (4.65) is linear and time varying, the varying parameter are the states of the slow subsystem $\boldsymbol{x}_1 = \theta$ but not in $\boldsymbol{x}_2 = \dot{\theta}$, hence it depends on the spatial configuration of the manipulator but not on the joint velocities. Conversely, the off-manifold system is highly non linear.

4.5 Model validation

The validation of the model has been carried out by means of comparison with the data obtained from the MERIt [83] dataset, thoroughly described in Section 3.2.2 and with simulations obtained from the model described in Chapter 3. It must be pointed out that the validation of the model raised several issues; the integral manifold approach is based on the partition of the system into a *on*-manifold subsystem and a *correction* subsystem with the hypothesis that the *off*-manifold fast dynamics reaches a steady state condition in a time-scale where the slow, *on*-manifold is quasi-constant. In other words, the integral manifold model, coupled with the $O(\varepsilon^3)$ approximation can be considered valid if a clear separation between the time-scales of the subsystems is present in the manipulator. This assumption can be valid in several contexts where the manipulator's motion is relatively slow with respect to the vibrations, like nuclear or agricoltural robot which don't require very high operational speeds. However, this is not the case of the MERIt dataset, where the bandwidth of the motion and vibrations intersect. As a consequence it has been decided to use the MERIt data only for the validation of the slow subsystem, while two simulation scenarios have been built with the aim of validating the *off*-manifold system. It must be mentioned that the implementation of the model in the Matlab/Simulink environment is not trivial, the details about coding and numerical simulation are omitted here for the sake of brevity, however some relevant aspects deserve to be mentioned:

- The theory of integral manifold lacks of a rigorous procedure for the expansion of the control input in terms of $\boldsymbol{u}_0$, $\boldsymbol{u}_1$ and $\boldsymbol{u}_2$, hence the control torque relative to the *on*-manifold subsystem only acts oh the $\bar{\boldsymbol{u}}_0$ term for the sake of simplicity. A possible way to cope with the $\bar{\boldsymbol{u}}_1$ and $\bar{\boldsymbol{u}}_2$ terms will be discussed in Chapter 5, but it turns out to be irrelevant in this phase of model validation.
- The formulation of the $\boldsymbol{h}_1^2$ term involves the derivative of $\boldsymbol{h}_2^1$, which is, in turn, the second derivative of $\boldsymbol{h}_1^0$. This term must be calculated nu-

merically, on the other hand the double numerical derivation would lead to unattainable results. In order to cope with this, the derivatives have been approximated with high-pass butterworth filters, tuned around a frequency of 30Hz.

4.5.1 Validation of the on-manifold subsystem

The *on*-manifold subsystem has been validated through a comparison with the MERIt dataset. The experimental setup and subset of data used for comparison are the same described in Section 3.2.2. The model described in this chapter naturally inherits part of the setup used to validate the closed-form model described in Chapter 3, hence the same approach has been adopted, two manually tuned PID regulators have been applied to the manipulator's joints in order to obtain a joint angle essentially identical between the experimental data and the simulations. A similar approach has been adopted in order to compare links' flexibility; the strains have been derived from the nodes' deflection by means of a linear interpolation and compared with MERIt's strain gauges measurements. It must be recalled that the comparison with MERIt is provided with the aim of validating the *on*-manifold subsystem, hence the output of the *off*-manifold system has not been considered in this phase[5]. As a consequence, during the simulations shown in the following one expects to see the *quasi steady state* dynamics of the strain reproduced by the state space of the system. That is exactly what happens, figures 4.1 and 4.2 show the comparison between measured and simulated strains in the case of a payload mass of 400 g, where the experimental data are represented in a grey dashed line while the simulatons are solid black lines. Moreover, in Figure 4.3 the normalizer spectra of the signals are shown. These figures clearly show that the integral manifold reduced order system represents a low frequency approximation of the original system.

4.5.2 Validation of the off-manifold subsystem

The validation of the off-manifold system is much more involved, as it has been explained at the beginning of this section, the boundary layer system has been derived under the hypothesis that the slow variables and the slow control input are in a steady state during the fast transient. In the experiments collected into the MERIt dataset, this assumption is not satisfied: slow variables (i.e. joints angular positions and velocities)and the slow input (i.e. torques at the joints) vary vary with a frequency content similar with respect of the links vibrations, due to the lack of a vibration damping system. Therefore, the boundary layer system has been validated by means of two different experiments, in both cases a comparison with the original, closed form model has been carried out.

[5] The $\boldsymbol{\eta}$ state variables have been fixed to zero

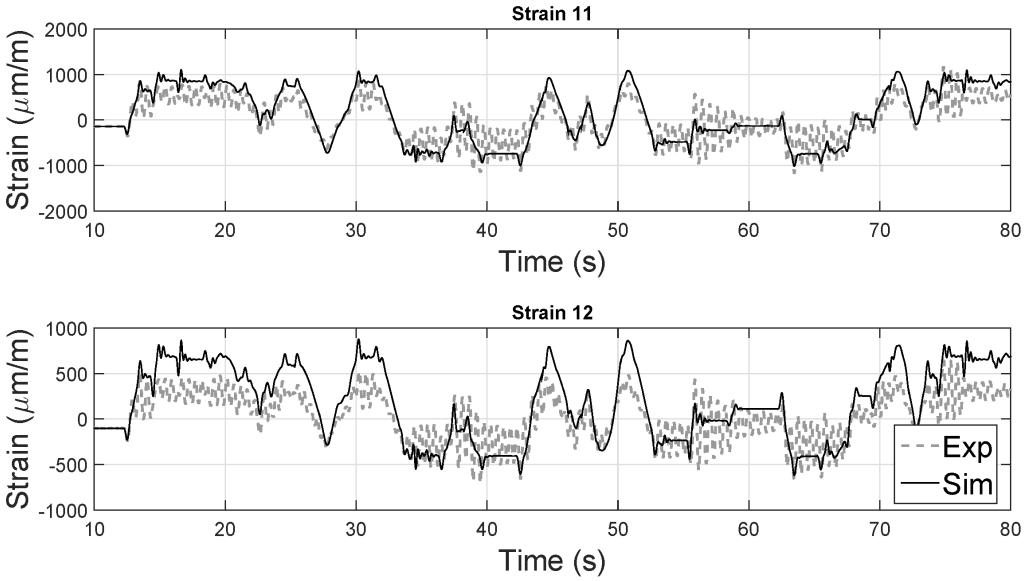

Figure 4.1: 1-st link - comparison between measured and simulated strains

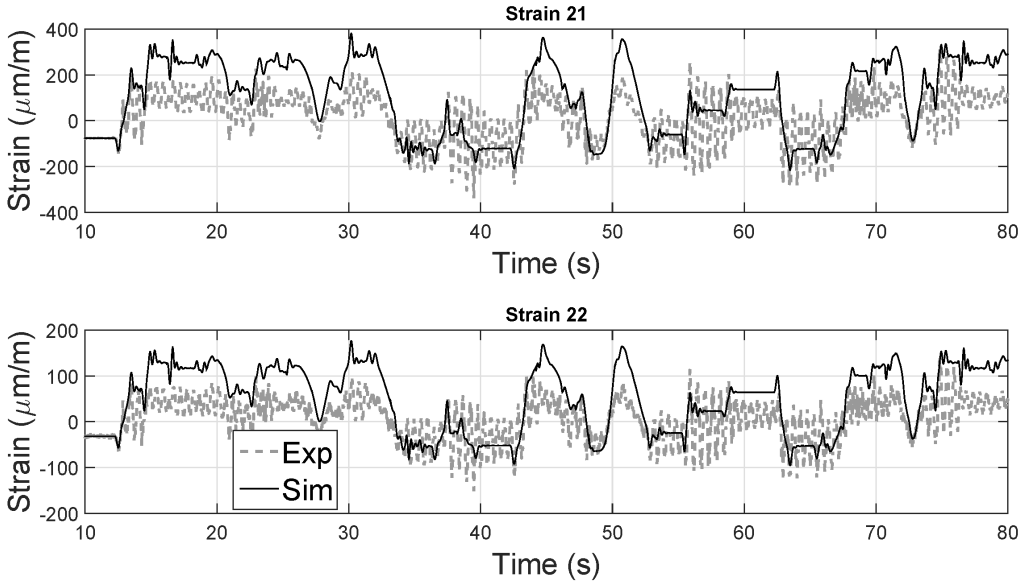

Figure 4.2: 2-nd link - comparison between measured and simulated strains

In the first simulation the TUDOR platform has been considered, but a different experiment with respect to the MERIt dataset has been carried out. The joint angles have been fixed to zero during the simulation, and a non-zero initial value has been assigned to the off-manifold state variables $\boldsymbol{\eta}$. The time evolution and frequency content of the tip transverse deflection have been compared to the corresponding quantity simulated with the complete model (described by Eqs. (3.1,3.2)). The aim of this procedure is to validate

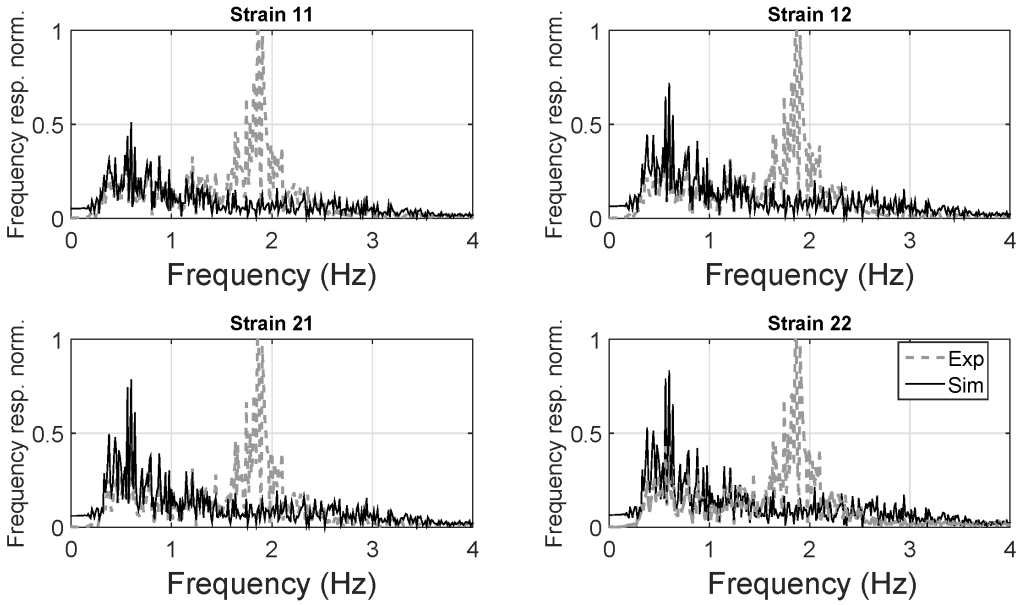

Figure 4.3: Strain FFT - comparison between measured and simulated strains

the analytical derivation of the manifold model with respect to the original one.

If the slow state variables $\boldsymbol{\theta}, \dot{\boldsymbol{\theta}}$ and the slow input $\boldsymbol{u}_s$ are fixed to zero, the timescale separation hypothesis is inherently satisfied; moreover, the quasi steady state trajectory $\bar{\boldsymbol{z}}$ is constant and therefore links deflections are only due to the off-manifold dynamics, which is described by the boundary layer system. In this configuration, links deflections computed by the boundary system and by the complete model can be compared. Non-zero initial value has been assigned to the $\boldsymbol{\eta}$ variables and the same has been done for the corresponding modal coordinates of the original model. The links vibrate around their constant quasi steady state trajectory. Figure 4.4 shows a comparison between the complete model (in dashed grey line) and the integral manifold model (in black solid line). Results demonstrate how the off-manifold system effectively reproduces the fast system dynamics. The initial perturbation of the fast system, and the corresponding perturbation of the $\boldsymbol{q}$ variables in the complete model do not have a comparable physical meaning, hence the deflections have been normalized in order to show the similar evolution in terms of vibration frequency, which can be further observed in the frequency domain plot.

Another simulation scenario, not based on the TUDOR experimental platform has been carried out: Consider a planar robot subject to gravity with two links and both joints in the horizontal plane. The quasi steady state trajectory is constant in the vertical plane which is out of the manipulator's motion space. The links' vibration on the vertical plane (which are due to the effect of gravity force) can be described by the boundary layer system. This

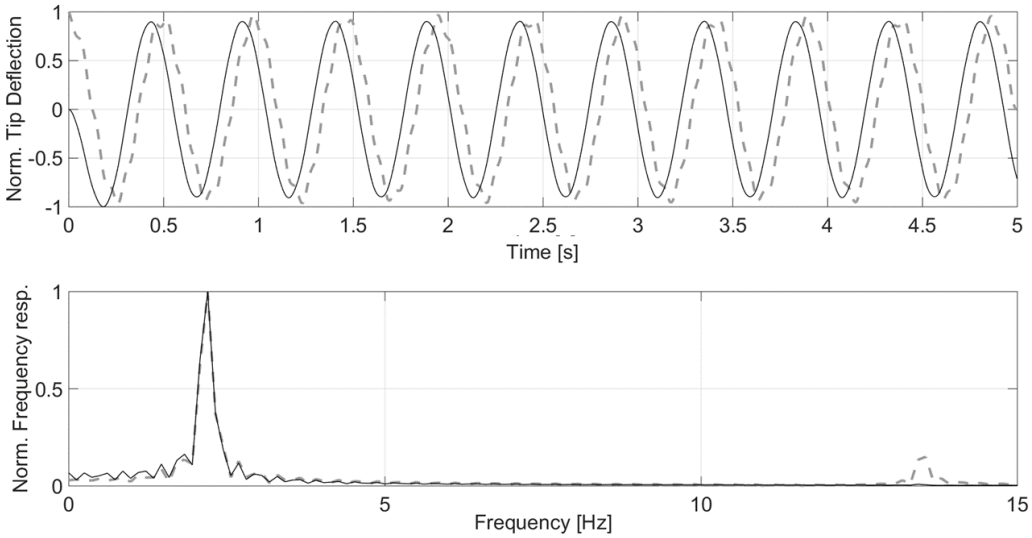

Figure 4.4: Comparison between link deflection of the boundary layer system and of the original model

Table 4.1: Planar robot link data

Length	300 mm
Thickness	2 mm
Height	50 mm
Density	2800 Kg/m^3
Young Modulus	700 GPa
Poisson's coefficient	0.33

configuration has been exploited to compare links deflection on the vertical direction computed by the boundary layer system with links deflection on the vertical direction computed by the original model.

The manipulator considered here is composed by two thin arms modeled with shell elements in the FE preprocessing and two joints whose axis are directed in the height direction of the links. The links' data are reported in Table 4.1[6] while the retained eigenvalues are shown in Fig 4.5. The shape and FE elements of the links have been choosen in order to show the three-dimensional deformation field of the manipulator, induced by the twisting compliance of the links.

Since the link section is thin, shell finite elements have been used to mesh the link. The value of the perturbation parameter ε for the links of this manipulator is 0.05 which is significantly lower then the value of TUDOR[7], hence the time scales are meaningfully separated and the hypothesis of the

[6] The damping ratio adopted in both cases is the lowest which guarantees numberical stability during the simulation

[7] The perturbation parameter for the TUDOR platform is 0.22. It must be recalled that $\varepsilon = \frac{1}{\sqrt{k_e}}$ i.e. the inverse of the lowest proper frequency of a link. However the frequencies of the system are usually significantly lower then the the frequencies of the single links, depending on the system's configuration

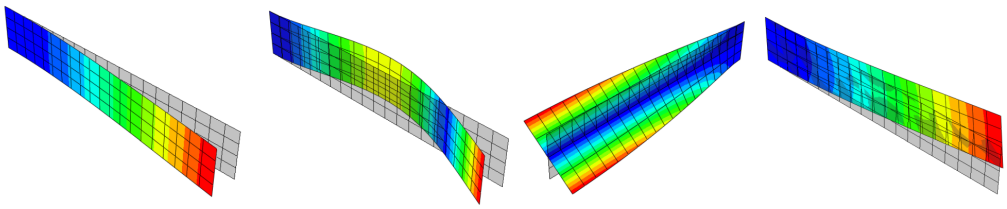

Figure 4.5: FE eigenmodes analysis of the links' frequency (from the left f=18.1,114.4,213.3,427.3 Hz)

Figure 4.6: Slow system input torque profile

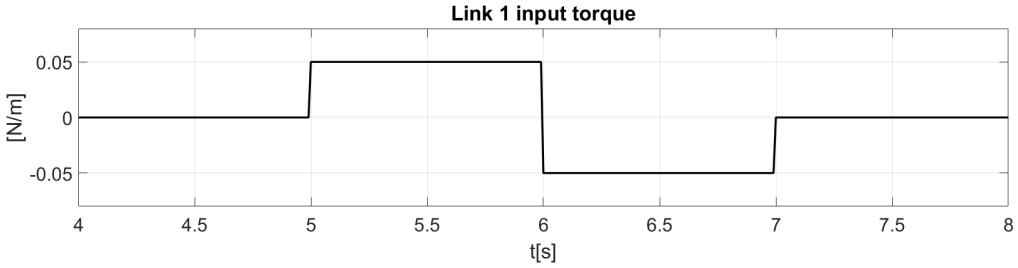

approach are observed.

The simulations have been performed by applying a bang-bang torque to the first joint, reported in 4.6, while the second has been fixed at $\vartheta_2 = \varpi/2$ by means of spring-damper system, in such a way to maximize the twisting on the first link.

Figure 4.7 compares links deflections of the original model and of the reduced order system. Again, the slow system represents the low frequency approximation of the original system.

Figures 4.8 and 4.9 show the time domain and the frequency domain comparison of links deflections in the horizontal plane between the original model and the complete integral manifold model (which is composed by the slow and the fast subsystem). This comparison confirms the hypothesis under which the boundary layer system has been derived, namely that the slow varibles must keep constant during the fast transient. Since this assumption is not verified in the plane of motion, the boundary layer system does not represents the off-manifold dyanmics correctely.

On the other hand, the assumption is verified in the vertical plane, where the quasi steady state trajectory $\bar{\boldsymbol{z}}$ is constant during the simulation. Since the assumption is verified, the boundary layer system correctly represents the off-manifold dynamics, as it can be seen from figure 4.10 and 4.11, which show good accordance between the models.

Figure 4.7: Links deflection in the horizontal plane (plane of motion): comparison between the original model and the reduced order model

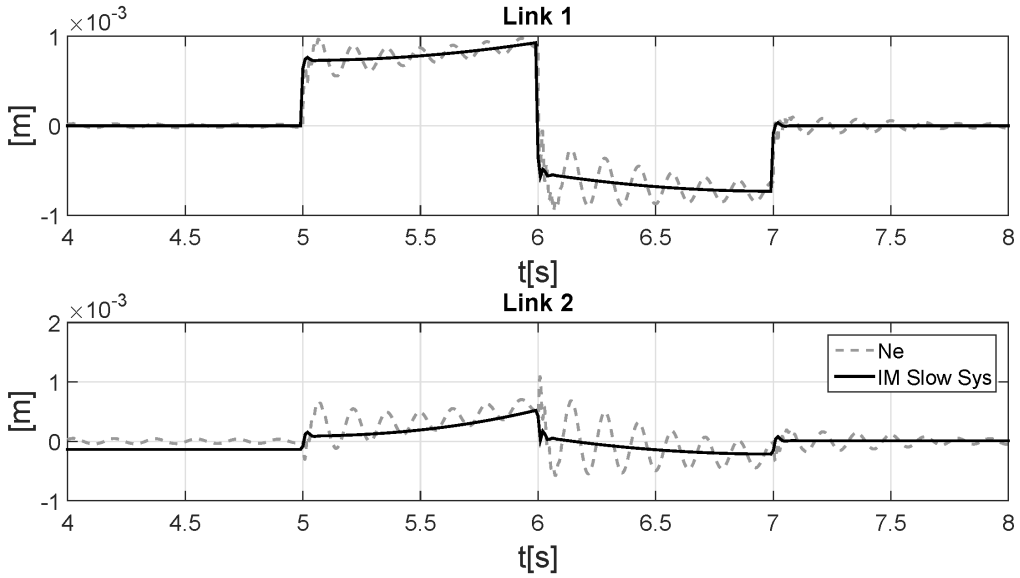

Figure 4.8: Links deflections in the horizontal plane (plane of motion): comparison between the original model and the complete integral manifold model

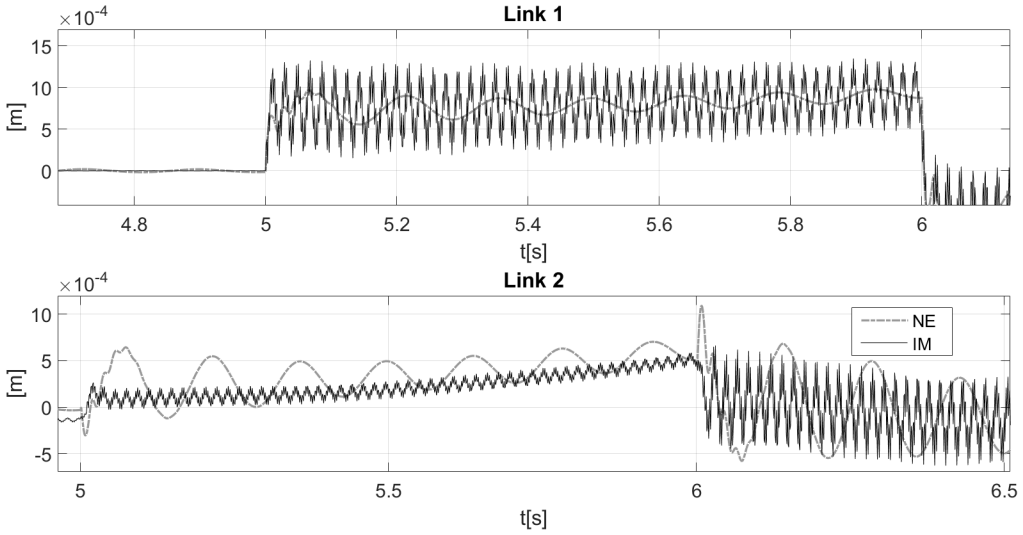

Figure 4.9: Links deflections in the horizontal plane (plane of motion): frequency domain comparison between the original model and the complete integral manifold model

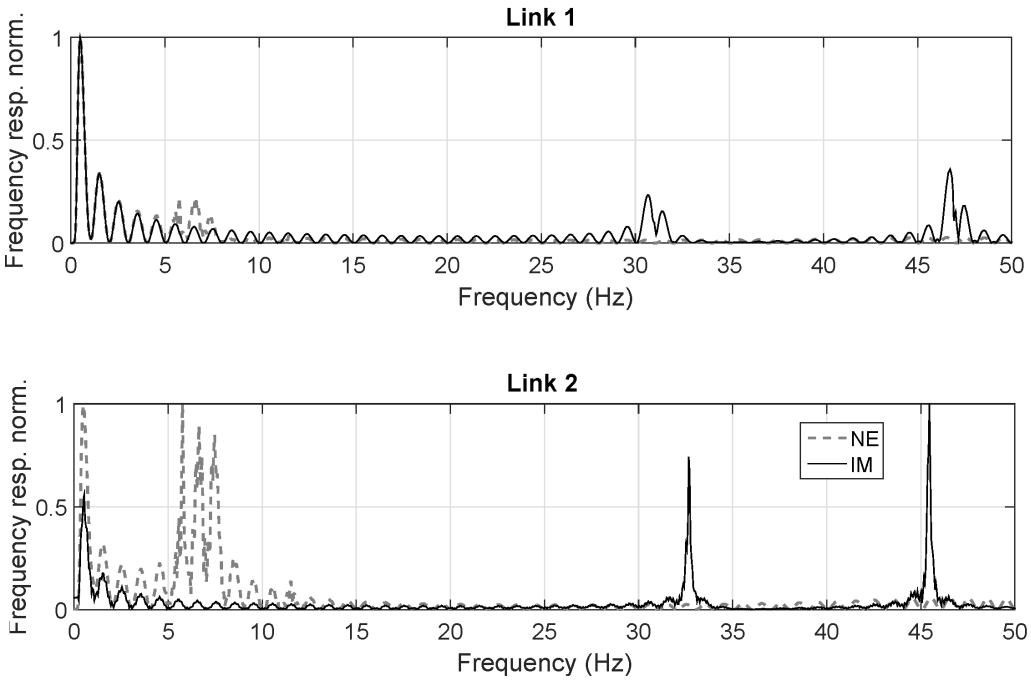

Figure 4.10: Links deflections in the vertical plane: comparison between the original model and the complete integral manifold model

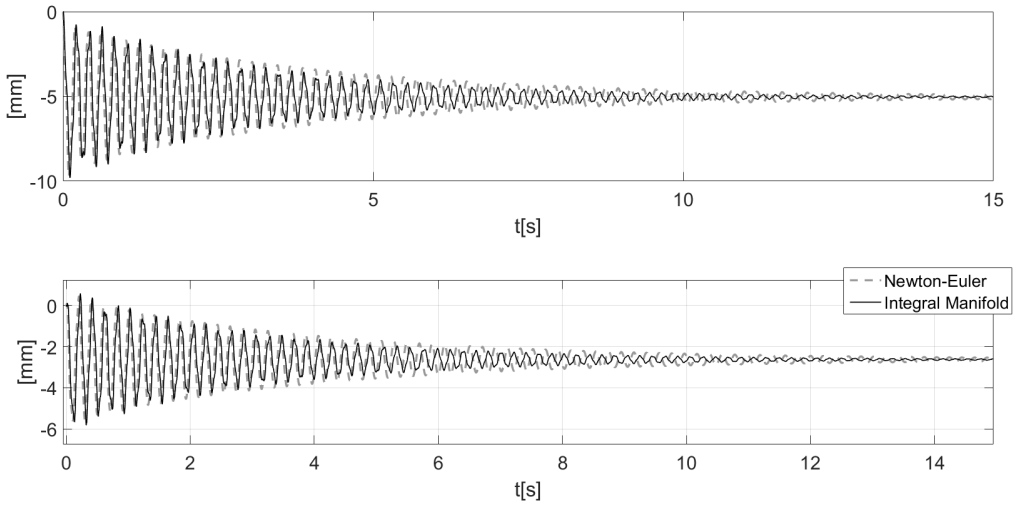

Figure 4.11: Links deflections in the vertical plane: frequency domain comparison between the original model and the complete integral manifold model

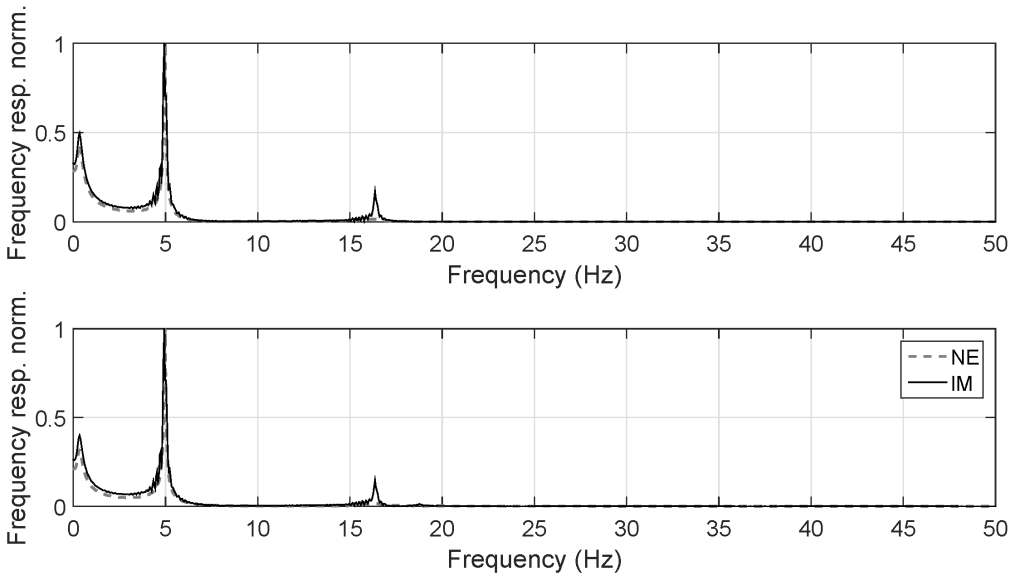

Chapter 5

Control strategies for vibration damping

In this chapter, the problem of the control of flexible manipulators will be tackled. One of the main objectives of the modelling work carried out in the previous chapter is to provide an effective framework for the synthesis of control schemes based on the separation of the system into two subsystems. Once the overall dynamics is divided in two subsystems, a different feedback controller can be synthesized for each subsystem and the resulting controls can be merged exploiting the theoretical framework provided by the composite control theory. The controller acting on the *on*-manifold system has to track the reference trajectory in the joint space, i.e. it deals with the motion of the manipulator; on the other hand, the fast controller is intended to damp links vibration around the quasi steady state equilibrium trajectory defined by the slow system.

The composite control technique was first proposed in [26] and it was originally conceived to cope with the design of a feedback control for a singularly perturbed system. However, since the integral manifold approach, together with the $O(\varepsilon^3)$ approximation can be considered as an extension of the singular perturbation approach, the composite control technique can be successfully applied even to the integral manifold model.

5.1 Tuning of the on-manifold subsystem control

According to the composite control technique, the composite control law for the singularly perturbed system

$$\dot{\boldsymbol{x}} = f(\boldsymbol{x}, \boldsymbol{z}, \boldsymbol{u}, \varepsilon, t) \tag{5.1}$$

$$\varepsilon\dot{\boldsymbol{z}} = g(\boldsymbol{x}, \boldsymbol{z}, \boldsymbol{u}, \varepsilon, t) \tag{5.2}$$

is set up as follows:

$$\boldsymbol{u} = \boldsymbol{u}_s + \boldsymbol{u}_f \tag{5.3}$$

The slow control $\boldsymbol{u}_s$ is a feedback control for the slow system, which has to track the reference trajectory of the slow state variables $\boldsymbol{x}$. On the other hand, the fast control $\boldsymbol{u}_f$ is a feedback control for the boundary layer system, which has to stabilize the fast states along the quasi-steady state equilibrium trajectory, i.e. it deals with the off manifold dynamics. Hence, the fast control must be inactive along the quasi-steady state equilibrium trajectory which represents the on manifold dynamics:

$$\boldsymbol{u}_f(\boldsymbol{x}, \bar{\boldsymbol{z}}) = 0 \tag{5.4}$$

Consequently, the quasi-steady state equilibrium trajectory $\bar{\boldsymbol{z}}$ of the $\boldsymbol{z}$ subset of state variable is a function of the slow control only:

$$\bar{\boldsymbol{z}} = \boldsymbol{h}(\bar{\boldsymbol{x}}, \boldsymbol{u}_s, \varepsilon, t) \tag{5.5}$$

The reduced order subsystem (obtained by the substitution of the equation (5.5) into the state equation (5.1)) is a function of the slow control only as well:

$$\dot{\bar{\boldsymbol{x}}} = f(\bar{\boldsymbol{x}}, \boldsymbol{h}(\bar{\boldsymbol{x}}, \boldsymbol{u}_s, \varepsilon, t), \boldsymbol{u}_s, t) \tag{5.6}$$

Therefore, the slow control law can be designed independently from the fast control. Moreover, it is a function of the $\boldsymbol{x}$ subset of state variables only:

$$\boldsymbol{u}_s = \boldsymbol{u}_s(\boldsymbol{x}) \tag{5.7}$$

On the other hand, the design of the fast control law depends on the slow control, because the boundary layer system ((5.8)) is a dynamic system parametrized in the slow variables $\boldsymbol{x}$ and in the slow control $\boldsymbol{u}_s$, which are assumed to be constant during the fast transients.

$$\frac{d\boldsymbol{\eta}}{d\tau} = g(\bar{\boldsymbol{x}}, \boldsymbol{\eta}(\tau) + \bar{\boldsymbol{z}}(\bar{\boldsymbol{x}}, \boldsymbol{u}_s, \varepsilon, t), \boldsymbol{u}_f, t) \tag{5.8}$$

Consequently,

$$\boldsymbol{u} = \boldsymbol{u}_s(\bar{\boldsymbol{x}}) + \boldsymbol{u}_f(\bar{\boldsymbol{x}}, \boldsymbol{\eta}) \tag{5.9}$$

In conclusion, the composite control technique significantly simplifies the controller design of a two time scale system. The design of a feedback control for the system described by the state equations (5.1) and (5.2) is split into the design of two control systems which can be synthesized independently, given that the *off*-manifold control is inactive along the quasi steady state equilibrium trajectory.

The composite control technique simplifies the stability analysis as well: the only hypothesis which must be satisfied is that the fast subsystem is

uniformly stabilizable for any slow trajectory $\bar{\boldsymbol{x}}$ [12]. The goal is now to design a control system of the *on*-manifold subsystem which allows to track a reference joint trajectory and a fast control system for the *off*-manifold subsystem which stabilizes the deflections along the quasi steady-state trajectory, i.e. damps the vibrations induced by the links' flexibility.

5.2 On-manifold subsystem control law

In the integral manifold approach, a Taylor series expansion of the control law is considered (see Section 4.4):

$$\boldsymbol{u}_s = \bar{\boldsymbol{u}}^0 + \varepsilon\bar{\boldsymbol{u}}^1 + \varepsilon^2\bar{\boldsymbol{u}}^2 \tag{5.10}$$

The derivation of each term is a consequence of the control scheme design; a possible choice, originally described in [128], is adapted here to the manipulator model. The *on*-manifold subsystem is initially approximated at $O(\varepsilon)$ and a control scheme based on the inverse model is computed, then higher order terms are introduced step-by-step and the equal-power terms of the control are computed accordingly.

5.2.1 Derivation of the first term of the on-manifold control input

Consider the system (4.61) approximated to $O(\varepsilon)$, where the *on*-manifold state variables are assumed $\dot{\boldsymbol{x}}_{\boldsymbol{1}} = \dot{\boldsymbol{\theta}}$ and $\dot{\boldsymbol{x}}_{\boldsymbol{2}} = \ddot{\boldsymbol{\theta}}$.

$$\ddot{\boldsymbol{\theta}} = -\boldsymbol{\mathcal{H}}_{\theta\theta}\left[\boldsymbol{\mathcal{C}}_\theta - \bar{\boldsymbol{u}}^0\right] - \boldsymbol{\mathcal{H}}_{\theta q}\left[\boldsymbol{\mathcal{C}}_{\boldsymbol{q}} + \boldsymbol{h}_1^0\right] \tag{5.11}$$

Recalling that

$$\boldsymbol{h}_1^0 = \bar{\boldsymbol{\mathcal{H}}}_{qq}^{-1}\bar{\boldsymbol{\mathcal{H}}}_{q\theta}\left[\bar{\boldsymbol{u}}^0 - \boldsymbol{\mathcal{C}}_\theta\right] - \boldsymbol{\mathcal{C}}_{\boldsymbol{q}} \tag{5.12}$$

and substituting eq. (5.12) into the slow system (5.11), one obtains

$$\begin{aligned}
\ddot{\boldsymbol{\theta}} &= -\boldsymbol{\mathcal{H}}_{\theta\theta}\left[\boldsymbol{\mathcal{C}}_\theta - \bar{\boldsymbol{u}}^0\right] \\
&\quad -\boldsymbol{\mathcal{H}}_{\theta q}\left[\boldsymbol{\mathcal{C}}_{\boldsymbol{q}} + \bar{\boldsymbol{\mathcal{H}}}_{qq}^{-1}\bar{\boldsymbol{\mathcal{H}}}_{q\theta}\left[\bar{\boldsymbol{u}}^0 - \boldsymbol{\mathcal{C}}_\theta\right] - \boldsymbol{\mathcal{C}}_{\boldsymbol{q}}\right] \\
&= \left[\boldsymbol{\mathcal{H}}_{\theta\theta} - \boldsymbol{\mathcal{H}}_{\theta q}\bar{\boldsymbol{\mathcal{H}}}_{qq}^{-1}\bar{\boldsymbol{\mathcal{H}}}_{q\theta}\right]\left[\bar{\boldsymbol{u}}^0 - \boldsymbol{\mathcal{C}}_\theta\right]
\end{aligned}$$

Using the Shur complement one obtains:

$$\ddot{\boldsymbol{\theta}} = \boldsymbol{\mathcal{M}}_{\theta\theta}^{-1}(\bar{\boldsymbol{x}}, \boldsymbol{0})\left[\bar{\boldsymbol{u}}^0 - \boldsymbol{\mathcal{C}}_\theta\right] \tag{5.13}$$

Equation (5.13) corresponds to the rigid system as alredy shown in section 4.2. [1]. Hence the control law for the $\boldsymbol{u}^0$ slow control term can be

[1] it must be remembered that all these matrices are evaluated in $(\bar{\boldsymbol{x}}, \boldsymbol{0})$

chosen arbitrarily among the well-known control techniques developed for rigid robots. One of these is the inverse model technique described in [130]. The control term $\bar{\boldsymbol{u}}^0$ is set up in order to compensate the nonlinear term $\boldsymbol{\mathcal{C}}_\theta$:

$$\bar{\boldsymbol{u}}^0(\boldsymbol{\theta}, \dot{\boldsymbol{\theta}}) = \boldsymbol{\mathcal{M}}_{\theta\theta}(\boldsymbol{\theta}, \dot{\boldsymbol{\theta}})\boldsymbol{v}(t) + \boldsymbol{\mathcal{C}}_\theta(\boldsymbol{\theta}, \dot{\boldsymbol{\theta}}) \tag{5.14}$$

where $\boldsymbol{v}(t)$ is the control variable. Consequently, the rigid system (5.13) can be considered as a double integrator system

$$\ddot{\boldsymbol{\theta}} = \boldsymbol{v} \tag{5.15}$$

The target input $\boldsymbol{v}$ is related to the reference trajectory which has to be tracked, namely it is defined as follows:

$$\boldsymbol{v} = \ddot{\boldsymbol{\theta}}_{ref} + \boldsymbol{K}_D[\dot{\boldsymbol{\theta}}_{ref}(t) - \dot{\boldsymbol{\theta}}(t)] + \boldsymbol{K}_P[\boldsymbol{\theta}_{ref}(t) - \boldsymbol{\theta}(t)] \tag{5.16}$$

The substitution of the target input expression (5.16) the system (5.15) yields the equation:

$$[\ddot{\boldsymbol{\theta}}_{ref} - \ddot{\boldsymbol{\theta}}] + \boldsymbol{K}_D[\dot{\boldsymbol{\theta}}_{ref}(t) - \dot{\boldsymbol{\theta}}(t)] + \boldsymbol{K}_P[\boldsymbol{\theta}_{ref}(t) - \boldsymbol{\theta}(t)] = 0 \tag{5.17}$$

where $\boldsymbol{K}_P$ and $\boldsymbol{K}_D$ are the matrices of the positions and velocities gains respectively.

By choosing:

$$\boldsymbol{K}_P = \text{diag}(\omega_1^2, \omega_2^2, \ldots, \omega_N^2) \tag{5.18}$$

$$\boldsymbol{K}_D = \text{diag}(2\xi_1\omega_1, 2\xi_2\omega_2, \ldots, 2\xi_N\omega_N) \tag{5.19}$$

the frequencies and the damping of the eigenvalues corresponding to each joint position error in (5.17) are determinated and consequently the rate of convergence of the joint position errors [12].

5.2.2 Derivation of the second term of the on-manifold control input

Once the slow control term $\bar{\boldsymbol{u}}^0$ has been determined, the $O(\varepsilon^2)$ reduced order model can be taken into account in order to find the expression of the control term $\bar{\boldsymbol{u}}^1$:

$$\ddot{\boldsymbol{\theta}} = -\boldsymbol{\mathcal{H}}_{\theta\theta}\left[\boldsymbol{\mathcal{C}}_\theta - \bar{\boldsymbol{u}}^0 - \varepsilon\bar{\boldsymbol{u}}^1\right] - \boldsymbol{\mathcal{H}}_{\theta q}\left[\boldsymbol{\mathcal{C}}_{\boldsymbol{q}} + \boldsymbol{h}_1^0 + \varepsilon\boldsymbol{h}_1^1\right] \tag{5.20}$$

Recalling that:

$$\boldsymbol{h}_1^1 = \bar{\boldsymbol{\mathcal{H}}}_{qq}^{-1}\bar{\boldsymbol{\mathcal{H}}}_{q\theta}\bar{\boldsymbol{u}}^1 \tag{5.21}$$

by substituting the expressions of $\boldsymbol{h}_1^0$ and of $\boldsymbol{h}_1^1$ into the reduced order system (5.20), one obtains:

$$\begin{aligned}\ddot{\boldsymbol{\theta}} = & - \boldsymbol{\mathcal{H}}_{\theta\theta}\left[\boldsymbol{\mathcal{C}}_\theta - \bar{\boldsymbol{u}}^0 - \varepsilon\bar{\boldsymbol{u}}^1\right] \\ & - \boldsymbol{\mathcal{H}}_{\theta q}\left[\boldsymbol{\mathcal{C}}_{\boldsymbol{q}} + \bar{\boldsymbol{\mathcal{H}}}_{qq}^{-1}\bar{\boldsymbol{\mathcal{H}}}_{q\theta}\left[\bar{\boldsymbol{u}}^0 - \boldsymbol{\mathcal{C}}_\theta\right] - \boldsymbol{\mathcal{C}}_{\boldsymbol{q}} + \varepsilon\bar{\boldsymbol{\mathcal{H}}}_{qq}^{-1}\bar{\boldsymbol{\mathcal{H}}}_{q\theta}\bar{\boldsymbol{u}}^1\right] \quad (5.22)\end{aligned}$$

and, simplifying:

$$\begin{aligned}\ddot{\boldsymbol{\theta}} &= \left[\boldsymbol{\mathcal{H}}_{\theta\theta} - \boldsymbol{\mathcal{H}}_{\theta q}\bar{\boldsymbol{\mathcal{H}}}_{qq}^{-1}\bar{\boldsymbol{\mathcal{H}}}_{q\theta}\right]\left[\bar{\boldsymbol{u}}^0 - \boldsymbol{\mathcal{C}}_\theta + \varepsilon\bar{\boldsymbol{u}}^1\right] \\ &= \boldsymbol{\mathcal{M}}_{\theta\theta}^{-1}\left[\bar{\boldsymbol{u}}^0 - \boldsymbol{\mathcal{C}}_\theta + \varepsilon\bar{\boldsymbol{u}}^1\right] \quad (5.23)\end{aligned}$$

recalling the expression of the slow control term $\bar{\boldsymbol{u}}^0$ given by the equation (5.14), one obtains:

$$\ddot{\boldsymbol{\theta}} = \boldsymbol{\mathcal{M}}_{\theta\theta}^{-1}\left[\boldsymbol{\mathcal{M}}_{\theta\theta}\boldsymbol{v} + \varepsilon\bar{\boldsymbol{u}}^1\right] \quad (5.24)$$

Therefore, $\bar{\boldsymbol{u}}^1 = 0$, since the aim of the slow control is to track the reference control variable $\boldsymbol{v}$.

5.2.3 Derivation of the third term of the on-manifold control input

Once the slow control terms $\bar{\boldsymbol{u}}^0$ and $\bar{\boldsymbol{u}}^1$ have been determined, the $O(\varepsilon^3)$ reduced order model is taken into account. The $\bar{\boldsymbol{u}}^2$ control term is obtained by means of a similar procedure. Consider the $O(\varepsilon^3)$ model written as follows:

$$\ddot{\boldsymbol{\theta}} = \boldsymbol{\mathcal{M}}_{\theta\theta}^{-1}\left[\bar{\boldsymbol{u}}^0 - \boldsymbol{\mathcal{C}}_\theta\right] + \varepsilon^2\left[\boldsymbol{\mathcal{H}}_{\theta\theta}\bar{\boldsymbol{u}}^2 + D(\boldsymbol{\theta}, \dot{\boldsymbol{x}}, \bar{\boldsymbol{u}}^0)\right] \quad (5.25)$$

where

$$D(\boldsymbol{\theta}, \dot{\boldsymbol{x}}, \bar{\boldsymbol{u}}^0) = -\boldsymbol{\mathcal{H}}_{\theta q}(\boldsymbol{h}_1^2 + \hat{\boldsymbol{\mathcal{C}}}_q) - \boldsymbol{\mathcal{H}}_{\theta\theta}\hat{\boldsymbol{\mathcal{C}}}_\theta - \hat{\boldsymbol{\mathcal{H}}}_{\theta\theta}(\boldsymbol{\mathcal{C}}_\theta - \bar{\boldsymbol{u}}^0) - \hat{\boldsymbol{\mathcal{H}}}_{\theta q}(\boldsymbol{\mathcal{C}}_{\boldsymbol{q}} + \boldsymbol{h}_1^0) \quad (5.26)$$

Recalling eq. (5.14), the control term $\bar{\boldsymbol{u}}^2$ can be calculated as:

$$\bar{\boldsymbol{u}}^2 = -\boldsymbol{\mathcal{H}}_{\theta\theta}^{-1}D(\boldsymbol{x}_1, \boldsymbol{x}_2, \bar{\boldsymbol{u}}^0) \quad (5.27)$$

Therefore, the slow control term $\bar{\boldsymbol{u}}^2$ can be interpreted as the control input which provides a compensation of the disturbance created by the effect of the flexibility acting on the reduced order system.

5.2.4 Simulation of the on-manifold control system

The *on*-manifold control law described in Section 5.2 has been tested through a simulation. The control system described in the previous section has been applied to the closed form model described in Chapter 3. In order to carry out the simulations the physical data of the TUDOR platform have been

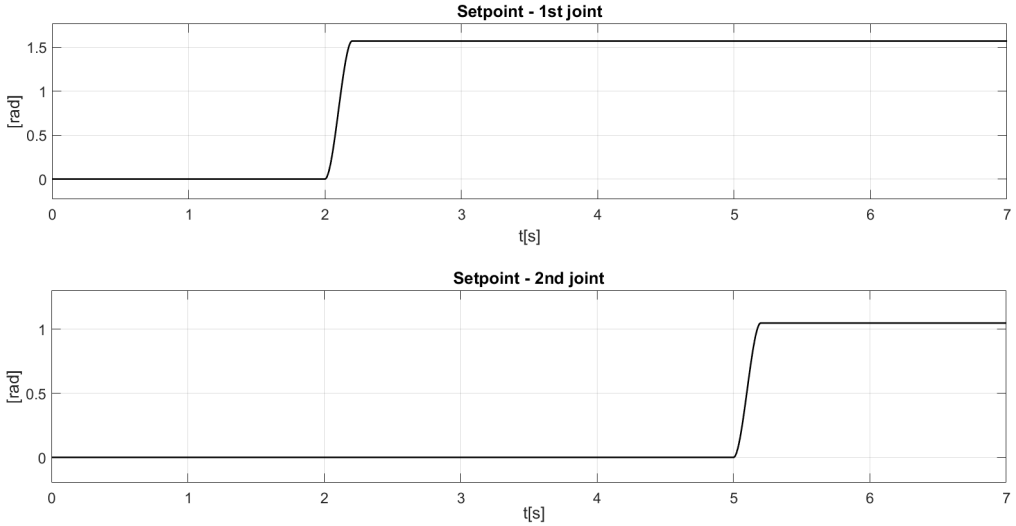

Figure 5.1: Setpoint of the manipulator's joints positions

used. The reference signals for the manipulator's joints are built interpolating a fifth order polynomial in order to obtain an analytic expression of the velocities and accelerations, which are inherently continuous. The reference positions are reported in Figure 5.1.

The control law has been set up as described previously in this section, i.e.:

$$\begin{aligned} \boldsymbol{u}_s &= \bar{\boldsymbol{u}}^0 + \varepsilon\bar{\boldsymbol{u}}^1 + \varepsilon^2\bar{\boldsymbol{u}}^2 && (5.28)\\ &= (\boldsymbol{\mathcal{M}}_{\theta\theta}\boldsymbol{v} + \boldsymbol{\mathcal{C}}_\theta) + \varepsilon^2\left(-\boldsymbol{\mathcal{H}}_{\theta\theta}^{-1}\boldsymbol{D}\right) && (5.29)\end{aligned}$$

while the frequencies and damping factors have been chosen as $\omega_1 = 12\,rad/s$, $\omega_2 = 16\,rad/s$ and $\psi_1 = \psi_2 = 1$; Figures 5.2 and 5.3 show a comparison of the system response to the setpoint variations, the setpoint is depicted with a black full line, in dark grey dashed line is represented the case where the $\bar{\boldsymbol{u}}^2$ term is not considered, while the light grey dotted line is the case where all the control terms are active. As mentioned before, the $\bar{\boldsymbol{u}}^2$ term aims to compensate the effect of the disturbances induced by the *off*-manifold dynamics (i.e. the fast, vanishing dynamics) which can be substantially neglected in this case. Therefore the contribution of the $\bar{\boldsymbol{u}}^2$ term is negligible, as shown by figure 5.4 where the torques corresponding to each control term are shown.

It must be pointed out that the choice of the frequencies and the damping factors which determine the rate of convergence of the joints errors is a challenging task in the presence of the fast controller. The separation of the slow and the fast time scale must be ensured also in closed loop, hence, a trade off among joints trajectories tracking accuracy and separation of the two time scale is necessary [129].

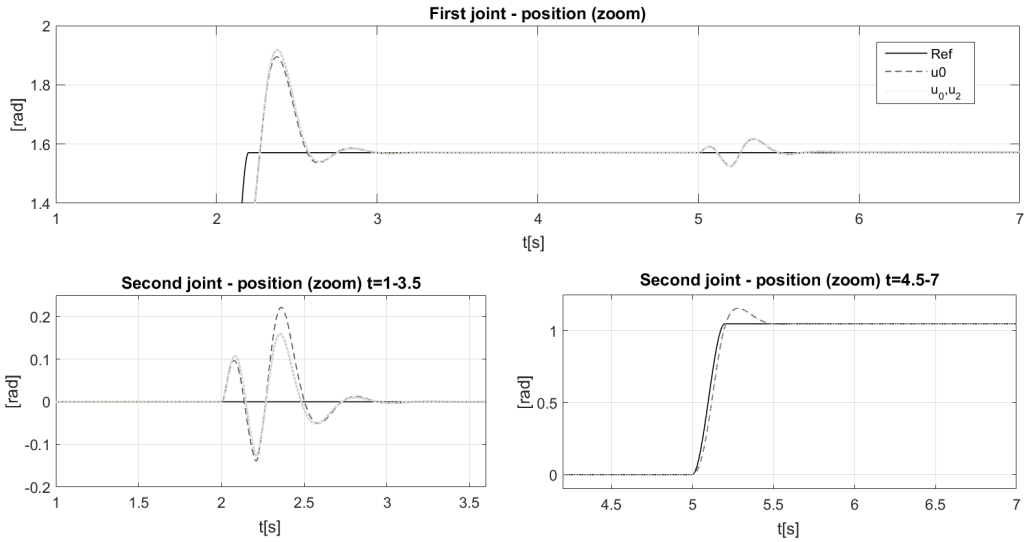

Figure 5.2: Position of the manipulator's joints (zoom)

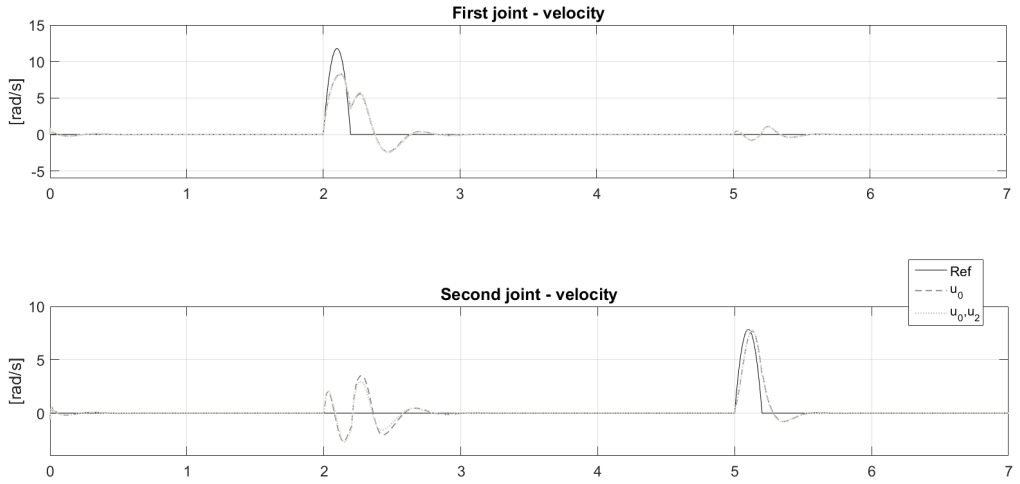

Figure 5.3: Velocities of the manipulator's joints

5.3 Robust control of the off-manifold subsystem

The *off*-manifold subsystem described by eqs. (4.65) is linear, but the dynamic matrices are parametric in $\boldsymbol{x}_1$. Assuming that $\boldsymbol{x}_1 = \boldsymbol{\theta}$ this dependency intuitively describes the influence of the manipulator's spatial configuration on the vibration dynamics, indeed, the system (4.65) is not dependent on the $\boldsymbol{x}_2$ states. As a consequence, parameters of the *off*-manifold system varies in a bounded set, which corresponds to the manipulator's joints space. As discussed in Section 4.4 the *off*-manifold dynamics describes the distance from the quasi steady state condition (i.e. the system on the manifold),

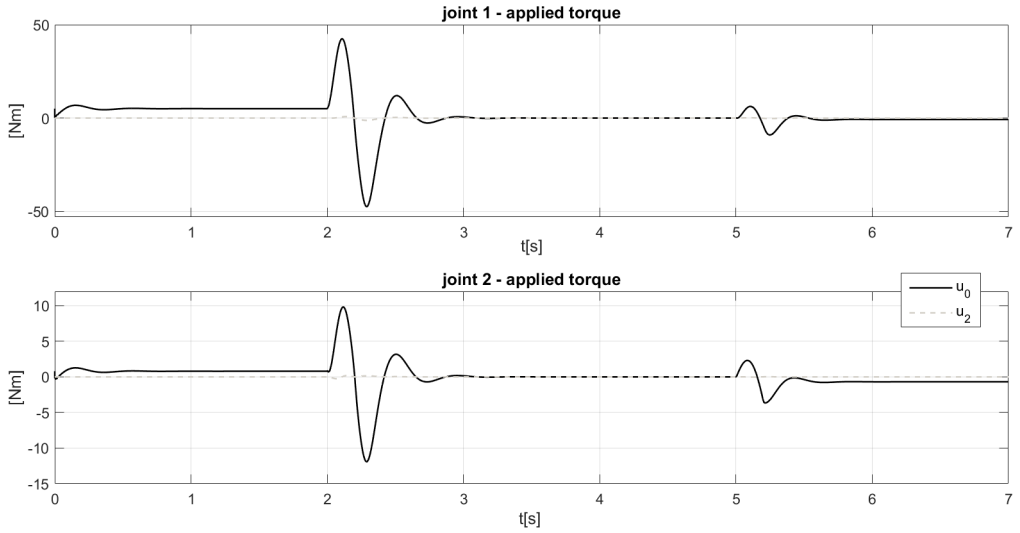

Figure 5.4: Torques acting on the joints

hence the goal of a control system acting on the joints is to bring back to zero the state variables of the *off*-manifold as consequence of disturbances, i.e. to damp the vibrations that arise from the manipulator's motion. In this context, the *off*-manifold system can be considered as a MIMO linear system, whose matrices vary in a bounded set and can be computed numerically for a finite subset of the same parameter. In this scenario, several control techniques can be applied, as discussed in Chapter 1. Nevertheless, most of these techniques have been developed with the assumption to have an explicit description of how the varying parameter influences the the dynamics matrices of the system. In the case discussed here, this dependency is deeply involved and its explicit formulation is very difficult to achieve, consequently, a technique based on the robust control has been carried out and simulated in order to test the effectiveness of the control.

5.3.1 Robust control synthesis

As a first attempt, a control scheme based on the classical robust control has been formulated. Consider the *off*-manifold system 4.65:

$$\frac{\mathrm{d}\boldsymbol{\eta}_1}{\mathrm{d}\tau} = \boldsymbol{\eta}_2 \tag{5.30}$$

$$\frac{\mathrm{d}\boldsymbol{\eta}_2}{\mathrm{d}\tau} = -\left(\bar{\boldsymbol{\mathcal{H}}}_{qq} + \varepsilon^2\bar{\hat{\boldsymbol{\mathcal{H}}}}_{qq}\right)\boldsymbol{\eta}_1 + \left(\bar{\boldsymbol{\mathcal{H}}}_{q\theta} + \varepsilon^2\bar{\hat{\boldsymbol{\mathcal{H}}}}_{q\theta}\right)\boldsymbol{u}_f \tag{5.31}$$

which, in the following will be represented in the traditional state space form as:

$$\frac{\mathrm{d}\boldsymbol{\eta}}{\mathrm{d}\tau} = \boldsymbol{\mathcal{A}}\boldsymbol{\eta} + \boldsymbol{\mathcal{B}}\boldsymbol{u}_f \tag{5.32}$$

where

$$\boldsymbol{\mathcal{A}} = \begin{bmatrix} \mathbf{0}_{M\times M} & \boldsymbol{I}_{M\times M} \\ -\left(\bar{\boldsymbol{\mathcal{H}}}_{qq} + \varepsilon^2 \bar{\hat{\boldsymbol{\mathcal{H}}}}_{qq}\right) & \mathbf{0}_{M\times M} \end{bmatrix} \in \mathbb{R}^{2M\times 2M} \tag{5.33}$$

is the state matrix, and

$$\boldsymbol{\mathcal{B}} = \begin{bmatrix} \mathbf{0}_{M\times N} \\ \left(\bar{\boldsymbol{\mathcal{H}}}_{q\theta} + \varepsilon^2 \bar{\hat{\boldsymbol{\mathcal{H}}}}_{q\theta}\right) \end{bmatrix} \in \mathbb{R}^{2M\times N} \tag{5.34}$$

is the matrix of control inputs. Recalling that the $\bar{\boldsymbol{\mathcal{H}}}_{q\theta}$ $\bar{\boldsymbol{\mathcal{H}}}_{qq}$ $\bar{\hat{\boldsymbol{\mathcal{H}}}}_{q\theta}$ *and* $\bar{\hat{\boldsymbol{\mathcal{H}}}}_{qq}$ matrices depend on the $\boldsymbol{\theta}$ state variables, one can rewrite the system (5.32) in transfer function form as follows:

$$\boldsymbol{y} = \boldsymbol{G}\boldsymbol{u}_f \tag{5.35}$$

Here the system is MIMO, $\boldsymbol{G} \in \mathbb{R}^{2M}$ can be reformulated as an uncertain matrix of transfer functions characterized by an output multiplicative uncertainty $\boldsymbol{\Delta} \in \mathbb{R}^{2M}$ and

$$\boldsymbol{G} = \boldsymbol{G}_0(\boldsymbol{I} + \boldsymbol{W}\boldsymbol{\Delta}) \tag{5.36}$$

where the matrix $\boldsymbol{G}_0$ is the *nominal* model, $\boldsymbol{\Delta}$ is a matrix of scalar functions which is unknown but assumed to be uniformly bounded in its induced matrix norm at all frequencies, i.e. for MIMO systems:

$$\bar{\sigma}(\boldsymbol{\Delta}(j\omega)) \leq 1, \ \forall\omega \tag{5.37}$$

or equivalently, recalling the definition of H_∞ norm for MIMO systems[2]

$$||\boldsymbol{\Delta}||_\infty \leq 1 \tag{5.38}$$

while the $\boldsymbol{W}$ term is commonly called *uncertainty weight* and describes the amount of uncertainty that characterize the system. [3] In the specific case of the system 5.32 the goal is to represent the variability of the $\boldsymbol{\mathcal{A}}$ and $\boldsymbol{\mathcal{B}}$ system matrices by means of the formulation 5.36 and synthesize a robust control able to stabilize the system robustly with respect to the varying parameter.

Figure 5.5, represents the upper linear fractional transformation (upper LFT) equivalent representation of (5.36). A common way to describe this representation of the system is $L_u(\boldsymbol{P}, \boldsymbol{\Delta})$ where the u subscript denotes the *upper* LFT, see [159] for further details. If it is possible to find a feedback controller $\boldsymbol{K}$ between y and u such that G is stable for all the norm bounded uncertainties $||\boldsymbol{\Delta}||_\infty \leq 1$ then the controller $\boldsymbol{K}$ is said to be *robustly stabilizing* and the system is *robustly stable*. The robust stabilization problem can be stated in terms of an equivalent $\boldsymbol{H}_\infty$ optimal control problem.

The system $\boldsymbol{P}$ of Figure 5.5 can be written as:

$$\boldsymbol{P} = \begin{bmatrix} \boldsymbol{P_{11}} & \boldsymbol{P_{12}} \\ \boldsymbol{P_{21}} & \boldsymbol{P_{22}} \end{bmatrix} = \begin{bmatrix} \mathbf{0} & \boldsymbol{G_0} \\ \boldsymbol{W} & \boldsymbol{G_0} \end{bmatrix} \tag{5.39}$$

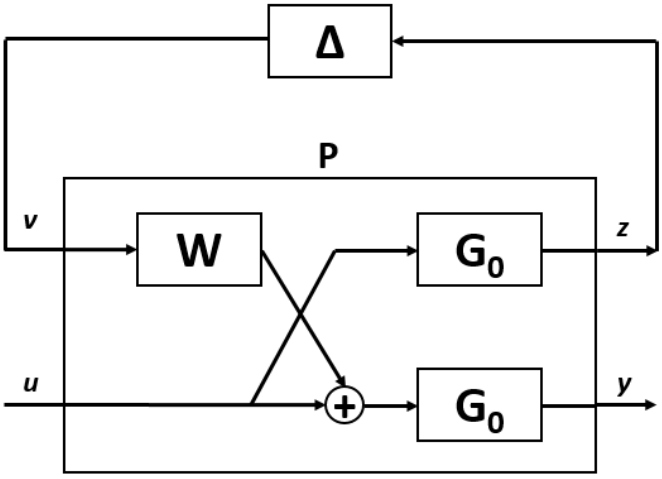

Figure 5.5: Uncertain model with multiplicative uncertainty

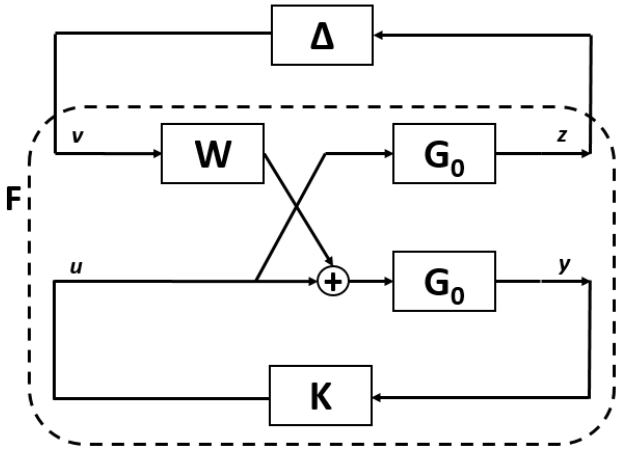

Figure 5.6: Uncertain model with multiplicative uncertainty and feedback controller

And the closed loop system including the controller, shown in Figure 5.6 can be written in an equivalent form:

$$z = (\boldsymbol{I} - \boldsymbol{F}\boldsymbol{\Delta})^{-1}\boldsymbol{F}v, \;\; \boldsymbol{F} = L_l(\boldsymbol{P}, \boldsymbol{K}) \tag{5.40}$$

where $\boldsymbol{F} = L_l(\boldsymbol{P}, \boldsymbol{K})$ denotes the lower LFT which, in turn, is the closed loop transfer function for the nominal system. According to the classical control theory for SISO systems, the feedback loop 5.6 is stable if $\boldsymbol{F} = L_l(\boldsymbol{P}, \boldsymbol{K})$ is stable and the loop transfer function $\boldsymbol{F}\boldsymbol{\Delta}$ has magnitude less then one at the cross-over frequency ω_c. This result is known as *small gain theorem*. By

[2] The Matrix norm is defined as the *maximum singular value* $\bar{\sigma}(\boldsymbol{\Delta}(j\omega))$, therefore the H_∞ is expressed as: $||\boldsymbol{\Delta}||_\infty = \sup \omega \bar{\sigma}(\boldsymbol{\Delta}(j\omega))$

[3] It must be recalled that in literature one can find other description of the uncartainty, for the sake of brevity not reported here. See [146, 159] for details.

the assumption that $\boldsymbol{\Delta}$ is norm-bounded $|\boldsymbol{\Delta}(j\boldsymbol{\omega})| < 1,\ \forall\omega$, robust stability is thus guaranteed if the transfer function $\boldsymbol{F}$ satisfies $|\boldsymbol{F}(j\omega)| < 1,\ \forall\omega$, or equivalently $||\boldsymbol{F}||_\infty < 1$. Regarding MIMO systems the transfer function equivalent to (5.40) can be written as:

$$z = (\boldsymbol{I} - \boldsymbol{F}\boldsymbol{\Delta})^{-1}\boldsymbol{F} = \frac{1}{det(\boldsymbol{I} - \boldsymbol{F}\boldsymbol{\Delta})} adj(\boldsymbol{I} - \boldsymbol{F}\boldsymbol{\Delta}) \cdot \boldsymbol{F} \tag{5.41}$$

Assuming that $\boldsymbol{F}$ and $\boldsymbol{\Delta}$ are both stable, the stability of 5.41 is determined by the roots of $det(\boldsymbol{I} - \boldsymbol{F}\boldsymbol{\Delta})$. Since the system shown in Figure 5.6 is stable for sufficiently small $\boldsymbol{\Delta}$, it follows that if a norm bounded $\boldsymbol{\Delta}$ exist such that (5.41) is unstable, then a Δ should exist such that (5.41) has a pole on the stability boundary, implying $det(\boldsymbol{I} - \boldsymbol{F}(j\omega)\boldsymbol{\Delta}(j\omega)) = 0$ for some ω. Consequently, the robust stability condition for MIMO systems can be written as:

$$det(\boldsymbol{I} - \boldsymbol{F}(j\omega)\boldsymbol{\Delta}(j\omega)) = 0,\ \forall\omega,\ \forall\ ||\boldsymbol{\Delta}||_\infty \leq 1 \tag{5.42}$$

After some analysis it can be shown that condition (5.42) holds if and only if $\bar{\sigma}(\boldsymbol{F}(j\omega)) < 1\ \forall\omega$ or equivalently $||\boldsymbol{F}||_\infty < 1$[4] The main significance of (5.42) is to give a quantitative characterization of the robust stability in terms of the H_∞ norm, hence the problem of finding a robust control for the *off*-manifold system can be recast into an optimal control problem where the following cost function is considered:

$$J_\infty(\boldsymbol{K}) = ||L_l(\boldsymbol{P}, \boldsymbol{K})||_\infty \tag{5.43}$$

The problem is to find a controller $\boldsymbol{K}$ such that the cost function $J_\infty(\boldsymbol{K})$ is minimized (under additional constraint considered later). The direct minimization of $J_\infty(\boldsymbol{K})$ turns out to be a tough problem [39, 52, 55], while it is much easier to construct a stabilizing controller which achieves a given bound. One can use this result to iteratively search for the sub-minimum $J_\infty(\boldsymbol{K})$ to a given degree of accuracy. This procedure is known as 'γ-*iteration*'.

Further considerations can be made if some more assumptions on the structure of the uncertainty are considered. In many cases the robust stability condition (5.42) can lead to unnecessarily conservative designs, but if the uncertainty Δ can be restricted to a diagonal structure, i.e.:

$$\boldsymbol{\Delta} = \begin{bmatrix} \boldsymbol{\Delta}_1 & 0 & \dots & 0 \\ 0 & \boldsymbol{\Delta}_2 & \dots & 0 \\ \vdots & \vdots & \ddots & \vdots \\ 0 & 0 & 0 & \boldsymbol{\Delta}_n \end{bmatrix},\ ||\boldsymbol{\Delta}_i|| < 1,\ i = 1, 2, \dots, n \tag{5.44}$$

[4] The result:

$$\boldsymbol{F}||_\infty < 1 \ \Rightarrow\ \text{robust stability}$$

is a classical result that follows the *small gain theorem*, while the dual:

$$\boldsymbol{F}||_\infty < 1 \ \Leftarrow\ \text{robust stability}$$

was proven only in the late 1980's and follows the fact that if $||\boldsymbol{F}||_\infty \geq 1$ then a $||\boldsymbol{\Delta}||_\infty \leq 1$, which can have arbitrary phase, can always be found to destabilize the system.

then, the robust stability condition (5.42) cannot be reduced to a simple condition on the H_∞ norm of the closed loop transfer function. However, a similar condition can be found defining a quantity:

$$\mu(\boldsymbol{F}(j\omega)) = \delta_{min}((\boldsymbol{F}(j\omega))^{-1} \tag{5.45}$$

where:

$$\delta_{min}(\boldsymbol{F}(j\omega)) = min\{\delta\colon det(I - \boldsymbol{F}(j\omega))\Delta(j\omega) = 0 \text{ for some } \Delta \in \boldsymbol{\Delta}_s(\delta)\} \tag{5.46}$$

and

$$\boldsymbol{\Delta}_s(\delta) = \{\Delta = block\ diag(\Delta_1, \Delta_2, \ldots, \Delta_n), ||\Delta_i||_\infty < \delta\} \tag{5.47}$$

The quantity $\mu(\boldsymbol{F})$ is called structural singular value (SSV) and was introduced in [38] in order to provide a condition for robust stability with respect to structured uncertainties, it can be considered as a generalization of the maximum singular value.

The definition of structured singular value does not provide a method for computing the actual value, moreover, the SSV turns out to be very hard to calculate numerically (see [142]) and no efficient algorithm exists. A more tractable approach is to compute an upper bound on μ, this approach is referred to as "DK-optimization" or "μ-synthesis" [106] and its description is not reported here.

Returning to the *off*-manifold system, the robust control approach described above can be useful to synthesize a controller where the uncertainty $\boldsymbol{\Delta}$ describes the dependency of the system from the parameter $\boldsymbol{x}_1$. However, it must be recalled that the final goal is to damp the vibrations (i.e. drive the state of the system to zero), but the described approach only guarantees the robust stability of the controlled system. As a consequence, a set of constraints on the resulting closed loop, aimed to force the dynamic behavior of the system must be formalized. In light of this, a result thoroughly described in [25] can be exploited. As shown in [52, 65] the H_∞ synthesis can be formulated as a convex optimization problem involving linear matrix inequalities. In this framework it is possible to add constraints to the optimization problem as LMI regions and solve the constrained problem, given that the intersection of the constraints define a convex region. By defining one or more LMI constraints, one can define the region of the complex plane in which the closed loop poles of the system should be placed.

Definition 8. Definition of the LMI region A subset Θ of the complex plane is called a n^{th} order LMI region if there exist a symmetric matrix $\Psi \in \mathbb{R}^{n,n}$ and a matrix $\Omega \in \mathbb{R}^{n,n}$ such that:

$$\Theta = \{z \in C\colon f_d(z) = \Psi + \Omega z + \Omega^T z < 0\} \tag{5.48}$$

In the specific case of the problem at hand, the goal is to introduce damping in the closed loop system as well as a minimum speed of the system

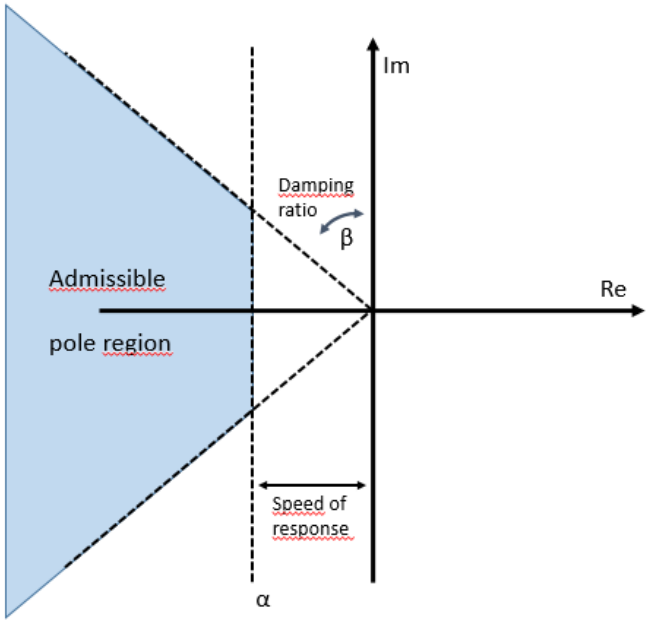

Figure 5.7: Admissible region of the closed loop poles

response. This constraints, which are graphically described in Figure 5.7, can be expressed through the convex intersection of two contraints, shown in the following.

The speed of response corresponds to restraining the real part of the poles to be under a minimum value α, i.e.:

$$\mathbb{R}(z) < \alpha \Leftrightarrow 2\alpha + z + z^T < 0 \tag{5.49}$$

hence it is sufficient to take $\Psi = 2\alpha$ and $\Omega = 1$

Similarly, in order to constrain the system to a given damping one can define the following:

$$a\mathbb{R}(z) + |b\mathbb{I}(z)| < 0 \Leftrightarrow \begin{pmatrix} a(z+\bar{z}) & -b(z+\bar{z}) \\ b(z+\bar{z}) & a(z+\bar{z}) \end{pmatrix} < 0 \tag{5.50}$$

which yelds:

$$\mathbf{\Psi} = \begin{pmatrix} 0 & 2 \\ 0 & 0 \end{pmatrix}, \ \mathbf{\Omega} = \begin{pmatrix} a & -b \\ b & a \end{pmatrix} \tag{5.51}$$

Summarizing, the procedure for the setup of the robust control problem consists in:

- Sampling the joints space with a resolution at choice.
- Identify a shaping filter $\boldsymbol{W}$ and a nominal model $\boldsymbol{G_0}$ in such a way that the array of *off*-manifold systems can be correctly described by (5.36)

Table 5.1: Manipulator's Link data

Length	400 mm
Section outer short axis	40 mm
Section outer long axis	60 mm
Width	2 mm
Density	270 Kg/m^3
Young Modulus	70 GPa

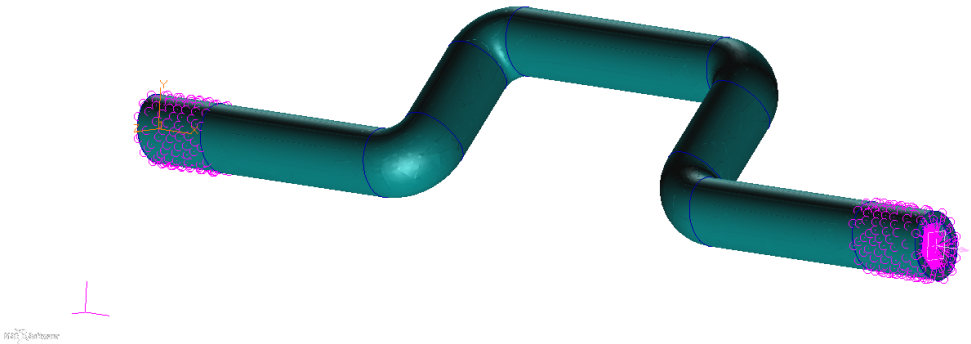

Figure 5.8: FE image of the manipulator's link

- Build an augmented system similar to the one described by eq.(5.39)
- Setup an optimization problem in order to find a controller $\boldsymbol{K}$ subject to the constraints described in (5.49,5.50) such that the H_∞ norm of the transfer function between v and z is $||\boldsymbol{P}_{vz}||_\infty < 1$

The procedure described above has been tested on a benchmark simulation case developed ad-hoc. A stabilizing robust controller has been synthesized starting from the *off*-manifold model and the results have been tested on the original closed-form model. The manipulator considered in this phase is still a two-links planar robot, but the links have been built starting from a three-dimensional shape, shown in 5.8 and the gravity field has been applied in such a way to be not parallel to the joints' axis, in order to appreciate the effect of gravity on the manipulator's configuration. The link's data are summarized in table 5.1. In Figure 5.8 the CAD model of the links is shown. The nodes of the FE model considered rigidly connected to the joints are highlighted in light red. For the sake of simplicity a minimal number of eigenmodes has been retained, namely 2 for every link. Such a low number greatly simplifies all the following phases, but at the same time allows to overcome the limits of the traditional manipulator's controls techniques where the control is tuned with the aim of having a closed-loop cutting-frequency ω_c lower then the first eigenfrequency of the system, in order not to excite the resonance.

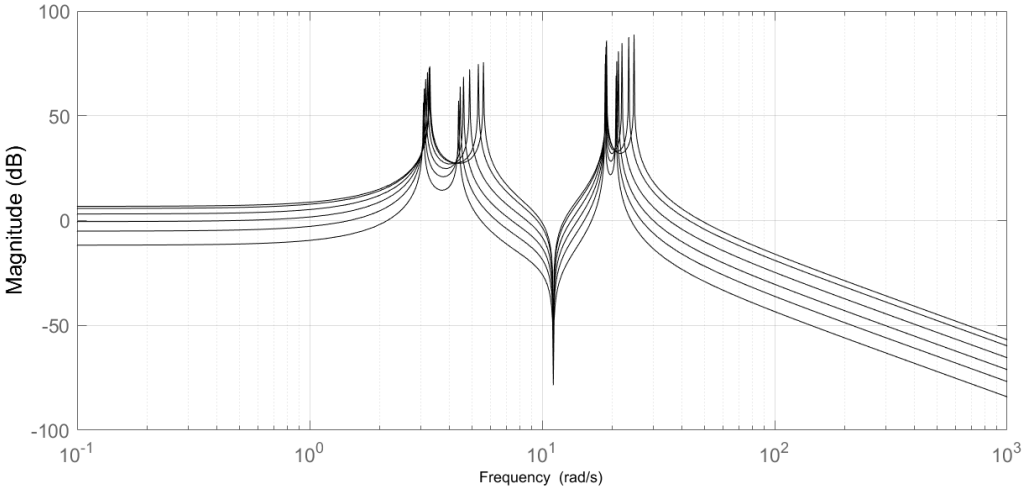

Figure 5.9: Bode diagram (Magnitude) of the transfer function from u(2) to $\eta(4)$

In order to determinate the shaping filters $\boldsymbol{W}$ and setup a control based on eq. (5.36) the joints space has been reduced to a bidimensional grid of points spacing from $-\pi$ to π with a step of $\pi/12$, yielding to an array of 144 systems. The Matlab function `ucover` has been used on the array of the transfer functions in order to obtain an uncertain model, the order of the covering filter has been set to 6. As an example, Fig. 5.9 shows the magnitudes of a subset of the transfer functions from $u(2)$ to $\eta(4)$. The system is affected by great variability with respect to the joints' position, moreover, it is not possible to obtain from *ucover* an uncertain model which describes the uncertainty of the system in such a way to be parametric with respect to inputs and and outputs[5]. The system is however MIMO with more outputs then inputs, hence an output multiplicative description of the uncertainty is able to capture the variability of the system with a more subtle granularity. As a consequence, an output multiplicative uncertainty (coherently with the description adopted in (5.36)) has been chosen. The magnitude of the filter corresponding to the subsystem array of Figure 5.9 is reported in Figure 5.10. As shown, the weighting filter has a significant magnitude at low frequencies, which is a phenomenon known to negatively affect the performances of the classical robust control schemes.

Subsequently, an augmented system of the form represented in (5.39) has been built and a stabilizing controller has been searched by means of the `h2hinfsyn` and by means of the `syndk` Matlab commands which respectively implement a procedure to synthesize a controller using the LMIs (based on the algorithm discussed in [25]) optimization and the μ-synthesis (based on [106]). In the first case additional constraints based on the LMIs described

[5] This statement deserves explanation: The `ucover` function gives a weighting filter as output, but accepts only a one-dimensional array as input, hence it is only possible to create an array of systems with both inputs for every output

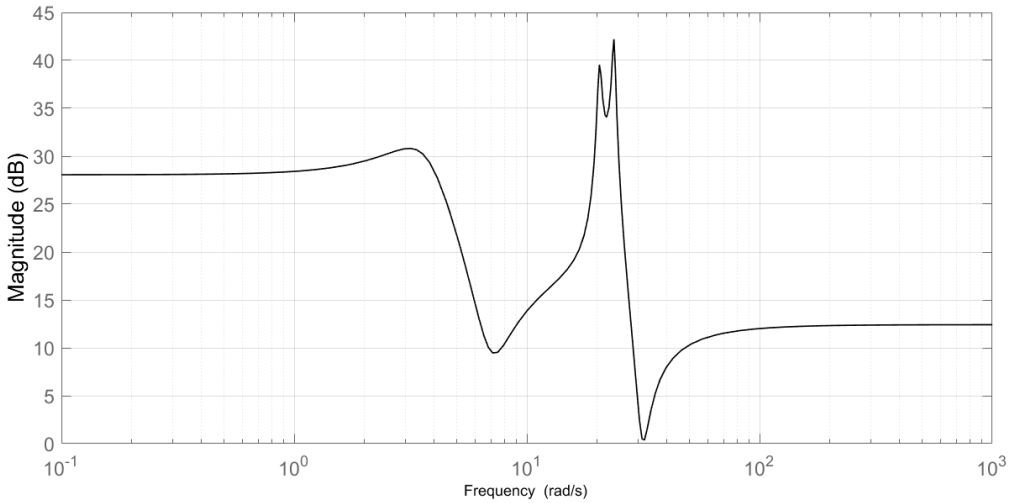

Figure 5.10: Bode diagram (Magnitude) of the filter covering the variability from u(2) to $\eta(4)$

above have been placed in the optimization procedure, the damping ratio of the closed loop poles has been set to $\psi = 0.3$ and the minimal speed of response to 10 rad/s. This procedure is carried out in a semi-automatic manner in Matlab, that is, a tool for the computation of the LMIs can be used. The matrices describing the admissible regions of the closed loop poles result as the intersection of the regions defined by eqs. (5.49,5.51). In particular, the minimum response speed is described by setting
$mathbfPsi_s = 20$ and
$mathbfOmega_s = 1$, while the matrices

$$\mathbf{\Psi_d} = \begin{pmatrix} 2 & 0 \\ 0 & 0 \end{pmatrix}, \ \mathbf{\Omega_d} = \begin{pmatrix} 0.866 & -0.5 \\ 0.5 & 0.866 \end{pmatrix} \tag{5.52}$$

describe the constraint related to damping, and the intersection of the regions is given by simply group the constraints together as follows:

$$\mathbf{\Psi} = \begin{pmatrix} 2 & 0 & 0 \\ 0 & 0 & 0 \\ 0 & 0 & 20 \end{pmatrix}, \ \mathbf{\Omega} = \begin{pmatrix} 0.866 & -0.5 & 0 \\ 0.5 & 0.866 & 0 \\ 0 & 0 & 1 \end{pmatrix} \tag{5.53}$$

Conversely, in the case where the μ-synthesis algorithm has been exploited, no additional constraint on the closed loop poles positions have been applied as optimization constraints, because the built-in functions in Matlab doesn't allow to set the relative constraints explicitly.

Despite the weakness of the dynamic constraints the LMI based optimizer could not find a feasible solution, while the μ-synthesis based solver found a solution, which is a controller of order 82. It must be recalled that no dynamic performance constraint was set during the μ-synthesis, as a consequence the solver has been able to find a solution, but the resulting

controller has unfeasible dynamic performances (i.e. no damping action). It must be pointed out that the feasibility of a solution greatly depends on the specific problem at hand, one could hope in the feasibility of the proposed method for manipulators whose dynamic vibrational behavior is less affected by spatial configuration, however some further considerations can be made. The proposed approach is simple in terms of model description and problem setup, nevertheless the dynamics of the system is complex and highly varying, moreover there are typically less inputs then outputs, leading to an even more complex control problem. Other control techniques with completely different approach could be explored, like a gain scheduling approach based on an LPV description of the system [5], but this techniques require to compute a function describing the dependency of the system's matrices from the parameters. This computation is very though for the model considered here and a robustly stabilizing controller is guaranteed only in the case of systems affine in the parameters [3]. Furthermore the controllers computed with the techniques described above often result in high-order systems and require great computational time to be synthesized.

In order to solve the problem within the framework adopted in the previous sections, a very effective method, based on the theoretical results described in [4, 7], has been adopted. This technique constitutes a practical alternative to the classical H_∞ control as it adopts a non-smooth and non convex optimization algorithm based on Clarke subdifferentials of the H_∞ norm. The mathematical treatise of this method is very involved, hence the reader is referred to [7] for a complete description and to [6] for further examples. This technique can be considered as an evolution of the robust control approach where several limitations of the classical results have been overcome. The main feature of this approach is to explicitly optimize the controller with respect to an array of closed loop models. Such kind of optimization problems is known to be non-smooth and non-convex[6], nevertheless an efficient optimization technique has been formulated. Other peculiar characteristics of this method are listed in the following.

- The structure of the controller must be defined *a priori*.
- Additional control objectives can be added to the problem as "*soft* constraints".
- Performance and stability margins requirements can be added as "*hard* constraints"
- The description of the model variability is not handled through weighting filters and structured uncertainties, instead it is considered explicitly by optimizing the cost functions over an array of closed loop systems.

[6] The non-smoothness is due to the finite array of systems with respect to which the optimizer must operate, while the non convexity is a consequence of the structural constraints on the controller

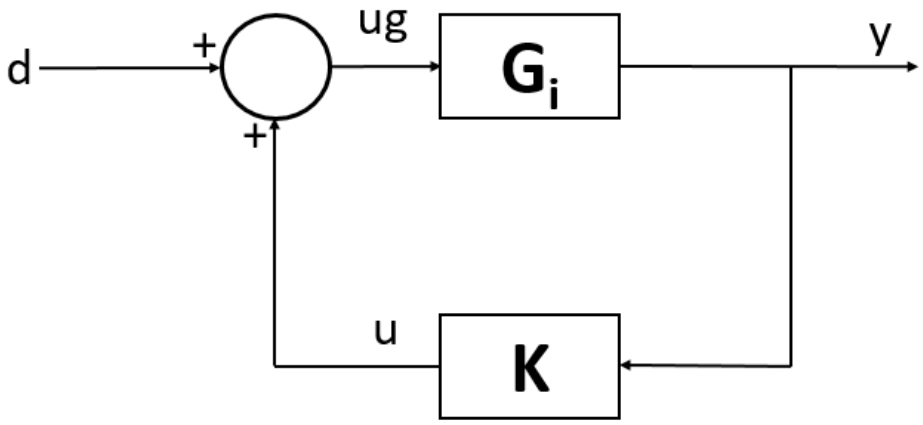

Figure 5.11: Block diagram of the closed loop systems.

The controller synthesis algorithm is implemented in Matlab through the `systune` command. The solver requires to define a controller structure and an array of closed loop systems where the signals subject to optimization or constraints are labelled. The block diagram of the systems is reported in Fig. 5.11, recalling that the final goal of the control system is to damp the vibrations an LQG control objective has been set up, where the output system response to a white noise input vector in d is considered as "*soft* constraints" or performance index. The output responses have been weighted in order to greatly penalize the lower frequency modes and particularly the η_1 variables. Additionally, "*hard* constraints" on the position of the closed loop poles and the stability margin has been placed into the optimization problem, in particular, the minimum damping ratio of the poles has been set to $\psi = 0.5$ and the minimum phase margin has been set to 50 degrees. The controller order has been fixed to 4. It must be pointed out that the specific values of the tuning goals for the closed loop system can vary as a consequence of the manipulator's task and hardness of the control synthesis problem. One of the advantages of this technique is to allow several different choices of the constraint within the same framework, leading to a fine tuning of performances and robustness.

With the constraints and performance costs described above, the solver `systune` has been able to find a stabilizing controller with the prescribed performances. Figure 5.12 shows the closed loop poles and zeros of all the elements of the transfer functions array from $d(1)$ to $y(2)$ as example, while Figue 5.13 shows the Nyquist diagram of the transfer functions. As shown, the constraints related to the poles position (i.e. damping) and phase margin have been fulfilled. As a further check, Figure 5.14 shows the impulse response of the open loop vs closed loop system.

The synthesized controller has been tested on the original closed-form model by means of the following procedure:

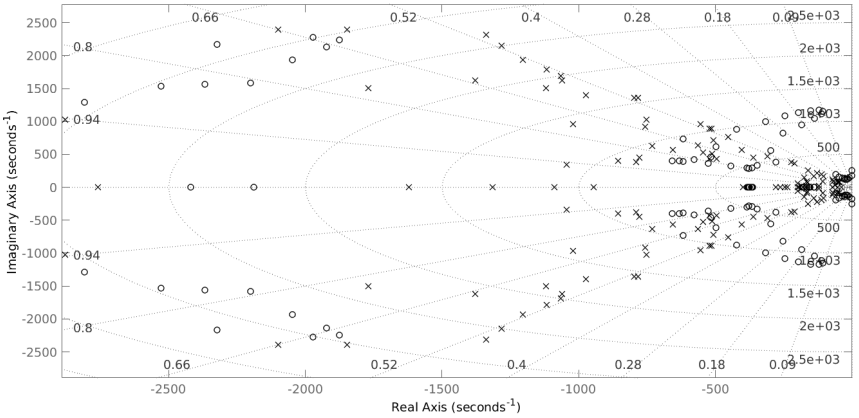

Figure 5.12: Pole/Zero map of the transfer function from $d(1)$ to $y(2)$

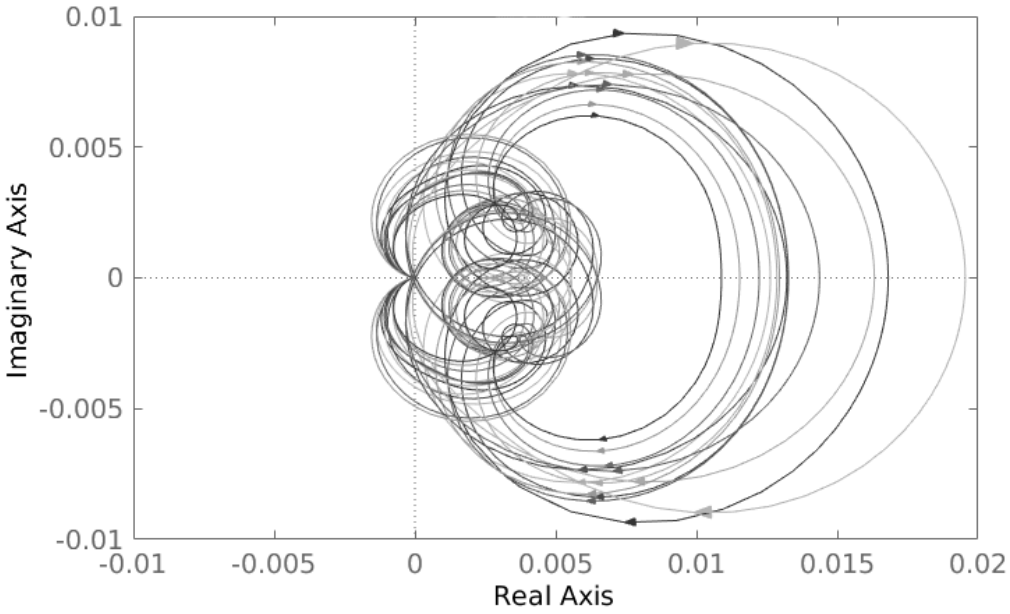

Figure 5.13: Nyquist diagram of the transfer function from $d(1)$ to $y(2)$

- Two joint position setpoints, mainly composed by interpolated steps have been created for both joints in such a way to test the influence of the disturbances created by the motion of the first joint on the second and vice versa.
- A position tracking task based on the developed trajectories has been given as input to the *on*-manifold controller acting on the closed-form model in the Matlab/Simulink simulation environment
- The gains of the *on*-manifold controller have been manually raised in order to increase the control action until vibrations in the manipulator

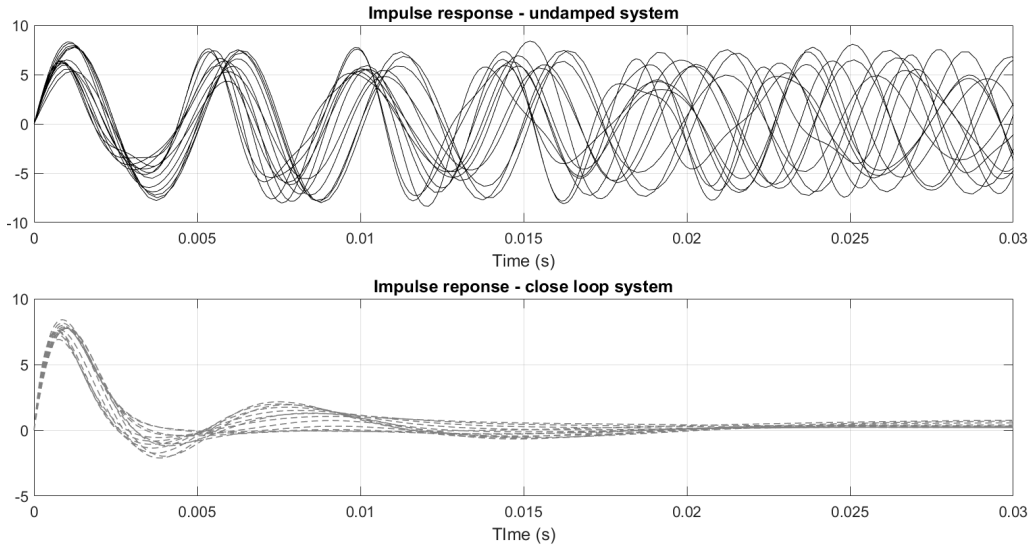

Figure 5.14: Impulse response of the open loop vs closed loop transfer function from $d(1)$ to $y(2)$

have been observed.

- Finally, the *off*-manifold controller has been introduced and the results have been observed.

Figures 5.15 and 5.16 shows a comparison of the positions of the tip of the links in the two cases. The simulation with the *off*-manifold controller inactive is reported in full black line, while the simulation reported in grey dashed line has been carried out with the controller active. Figure 5.17 shows a frequency analysis of the transverse tip position of the second link, the controller effectively damps the vibrations of the system induced by the motion.

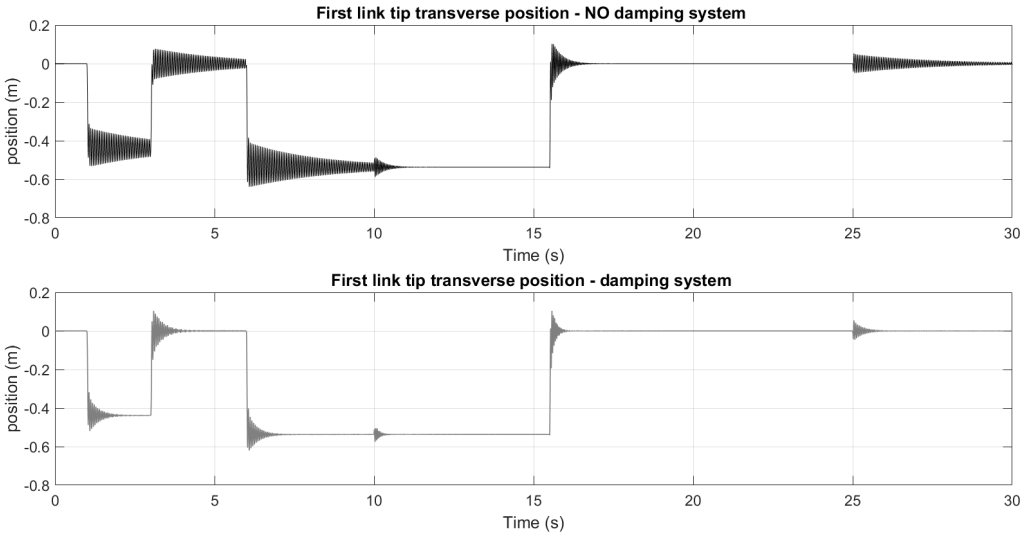

Figure 5.15: Comparison of the first links' tips transverse position with the *off*-manifold control system off (black line) and on (grey line)

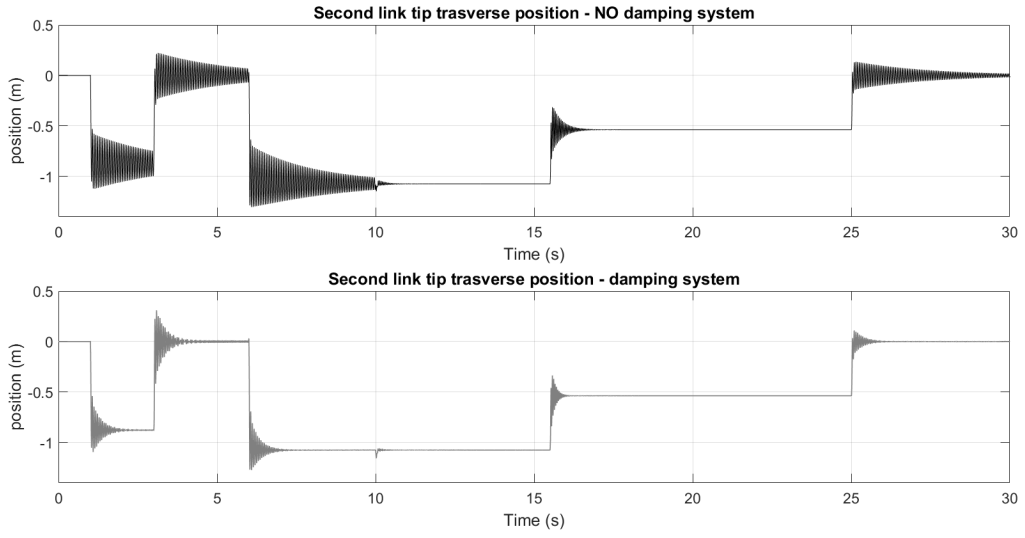

Figure 5.16: Comparison of the second links' tips transverse position with the *off*-manifold control system off (black line) and on (grey line)

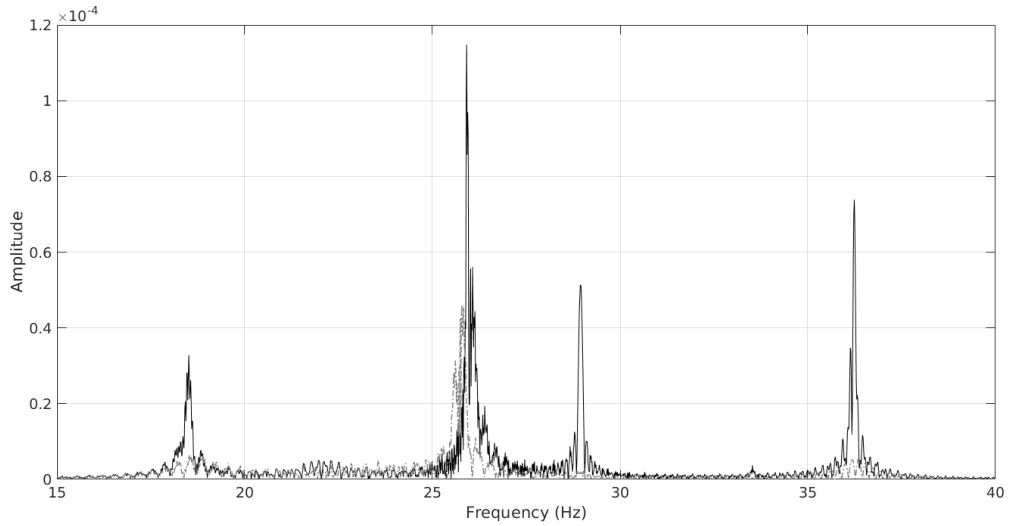

Figure 5.17: Comparison of the links' tips transverse positions frequency content, *off*-manifold control system off (full black line) and on (dashed grey line)

Chapter 6

Conclusions and future developments

6.1 Conclusions

In this thesis, the problem of modelling and control of a flexible manipulator has been tackled. This topic has been matter of research for decades, nevertheless, the great majority of the scientific work has been carried out on single link or two-links planar models derived by means of the Lagrangian approach. Here, a modular model, able to describe three-dimensional manipulators with flexible links of general shape, has been carried out by means of the Newton-Euler approach. It must be pointed out that this model has been computed starting from the Newton-Euler equations of motion of the generic flexible body. In this context, a preliminary object-oriented model has been developed and a remarkable result has been obtained, that is, the explicit computation of the Coriolis and centripetal terms of the inertial forces acting on the elastic degrees of freedom. The development of this model can be considered as the fundamental element for the realization of the subsequent results as it provides a tool for the simulation and testing in an independent multibody environment. Moreover, it constitutes as a substantial contribution in the field of object-oriented mechanical modelling, as witnessed by several feedbacks recieved by the Modelica community.

Starting from the Newton-Euler generic body model and taking advantage of the spatial vector algebra, the flexible manipulator model has been derived. The examples found in literature that follow a similar approach, although limited to planar deformation field and beam-like structures, usually solve the equations of motion by means of a recursive technique. Unlike the commonly adopted approaches, in this work the model has been derived in closed form with respect to the joint angles and the elastic variables, leading to a model suitable for simulation and analysis. Another remarkable result consists in the ability of the model to consider links of general shape by using the substructuring feature provided by finite elements solver. Further

improvements have been carried to the model by considering links with high flexibility and the presence of payloads as well as time-varying forces acting on the tip. The model has been validated with respect to benchmarks found in literature, moreover, thanks to the MERIt dataset provided by TU Dortmund, it has been possible to validate the aforementioned model with respect to experimental data.

The model disclosed in this work is highly nonlinear and its inherent complexity makes it unsuitable for the synthesis of an active vibration damping system. To this purpose, an approximated model, based on the integral manifold approach has been derived. Since the integral manifold is an extension of the singular perturbation theory, a singularly perturbed model has been initially developed and subsequently decomposed in two interacting subsystems, a *on*-manifold system representing the slow dynamics and the *off*-manifold system describing the fast dynamics, i.e. the vibrations. While the *on*-manifold system turned out to be highly nonlinear and weakly influenced by the vibratory dynamic, the *off*-manifold system is instead linear, time varying, and heavily dependent on the state of the slow system, i.e. on the spatial configuration of the manipulator.

Making use of the approximated models, the problem of model-based control design has been addressed. In order to simplify the control problem, and following the approach adopted in the modelling phase, the two time-scales composite control theory has been used to derive two separate model-based control systems. The controller for the slow system has been computed by means of a technique based on the model inversion, and it is aimed to track trajectories in the joint space. Conversely, the control system relative to the *off*-manifold, fast system, is directed toward damping the vibrations and stabilizing the system along the steady state. To this purpose, a controller based on an evolution of the robust control approach has been derived. Particularly, a novel technique, based on the optimization of the the controller with respect to an array of system models, has been applied. Moreover, this approach allows to force structural constraints on the controller and to explicitly ensure the closed loop stability. The controller has finally been tested by means of simulations, demonstrating good results in terms of vibrations damping.

6.2 Future developments

Despite the amount of theoretical and engineering work that has been carried out, several open issues still deserve to be explored. From the theoretical point of view, there are several aspects related to the observability and controllability of the system which should be discussed. Furthermore, this topic is strictly related to the issue of state estimation. The matter was not discussed in the contest of this thesis, nevertheless, an effective technique aimed to provide the estimation of the elastic modal variable is essential.

Many results related to this subject can be found in literature, however, an effective estimation method for three dimensional manipulators is still missing and the problem is further complicated by the generality of the links' geometry.

Further research would be suitable in the context of the control systems as well. The dependency of the *off*-manifold system from the joints configuration naturally calls for an LPV control scheme based on the recent results on the stability of affinely controlled LPV systems. Nevertheless it must be recalled that the dependency is very involved, hence, further work is required in order to consider this techniques. Furthermore, other model-based control techniques usually applied to flexible manipulators, briefly recalled in Chapter 1 deserve to be explored.

Finally, the realization of a three dimensional experimental platform is essential for the testing and validation of the techniques presented here, as much as for the study of further developments in terms of modelling, identification and control.

Bibliography

[1] A.A.Shabana. Dynamics of flexible bodies using generalized newton-euler equations. *Dyn. Sys., Meas., Control*, 112(3)(8):496–50, 1990.

[2] Ansys Corp. *Ansys Release 11.0 Documentation*, 2009.

[3] P. Apkarian and R. Adams. Advanced gain-scheduling techniques for uncertain systems. *IEEE Transactions on control systems technology*, 6(1):21–32, 1998.

[4] P. Apkarian, M. N. Dao, and D. Noll. Parametric robust structured control design. *IEEE Transactions on Automatic Control*, 60(7):1857–1869, July 2015.

[5] P. Apkarian and P. Gahinet. A convex characterization of gain-scheduled H∞ controllers. *IEEE Transactions on Automatic Control*, 40(5):853–864, May 1995.

[6] P. Apkarian, P. Gahinet, and C. Buhr. Multi-model, multi-objective tuning of fixed-structure controllers. In *2014 European Control Conference (ECC)*, pages 856–861. IEEE Publ. Piscataway, NJ, 2014.

[7] P. Apkarian and D. Noll. Nonsmooth H∞ synthesis. *IEEE Transactions on Automatic Control*, 51(1):71–86, 2006.

[8] H Asada, Z-D Ma, and H Tokumaru. Inverse dynamics of flexible robot arms: modeling and computation for trajectory control. *Journal of dynamic systems, Measurement, and Control*, 112(2):177–185, 1990.

[9] Dong H. Bai, M. and H. Schwarz. Adaptive augmented state feedback control for an experimental planar two-link flexible manipulator. *IEEE Transactions on Robotics and Automation*, 14(6):940–950, 1998.

[10] R. Banavar and P. Dominic. An LQG/H∞ controller for a flexible manipulator. *IEEE Transactions on control systems technology*, 3(4):409–416, 1995.

[11] H Baruh and SSK Tadikonda. Issues in the dynamics and control of flexible robot manipulators. *Journal of Guidance, Control, and Dynamics*, 12(5):659–671, 1989.

[12] L. Bascetta. *Visual servoing of flexible manipulators.* PhD thesis, Politecnico di Milano, 2004.

[13] L. Bascetta, G. Ferretti, and B. Scaglioni. Closed-form Newton-Euler dynamic model of flexible manipulators. *Robotica (in press).*

[14] M. Benosman and G Le Vey. Control of flexible manipulators: A survey. *Robotica*, 22(05):533–545, 2004.

[15] M Benosman, G Le Vey, L Lanari, and A. De Luca. Rest-to-rest motion for planar multi-link flexible manipulator through backward recursion. *Journal of dynamic systems, measurement, and control*, 126(1):115–123, 2004.

[16] M. Berzeri and A.A. Shabana. Study of the centrifugal stiffening effect using the finite element absolute nodal coordinate formulation. *Multibody System Dynamics*, 7(4):357–387, 2002.

[17] W. J. Book. Recursive Lagrangian dynamics of flexible manipulator arms. *The international Journal of Robotics Research*, 3(3):87–101, 1984.

[18] F. Boyer and P. Coiffet. Generalization of Newton-Euler model for flexible manipulators. *Journal of Robotic Systems*, 13(1):11–24, 1996.

[19] Wen C. Dynamic modeling of multi-link flexible robotic manipulators. *Computers & Structures*, 79(2):183–195, 2001.

[20] T. Chan and K. Stelson. Point-to-point motion commands that eliminate residual vibration. In *American Control Conference, Proceedings of the 1995*, volume 1, pages 909–913. IEEE, 1995.

[21] L. Chang and K. Gannon. A dynamic model on a single-link flexible manipulator. *Journal of vibration and acoustics*, 112(1):138–143, 1990.

[22] J. S. Chen and C. L. Huang. Dynamic analysis of flexible slider-crank mechanisms with non-linear finite element method. *Journal of Sound and Vibration*, 246(3):389–402, 2001.

[23] F. Cheung, E. Fung, and T. Leung. A two-switching surface variable structure control scheme for a flexible manipulator. In *American Control Conference, Proceedings of the 1995*, volume 1, pages 830–836. IEEE, 1995.

[24] C Chevallereau and Y Aoustin. Nonlinear control of a two flexible link robot: experimental and theoretical comparisons. In *European Control Conference*, pages 1051–1056, 1987.

[25] M. Chilali and P. Gahinet. $H\infty$ design with pole placement contraints: an LMI approach. *IEEE transactions of automation control*, 41(3):358–367, 1996.

[26] J. Chow and P.V. Kokotovic. Two time-scale feedback design of a class of nonlinear systems. *Proc of the Jt Autom Control Conf; San Francisco, CA, USA*, 2:556–561, 1977.

[27] R. Craig and A. Kurdila. *Fundamentals of structural dynamics*. John Wiley & Sons, New York, 2006.

[28] R. R. Craig and M. C. C. Bampton. Coupling of substructures for dynamic analyses. *AIAA Journal*, 6(7):1313–1319, 1968.

[29] Dassault Systemès. *Dymola*. http://www.3ds.com/products-services/catia/products/dymola.

[30] Dassault Systemès. *Dassault Systèmes Simulia Corp. Abaqus Analysis Users Manual, Version 6.9.*, 2009.

[31] A De Luca and G Di Giovanni. Rest-to-rest motion of a one-link flexible arm. In *Advanced Intelligent Mechatronics, 2001. Proceedings. 2001 IEEE/ASME International Conference on*, volume 2, pages 923–928. IEEE, 2001.

[32] A. De Luca and B. Siciliano. Joint-based control of a nonlinear model of a flexible arm. In *American Control Conference, 1988*, pages 935–940. IEEE, 1988.

[33] A. De Luca and B Siciliano. Trajectory control of a non-linear one-link flexible arm. *International Journal of Control*, 50(5):1699–1715, 1989.

[34] A. De Luca and B. Siciliano. Explicit dynamic modeling of a planar two-link flexible manipulator. In *Decision and Control, 1990., Proceedings of the 29th IEEE Conference on*, pages 528–530. IEEE, 1990.

[35] A. De Luca and B. Siciliano. Closed-form dynamic model of planar multilink lightweight robots. *IEEE Transactions on Systems, Man, and Cybernetics*, 21(4):826–839, 1991.

[36] A. De Luca and B. Siciliano. Regulation of flexible arms under gravity. *IEEE Transactions on Robotics and Automation*, 9(4):463–467, 1993.

[37] J. Denavit and R. S. Hartenberg. A kinematic notation for lower–pair mechanisms based on matrices. *Transaction of ASME E, Journal of Applied Mechanics*, 22:215–221, June 1955.

[38] J. Doyle et al. Analysis of feedback systems with structured uncertainties. In *IEE proceedings*, volume 129, pages 242–250, 1982.

[39] J. Doyle, K. Glover, P. Khargonekar, and Bruce A Francis. State-space solutions to standard H2 and $H\infty$ control problems. *IEEE Transactions on Automatic control*, 34(8):831–847, 1989.

[40] S. Dubowsky et al. Dealing with vibrations in the deployment structures of space robotic systems. In *Proceedings of the 5th International Conference on Adaptive Structures*, pages 5–7, 1994.

[41] J.L. Escalona, H.A. Hussien, and A.A. Shabana. Application of the absolute nodal coordinate formulation to multibody system dynamics. *Journal of Sound and Vibration*, 214(5):833–851, 1998.

[42] ESI software. *SimulationX*. https://www.simulationx.com/.

[43] R. Featherstone. *Rigid Body Dynamics Algorithms*. Springer, New York, 2008.

[44] R. Featherstone, D.E. Orin, B. Siciliano, and O. Khatib. *Springer Handbook of Robotics*, chapter Dynamics, pages 35–65. Springer, Berlin, 2008.

[45] J. Fehr and P. Eberhard. Improving the simulation process in flexible multibody dynamics by enhanced model order reduction techniques. In *Multibody Dynamics 2009 - ECCOMAS Thematic Conferences. June 29 - July 2, 2009, Warsaw, Poland.*, 2009.

[46] J. Fehr and P. Eberhard. Simulation process of flexible multibody systems with non-modal model order reduction techniques. *Multibody System Dynamics*, 25:313–334, 2011.

[47] G. Ferretti, G. Magnani, and P. Rocco. Virtual prototyping of mechatronic systems. *IFAC Journal Annual Reviews in Control*, 28(2):193–206, 2004.

[48] G. Ferretti, B. Scaglioni, and A. Rossi. Multibody model of a motorbike with a flexible swingarm. In *Proceedings of the 10th international Modelica Conference, Lund, March 10-12 2014*, 2014.

[49] G. Ferretti, F. Schiavo, and L. Viganò. Object–oriented modelling and simulation of flexible multibody thin beams in Modelica with the finite element method. In 4^{th} *Modelica Conference*, Hamburg-Harburg, Germany, March 7-8 2005.

[50] A. Fijany and R. Featherstone. A new factorization of the mass matrix for optimal serial and parallel calculation of multibody dynamics. *Multibody sysyem Dynamics*, 1(29):169–187, 2013.

[51] P. Fritzson, P. Aronsson, H. Lundvall, K. Nyström, A. Pop, L. Saldamli, and D. Broman. The openmodelica modeling, simulation, and software development environment. *Simulation News Europe*, 44:8–16, 2005.

[52] P. Gahinet, P.and Apkarian. A linear matrix inequality approach to H∞ control. *International journal of robust and nonlinear control*, 4(4):421–448, 1994.

[53] V. Gamarra-Rosado and E. Yuhara. Dynamic modeling and simulation of a flexible robotic manipulator. *Robotica*, 17(05):523–528, 1999.

[54] J. Gerstmayr and J. Schöberl. A 3D finite element method for flexible multibody systems. *Multibody System Dynamics*, 15:305–320, 2006.

[55] K. Glover and J. Doyle. State-space formulae for all stabilizing controllers that satisfy an h-infinity norm bound and relations to relations to risk sensitivity. *Systems & Control Letters*, 11(3):167–172, 1988.

[56] G. Hastings and W. Book. Verification of a linear dynamic model for flexible robotic manipulators. In *Robotics and Automation. Proceedings. 1986 IEEE International Conference on*, volume 3, pages 1024–1029. IEEE, 1986.

[57] G. Hastings and W.J. Book. A linear dynamic model for flexible robotic manipulators. *Control Systems Magazine, IEEE*, 7(1):61–64, February 1987.

[58] A. Heckmann. On the choice of boundary conditions for mode shapes in flexible multibody systems. *Multibody System Dynamics*, 23(2):141–163, 2010.

[59] A. Heckmann, M. Otter, S. Dietz, and J. D. López. The DLR FlexibleBodies library to model large motions of beams and of flexible bodies exported from finite element programs. In 5^{th} *Modelica Conference*, Vienna, Austria, September 4-5 2006.

[60] M. Hermle and P. Eberhard. Control and parameter optimization of flexible robots. *Mechanics of Structures and Machines*, 28(2-3):137–168, 2000.

[61] F. Hoppensteadt. Stability in systems with parameter. *Journal of Mathematical Analysis and Applications*, 18(1):129–134, 1967.

[62] Y. Huang and CS G. Lee. Generalization of newton-euler formulation of dynamic equations to nonrigid manipulators. *Journal of dynamic systems, measurement, and control*, 110(3):308–315, 1988.

[63] Y. Hwang. Recursive newton-euler formulation for flexible dynamic manufacturing analysis of open-loop robotic systems. *The International Journal of Advanced Manufacturing Technology*, 29(5-6):598–604, 2006.

[64] M. Isogai, F. Arai, and T. Fukuda. Modeling and vibration control with neural network for flexible multi-link structures. In *Robotics and Automation, 1999. Proceedings. 1999 IEEE International Conference on*, volume 2, pages 1096–1101. IEEE, 1999.

[65] T. Iwasaki and R. Skelton. All controllers for the general $h\infty$ control problem: Lmi existence conditions and state space formulas. *Automatica*, 30(8):1307–1317, 1994.

[66] B. Jonker. A finite element dynamic analysis of flexible manipulators. *The International Journal of Robotics Research*, 9(4):59–74, 1990.

[67] M. Karkoub, G. Balas, K. Tamma, and M. Donath. Robust control of flexible manipulators via μ-synthesis. *Control engineering practice*, 8(7):725–734, 2000.

[68] M Khairudin, Z Mohamed, AR Husain, and MA Ahmad. Dynamic modelling and characterisation of a two-link flexible robot manipulator. *Low Frequency Noise, Vibration and Active Control*, 29(3):207–219, 2010.

[69] W. Khalil. Dynamic modeling of robots using recursive newton-euler techniques. In *ICINCO2010*, 2010.

[70] W. Khalil and F. Boyer. An efficient calculation of computed torque control of flexible manipulators. In *Robotics and Automation, 1995. Proceedings., 1995 IEEE International Conference on*, volume 1, pages 609–614. IEEE, 1995.

[71] M Kirćanski, M Vukobratović, N Kirćanski, and A Timčenko. A new program package for the generation of efficient manipulator kinematic and dynamic equations in symbolic form. *Robotica*, 6(04):311–318, 1988.

[72] P. Kokotovic, H.K. Khali, and J. O'Reilly. *Singular Perturbation Methods in Control: Analysis and Design*, chapter Singular perturbation techniques in control theory. Society for Industrial and Applied Mathematics, 1986.

[73] P. Koutsovasilis and M. Beitelschmidt. Comparison of model reduction techniques for large mechanical systems. *Multibody System Dynamics*, 20(2):111–128, 2008.

[74] L. Lanari and J.T. Wen. Asymptotically stable set point control laws for flexible robots. *Systems & control letters*, 19(2):119–129, 1992.

[75] EK Lavrovskii and AM Formal'skii. Control of an elastic manipulator arm using load position and velocity feedback. *Journal of Applied Mathematics and Mechanics*, 57(6):1005–1014, 1993.

[76] K. Lee and G. Wang, Y.and Chirikjian. O(n) mass matrix inversion for serial manipulators and polypeptide chains using lie derivatives. *Robotica*, 25(06):739–750, 2007.

[77] M. Lehner and P. Eberhard. A two–step approach for model reduction in flexible multibody dynamics. *Multibody System Dynamics*, 17:157–176, 2007.

[78] ChangJin Li and T. S. Sankar. Systematic methods for efficient modeling and dynamics computation of flexible robot manipulators. *Systems, Man and Cybernetics, IEEE Transactions on*, 23(1):77–95, 1993.

[79] B. Litkouhi and H. Khalil. Multirate and composite control of two-time-scale discrete-time systems. *IEEE Transactions on Automatic Control*, 30(7):645–651, Jul 1985.

[80] Z. Luo. Direct strain feedback control of flexible robot arms: new theoretical and experimental results. *IEEE Transactions on Automatic Control*, 38(11):1610–1622, 1993.

[81] C. Maffezzoni and R. Girelli. MOSES: modular modeling of physical systems in an object–oriented database. *Mathematical Modeling of Systems*, 4(2):121–147, 1998.

[82] D. J. Malzahn. *Modeling and control of multi-elastic-link robots under gravity*. PhD thesis, TU Dortmund University, 2014.

[83] J. Malzahn and T. Bertram. MERIt - a Multi-Elastic-Link Robot Identification Dataset, Institute of Control Theory and Systems Engineering (RST), TU Dortmund, Germany. Dataset TUD01-APRBS responses without damping, 2015.

[84] R. F. Reinhart Malzahn, J. and T. Bertram. Dynamics identification of a damped multi elastic link robot arm under gravity. In *IEEE International Conference on Robotics and Automation*, Honkong, China, May 31-June 7 2014.

[85] MathCore AB. *MathModelica*. http://www.mathcore.com/. A Wolfram Company.

[86] S.E. Mattsson and M. Andersson. *Omola - An Object-Oriented Modeling Language*, pages 291–310. Recent Advances in Computer Aided Control Systems. Elsevier Science, 1993.

[87] J. Mayo and J. Domínguez. Geometrically non-linear formulation of flexible multibody systems in terms of beam elements: Geometric stiffness. *Computers Structures*, 59(6):1039—-1050, 1996.

[88] J. Mayo, D. Garcia-Vallejo, and J. Dominguez. Study of the geometric stiffening effect: comparison of different formulations. *Multibody System Dynamics*, 11(4):321–341, 2004.

[89] S.. Megahed and K. Hamza. Modeling and simulation of planar flexible link manipulators with rigid tip connections to revolute joints. *Robotica*, 22(03):285–300, 2004.

[90] L. Meirovitch. *Analytical Methods in Vibration*. Macmillan Publishing, New York, 1967.

[91] P. Misra. Robust control of flexible manipulators. In *Systems Engineering, 1989., IEEE International Conference on*, pages 73–76. IEEE, 1989.

[92] M. Moallem, K. Khorasani, and R. Patel. An integral manifold approach for tip-position tracking of flexible multi-link manipulators. *IEEE Transactions on Robotics and Automation*, 13(6):823–837, 1997.

[93] A. Mohri, P. Sarkar, and M. Yamamoto. An efficient motion planning of flexible manipulator along specified path. In *Robotics and Automation, 1998. Proceedings. 1998 IEEE International Conference on*, volume 2, pages 1104–1109. IEEE, 1998.

[94] MSC Software Corporation. *MSC/ADAMS reference Manual*, 1994.

[95] MSC Software Corporation. *MSC/NASTRAN Reference Manual, Version 68 – Lahey, Miller, et al.*, 1994.

[96] MSC Software Corporation. *ADAMS/Flex – Theory of Flexible Bodies*, 2003.

[97] A. Nada, B. Hussein, S. Megahed, and A. Shabana. Floating frame of reference and absolute nodal coordinate formulations in the large deformation analysis of robotic manipulators: a comparative experimental and numerical study. In *ASME 2009 International Design Engineering Technical Conferences and Computers and Information in Engineering Conference*, pages 889–900. American Society of Mechanical Engineers, 2009.

[98] B. Nagaraj, B. Nataraju, and D. Chandrasekhar. Nondimensional parameters for the dynamics of a single flexible link. In *International Conference on Theoretical, Applied, Computational and Experimental Mechanics (ICTACEM)*, 2001.

[99] P. Naude. *Create Flexible bodies for Adams using Patran*. ESTEQ Engineering.

[100] C. Nowakowski, J. Fehr, M. Fischer, and P. Eberhard. Model order reduction in elastic multibody systems using the floating frame of reference formulation. In 7^{th} *Vienna International Conference on Mathematical Modelling – MATHMOD 2012*, Vienna, Austria, February 15—-17 2012.

[101] C. Oakley and R. Cannon. Initial experiments on the control of a two-link manipulator with a very flexible forearm. In *American Control Conference, 1988*, pages 996–1003. IEEE, 1988.

[102] M. Oh and C.C. Pantelides. A modeling and simulation language for combined lumped and distributed parameter systems. *Computers and Chemical Engineering*, 20:611–633, 1996.

[103] V. Orlando Gamarra-Rosado. A planar flexible robotic manipulator. *Kybernetes*, 29(5/6):787–797, 2000.

[104] M. Otter, H. Elmqvist, and S.E. Mattsson. The new Modelica multibody library. In 3^{rd} *Modelica Conference*, Linköping, Sweden, November 3–4, 2003.

[105] J Ower and J De Vegte. Classical control design for a flexible manipulator: modeling and control system design. *IEEE Journal on Robotics and Automation*, 5(3):485–489, 1987.

[106] A. Packard, J. Doyle, and G. Balas. Linear, multivariable robust control with a μ perspective. *Journal of dynamic systems, measurement, and control*, 115(2B):426–438, 1993.

[107] M. Pascal. Some Ooen problems in dynamic analysis of flexible multibody systems. *Multibody System Dynamics*, 5(4):315–334, 2001.

[108] N. Pedersen and M. Pedersen. A direct derivation of the equations of motion for 3d–flexible mechanical systems. *International Journal for Numerical Methods in Engineering*, 41(4):697—-719, 1998.

[109] F. Pfeiffer and B. Gebler. A multistage-approach to the dynamics and control of elastic robots. In *Robotics and Automation, 1988. Proceedings., 1988 IEEE International Conference on*, pages 2–8 vol.1, 1988.

[110] P.C. Piela, T.G. Epperly, K.M. Westerberg, and A.W. Westerberg. ASCEND: an object-oriented computer environment for modelling and analysis: the modelling language. *Computers and Chemical Engineering*, 15(1):53–72, 1991.

[111] J. Qingxuan, Z. Xiaodong, S. Hanxu, and C. Ming. Active control of space flexible-joint/flexible-link manipulator. In *2008 IEEE Conference on Robotics, Automation and Mechatronics*, pages 812–818. IEEE, 2008.

[112] F Rakhsha and A Goldenberg. Dynamics modelling of a single-link flexible robot. In *Robotics and Automation. Proceedings. 1985 IEEE International Conference on*, volume 2, pages 984–989. IEEE, 1985.

[113] M. Reiner, M. Otter, and H. Ulbrich. Modeling and feed-forward control of structural elastic robots. In *ICNAAM 2010: International Conference of Numerical Analysis and Applied Mathematics 2010*, volume 1281, pages 378—-381, Rhodes (Greece), 19—-25 September 2010. AIP.

[114] M. Rognant, E. Courteille, and P. Maurine. A systematic procedure for the elastodynamic modeling and identification of robot manipulators. *Robotics, IEEE Transactions on*, 26(6):1085—-1093, 2010.

[115] M. Sabatini, P. Gasbarri, R. Monti, and G.B. Palmerini. Vibration control of a flexible space manipulator during on orbit operations. *Acta astronautica*, 73:109–121, 2012.

[116] J.P. Sadler and Z. Yang. A comprehensive study of modal characteristics of a cylindrical manipulator with both link and joint flexibility. *Mechanism and Machine Theory*, 32(8):941—-956, 1997.

[117] M. Sayahkarajy, Z Mohamed, and A. Faudzi. Review of modelling and control of flexible-link manipulators. *Proceedings of the Institution of Mechanical Engineers, Part I: Journal of Systems and Control Engineering*, page 0959651816642099, 2016.

[118] F. Schiavo, L. Viganò, and G. Ferretti. Object-oriented modelling of flexible beams. *Multibody System Dynamics*, 15(3):263–286, 2006.

[119] R. Schloss. *End effector load force estimation and control for a multi elastic link robot arm*. PhD thesis, Citeseer, 2014.

[120] E. Schmitz. *Experiments on the end point position control of a very flexible one link manipulator*. Stanford University, 1985.

[121] R. Schwertassek and O. Wallrapp. *Dynamik flexibler Mehrkörpersysteme*. Vieweg, Wiesbaden, 1999.

[122] R. Schwertassek, O. Wallrapp, and A. A. Shabana. Flexible multibody simulation and choice of shape functions. *Nonlinear Dynamics*, 20:361–380, 1999.

[123] S.Dwivedy and P.Eberhard. Dynamic analysis of flexible manipulators, a literature review. *Mechanism and Machine Theory*, 41(7):749–777, 2006.

[124] A. A. Shabana. *Dynamics of Multibody Systems*. Cambridge University Press, New York, 1998.

[125] A. A. Shabana and R. Y. Yakoub. Three dimensional absolute nodal coordinate formulation for beam elements: Theory. *Journal of Mechanical Design*, 123(4):606—-613, 2000.

[126] A.A. Shabana and R. Schwertassek. Equivalence of the floating frame of reference approach and finite element formulations. *International Journal of Non–Linear Mechanics*, 33(3):417 – 432, 1998.

[127] P. Shi, J. McPhee, and G.R. Heppler. A deformation field for Euler–Bernoulli beams with applications to flexible multibody dynamics. *Multibody System Dynamics*, 5:79–104, 2001.

[128] B. Siciliano and W. Book. A singular perturbation approach to control of lightweight flexible manipulators. *The International Journal of Robotics Research*, 7(4):79–90, 1988.

[129] B. Siciliano, W. Book, and G. De Maria. An integral manifold approach to control of a one link flexible arm. In *Decision and Control, 1986 25th IEEE Conference on*, pages 1131–1134. IEEE, 1986.

[130] B. Siciliano and L. Sciavicco. *Modelling and control of robot manipualators*. Springer-Verlag London, 2000.

[131] SIMPACK AG. *FEMBS, The SIMPACK interface to FE Tools*. Gilching, Germany.

[132] S. Singh and A.A. Schy. Robust torque control of an elastic robotic arm based on invertibility and feedback stabilization. In *Decision and Control, 1985 24th IEEE Conference on*, pages 1317–1322. IEEE, 1985.

[133] S. N. Singh and AA Schy. Control of elastic robotic systems by nonlinear inversion and modal damping. *Journal of dynamic systems, measurement, and control*, 108(3):180–189, 1986.

[134] S. N. Singh and AA Schy. Elastic robot control: nonlinear inversion and linear stabilization. *IEEE transactions on aerospace and electronic systems*, 105(4):340–348, 1986.

[135] V.A. Sobolev. Integral manifolds and decomposition of singularly perturbed systems. *Systems and Control Letters*, 5(3):169–179, 1984.

[136] M.W. Spong, K. Khorasani, and P.V. Kokotovic. An integral manifold approach to the feedback control of flexible joint robots. *IEEE Journal of Robotics and Automation*, 3(4):291–300, August 1987.

[137] P. Staufer and H. Gattringer. Passivity-based tracking control of a flexible link robot. In *Multibody System Dynamics, Robotics and Control*, pages 95–112. Springer, 2013.

[138] W Sunada and S Dubowsky. The application of finite element methods to the dynamic analysis of flexible spatial and co-planar linkage systems. *Journal of Mechanical Design*, 103(3):643–651, 1981.

[139] The Modelica Association. *Modelica – A Unified Object–Oriented Language for Physical Systems Modeling*. Language Specification Version 3.1, 2009.

[140] R. J. Theodore and A. Ghosal. Comparison of the assumed modes and finite element models for flexible multilink manipulators. *The International Journal of Robotics Research*, 14(2):91—-111, 1995.

[141] A. Tikhonov. Systems of differential equations containing small parameters in the derivatives. *Matematicheskii sbornik*, 73(3):575–586, 1952.

[142] O Toker and H Ozbay. On the np-hardness of the purely complex μ computation, analysis/synthesis, and some related problems in multidimensional systems. In *American Control Conference, Proceedings of the 1995*, volume 1, pages 447–451. IEEE, 1995.

[143] P. Tomei and A. Tornambe. Approximate modeling of robots having elastic links. *IEEE Transactions on Systems, Man, and Cybernetics*, 18(5):831–840, 1988.

[144] C. Trautman and D. Wang. Experimental H∞ control of a single flexible link with a shoulder joint. In *Robotics and Automation, 1995. Proceedings., 1995 IEEE International Conference on*, volume 1, pages 1235–1241. IEEE, 1995.

[145] R. E. Valembois, P. Fisette, and J. C. Samin. Comparison of various techniques for modelling flexible beams in multibody dynamics. *Nonlinear Dynamics*, 12:367–397, 1997.

[146] M Vidyasagar and H Kimura. Robust controllers for uncertain linear multivariable systems. *Automatica*, 22(1):85–94, 1986.

[147] O. Wallrapp. Standardization of flexible body modeling in multibody system codes, Part I: Definition of Standard Input Data. *Mechanics Based Design of Structures and Machines*, 22(3):283 – 304, 1994.

[148] W.J. Wang, S.S. Lu, and C.F. Hsu. Experiments on the position control of a one-link flexible robot arm. *IEEE transactions on robotics and automation*, 5(3):373–377, 1989.

[149] X. Wang and J. K. Mills. Dynamic modeling of a flexible-link planar parallel platform using a substructuring approach. *Mechanism and Machine Theory*, 41(6):671—-687, 2006.

[150] T. Wasfy. Modeling contact/impact of flexible manipulators with a fixed rigid surface. In *Robotics and Automation, 1995. Proceedings., 1995 IEEE International Conference on*, volume 1, pages 621–626 vol.1, 1995.

[151] S.C. Wu and E.J. Haug. Geometric non-linear substructuring for dynamics of flexible mechanical systems. *International Journal for Numerical Methods in Engineering*, 26:2211–2276, 1988.

[152] H Yang, Hariharan Krishnan, and MH Ang. A simple rest-to-rest control command for a flexible link robot. In *Robotics and Automation, 1997. Proceedings., 1997 IEEE International Conference on*, volume 4, pages 3312–3317. IEEE, 1997.

[153] J.H. Yang, F. Lian, and L. Fu. Nonlinear adaptive control for flexible-link manipulators. *IEEE Transactions on Robotics and Automation*, 13(1):140–148, 1997.

[154] T. Yoshikawa, H. Murakami, and K. Hosoda. Modeling and control of a three degree of freedom manipulator with two flexible links. In *Experimental Robotics II*, pages 531–545. Springer, 1993.

[155] K. Zaad and K Khorasani. Control of non-minimum phase singularly perturbed systems with application to flexible-link manipulators. *International Journal of Control*, 63(4):679–701, 1996.

[156] C. Zhang and S. Song. An efficient method for inverse dynamics of manipulators based on the virtual work principle. *Journal of Robotic Systems*, 10(5):605–627, 1993.

[157] D. Zhang and S. Zhou. Dynamic analysis of flexible-link and flexible-joint robots. *Applied Mathematics and Mechanics*, 27(5):695—-704, 2006.

[158] L Zhang and J Liu. Observer-based partial differential equation boundary control for a flexible two-link manipulator in task space. *IET Control Theory & Applications*, 6(13):2120–2133, 2012.

[159] K. Zhou, J. Doyle, K. Glover, et al. *Robust and optimal control*, volume 40. Prentice hall New Jersey, 1996.

[160] G Zhu, S.. Ge, and T.H. Lee. Simulation studies of tip tracking control of a single-link flexible robot based on a lumped model. *Robotica*, 17(1):71–78, 1999.

Appendix A

Computation of the Coriolis and centripetal terms relative to the elastic degrees of freedom

The Coriolis and centripetal terms for the elastic degrees of freedom are computed from the formulation originally described in [1], i.e.:

$$\begin{aligned} \mathbf{h}_{\omega}^{f} &= -\int_{V} \rho \mathbf{S}^{T} \left(\tilde{\bar{\boldsymbol{\omega}}}^{2} \bar{\mathbf{u}} + 2\tilde{\bar{\boldsymbol{\omega}}} \dot{\bar{u}}_{f} \right) dV \\ &= -\int_{V} \rho \mathbf{S}^{T} \tilde{\bar{\boldsymbol{\omega}}}^{2} \bar{\mathbf{u}} \, dV - 2 \int_{V} \rho \mathbf{S}^{T} \tilde{\bar{\boldsymbol{\omega}}} \mathbf{S} \dot{\mathbf{q}} \, dV \end{aligned} \tag{A.1}$$

which can be divided in two terms corresponding to the two integrals, that will be analysed separately. Consider the first integral,

$$\int_{V} \rho \mathbf{S}^{T} \tilde{\bar{\boldsymbol{\omega}}}^{2} \bar{\mathbf{u}} \, dV = \int_{V} \rho \mathbf{H} \, dV \tag{A.2}$$

where the function $\mathbf{H}$ is defined as follows

$$\begin{aligned} \mathbf{H} &= -\mathbf{S}^{T} \tilde{\bar{\boldsymbol{\omega}}}^{2} \bar{\mathbf{u}} = -\mathbf{S}^{T} \bar{\omega} \times (\bar{\omega} \times \bar{\mathbf{u}}) \\ &= \mathbf{S}^{T} (\bar{\omega} \times \bar{\mathbf{u}}) \times \bar{\omega} = \mathbf{S}^{T} \widetilde{(\bar{\omega} \times \bar{\mathbf{u}})} \bar{\omega} = \mathbf{C}^{T} \bar{\boldsymbol{\omega}} \end{aligned} \tag{A.3}$$

Consequently, defining the $\mathbf{S}^{T}$ matrix as

$$\mathbf{S}^{T} = \left[\begin{array}{ccc} \hat{\mathbf{s}}_{1}^{T} & \hat{\mathbf{s}}_{2}^{T} & \hat{\mathbf{s}}_{3}^{T} \end{array} \right], \tag{A.4}$$

the $\mathbf{C}$ matrix can be written as:

$$\mathbf{C} = \widetilde{(\bar{\boldsymbol{\omega}} \times \bar{\mathbf{u}})}^{T} \mathbf{S} = -\widetilde{(\bar{\boldsymbol{\omega}} \times \bar{\mathbf{u}})} \mathbf{S} = -\widetilde{(\bar{\boldsymbol{\omega}} \times \bar{\mathbf{u}})} \left[\begin{array}{c} \hat{\mathbf{s}}_{1} \\ \hat{\mathbf{s}}_{2} \\ \hat{\mathbf{s}}_{3} \end{array} \right], \tag{A.5}$$

and recalling that

$$
\begin{aligned}
\widetilde{(\bar{\boldsymbol{\omega}} \times \bar{\mathbf{u}})} &= \begin{bmatrix} \widetilde{\bar{\omega}_2\bar{u}_3 - \bar{\omega}_3\bar{u}_2} \\ \bar{\omega}_3\bar{u}_1 - \bar{\omega}_1\bar{u}_3 \\ \bar{\omega}_1\bar{u}_2 - \bar{\omega}_2\bar{u}_1 \end{bmatrix} \\
&= \begin{bmatrix} 0 & -\bar{\omega}_1\bar{u}_2 + \bar{\omega}_2\bar{u}_1 & \bar{\omega}_3\bar{u}_1 - \bar{\omega}_1\bar{u}_3 \\ \bar{\omega}_1\bar{u}_2 - \bar{\omega}_2\bar{u}_1 & 0 & -\bar{\omega}_2\bar{u}_3 + \bar{\omega}_3\bar{u}_2 \\ -\bar{\omega}_3\bar{u}_1 + \bar{\omega}_1\bar{u}_3 & \bar{\omega}_2\bar{u}_3 - \bar{\omega}_3\bar{u}_2 & 0 \end{bmatrix} \qquad \text{(A.6)}
\end{aligned}
$$

$$\text{(A.7)}$$

One can compute $\mathbf{C}$ as:

$$
\begin{aligned}
\mathbf{C} &= -\widetilde{(\bar{\boldsymbol{\omega}} \times \bar{\mathbf{u}})} \begin{bmatrix} \hat{\mathbf{s}}_1 \\ \hat{\mathbf{s}}_2 \\ \hat{\mathbf{s}}_3 \end{bmatrix} \\
&= \begin{bmatrix} \bar{u}_1\bar{\omega}_2\hat{\mathbf{s}}_2 - \bar{u}_2\bar{\omega}_1\hat{\mathbf{s}}_2 + \bar{u}_1\bar{\omega}_3\hat{\mathbf{s}}_3 - \bar{u}_3\bar{\omega}_1\hat{\mathbf{s}}_3 \\ -\bar{u}_1\bar{\omega}_2\hat{\mathbf{s}}_1 + \bar{u}_2\bar{\omega}_1\hat{\mathbf{s}}_1 + \bar{u}_2\bar{\omega}_3\hat{\mathbf{s}}_3 - \bar{u}_3\bar{\omega}_2\hat{\mathbf{s}}_3 \\ -\bar{u}_1\bar{\omega}_3\hat{\mathbf{s}}_1 + \bar{u}_3\bar{\omega}_1\hat{\mathbf{s}}_1 - \bar{u}_2\bar{\omega}_3\hat{\mathbf{s}}_2 + \bar{u}_3\bar{\omega}_2\hat{\mathbf{s}}_2 \end{bmatrix} \qquad \text{(A.8)}
\end{aligned}
$$

Every line of the matrix (A.8) can be expressed as a combination of two elements. Focusing on the firts row, the positive terms $\bar{u}_2\bar{\boldsymbol{\omega}}_1\hat{\mathbf{s}}_2$ and $\bar{u}_3\bar{\boldsymbol{\omega}}_1\hat{\mathbf{s}}_3$ can be computed from the the following expression

$$\bar{\omega}_1 \begin{bmatrix} \bar{u}_1 & \bar{u}_2 & \bar{u}_3 \end{bmatrix} \begin{bmatrix} \hat{\mathbf{s}}_1 \\ \hat{\mathbf{s}}_2 \\ \hat{\mathbf{s}}_3 \end{bmatrix} = \bar{u}_1\bar{\omega}_1\hat{\mathbf{s}}_1 + \bar{u}_2\bar{\omega}_1\hat{\mathbf{s}}_2 + \bar{u}_3\bar{\omega}_1\hat{\mathbf{s}}_3 \qquad \text{(A.9)}$$

and the negative terms $-\bar{\omega}_2\bar{u}_1\hat{\mathbf{s}}_2$ and $-\bar{\omega}_3\bar{u}_1\hat{\mathbf{s}}_3$ are computed recalling that

$$-\begin{bmatrix} \bar{\omega}_1 & \bar{\omega}_2 & \bar{\omega}_3 \end{bmatrix} \bar{u}_1 \begin{bmatrix} \hat{\mathbf{s}}_1 \\ \hat{\mathbf{s}}_2 \\ \hat{\mathbf{s}}_3 \end{bmatrix} = -\bar{\omega}_1\bar{u}_1\hat{\mathbf{s}}_1 - \bar{\omega}_2\bar{u}_1\hat{\mathbf{s}}_2 - \bar{\omega}_3\bar{u}_1\hat{\mathbf{s}}_3. \qquad \text{(A.10)}$$

As a consequence, the first row of the matrix (A.8) can be expressed as

$$\bar{\omega}_1\bar{\mathbf{u}}^T\mathbf{S} - \bar{\boldsymbol{\omega}}^T\bar{u}_1\mathbf{S}. \qquad \text{(A.11)}$$

Extending this expression to the other rows, matrix $\mathbf{C}$ is:

$$\mathbf{C} = \begin{bmatrix} \bar{\omega}_1\bar{\mathbf{u}}^T\mathbf{S} - \bar{\boldsymbol{\omega}}^T\bar{u}_1\mathbf{S} \\ \bar{\omega}_2\bar{\mathbf{u}}^T\mathbf{S} - \bar{\boldsymbol{\omega}}^T\bar{u}_2\mathbf{S} \\ \bar{\omega}_3\bar{\mathbf{u}}^T\mathbf{S} - \bar{\boldsymbol{\omega}}^T\bar{u}_3\mathbf{S} \end{bmatrix} \qquad \text{(A.12)}$$

Consequently, the first part of $\mathbf{h}^f_\omega$ can be written as:

$$\int_V \rho\mathbf{S}^T\tilde{\bar{\boldsymbol{\omega}}}^2\bar{\mathbf{u}}\, dV = \int_V \rho\mathbf{H}\, dV = \int_V \rho\mathbf{C}^T dV\bar{\boldsymbol{\omega}} = \left(\int_V \rho\mathbf{C}\, dV\right)^T \bar{\boldsymbol{\omega}} \qquad \text{(A.13)}$$

Where

$$\int_V \rho \mathbf{C}\ dV = \begin{bmatrix} \bar{\omega}_1 \int_V \rho \bar{u}^T \mathbf{S}\ dV - \bar{\boldsymbol{\omega}}^T \int_V \rho \bar{u}_1 \mathbf{S} dV \\ \bar{\omega}_2 \int_V \rho \bar{u}^T \mathbf{S}\ dV - \bar{\boldsymbol{\omega}}^T \int_V \rho \bar{u}_2 \mathbf{S} dV \\ \bar{\omega}_3 \int_V \rho \bar{u}^T \mathbf{S}\ dV - \bar{\boldsymbol{\omega}}^T \int_V \rho \bar{u}_3 \mathbf{S} dV \end{bmatrix} \tag{A.14}$$

In order to compute (A.14), one can conveniently define a matrix $\mathbf{D}_i$ as:

$$\mathbf{D}_i = \begin{bmatrix} \mathbf{d}_{i1} \\ \mathbf{d}_{i2} \\ \mathbf{d}_{i3} \end{bmatrix} = \begin{bmatrix} \int_V \rho \bar{u}_{i1} \mathbf{S} dV \\ \int_V \rho \bar{u}_{i2} \mathbf{S} dV \\ \int_V \rho \bar{u}_{i3} \mathbf{S} dV \end{bmatrix} \tag{A.15}$$

For the purpose explicitly computing $\mathbf{D}$, the $\mathbf{I}^{10}$ and $\mathbf{I}^{11}$ inertia invariants can be introduced as follows:

$$\mathbf{I}^{10}_{ij} = \int_V \rho \bar{u}_{0i} \hat{\mathbf{s}}_j\ dV \tag{A.16}$$

$$\mathbf{I}^{11}_{ij} = \int_V \rho \hat{\mathbf{s}}_i^T \hat{\mathbf{s}}_j\ dV \tag{A.17}$$

$$\tag{A.18}$$

As a consequence of the introduction of the invariants, matrix $\mathbf{D}$, is given by:

$$\begin{aligned} \mathbf{D}_i &= \int_V \rho \bar{u}_i \mathbf{S}\ \mathrm{d}V = \int_V \rho \left(\bar{\mathbf{u}}_0 + \mathbf{S}\mathbf{q}\right)_i \mathbf{S}\ \mathrm{d}V \\ &= \int_V \rho \bar{u}_{0i} \mathbf{S}\ \mathrm{d}V + \int_V \rho \left(\mathbf{S}\mathbf{q}\right)_i \mathbf{S}\ \mathrm{d}V = \begin{bmatrix} \mathbf{I}^{10}_{i1} \\ \mathbf{I}^{10}_{i2} \\ \mathbf{I}^{10}_{i3} \end{bmatrix} + \int_V \rho \hat{\mathbf{s}}_i \mathbf{q} \mathbf{S}\ \mathrm{d}V \\ &= \begin{bmatrix} \mathbf{I}^{10}_{i1} \\ \mathbf{I}^{10}_{i2} \\ \mathbf{I}^{10}_{i3} \end{bmatrix} + \int_V \rho \mathbf{q}^T \hat{\mathbf{s}}_i^T \mathbf{S}\ \mathrm{d}V = \begin{bmatrix} \mathbf{I}^{10}_{i1} \\ \mathbf{I}^{10}_{i2} \\ \mathbf{I}^{10}_{i3} \end{bmatrix} + \begin{bmatrix} \mathbf{q}^T \mathbf{I}^{11}_{i1} \\ \mathbf{q}^T \mathbf{I}^{11}_{i2} \\ \mathbf{q}^T \mathbf{I}^{11}_{i3} \end{bmatrix} \quad i = 1, 2, 3 \end{aligned}$$

Focus on the first term of the first line of matrix (A.14), it can be rewritten in terms of the $\mathbf{I}^{10}$ and $\mathbf{I}^{11}$ inertia invariants as follows.

$$\begin{aligned}
\bar{\omega}_1 \int_V \rho \bar{\mathbf{u}}^T \mathbf{S}\ dV &= \bar{\omega}_1 \int_V \rho \begin{bmatrix} \bar{u}_1 & \bar{u}_2 & \bar{u}_3 \end{bmatrix} \begin{bmatrix} \hat{\mathbf{s}}_1 \\ \hat{\mathbf{s}}_2 \\ \hat{\mathbf{s}}_3 \end{bmatrix} dV \\
&= \bar{\omega}_1 \int_V \rho \bar{u}_1 \hat{\mathbf{s}}_1 + \bar{u}_2 \hat{\mathbf{s}}_2 + \bar{u}_3 \hat{\mathbf{s}}_3) dV \\
&= \bar{\omega}_1 \left[\int_V \rho \bar{u}_1 \hat{\mathbf{s}}_1\ dV + \int_V \rho \bar{u}_2 \hat{\mathbf{s}}_2\ dV + \int_V \rho \bar{u}_3 \hat{\mathbf{s}}_3\ dV \right] \\
&= \bar{\omega}_1 \left[\mathbf{I}_{11}^{10} + q^T \mathbf{I}_{11}^{11} + \mathbf{I}_{22}^{10} + q^T \mathbf{I}_{22}^{11} + \mathbf{I}_{33}^{10} + q^T \mathbf{I}_{33}^{11} \right] \\
&= \sum_{j=1}^{3} \mathbf{d}_{ii} \qquad \text{(A.19)}
\end{aligned}$$

While the second term of the first line of matrix (A.14) can be rewritten in terms of the $\mathbf{D}$ matrix as follows:

$$\begin{aligned}
-\bar{\boldsymbol{\omega}}^T \int_V \rho \bar{u}_1 \mathbf{S} dV &= -\bar{\boldsymbol{\omega}}^T \int_V \rho u_1 \begin{bmatrix} \hat{\mathbf{s}}_1 \\ \hat{\mathbf{s}}_2 \\ \hat{\mathbf{s}}_3 \end{bmatrix} dV \\
&= -\bar{\boldsymbol{\omega}}^T \int_V \rho \begin{bmatrix} \bar{u}_1 \hat{\mathbf{s}}_1 \\ \bar{u}_1 \hat{\mathbf{s}}_2 \\ \bar{u}_1 \hat{\mathbf{s}}_3 \end{bmatrix} dV = -\bar{\boldsymbol{\omega}}^T \mathbf{D}_1 \qquad \text{(A.20)}
\end{aligned}$$

Summarizing, the first row of (A.14) can be written as:

$$\bar{\omega}_1 \int_V \rho \bar{\mathbf{u}}^T \mathbf{S}\ dV - \bar{\boldsymbol{\omega}}^T \int_V \rho \bar{u}_1 \mathbf{S} dV = \bar{\omega}_1 (\sum_{i=1}^{3} \mathbf{d}_{ii}) - \bar{\boldsymbol{\omega}}^T \mathbf{D}_1 \qquad \text{(A.21)}$$

Extending the same computation to the other lines of (A.14), the first term of $\mathbf{h}_\omega^f$ can be computed as follows:

$$-\int_V \rho \mathbf{S}^T \tilde{\bar{\boldsymbol{\omega}}}^2 \bar{\mathbf{u}}\ dV = \begin{bmatrix} \bar{\omega}_1 (\sum_{i=1}^{3} \mathbf{d}_{ii}) - \bar{\boldsymbol{\omega}}^T \mathbf{D}_1 \\ \bar{\omega}_2 (\sum_{i=1}^{3} \mathbf{d}_{ii}) - \bar{\boldsymbol{\omega}}^T \mathbf{D}_2 \\ \bar{\omega}_3 (\sum_{i=1}^{3} \mathbf{d}_{ii}) - \bar{\boldsymbol{\omega}}^T \mathbf{D}_3 \end{bmatrix}^T \bar{\boldsymbol{\omega}} \qquad \text{(A.22)}$$

Regarding the second term of $\mathbf{h}_\omega^f$ further elaborations are necessary, it can be written as:

$$-2 \int_V \rho \mathbf{S}^T \tilde{\bar{\boldsymbol{\omega}}} \mathbf{S} \dot{\mathbf{q}}\ dV = -2 (\int_V \rho \mathbf{S}^T \tilde{\bar{\boldsymbol{\omega}}} \mathbf{S}\ dV) \dot{\mathbf{q}} = -2 \mathbf{F} \dot{\mathbf{q}} \qquad \text{(A.23)}$$

where $\mathbf{F}$ is defined as:

$$\mathbf{F} = \int_V \rho \mathbf{S}^T \tilde{\bar{\boldsymbol{\omega}}} \mathbf{S} \, dV \tag{A.24}$$

Recalling that $\mathbf{S}^T \left(\tilde{\bar{\boldsymbol{\omega}}} \mathbf{S} \right)$ can be written as:

$$\begin{aligned} \mathbf{S}^T \tilde{\bar{\boldsymbol{\omega}}} \mathbf{S} &= \begin{bmatrix} \hat{\mathbf{s}}_1^T & \hat{\mathbf{s}}_2^T & \hat{\mathbf{s}}_3^T \end{bmatrix} \begin{bmatrix} 0 & -\bar{\omega}_3 & \bar{\omega}_2 \\ \bar{\omega}_3 & 0 & -\bar{\omega}_1 \\ -\bar{\omega}_2 & \bar{\omega}_1 & 0 \end{bmatrix} \begin{bmatrix} \hat{\mathbf{s}}_1 \\ \hat{\mathbf{s}}_2 \\ \hat{\mathbf{s}}_3 \end{bmatrix} \qquad \text{(A.25)} \\ &= -\hat{\mathbf{s}}_1^T \bar{\omega}_3 \hat{\mathbf{s}}_2 + \hat{\mathbf{s}}_1^T \bar{\omega}_2 \hat{\mathbf{s}}_3 \\ &\quad + \hat{\mathbf{s}}_2^T \bar{\omega}_3 \hat{\mathbf{s}}_1 - \hat{\mathbf{s}}_2^T \bar{\omega}_1 \hat{\mathbf{s}}_3 \\ &\quad - \hat{\mathbf{s}}_3^T \bar{\omega}_2 \hat{\mathbf{s}}_1 + \hat{\mathbf{s}}_3^T \bar{\omega}_1 \hat{\mathbf{s}}_2 \\ &= \bar{\omega}_1 (\hat{\mathbf{s}}_3^T \hat{\mathbf{s}}_2 - \hat{\mathbf{s}}_2^T \hat{\mathbf{s}}_3) + \bar{\omega}_2 (\hat{\mathbf{s}}_1^T \hat{\mathbf{s}}_3 - \hat{\mathbf{s}}_3^T \hat{\mathbf{s}}_1) \\ &\quad + \bar{\omega}_3 (\hat{\mathbf{s}}_2^T \hat{\mathbf{s}}_1 - \hat{\mathbf{s}}_1^T \hat{\mathbf{s}}_2) \qquad \text{(A.26)} \end{aligned}$$

One can write $\mathbf{F}$ in terms of the invariants by computing the elements as follows:

$$\begin{aligned} \mathbf{F} &= \bar{\omega}_1 \int_V \rho (\hat{\mathbf{s}}_3^T \hat{\mathbf{s}}_2 - \hat{\mathbf{s}}_2^T \hat{\mathbf{s}}_3) \, dV + \bar{\omega}_2 \int_V \rho (\hat{\mathbf{s}}_1^T \hat{\mathbf{s}}_3 - \hat{\mathbf{s}}_3^T \hat{\mathbf{s}}_1) \, dV \\ &+ \bar{\omega}_3 \int_V \rho (\hat{\mathbf{s}}_2^T \hat{\mathbf{s}}_1 - \hat{\mathbf{s}}_1^T \hat{\mathbf{s}}_2) \, dV \\ &= \bar{\omega}_1 (\mathbf{I}_{32}^{11} - \mathbf{I}_{23}^{11}) + \bar{\omega}_2 (\mathbf{I}_{13}^{11} - \mathbf{I}_{31}^{11}) + \bar{\omega}_3 (\mathbf{I}_{21}^{11} - \mathbf{I}_{12}^{11}) \qquad \text{(A.27)} \end{aligned}$$

Consequently, the complete expression of $\mathbf{h}_\omega^f$ in terms of the $\mathbf{I}^{10}$ and $\mathbf{I}^{11}$ inertia invariants is the following:

$$\begin{aligned} \mathbf{h}_\omega^f &= \begin{bmatrix} \bar{\omega}_1 (\sum_{i=1}^{3} \mathbf{d}_{ii}) - \bar{\boldsymbol{\omega}}^T \mathbf{D}_1 \\ \bar{\omega}_2 (\sum_{i=1}^{3} \mathbf{d}_{ii}) - \bar{\boldsymbol{\omega}}^T \mathbf{D}_2 \\ \bar{\omega}_3 (\sum_{i=1}^{3} \mathbf{d}_{ii}) - \bar{\boldsymbol{\omega}}^T \mathbf{D}_3 \end{bmatrix}^T \bar{\boldsymbol{\omega}} \qquad \text{(A.28)} \\ &- 2 \left[\bar{\omega}_1 (\mathbf{I}_{32}^{11} - \mathbf{I}_{23}^{11}) + \bar{\omega}_2 (\mathbf{I}_{13}^{11} - \mathbf{I}_{31}^{11}) + \bar{\omega}_3 (\mathbf{I}_{21}^{11} - \mathbf{I}_{12}^{11}) \right] \dot{\mathbf{q}} \end{aligned}$$

where

$$\mathbf{D}_i = \begin{bmatrix} \mathbf{d}_{i1} \\ \mathbf{d}_{i2} \\ \mathbf{d}_{i3} \end{bmatrix} = \begin{bmatrix} \mathbf{I}_{i1}^{10} + \mathbf{q}^T \mathbf{I}_{i1}^{11} \\ \mathbf{I}_{i2}^{10} + \mathbf{q}^T \mathbf{I}_{i2}^{11} \\ \mathbf{I}_{i3}^{10} + \mathbf{q}^T \mathbf{I}_{i3}^{11} \end{bmatrix} \tag{A.29}$$

However, an explicit expression for the $\mathbf{I}^{10}$ and $\mathbf{I}^{11}$ inertia invariants still has to be computed.

Recalling that the $\mathbf{I}^8$ invariant can be expressed as follows:

$$\mathbf{I}^8_k = \int_v \rho \begin{bmatrix} -\bar{u}_{02}s_{2k} - \bar{u}_{03}s_{3k} & \bar{u}_{01}s_{2k} & \bar{u}_{01}s_{3k} \\ \bar{u}_{02}s_{1k} & -\bar{u}_{01}s_{1k} - \bar{u}_{03}s_{3k} & \bar{u}_{02}s_{3k} \\ \bar{u}_{03}s_{1k} & \bar{u}_{03}s_{2k} & -\bar{u}_{01}s_{1k} - \bar{u}_{02}s_{2k} \end{bmatrix} dV$$

One can calculate $\mathbf{I}^{10}_k$ from eq. (A.16) by expanding the terms inside the integral of the expression above, as follows:

$$\begin{aligned} u_{0i}\hat{\mathbf{s}}_j &= \bar{u}_{0i}\begin{bmatrix}(\hat{\mathbf{s}}_j)_1 & (\hat{\mathbf{s}}_j)_2 & (\hat{\mathbf{s}}_j)_3 & \dots & (\hat{\mathbf{s}}_j)_M\end{bmatrix} && \text{(A.30)} \\ &= \begin{bmatrix} \bar{u}_{0i}(\hat{\mathbf{s}}_j)_1 & \bar{u}_{0i}(\hat{\mathbf{s}}_j)_2 & \bar{u}_{0i}(\hat{\mathbf{s}}_j)_3 & \dots & \bar{u}_{0i}(\hat{\mathbf{s}}_j)_M \end{bmatrix} && \text{(A.31)} \end{aligned}$$

yielding

$$\mathbf{I}^{10}_{ij} = \int_V \begin{bmatrix} \bar{u}_{0i}(\hat{\mathbf{s}}_j)_1 & \bar{u}_{0i}(\hat{\mathbf{s}}_j)_2 & \bar{u}_{0i}(\hat{\mathbf{s}}_j)_3 & \dots & \bar{u}_{0i}(\hat{\mathbf{s}}_j)_M \end{bmatrix} dV \qquad \text{(A.32)}$$

Having defined

$$\mathbf{S}^T = \begin{bmatrix} \hat{\mathbf{s}}_1^T & \hat{\mathbf{s}}_2^T & \hat{\mathbf{s}}_3^T \end{bmatrix} = \begin{bmatrix} \mathbf{s}_1 & \mathbf{s}_2 & \mathbf{s}_3 & \dots & \mathbf{s}_M \end{bmatrix}^T \qquad \text{(A.33)}$$

with the notation adopted so far, s_{ij} is the ij^{th} element of matrix $\mathbf{S}$, corrisponding to the j^{th} element of the vector $\mathbf{s}_i$ or, adopting the notation based on vectors $\hat{\mathbf{s}}$, is the i^{th} element of vector $\hat{\mathbf{s}}_j$. summarizing:

$$s_{ij} = (\mathbf{s}_j)_i = (\hat{\mathbf{s}}_i)_j \qquad \text{(A.34)}$$

it follows that the scalars $(\hat{\mathbf{s}}_i)_j$ are in fact the scalars $\mathbf{s}_{ij}$. Consequently, the scalar elements of $\mathbf{I}^{10}_k$ can be computed starting from the elements of $\mathbf{I}^8_i$ as follows:

$$\left(\mathbf{I}^{10}_{ij}\right)_k = \begin{cases} (\mathbf{I}^8_k)_{ji} & i \neq j = 1,2,3 \quad k = 1,\dots,M \\ \frac{1}{2}\left[(\mathbf{I}^8_k)_{ii} - (\mathbf{I}^8_k)_{ll} - (\mathbf{I}^8_k)_{mm}\right] & \begin{matrix} i = j = 1,2,3 \\ l,m = 1,2,3 \end{matrix} \quad k = 1,\dots,M \end{cases} \qquad \text{(A.35)}$$

The relation (A.35) for the out-of-diagional terms is trivial, while regarding the the diagonal terms of the $\mathbf{I}^{10}$, one can obtain these terms from invariant from $\mathbf{I}^8$ in the following way.

$$\begin{aligned} (\mathbf{I}^{10}_{11})_k &= \frac{1}{2}\left[(\mathbf{I}^8_k)_{11} - (\mathbf{I}^8_k)_{22} - (\mathbf{I}^8_k)_{33}\right] \\ &= \frac{1}{2}\left[-\bar{u}_{02}s_{2k} - \bar{u}_{03}s_{3k} - (-\bar{u}_{01}s_{1k} - \bar{u}_{03}s_{3k}) - (-\bar{u}_{01}s_{1k} - \bar{u}_{02}s_{2k})\right] \\ &= \frac{1}{2}\left[+(\bar{u}_{01}s_{1k} + \bar{u}_{01}s_{1k}) + (\bar{u}_{03}s_{3k} - \bar{u}_{03}s_{3k}) + (\bar{u}_{02}s_{2k} - \bar{u}_{02}s_{2k})\right] \\ &= \bar{u}_{01}s_{1k} \qquad \text{(A.36)} \end{aligned}$$

$$\begin{aligned}(\mathbf{I}^{10}_{22})_k &= \frac{1}{2}\left[(\mathbf{I}^{8}_{k})_{22} - (\mathbf{I}^{8}_{k})_{11} - (\mathbf{I}^{8}_{k})_{33}\right] \\ &= \frac{1}{2}\left[-\bar{u}_{01}s_{1k} - \bar{u}_{03}s_{3k} - (-\bar{u}_{02}s_{2k} - \bar{u}_{03}s_{3k}) - (-\bar{u}_{01}s_{1k} - \bar{u}_{02}s_{2k})\right] \\ &= \bar{u}_{02}s_{2k} \end{aligned} \tag{A.37}$$

$$\begin{aligned}(\mathbf{I}^{10}_{33})_k &= \frac{1}{2}\left[(\mathbf{I}^{8}_{k})_{33} - (\mathbf{I}^{8}_{k})_{11} - (\mathbf{I}^{8}_{k})_{22}\right] \\ &= \frac{1}{2}\left[-\bar{u}_{01}s_{1k} - \bar{u}_{02}s_{2k} - (-\bar{u}_{02}s_{2k} - \bar{u}_{03}s_{3k}) - (-\bar{u}_{01}s_{1k} - \bar{u}_{03}s_{3k})\right] \\ &= \bar{u}_{03}s_{3k} \end{aligned} \tag{A.38}$$

Invariant $\mathbf{I}^{11}$ is computed in a similar way with respect to invariant $\mathbf{I}^{10}$, starting from the scalar elements of $\mathbf{I}^{9}$. Recalling that $\mathbf{I}^{9}$ can be defined expressed as:

$$\mathbf{I}^{9}_{kl} = \int_V \rho \begin{bmatrix} -s_{3k}s_{3l} - s_{2k}s_{2l} & s_{2k}s_{1l} & s_{3k}s_{1l} \\ s_{1k}s_{2l} & -s_{3k}s_{3l} - s_{1k}s_{1l} & s_{3k}s_{2l} \\ s_{1k}s_{3l} & s_{2k}s_{3l} & -s_{2k}s_{2l} - s_{1k}s_{1l} \end{bmatrix} \mathrm{d}V \ , \tag{A.39}$$

One can calculate the scalar terms of $\mathbf{I}^{11}_{kl}$ by expanding the term $\hat{\mathbf{s}}_i^T\hat{\mathbf{s}}_j$ as follows:

$$\hat{\mathbf{s}}_i^T\hat{\mathbf{s}}_i = \begin{bmatrix} (\hat{\mathbf{s}}_i)_1(\hat{\mathbf{s}}_j)_1 & (\hat{\mathbf{s}}_i)_1(\hat{\mathbf{s}}_j)_2 & (\hat{\mathbf{s}}_i)_1(\hat{\mathbf{s}}_j)_3 & \dots & (\hat{\mathbf{s}}_i)_1(\hat{\mathbf{s}}_j)_M \\ (\hat{\mathbf{s}}_i)_2(\hat{\mathbf{s}}_j)_1 & (\hat{\mathbf{s}}_i)_2(\hat{\mathbf{s}}_j)_2 & (\hat{\mathbf{s}}_i)_2(\hat{\mathbf{s}}_j)_3 & \dots & (\hat{\mathbf{s}}_i)_2(\hat{\mathbf{s}}_j)_M \\ \vdots & \vdots & \ddots & \vdots & \vdots \\ (\hat{\mathbf{s}}_i)_M(\hat{\mathbf{s}}_j)_1 & (\hat{\mathbf{s}}_i)_M(\hat{\mathbf{s}}_j)_2 & (\hat{\mathbf{s}}_i)_M(\hat{\mathbf{s}}_j)_3 & \dots & (\hat{\mathbf{s}}_i)_M(\hat{\mathbf{s}}_j)_M \end{bmatrix} \tag{A.40}$$

Again, as a consequence of eq.(A.34), the elements of invariant $\mathbf{I}^{11}$ can be computed as:

$$\left(\mathbf{I}^{11}_{ij}\right)_{kl} = \begin{cases} \left(\mathbf{I}^{9}_{kl}\right)_{ji} & i \neq j = 1,2,3 \quad k,l = 1,\dots,M \\ \\ \frac{1}{2}\left[(\mathbf{I}^{9}_{kl})_{ii} - (\mathbf{I}^{9}_{kl})_{mm} - (\mathbf{I}^{9}_{kl})_{nn}\right] & \begin{matrix} i = j = 1,2,3 \\ m,n = 1,2,3 \end{matrix} \quad k,l = 1,\dots,M \end{cases}$$

and again, the out-of-diagonal terms are obtained directly from the elements of $\mathbf{I}^{9}_{kl}$, while the diagonal terms are obtained as follows:

$$\begin{aligned}(\mathbf{I}^{11}_{11})_{kl} &= \frac{1}{2}\left[(\mathbf{I}^{9}_{kl})_{11} - (\mathbf{I}^{9}_{kl})_{22} - (\mathbf{I}^{9}_{kl})_{33}\right] \\ &= \frac{1}{2}\left[-s_{3k}s_{3l} - s_{2k}s_{2l} - (-s_{3k}s_{3l} - s_{1k}s_{1l}) - (-s_{2k}s_{2l} - s_{1k}s_{1l})\right] \\ &= s_{1k}s_{1l} \end{aligned} \tag{A.41}$$

$$
\begin{aligned}
(\mathbf{I}^{11}_{22})_{kl} &= \frac{1}{2}\left[(\mathbf{I}^{9}_{kl})_{22} - (\mathbf{I}^{9}_{kl})_{11} - (\mathbf{I}^{9}_{kl})_{33}\right] \\
&= \frac{1}{2}\left[-s_{3k}s_{3l} - s_{1k}s_{1l} - (-s_{3k}s_{3l} - s_{2k}s_{2l}) - (-s_{2k}s_{2l} - s_{1k}s_{1l})\right] \\
&= s_{2k}s_{2l} \qquad \text{(A.42)}
\end{aligned}
$$

$$
\begin{aligned}
(\mathbf{I}^{11}_{33})_{kl} &= \frac{1}{2}\left[(\mathbf{I}^{9}_{kl})_{33} - (\mathbf{I}^{9}_{kl})_{11} - (\mathbf{I}^{9}_{kl})_{11}\right] \\
&= \frac{1}{2}\left[-s_{3k}s_{3l} - s_{1k}s_{1l} - (-s_{2k}s_{2l} - s_{1k}s_{1l}) - (-s_{3k}s_{3l} - s_{2k}s_{2l})\right] \\
&= s_{3k}s_{3l} \qquad \text{(A.43)}
\end{aligned}
$$

Appendix B

Partial derivatives of the inertia matrix

In this Appendix, the partial derivatives of the terms of inertia matrix with respect to the elastic coordinates are derived.

The inertia matrix is subdivided in four submatrices, namely $\boldsymbol{\mathcal{M}}_{\theta\theta}$, $\boldsymbol{\mathcal{M}}_{\theta q}$, Mqq and the transpose of $\boldsymbol{\mathcal{M}}_{\theta q}$. Their partial derivatives with respect to the elastic coordinates will be derived in the following, expanding the constitutive terms of every matrix element.

The partial drivative of $\boldsymbol{\mathcal{M}}_{\theta\theta}$ is:

$$\begin{aligned}\frac{\partial \boldsymbol{\mathcal{M}}_{\theta\theta}}{\partial q_{j,i}} &= \frac{\partial \boldsymbol{\mathcal{B}}_\theta^T}{\partial q_{j,i}} \boldsymbol{\mathcal{P}}^{-1} \boldsymbol{\mathcal{I}}_{vv} \boldsymbol{\mathcal{P}}^{-T} \boldsymbol{\mathcal{B}}_\theta + \boldsymbol{\mathcal{B}}_\theta^T \frac{\partial \boldsymbol{\mathcal{P}}^{-1}}{\partial q_{j,i}} \boldsymbol{\mathcal{I}}_{vv} \boldsymbol{\mathcal{P}}^{-T} \boldsymbol{\mathcal{B}}_\theta \\ &+ \boldsymbol{\mathcal{B}}_\theta^T \boldsymbol{\mathcal{P}}^{-1} \frac{\partial \boldsymbol{\mathcal{I}}_{vv}}{\partial q_{j,i}} \boldsymbol{\mathcal{P}}^{-T} \boldsymbol{\mathcal{B}}_\theta \\ &+ \boldsymbol{\mathcal{B}}_\theta^T \boldsymbol{\mathcal{P}}^{-1} \boldsymbol{\mathcal{I}}_{vv} \frac{\partial \boldsymbol{\mathcal{P}}^{-T}}{\partial q_{j,i}} \boldsymbol{\mathcal{B}}_\theta \\ &+ \boldsymbol{\mathcal{B}}_\theta^T \boldsymbol{\mathcal{P}}^{-1} \boldsymbol{\mathcal{I}}_{vv} \boldsymbol{\mathcal{P}}^{-T} \frac{\partial \boldsymbol{\mathcal{B}}_\theta}{\partial q_{j,i}}\end{aligned} \tag{B.1}$$

where

$$\frac{\partial \boldsymbol{\mathcal{B}}_\theta}{\partial q_{j,i}} = \begin{bmatrix} \frac{\partial \boldsymbol{B}_{\theta,0}}{\partial q_{j,i}} & \mathbf{0} & \mathbf{0} & \cdots & \mathbf{0} & \mathbf{0} \\ \mathbf{0} & \frac{\partial \boldsymbol{B}_{\theta,1}}{\partial q_{j,i}} & \mathbf{0} & \cdots & \mathbf{0} & \mathbf{0} \\ \mathbf{0} & \mathbf{0} & \frac{\partial \boldsymbol{B}_{\theta,2}}{\partial q_{j,i}} & \cdots & \mathbf{0} & \mathbf{0} \\ \vdots & \vdots & \vdots & \ddots & \vdots & \vdots \\ \mathbf{0} & \mathbf{0} & \mathbf{0} & \cdots & \frac{\partial \boldsymbol{B}_{\theta,N-2}}{\partial q_{j,i}} & \mathbf{0} \\ \mathbf{0} & \mathbf{0} & \mathbf{0} & \mathbf{0} & \mathbf{0} & \frac{\partial \boldsymbol{B}_{\theta,N-1}}{\partial q_{j,i}} \end{bmatrix} \tag{B.2}$$

and the terms of the last matrix can be calculated as:

$$\frac{\partial \boldsymbol{B}_{\theta,k}}{\partial q_{j,i}} = \begin{bmatrix} \frac{\partial \left(\boldsymbol{A}_k \hat{\boldsymbol{A}}_k \hat{\boldsymbol{z}}_k\right)}{\partial q_{j,i}} \\ \boldsymbol{0} \end{bmatrix} \tag{B.3}$$

Moreover:

$$\frac{\partial \left(\boldsymbol{A}_k \hat{\boldsymbol{A}}_k \hat{\boldsymbol{z}}_k\right)}{\partial q_{j,i}} = \begin{cases} \boldsymbol{0} & , \quad i > k \\ \boldsymbol{A}_i \frac{\partial \hat{\boldsymbol{A}}_i}{\partial q_{j,i}} \hat{\boldsymbol{z}}_i = \boldsymbol{A}_i \frac{\partial \widetilde{\left(\hat{\boldsymbol{S}}_i \boldsymbol{q}_i\right)}}{\partial q_{j,i}} \hat{\boldsymbol{z}}_i = \boldsymbol{A}_i \widetilde{\left(\hat{\boldsymbol{S}}_i \boldsymbol{\sigma}_{j,i}\right)} \hat{\boldsymbol{z}}_i & , \quad i = k \\ \frac{\partial \boldsymbol{A}_k}{\partial q_{j,i}} \hat{\boldsymbol{A}}_k \hat{\boldsymbol{z}}_k & , \quad i < k \end{cases} \tag{B.4}$$

$$\frac{\partial \boldsymbol{A}_k}{\partial q_{j,i}} = \begin{cases} \boldsymbol{0} & , \quad i \geq k \\ \hat{\boldsymbol{A}}_0 \bar{\boldsymbol{A}}_0 \cdots \widetilde{\left(\hat{\boldsymbol{S}}_i \boldsymbol{\sigma}_{j,i}\right)} \bar{\boldsymbol{A}}_i \cdots \hat{\boldsymbol{A}}_{k-1} \bar{\boldsymbol{A}}_{k-1}, i < k & , \quad i < k \end{cases} \tag{B.5}$$

where $\boldsymbol{\sigma}_{j,k}$ is a vector of M_k null elements but the j-th, equal to 1. The derivative of $\boldsymbol{\mathcal{P}}^{-1}$ can be calculated as follows:

$$\frac{\partial \boldsymbol{\mathcal{P}}^{-1}}{\partial q_{j,i}} = -\boldsymbol{\mathcal{P}}^{-1} \frac{\partial \boldsymbol{\mathcal{P}}}{\partial q_{j,i}} \boldsymbol{\mathcal{P}}^{-1} \tag{B.6}$$

$$\frac{\partial \boldsymbol{\mathcal{P}}}{\partial q_{j,i}} = \begin{bmatrix} \boldsymbol{0} & -\frac{\partial \boldsymbol{P}_1^T}{\partial q_{j,i}} & \boldsymbol{0} & \cdots & \boldsymbol{0} & \boldsymbol{0} \\ \boldsymbol{0} & \boldsymbol{0} & -\frac{\partial \boldsymbol{P}_2^T}{\partial q_{j,i}} & \cdots & \boldsymbol{0} & \boldsymbol{0} \\ \boldsymbol{0} & \boldsymbol{0} & \boldsymbol{0} & \cdots & \boldsymbol{0} & \boldsymbol{0} \\ \vdots & \vdots & \vdots & \ddots & \vdots & \vdots \\ \boldsymbol{0} & \boldsymbol{0} & \boldsymbol{0} & \cdots & \boldsymbol{0} & -\frac{\partial \boldsymbol{P}_{N-1}^T}{\partial q_{j,i}} \\ \boldsymbol{0} & \boldsymbol{0} & \boldsymbol{0} & \boldsymbol{0} & \boldsymbol{0} & \boldsymbol{0} \end{bmatrix} \tag{B.7}$$

$$\frac{\partial \boldsymbol{P}_k}{\partial q_{j,i}} = \begin{bmatrix} \boldsymbol{0} & \boldsymbol{0} \\ -\frac{\partial \tilde{\boldsymbol{p}}_{k+1,k}}{\partial q_{j,i}} & \boldsymbol{0} \end{bmatrix} \tag{B.8}$$

$$\frac{\partial \tilde{\boldsymbol{p}}_{k+1,k}}{\partial q_{j,i}} = \frac{\partial \widetilde{\left(\boldsymbol{A}_k \bar{\boldsymbol{u}}_{0,k}\right)}}{\partial q_{j,i}} + \frac{\partial \widetilde{\left(\boldsymbol{A}_k \boldsymbol{S}_k \boldsymbol{q}_k\right)}}{\partial q_{j,i}} \tag{B.9}$$

$$\frac{\partial \widetilde{\left(\boldsymbol{A}_k \bar{\boldsymbol{u}}_{0,k}\right)}}{\partial q_{j,i}} + \frac{\partial \widetilde{\left(\boldsymbol{A}_k \boldsymbol{S}_k \boldsymbol{q}_k\right)}}{\partial q_{j,i}} = \begin{cases} \boldsymbol{0} & , \quad i > k \\ \boldsymbol{A}_i \boldsymbol{S}_i \boldsymbol{\sigma}_{j,i} & , \quad i = k \\ \frac{\partial \boldsymbol{A}_k}{\partial q_{j,i}} \left(\bar{\boldsymbol{u}}_{0,k} + \boldsymbol{S}_k \boldsymbol{q}_k\right) & , \quad i < k \end{cases} \tag{B.10}$$

Subsequently, the partial derivative of $\boldsymbol{\mathcal{I}}_{vv}$ must be computed.

$$\frac{\partial \boldsymbol{\mathcal{I}}_{vv}}{\partial q_{j,i}} = \operatorname{diag}\left\{ \frac{\partial \boldsymbol{I}_{vv,k}}{\partial q_{j,i}} \right\} \tag{B.11}$$

$$\frac{\partial \boldsymbol{I}_{vv,k}}{\partial q_{j,i}} = \begin{bmatrix} \frac{\partial\left(\boldsymbol{A}_k \bar{\boldsymbol{J}}_k \boldsymbol{A}_k^T\right)}{\partial q_{j,i}} & \frac{\partial\left(\boldsymbol{A}_k m_k \tilde{\bar{\boldsymbol{d}}}_{C,k} \boldsymbol{A}_k^T\right)}{\partial q_{j,i}} \\ \frac{\partial\left(\boldsymbol{A}_k m_k \tilde{\bar{\boldsymbol{d}}}_{C,k} \boldsymbol{A}_k^T\right)^T}{\partial q_{j,i}} & \boldsymbol{0} \end{bmatrix} \tag{B.12}$$

$$\frac{\partial\left(\boldsymbol{A}_k \bar{\boldsymbol{J}}_k \boldsymbol{A}_k^T\right)}{\partial q_{j,i}} = \frac{\partial \boldsymbol{A}_k}{\partial q_{j,i}} \bar{\boldsymbol{J}}_k \boldsymbol{A}_k^T + \boldsymbol{A}_k \frac{\partial \bar{\boldsymbol{J}}_k}{\partial q_{j,i}} \boldsymbol{A}_k^T + \boldsymbol{A}_k \bar{\boldsymbol{J}}_k \frac{\partial \boldsymbol{A}_k^T}{\partial q_{j,i}} \tag{B.13}$$

$$\frac{\partial\left(\boldsymbol{A}_k m_k \tilde{\bar{\boldsymbol{d}}}_{C,k} \boldsymbol{A}_k^T\right)}{\partial q_{j,i}} = \frac{\partial \boldsymbol{A}_k}{\partial q_{j,i}} m_k \tilde{\bar{\boldsymbol{d}}}_{C,k} \boldsymbol{A}_k^T + \boldsymbol{A}_k \frac{\partial\left(m_k \tilde{\bar{\boldsymbol{d}}}_{C,k}\right)}{\partial q_{j,i}} \boldsymbol{A}_k^T + \boldsymbol{A}_k m_k \tilde{\bar{\boldsymbol{d}}}_{C,k} \frac{\partial \boldsymbol{A}_k^T}{\partial q_{j,i}} \tag{B.14}$$

$$\frac{\partial \bar{\boldsymbol{J}}_k}{\partial q_{j,i}} = \begin{cases} \boldsymbol{0} & , \quad i \neq k \\ -\left(\boldsymbol{I}_{j,i}^{8T} + \boldsymbol{I}_{j,i}^{8}\right) - \sum_{l=1}^{M_i} \left(\boldsymbol{I}_{jl,i}^{9} + \boldsymbol{I}_{lj,i}^{9}\right) q_{l,i} & , \quad i = k \end{cases} \tag{B.15}$$

$$\frac{\partial\left(m_k \tilde{\bar{\boldsymbol{d}}}_{C,k}\right)}{\partial q_{j,i}} = \begin{cases} \boldsymbol{0} & , \quad i \neq k \\ \tilde{\boldsymbol{I}}_{j,i}^{3} & , \quad i = k \end{cases} \tag{B.16}$$

The partial derivatives of the other submatrices are calculated in a similar way.

$$\begin{aligned} \frac{\partial \boldsymbol{\mathcal{M}}_{\theta q}}{\partial q_{j,i}} \quad = \quad & \frac{\partial \boldsymbol{\mathcal{B}}_\theta^T}{\partial q_{j,i}} \boldsymbol{\mathcal{P}}^{-1} \boldsymbol{\mathcal{I}}_{vq} + \boldsymbol{\mathcal{B}}_\theta^T \frac{\partial \boldsymbol{\mathcal{P}}^{-1}}{\partial q_{j,i}} \boldsymbol{\mathcal{I}}_{vq} \\ & + \boldsymbol{\mathcal{B}}_\theta^T \boldsymbol{\mathcal{P}}^{-1} \frac{\partial \boldsymbol{\mathcal{I}}_{vq}}{\partial q_{j,i}} \\ & + \frac{\partial \boldsymbol{\mathcal{B}}_\theta^T}{\partial q_{j,i}} \boldsymbol{\mathcal{P}}^{-1} \boldsymbol{\mathcal{I}}_{vv}^T \boldsymbol{\mathcal{P}}^{-T} \boldsymbol{\mathcal{B}}_q + \boldsymbol{\mathcal{B}}_\theta^T \frac{\partial \boldsymbol{\mathcal{P}}^{-1}}{\partial q_{j,i}} \boldsymbol{\mathcal{I}}_{vv}^T \boldsymbol{\mathcal{P}}^{-T} \boldsymbol{\mathcal{B}}_q \\ & + \boldsymbol{\mathcal{B}}_\theta^T \boldsymbol{\mathcal{P}}^{-1} \frac{\partial \boldsymbol{\mathcal{I}}_{vv}^T}{\partial q_{j,i}} \boldsymbol{\mathcal{P}}^{-T} \boldsymbol{\mathcal{B}}_q \\ & + \boldsymbol{\mathcal{B}}_\theta^T \boldsymbol{\mathcal{P}}^{-1} \boldsymbol{\mathcal{I}}_{vv}^T \frac{\partial \boldsymbol{\mathcal{P}}^{-T}}{\partial q_{j,i}} \boldsymbol{\mathcal{B}}_q + \boldsymbol{\mathcal{B}}_\theta^T \boldsymbol{\mathcal{P}}^{-1} \boldsymbol{\mathcal{I}}_{vv}^T \boldsymbol{\mathcal{P}}^{-T} \frac{\partial \boldsymbol{\mathcal{B}}_q}{\partial q_{j,i}} \end{aligned} \tag{B.17}$$

and the subterms are computed as:

$$\frac{\partial \boldsymbol{\mathcal{I}}_{vq}}{\partial q_{j,i}} = \begin{bmatrix} \frac{\partial \boldsymbol{I}_{vq,1}}{\partial q_{j,i}} & \boldsymbol{0} & \boldsymbol{0} & \cdots & \boldsymbol{0} & \boldsymbol{0} \\ \boldsymbol{0} & \frac{\partial \boldsymbol{I}_{vq,2}}{\partial q_{j,i}} & \boldsymbol{0} & \cdots & \boldsymbol{0} & \boldsymbol{0} \\ \boldsymbol{0} & \boldsymbol{0} & \frac{\partial \boldsymbol{I}_{vq,3}}{\partial q_{j,i}} & \cdots & \boldsymbol{0} & \boldsymbol{0} \\ \vdots & \vdots & \vdots & \ddots & \vdots & \vdots \\ \boldsymbol{0} & \boldsymbol{0} & \boldsymbol{0} & \cdots & \frac{\partial \boldsymbol{I}_{vq,N-1}}{\partial q_{j,i}} & \boldsymbol{0} \\ \boldsymbol{0} & \boldsymbol{0} & \boldsymbol{0} & \boldsymbol{0} & \boldsymbol{0} & \frac{\partial \boldsymbol{I}_{vq,N}}{\partial q_{j,i}} \end{bmatrix} \tag{B.18}$$

$$\frac{\partial \boldsymbol{I}_{vq,k}}{\partial q_{j,i}} = \begin{bmatrix} \frac{\partial \boldsymbol{A}_k}{\partial q_{j,i}} \bar{\boldsymbol{C}}_{r,k}^T + \boldsymbol{A}_k \frac{\partial \bar{\boldsymbol{C}}_{r,k}^T}{\partial q_{j,i}} \\ \frac{\partial \boldsymbol{A}_k}{\partial q_{j,i}} \bar{\boldsymbol{C}}_{t,k}^T \end{bmatrix} \tag{B.19}$$

$$\frac{\partial \bar{\boldsymbol{C}}_{r,k}^T}{\partial q_{j,i}} = \begin{cases} \boldsymbol{0} & , \quad i \neq k \\ \boldsymbol{I}_{j,i}^5 & , \quad i = k \end{cases} \tag{B.20}$$

$$\frac{\partial \boldsymbol{\mathcal{B}}_q}{\partial q_{j,i}} = \begin{bmatrix} \boldsymbol{0} & \boldsymbol{0} & \boldsymbol{0} & \cdots & \boldsymbol{0} & \boldsymbol{0} \\ \frac{\partial \boldsymbol{B}_{q,1}}{\partial q_{j,i}} & \boldsymbol{0} & \boldsymbol{0} & \cdots & \boldsymbol{0} & \boldsymbol{0} \\ \boldsymbol{0} & \frac{\partial \boldsymbol{B}_{q,2}}{\partial q_{j,i}} & \boldsymbol{0} & \cdots & \boldsymbol{0} & \boldsymbol{0} \\ \vdots & \vdots & \vdots & \ddots & \vdots & \vdots \\ \boldsymbol{0} & \boldsymbol{0} & \boldsymbol{0} & \cdots & \boldsymbol{0} & \boldsymbol{0} \\ \boldsymbol{0} & \boldsymbol{0} & \boldsymbol{0} & \boldsymbol{0} & \frac{\partial \boldsymbol{B}_{q,N-1}}{\partial q_{j,i}} & \boldsymbol{0} \end{bmatrix} \tag{B.21}$$

$$\frac{\partial \boldsymbol{B}_{q,k}}{\partial q_{j,i}} = \begin{bmatrix} \frac{\partial \boldsymbol{A}_k}{\partial q_{j,i}} \hat{\boldsymbol{S}}_k \\ \frac{\partial \boldsymbol{A}_k}{\partial q_{j,i}} \boldsymbol{S}_i \end{bmatrix} \tag{B.22}$$

Finally, the partial derivative of $\boldsymbol{\mathcal{M}}_{qq}$ is computed as follows.

$$\begin{aligned} \frac{\partial \boldsymbol{\mathcal{M}}_{qq}}{\partial q_{j,i}} \quad = \quad & \frac{\partial \boldsymbol{\mathcal{B}}_q^T}{\partial q_{j,i}} \boldsymbol{\mathcal{P}}^{-1} \boldsymbol{\mathcal{I}}_{vv} \boldsymbol{\mathcal{P}}^{-T} \boldsymbol{\mathcal{B}}_q + \boldsymbol{\mathcal{B}}_q^T \frac{\partial \boldsymbol{\mathcal{P}}^{-1}}{\partial q_{j,i}} \boldsymbol{\mathcal{I}}_{vv} \boldsymbol{\mathcal{P}}^{-T} \boldsymbol{\mathcal{B}}_q \\ & + \boldsymbol{\mathcal{B}}_q^T \boldsymbol{\mathcal{P}}^{-1} \frac{\partial \boldsymbol{\mathcal{I}}_{vv}}{\partial q_{j,i}} \boldsymbol{\mathcal{P}}^{-T} \boldsymbol{\mathcal{B}}_q \\ & + \boldsymbol{\mathcal{B}}_q^T \boldsymbol{\mathcal{P}}^{-1} \boldsymbol{\mathcal{I}}_{vv} \frac{\partial \boldsymbol{\mathcal{P}}^{-T}}{\partial q_{j,i}} \boldsymbol{\mathcal{B}}_q + \boldsymbol{\mathcal{B}}_q^T \boldsymbol{\mathcal{P}}^{-1} \boldsymbol{\mathcal{I}}_{vv} \boldsymbol{\mathcal{P}}^{-T} \frac{\partial \boldsymbol{\mathcal{B}}_q}{\partial q_{j,i}} \\ & + \frac{\partial \boldsymbol{\mathcal{I}}_{vq}^T}{\partial q_{j,i}} \boldsymbol{\mathcal{P}}^{-T} \boldsymbol{\mathcal{B}}_q + \boldsymbol{\mathcal{I}}_{vq}^T \frac{\partial \boldsymbol{\mathcal{P}}^{-T}}{\partial q_{j,i}} \boldsymbol{\mathcal{B}}_q \\ & + \boldsymbol{\mathcal{I}}_{vq}^T \boldsymbol{\mathcal{P}}^{-T} \frac{\partial \boldsymbol{\mathcal{B}}_q}{\partial q_{j,i}} + \frac{\partial \boldsymbol{\mathcal{B}}_q^T}{\partial q_{j,i}} \boldsymbol{\mathcal{P}}^{-1} \boldsymbol{\mathcal{I}}_{vq} + \boldsymbol{\mathcal{B}}_q^T \frac{\partial \boldsymbol{\mathcal{P}}^{-1}}{\partial q_{j,i}} \boldsymbol{\mathcal{I}}_{vq} + \boldsymbol{\mathcal{B}}_q^T \boldsymbol{\mathcal{P}}^{-1} \frac{\partial \boldsymbol{\mathcal{I}}_{vq}}{\partial q_{j,i}} \end{aligned} \tag{B.23}$$

The derivatives of $\boldsymbol{\mathcal{C}_\theta}$ and $\boldsymbol{\mathcal{C}_q}$ are calculated with a similar procedure.

$$\begin{aligned} \frac{\partial \boldsymbol{\mathcal{C}}_\theta}{\partial q_{j,i}} \quad = \quad & \frac{\partial \boldsymbol{\mathcal{B}}_\theta^T}{\partial q_{j,i}} \boldsymbol{\mathcal{P}}^{-1} \boldsymbol{\mathcal{I}}_{vv} \boldsymbol{\mathcal{P}}^{-T} \dot{\boldsymbol{\mathcal{V}}}' + \boldsymbol{\mathcal{B}}_\theta^T \frac{\partial \boldsymbol{\mathcal{P}}^{-1}}{\partial q_{j,i}} \boldsymbol{\mathcal{I}}_{vv} \boldsymbol{\mathcal{P}}^{-T} \dot{\boldsymbol{\mathcal{V}}}' + \boldsymbol{\mathcal{B}}_\theta^T \boldsymbol{\mathcal{P}}^{-1} \frac{\partial \boldsymbol{\mathcal{I}}_{vv}}{\partial q_{j,i}} \boldsymbol{\mathcal{P}}^{-T} \dot{\boldsymbol{\mathcal{V}}}' \\ & + \boldsymbol{\mathcal{B}}_\theta^T \boldsymbol{\mathcal{P}}^{-1} \boldsymbol{\mathcal{I}}_{vv} \frac{\partial \boldsymbol{\mathcal{P}}^{-T}}{\partial q_{j,i}} \dot{\boldsymbol{\mathcal{V}}}' + \boldsymbol{\mathcal{B}}_\theta^T \boldsymbol{\mathcal{P}}^{-1} \boldsymbol{\mathcal{I}}_{vv} \boldsymbol{\mathcal{P}}^{-T} \frac{\partial \dot{\boldsymbol{\mathcal{V}}}'}{\partial q_{j,i}} - \frac{\partial \boldsymbol{\mathcal{B}}_\theta^T}{\partial q_{j,i}} \boldsymbol{\mathcal{P}}^{-1} \boldsymbol{\mathcal{C}}_v \\ & - \boldsymbol{\mathcal{B}}_\theta^T \frac{\partial \boldsymbol{\mathcal{P}}^{-1}}{\partial q_{j,i}} \boldsymbol{\mathcal{C}}_v - \boldsymbol{\mathcal{B}}_\theta^T \boldsymbol{\mathcal{P}}^{-1} \frac{\partial \boldsymbol{\mathcal{C}}_v}{\partial q_{j,i}} \end{aligned} \tag{B.24}$$

where

$$\frac{\partial \dot{\boldsymbol{\mathcal{V}}}'}{\partial q_{j,i}} = \operatorname{col}\left\{\frac{\partial \dot{\boldsymbol{V}}_k'}{\partial q_{j,i}}\right\} \tag{B.25}$$

$$\frac{\partial \dot{\boldsymbol{V}}_k'}{\partial q_{j,i}} = \begin{bmatrix} \frac{\partial \dot{\boldsymbol{\omega}}_k'}{\partial q_{j,i}} \\ \frac{\partial \dot{\boldsymbol{v}}_k'}{\partial q_{j,i}} \end{bmatrix} \tag{B.26}$$

$$\begin{aligned}\left.\frac{\partial \dot{\boldsymbol{\omega}}_k'}{\partial q_{j,i}}\right|_{\substack{\boldsymbol{q}=\boldsymbol{0}\\ \dot{\boldsymbol{q}}=\boldsymbol{0}}} = {} & \frac{\partial \tilde{\boldsymbol{\omega}}_{k-1}}{\partial q_{j,i}} \boldsymbol{A}_{k-1}\hat{\boldsymbol{A}}_{k-1}\hat{\boldsymbol{z}}_{k-1}'\dot{\theta}_k + \tilde{\boldsymbol{\omega}}_{k-1}\frac{\partial \boldsymbol{A}_{k-1}}{\partial q_{j,i}}\hat{\boldsymbol{A}}_{k-1}\hat{\boldsymbol{z}}_{k-1}'\dot{\theta}_k \\ & + \tilde{\boldsymbol{\omega}}_{k-1}\boldsymbol{A}_{k-1}\frac{\partial \hat{\boldsymbol{A}}_{k-1}}{\partial q_{j,i}}\hat{\boldsymbol{z}}_{k-1}'\dot{\theta}_k \end{aligned} \tag{B.27}$$

$$\left.\frac{\partial \boldsymbol{\omega}_{k-1}}{\partial q_{j,i}}\right|_{\substack{\boldsymbol{q}=\boldsymbol{0}\\ \dot{\boldsymbol{q}}=\boldsymbol{0}}} = \sum_{l=0}^{k-2}\left(\frac{\partial \boldsymbol{A}_l}{\partial q_{j,i}}\hat{\boldsymbol{A}}_l\hat{\boldsymbol{z}}_l'\dot{\theta}_{l+1} + \boldsymbol{A}_l\frac{\partial \hat{\boldsymbol{A}}_l}{\partial q_{j,i}}\hat{\boldsymbol{z}}_l'\dot{\theta}_{l+1}\right) \tag{B.28}$$

$$\left.\frac{\partial \dot{\boldsymbol{v}}_k'}{\partial q_{j,i}}\right|_{\substack{\boldsymbol{q}=\boldsymbol{0}\\ \dot{\boldsymbol{q}}=\boldsymbol{0}}} = \frac{\partial \tilde{\boldsymbol{\omega}}_{k-1}}{\partial q_{j,i}}\left(\tilde{\boldsymbol{\omega}}_{k-1}\boldsymbol{p}_{k,k-1}\right) + \tilde{\boldsymbol{\omega}}_{k-1}\left(\frac{\partial \tilde{\boldsymbol{\omega}}_{k-1}}{\partial q_{j,i}}\boldsymbol{p}_{k,k-1}\right) + \tilde{\boldsymbol{\omega}}_{k-1}\left(\tilde{\boldsymbol{\omega}}_{k-1}\frac{\partial \boldsymbol{p}_{k,k-1}}{\partial q_{j,i}}\right) \tag{B.29}$$

$$\frac{\partial \boldsymbol{\mathcal{C}}_v}{\partial q_{j,i}} = \operatorname{col}\left\{\frac{\partial \boldsymbol{C}_{v,k}}{\partial q_{j,i}}\right\} \tag{B.30}$$

$$\frac{\partial \boldsymbol{C}_{v,k}}{\partial q_{j,i}} = \begin{bmatrix} \frac{\partial \boldsymbol{A}_k}{\partial q_{j,i}}\boldsymbol{h}_{\omega,k}^{\theta} + \boldsymbol{A}_k\frac{\partial \boldsymbol{h}_{\omega,k}^{\theta}}{\partial q_{j,i}} \\ \frac{\partial \boldsymbol{A}_k}{\partial q_{j,i}}\boldsymbol{h}_{\omega,k}^{r} + \boldsymbol{A}_k\frac{\partial \boldsymbol{h}_{\omega,k}^{r}}{\partial q_{j,i}} \end{bmatrix} \tag{B.31}$$

$$\left.\frac{\partial \boldsymbol{h}_{\omega,k}^{\theta}}{\partial q_{j,i}}\right|_{\substack{\boldsymbol{q}=\boldsymbol{0}\\ \dot{\boldsymbol{q}}=\boldsymbol{0}}} = -\frac{\partial \tilde{\bar{\boldsymbol{\omega}}}_k}{\partial q_{j,i}}\bar{\boldsymbol{J}}_k\bar{\boldsymbol{\omega}}_k - \tilde{\bar{\boldsymbol{\omega}}}_k\frac{\partial \bar{\boldsymbol{J}}_k}{\partial q_{j,i}}\bar{\boldsymbol{\omega}}_k - \tilde{\bar{\boldsymbol{\omega}}}_k\bar{\boldsymbol{J}}_k\frac{\partial \bar{\boldsymbol{\omega}}_k}{\partial q_{j,i}} \tag{B.32}$$

$$\frac{\partial \bar{\boldsymbol{\omega}}_k}{\partial q_{j,i}} = \frac{\partial \boldsymbol{A}_k^T}{\partial q_{j,i}}\boldsymbol{\omega}_k + \boldsymbol{A}_k^T\frac{\partial \boldsymbol{\omega}_k}{\partial q_{j,i}} \tag{B.33}$$

$$\left.\frac{\partial \boldsymbol{h}_{\omega,k}^{r}}{\partial q_{j,i}}\right|_{\substack{\boldsymbol{q}=\boldsymbol{0}\\ \dot{\boldsymbol{q}}=\boldsymbol{0}}} = -\frac{\partial \tilde{\bar{\boldsymbol{\omega}}}_k}{\partial q_{j,i}}\tilde{\bar{\boldsymbol{\omega}}}_k m_k\bar{\boldsymbol{d}}_{C,k} - \tilde{\bar{\boldsymbol{\omega}}}_k\frac{\partial \tilde{\bar{\boldsymbol{\omega}}}_k}{\partial q_{j,i}}m_k\bar{\boldsymbol{d}}_{C,k} - \tilde{\bar{\boldsymbol{\omega}}}_k\tilde{\bar{\boldsymbol{\omega}}}_k\frac{\partial\left(m_k\bar{\boldsymbol{d}}_{C,k}\right)}{\partial q_{j,i}} \tag{B.34}$$

and

$$\frac{\partial \boldsymbol{\mathcal{C}}_\theta}{\partial \dot{q}_{j,i}} = \boldsymbol{\mathcal{B}}_\theta^T\boldsymbol{\mathcal{P}}^{-1}\boldsymbol{\mathcal{I}}_{vv}\boldsymbol{\mathcal{P}}^{-T}\frac{\partial \dot{\boldsymbol{\mathcal{V}}}'}{\partial \dot{q}_{j,i}} - \boldsymbol{\mathcal{B}}_\theta^T\boldsymbol{\mathcal{P}}^{-1}\frac{\partial \boldsymbol{\mathcal{C}}_v}{\partial \dot{q}_{j,i}} \tag{B.35}$$

where

$$\frac{\partial \dot{\boldsymbol{\mathcal{V}}}'}{\partial \dot{q}_{j,i}} = \mathrm{col}\left\{ \frac{\partial \dot{\boldsymbol{V}}'_k}{\partial \dot{q}_{j,i}} \right\} \tag{B.36}$$

$$\frac{\partial \dot{\boldsymbol{V}}'_k}{\partial \dot{q}_{j,i}} = \begin{bmatrix} \frac{\partial \dot{\boldsymbol{\omega}}'_k}{\partial \dot{q}_{j,i}} \\ \frac{\partial \dot{\boldsymbol{v}}'_k}{\partial \dot{q}_{j,i}} \end{bmatrix} \tag{B.37}$$

$$\begin{aligned} \left.\frac{\partial \dot{\boldsymbol{\omega}}'_k}{\partial \dot{q}_{j,i}}\right|_{\substack{\boldsymbol{q}=\boldsymbol{0}\\ \dot{\boldsymbol{q}}=\boldsymbol{0}}} &= \frac{\partial \tilde{\boldsymbol{\omega}}_{k-1}}{\partial \dot{q}_{j,i}} \boldsymbol{A}_{k-1} \hat{\boldsymbol{S}}_{k-1} \dot{\boldsymbol{q}}_{k-1} + \tilde{\boldsymbol{\omega}}_{k-1} \boldsymbol{A}_{k-1} \hat{\boldsymbol{S}}_{k-1} \frac{\partial \dot{\boldsymbol{q}}_{k-1}}{\partial \dot{q}_{j,i}} \\ &\quad + \frac{\partial \tilde{\boldsymbol{\omega}}_{k-1}}{\partial \dot{q}_{j,i}} \boldsymbol{A}_{k-1} \hat{\boldsymbol{A}}_{k-1} \hat{\boldsymbol{z}}'_{k-1} \dot{\theta}_k + \boldsymbol{A}_{k-1} \widetilde{\left(\hat{\boldsymbol{S}}_{k-1} \frac{\partial \dot{\boldsymbol{q}}_{k-1}}{\partial \dot{q}_{j,i}} \right)} \hat{\boldsymbol{z}}'_{k-1} \dot{\theta}_k \end{aligned}$$

$$\frac{\partial \boldsymbol{\omega}_{k-1}}{\partial \dot{q}_{j,i}} = \begin{cases} \boldsymbol{0} & , \quad i > k-2 \\ \boldsymbol{A}_i \hat{\boldsymbol{S}}_i \boldsymbol{\sigma}_{j,i} & , \quad i \leq k-2 \end{cases} \tag{B.38}$$

$$\frac{\partial \dot{\boldsymbol{q}}_{k-1}}{\partial \dot{q}_{j,i}} = \begin{cases} \boldsymbol{0} & , \quad i \neq k-1 \\ \boldsymbol{\sigma}_{j,i} & , \quad i = k-1 \end{cases} \tag{B.39}$$

$$\begin{aligned} \left.\frac{\partial \dot{\boldsymbol{v}}'_k}{\partial \dot{q}_{j,i}}\right|_{\substack{\boldsymbol{q}=\boldsymbol{0}\\ \dot{\boldsymbol{q}}=\boldsymbol{0}}} &= \frac{\partial \tilde{\boldsymbol{\omega}}_{k-1}}{\partial \dot{q}_{j,i}} \tilde{\boldsymbol{\omega}}_{k-1} \boldsymbol{p}_{k,k-1} + \tilde{\boldsymbol{\omega}}_{k-1} \frac{\partial \tilde{\boldsymbol{\omega}}_{k-1}}{\partial \dot{q}_{j,i}} \boldsymbol{p}_{k,k-1} \\ &\quad + \frac{\partial \tilde{\boldsymbol{\omega}}_{k-1}}{\partial \dot{q}_{j,i}} \boldsymbol{A}_{k-1} \boldsymbol{S}_{k-1} \dot{\boldsymbol{q}}_{k-1} + \tilde{\boldsymbol{\omega}}_{k-1} \boldsymbol{A}_{k-1} \boldsymbol{S}_{k-1} \frac{\partial \dot{\boldsymbol{q}}_{k-1}}{\partial \dot{q}_{j,i}} \end{aligned} \tag{B.40}$$

$$\frac{\partial \boldsymbol{\mathcal{C}}_v}{\partial \dot{q}_{j,i}} = \mathrm{col}\left\{ \frac{\partial \boldsymbol{C}_{v,k}}{\partial \dot{q}_{j,i}} \right\} \tag{B.41}$$

$$\frac{\partial \boldsymbol{C}_{v,k}}{\partial \dot{q}_{j,i}} = \begin{bmatrix} \boldsymbol{A}_k \frac{\partial \boldsymbol{h}^{\theta}_{\omega,k}}{\partial \dot{q}_{j,i}} \\ \boldsymbol{A}_k \frac{\partial \boldsymbol{h}^{r}_{\omega,k}}{\partial \dot{q}_{j,i}} \end{bmatrix} \tag{B.42}$$

$$\begin{aligned} \left.\frac{\partial \boldsymbol{h}^{\theta}_{\omega,k}}{\partial \dot{q}_{j,i}}\right|_{\substack{\boldsymbol{q}=\boldsymbol{0}\\ \dot{\boldsymbol{q}}=\boldsymbol{0}}} &= -\frac{\partial \tilde{\bar{\boldsymbol{\omega}}}_k}{\partial \dot{q}_{j,i}} \bar{\boldsymbol{J}}_k \bar{\boldsymbol{\omega}}_k - \tilde{\bar{\boldsymbol{\omega}}}_k \bar{\boldsymbol{J}}_k \frac{\partial \bar{\boldsymbol{\omega}}_k}{\partial \dot{q}_{j,i}} - \frac{\partial \tilde{\bar{\boldsymbol{\omega}}}_k}{\partial \dot{q}_{j,i}} \bar{\boldsymbol{C}}^T_{r,k} \dot{\boldsymbol{q}}_k \\ &\quad - \tilde{\bar{\boldsymbol{\omega}}}_k \bar{\boldsymbol{C}}^T_{r,k} \frac{\partial \dot{\boldsymbol{q}}_k}{\partial \dot{q}_{j,i}} - \frac{\partial \dot{\bar{\boldsymbol{J}}}_k}{\partial \dot{q}_{j,i}} \bar{\boldsymbol{\omega}}_k - \dot{\bar{\boldsymbol{J}}}_k \frac{\partial \bar{\boldsymbol{\omega}}_k}{\partial \dot{q}_{j,i}} \end{aligned} \tag{B.43}$$

$$\frac{\partial \dot{\bar{\boldsymbol{J}}}_k}{\partial \dot{q}_{j,i}} = \begin{cases} \boldsymbol{0} & , \quad i \neq k \\ -\boldsymbol{I}^{8T}_{j,i} + \boldsymbol{I}^{8T}_{j,i} - \sum\limits_{l=1}^{M_k} \left(\boldsymbol{I}^{9}_{jl,i} + \boldsymbol{I}^{9}_{lj,i} \right) q_{l,i} & , \quad i = k \end{cases} \tag{B.44}$$

$$\begin{aligned}\frac{\partial \boldsymbol{h}^r_{\omega,k}}{\partial \dot{q}_{j,i}} &= -\frac{\partial \tilde{\bar{\boldsymbol{\omega}}}_k}{\partial \dot{q}_{j,i}} \tilde{\bar{\boldsymbol{\omega}}}_k m_k \bar{\boldsymbol{d}}_{C,k} - \tilde{\bar{\boldsymbol{\omega}}}_k \frac{\partial \tilde{\bar{\boldsymbol{\omega}}}_k}{\partial \dot{q}_{j,i}} m_k \bar{\boldsymbol{d}}_{C,k} \\ &\quad -\frac{\partial \tilde{\bar{\boldsymbol{\omega}}}_k}{\partial \dot{q}_{j,i}} 2\bar{\boldsymbol{C}}^T_{t,k} \dot{\boldsymbol{q}}_k - \tilde{\bar{\boldsymbol{\omega}}}_k 2\bar{\boldsymbol{C}}^T_{t,k} \frac{\partial \dot{\boldsymbol{q}}_k}{\partial \dot{q}_{j,i}} \end{aligned} \tag{B.45}$$

and finally

$$\begin{aligned}\frac{\partial \boldsymbol{\mathcal{C}}_q}{\partial q_{j,i}} &= \frac{\partial \boldsymbol{\mathcal{I}}^T_{vq}}{\partial q_{j,i}} \boldsymbol{\mathcal{P}}^{-T} \dot{\boldsymbol{\mathcal{V}}}' + \boldsymbol{\mathcal{I}}^T_{vq} \frac{\partial \boldsymbol{\mathcal{P}}^{-T}}{\partial q_{j,i}} \dot{\boldsymbol{\mathcal{V}}}' + \boldsymbol{\mathcal{I}}^T_{vq} \boldsymbol{\mathcal{P}}^{-T} \frac{\partial \dot{\boldsymbol{\mathcal{V}}}'}{\partial q_{j,i}} \\ &\quad + \frac{\partial \boldsymbol{\mathcal{B}}^T_q}{\partial q_{j,i}} \boldsymbol{\mathcal{P}}^{-1} \boldsymbol{\mathcal{I}}_{vv} \boldsymbol{\mathcal{P}}^{-T} \dot{\boldsymbol{\mathcal{V}}}' \\ &\quad + \boldsymbol{\mathcal{B}}^T_q \frac{\partial \boldsymbol{\mathcal{P}}^{-1}}{\partial q_{j,i}} \boldsymbol{\mathcal{I}}_{vv} \boldsymbol{\mathcal{P}}^{-T} \dot{\boldsymbol{\mathcal{V}}}' + \boldsymbol{\mathcal{B}}^T_q \boldsymbol{\mathcal{P}}^{-1} \frac{\partial \boldsymbol{\mathcal{I}}_{vv}}{\partial q_{j,i}} \boldsymbol{\mathcal{P}}^{-T} \dot{\boldsymbol{\mathcal{V}}}' \\ &\quad + \boldsymbol{\mathcal{B}}^T_q \boldsymbol{\mathcal{P}}^{-1} \boldsymbol{\mathcal{I}}_{vv} \frac{\partial \boldsymbol{\mathcal{P}}^{-T}}{\partial q_{j,i}} \dot{\boldsymbol{\mathcal{V}}}' + \boldsymbol{\mathcal{B}}^T_q \boldsymbol{\mathcal{P}}^{-1} \boldsymbol{\mathcal{I}}_{vv} \boldsymbol{\mathcal{P}}^{-T} \frac{\partial \dot{\boldsymbol{\mathcal{V}}}'}{\partial q_{j,i}} - \frac{\partial \boldsymbol{\mathcal{B}}^T_q}{\partial q_{j,i}} \boldsymbol{\mathcal{P}}^{-1} \boldsymbol{\mathcal{C}}_v \\ &\quad - \boldsymbol{\mathcal{B}}^T_q \frac{\partial \boldsymbol{\mathcal{P}}^{-1}}{\partial q_{j,i}} \boldsymbol{\mathcal{C}}_v - \boldsymbol{\mathcal{B}}^T_q \boldsymbol{\mathcal{P}}^{-1} \frac{\partial \boldsymbol{\mathcal{C}}_v}{\partial q_{j,i}} - \frac{\partial \boldsymbol{\mathcal{C}}_f}{\partial q_{j,i}} \end{aligned} \tag{B.46}$$

It must be pointed out that the calculation of the derivatives for the Coriolis and quadratic terms is very involved, namely:

$$\frac{\partial \boldsymbol{\mathcal{C}}_f}{\partial q_{j,i}} = \mathrm{col}\left\{ \frac{\partial \boldsymbol{h}^f_{\omega,k}}{\partial q_{j,i}} \right\} \tag{B.47}$$

$$\begin{aligned}\frac{\partial \boldsymbol{h}^f_{\omega,k}}{\partial q_{j,i}} &= \begin{bmatrix} \frac{\partial \bar{\omega}_{1,k}}{\partial q_{j,i}} \left(\sum_{l=1}^{k} \boldsymbol{d}_{ll,k} \right) + \bar{\omega}_{1,k} \left(\sum_{l=1}^{k} \frac{\partial \boldsymbol{d}_{ll,k}}{\partial q_{j,i}} \right) - \frac{\partial \bar{\boldsymbol{\omega}}^T_k}{\partial q_{j,i}} \boldsymbol{D}_{1,k} - \bar{\boldsymbol{\omega}}^T_k \frac{\partial \boldsymbol{D}_{1,k}}{\partial q_{j,i}} \\ \frac{\partial \bar{\omega}_{2,k}}{\partial q_{j,i}} \left(\sum_{l=1}^{k} \boldsymbol{d}_{ll,k} \right) + \bar{\omega}_{2,k} \left(\sum_{l=1}^{k} \frac{\partial \boldsymbol{d}_{ll,k}}{\partial q_{j,i}} \right) - \frac{\partial \bar{\boldsymbol{\omega}}^T_k}{\partial q_{j,i}} \boldsymbol{D}_{2,k} - \bar{\boldsymbol{\omega}}^T_k \frac{\partial \boldsymbol{D}_{2,k}}{\partial q_{j,i}} \\ \frac{\partial \bar{\omega}_{3,k}}{\partial q_{j,i}} \left(\sum_{l=1}^{k} \boldsymbol{d}_{ll,k} \right) + \bar{\omega}_{3,k} \left(\sum_{l=1}^{k} \frac{\partial \boldsymbol{d}_{ll,k}}{\partial q_{j,i}} \right) - \frac{\partial \bar{\boldsymbol{\omega}}^T_k}{\partial q_{j,i}} \boldsymbol{D}_{3,k} - \bar{\boldsymbol{\omega}}^T_k \frac{\partial \boldsymbol{D}_{3,k}}{\partial q_{j,i}} \end{bmatrix}^T \bar{\boldsymbol{\omega}}_k \\ &\quad + \begin{bmatrix} \bar{\omega}_{1,k} \left(\sum_{l=1}^{k} \boldsymbol{d}_{ll,k} \right) - \bar{\boldsymbol{\omega}}^T_k \boldsymbol{D}_{1,k} \\ \bar{\omega}_{2,k} \left(\sum_{l=1}^{k} \boldsymbol{d}_{ll,k} \right) - \bar{\boldsymbol{\omega}}^T_k \boldsymbol{D}_{2,k} \\ \bar{\omega}_{3,k} \left(\sum_{l=1}^{k} \boldsymbol{d}_{ll,k} \right) - \bar{\boldsymbol{\omega}}^T_k \boldsymbol{D}_{3,k} \end{bmatrix}^T \frac{\partial \bar{\boldsymbol{\omega}}_k}{\partial q_{j,i}} \\ &\quad - 2\frac{\partial \bar{\omega}_{1,k}}{\partial q_{j,i}} \left(\boldsymbol{I}^{11}_{32,k} - \boldsymbol{I}^{11}_{23,k} \right) \dot{\boldsymbol{q}}_k - 2\frac{\partial \bar{\omega}_{2,k}}{\partial q_{j,i}} \left(\boldsymbol{I}^{11}_{13,k} - \boldsymbol{I}^{11}_{31,k} \right) \dot{\boldsymbol{q}}_k \\ &\quad - 2\frac{\partial \bar{\omega}_{3,k}}{\partial q_{j,i}} \left(\boldsymbol{I}^{11}_{21,k} - \boldsymbol{I}^{11}_{12,k} \right) \dot{\boldsymbol{q}}_k \end{aligned} \tag{B.48}$$

$$\frac{\partial \boldsymbol{D}_{m,k}}{\partial q_{j,i}} = \begin{bmatrix} \frac{\partial \mathbf{q}_k^T}{\partial q_{j,i}} \boldsymbol{I}_{m1,k}^{11} \\ \frac{\partial \mathbf{q}_k^T}{\partial q_{j,i}} \boldsymbol{I}_{m2,k}^{11} \\ \frac{\partial \mathbf{q}_k^T}{\partial q_{j,i}} \boldsymbol{I}_{m3,k}^{11} \end{bmatrix} \tag{B.49}$$

$$\frac{\partial \boldsymbol{\mathcal{C}}_q}{\partial \dot{q}_{j,i}} = \boldsymbol{\mathcal{I}}_{vq}^T \boldsymbol{\mathcal{P}}^{-T} \frac{\partial \dot{\boldsymbol{\mathcal{V}}}'}{\partial \dot{q}_{j,i}} + \boldsymbol{\mathcal{B}}_q^T \boldsymbol{\mathcal{P}}^{-1} \boldsymbol{\mathcal{I}}_{vv} \boldsymbol{\mathcal{P}}^{-T} \frac{\partial \dot{\boldsymbol{\mathcal{V}}}'}{\partial \dot{q}_{j,i}} - \boldsymbol{\mathcal{B}}_q^T \boldsymbol{\mathcal{P}}^{-1} \frac{\partial \boldsymbol{\mathcal{C}}_v}{\partial \dot{q}_{j,i}} - \frac{\partial \boldsymbol{\mathcal{C}}_f}{\partial \dot{q}_{j,i}} \tag{B.50}$$

$$\frac{\partial \boldsymbol{\mathcal{C}}_f}{\partial \dot{q}_{j,i}} = \mathrm{col} \left\{ \frac{\partial \boldsymbol{h}_{\omega,k}^f}{\partial q_{j,i}} \right\} \tag{B.51}$$

$$\begin{aligned} \frac{\partial \boldsymbol{h}_{\omega,k}^f}{\partial q_{j,i}} \quad = \quad & \begin{bmatrix} \frac{\partial \bar{\omega}_{1,k}}{\partial \dot{q}_{j,i}} \left(\sum_{l=1}^{k} \boldsymbol{d}_{ll,k} \right) - \frac{\partial \bar{\boldsymbol{\omega}}_k^T}{\partial \dot{q}_{j,i}} \boldsymbol{D}_{1,k} \\ \frac{\partial \bar{\omega}_{2,k}}{\partial \dot{q}_{j,i}} \left(\sum_{l=1}^{k} \boldsymbol{d}_{ll,k} \right) - \frac{\partial \bar{\boldsymbol{\omega}}_k^T}{\partial \dot{q}_{j,i}} \boldsymbol{D}_{2,k} \\ \frac{\partial \bar{\omega}_{3,k}}{\partial \dot{q}_{j,i}} \left(\sum_{l=1}^{k} \boldsymbol{d}_{ll,k} \right) - \frac{\partial \bar{\boldsymbol{\omega}}_k^T}{\partial \dot{q}_{j,i}} \boldsymbol{D}_{3,k} \end{bmatrix}^T \bar{\boldsymbol{\omega}}_k \\ & + \begin{bmatrix} \bar{\omega}_{1,k} \left(\sum_{l=1}^{k} \boldsymbol{d}_{ll,k} \right) - \bar{\boldsymbol{\omega}}_k^T \boldsymbol{D}_{1,k} \\ \bar{\omega}_{2,k} \left(\sum_{l=1}^{k} \boldsymbol{d}_{ll,k} \right) - \bar{\boldsymbol{\omega}}_k^T \boldsymbol{D}_{2,k} \\ \bar{\omega}_{3,k} \left(\sum_{l=1}^{k} \boldsymbol{d}_{ll,k} \right) - \bar{\boldsymbol{\omega}}_k^T \boldsymbol{D}_{3,k} \end{bmatrix}^T \frac{\partial \bar{\boldsymbol{\omega}}_k}{\partial \dot{q}_{j,i}} \\ & -2 \frac{\partial \bar{\omega}_{1,k}}{\partial \dot{q}_{j,i}} \left(\boldsymbol{I}_{32,k}^{11} - \boldsymbol{I}_{23,k}^{11} \right) \dot{\boldsymbol{q}}_k - 2 \frac{\partial \bar{\omega}_{2,k}}{\partial \dot{q}_{j,i}} \left(\boldsymbol{I}_{13,k}^{11} - \boldsymbol{I}_{31,k}^{11} \right) \dot{\boldsymbol{q}}_k \\ & -2 \frac{\partial \bar{\omega}_{3,k}}{\partial \dot{q}_{j,i}} \left(\boldsymbol{I}_{21,k}^{11} - \boldsymbol{I}_{12,k}^{11} \right) \dot{\boldsymbol{q}}_k - 2 \bar{\omega}_{1,k} \left(\boldsymbol{I}_{32,k}^{11} - \boldsymbol{I}_{23,k}^{11} \right) \frac{\partial \dot{\boldsymbol{q}}_k}{\partial \dot{q}_{j,i}} \\ & -2 \bar{\omega}_{2,k} \left(\boldsymbol{I}_{13,k}^{11} - \boldsymbol{I}_{31,k}^{11} \right) \frac{\partial \dot{\boldsymbol{q}}_k}{\partial \dot{q}_{j,i}} - 2 \bar{\omega}_{3,k} \left(\boldsymbol{I}_{21,k}^{11} - \boldsymbol{I}_{12,k}^{11} \right) \frac{\partial \dot{\boldsymbol{q}}_k}{\partial \dot{q}_{j,i}} \end{aligned}$$